The Synergistic Effect of Bone Graft Substitute Architecture and Mechanical Environment on hMSCs Responses *in vitro*

Feng Yang

Supervisors: Dr Karin A. Hing and Dr Simon C.F. Rawlinson

Submitted in partial fulfilment of the requirements of the Degree of Doctor of Philosophy

School of Engineering and Material Science

Queen Mary University of London

December 2018

Statement of Originality

I, Feng Yang, confirm that the research included within this thesis is my own work or that where it has been carried out in collaboration with, or supported by others, that this is duly acknowledged below, and my contribution indicated. Previously published material is also acknowledged below.

I attest that I have exercised reasonable care to ensure that the work is original and does not to the best of my knowledge break any UK law, infringe any third party's copyright or other Intellectual Property Right, or contain any confidential material.

I accept that the College has the right to use plagiarism detection software to check the electronic version of the thesis.

I confirm that this thesis has not been previously submitted for the award of a degree by this or any other university.

The copyright of this thesis rests with the author and no quotation from it or information derived from it may be published without the prior written consent of the author.

Signature:

Date:

Acknowledgements

I would like to sincerely thank my supervisors, Dr Karin A. Hing and Dr Simon C.F. Rawlinson for giving me a wonderful opportunity to be part of the research group. This research would not have been possible without their support, advice and guidance throughout my PhD.

My gratitude also goes to all members of the Hing group, past and present, who are my colleagues as well as friends of mine. Special thanks to Dr Krystelle Mafina for helping me with materials characterisation training, Dr Navinderpal Kaur Chana for teaching me foundation of cell culture and perfusion system, Dinara Ikramova for sharing the lab bench and excitements at day and night together.

I would like to express my gratitude to Dr Stephen Thorpe, Dr Clare Thompson and Dr Estell Collin for teaching me molecular biology techniques and for helpful discussion. Many thanks to the people I worked with in Baxter Inc for providing me with biomaterials and helping me with characterisation equipment. I further would like to thank our wonderful SEMS lab management and technician team for their technical support.

Finally, a very special thanks to my family and friends, especially my parents and my husband Adam, for their endless love, support and encouragement.

Abstract

Porous silicate substituted hydroxyapatite (SiHA) as synthetic bone graft substitute (BGS) shows excellent bone repair *in vivo*. It is accepted that the mechanical environment to which cells are exposed regulates cellular differentiation. One mechanism by which BGS architecture may regulate bone formation could be through influencing the shear stress distribution of interstitial fluid. The aim of this study was to investigate the combined influence of BGS architecture and fluid shear environment on human mesenchymal stem cells (hMSCs) responses.

hMSCs were cultured on SiHA BGS with defined porosity. A 3D in-house perfusion bioreactor system was established, and two shear stress profiles were applied in this study: 1) continuous basal perfusion rate (BPR) at 0.07 ml/min; 2) BPR with a period of high perfusion rate (pHPR) every day at 2.5 ml/min. The cytoskeleton of hMSCs was reorganized under perfusion conditions compared with under static condition. Shear stress induced both ERK1/2 and pEKR1/2 translocation from the cytoplasm to nucleus. hMSCs cultured in BPR profile differentiated towards osteogenic lineage, while pHPR induced hMSCs to differentiate towards chondrogenic lineage. Gene expression of *osx*, *sox9*, *runx2* and *col ii* was not dependent on BGS micro-porosity under static condition. However, the expression of osteogenic transcription factor *osx* increased significantly with increasing BGS micro-porosity under BPR condition, whereas the expression of chondrogenic markers like *sox9*, *runx2* and *col ii* decreased with increasing BGS micro-porosity under pHPR condition after 3 days.

Nifedipine was used to block L-type voltage-sensitive Ca^{2+} channel (VSCC) activity. The translocation of ERK1/2 and pEKR1/2 from the cytoplasm to nucleus was found to be dependent on L-type VSCCs. Both BPR induced osteogenic differentiation and pHPR induced chondrogenic differentiation were found to be modulated by L-type VSCCs. The findings of this PhD thesis demonstrate that the future evaluation of porous BGS bioactivity should be conducted under carefully selected perfusion conditions, and the results of this thesis suggest that chondrogenic markers should also be used as one of the indicators for BGS performance in addition to conventional osteogenic markers, as early chondrogenic activity may denote the onset of osteochondral bone formation. This would also argue for longer term culture to

further monitor cell fate and the development of any extracellular matrix (ECM) produced.

Table of Contents

List of Abbreviations and Symbols

Key abbreviations and symbols used in this PhD thesis are defined here. Some less frequently used ones are defined in the main body of the text.

3D	3 dimensional
ALP	alkaline phosphatase
ANOVA	analysis of variance
BCP	biphasic calcium phosphate
BGS	Bone graft substitute
BM	basic cell culture medium
BMO	BM supplemented with osteogenic induction medium
BMP	bone morphogenetic protein
β-TCP	β-tricalcium phosphate
BPR	basal perfusion rate
BPR + C	basal perfusion rate with one hour daily cyclic compression
BSA	bovine serum albumin
BSP	bone sialoprotein
Ca^{2+}	calcium ions
CO_2	carbon dioxide
COL I	type 1 collagen
COL II	type 2 collagen
COX-2	cyclooxygenase-2
DAPI	4',6-diamidino-2-phenylindole
DMP1	dentin matrix acidic phosphoprotein
DNA	deoxyribonucleic acid
ECM	extracellular matrix
ERK	extracellular signal-regulated kinase
FAK	focal adhesion kinase
FBS	fetal bovine serum

GAPDH	glyceraldehyde 3-phosphate dehydrogenase
HA	hydroxyapatite
hMSCs	human mesenchymal stem cells
IF	immunofluorescence
MC3T3-E1	mouse calvaria osteoblastic cells
MAPK	mitogen-activated protein kinase
myoD	myoblast determination protein
mRNA	messenger ribonucleic acid
MG63	human osteosarcoma cells
MSCs	mesenchymal stem cells
OC	osteocalcin
ON	osteonetin
OPN	osteopontin
OSX	osterix
PBS	phosphate buffered saline
PCR	polymerase chain reaction
pERK	phosphorylated ERK
PGE2	prostaglandin E2
PM	MSC growth medium 2 from PromoCell
PMO	PM supplemented with osteogenic induction medium
RUNX2	runt-related transcription factor 2
SEM	scanning electron microscope
SiHA	silicate substituted hydroxyapatite
SOX9	SRY-box 9
TBS	tris buffered saline
VEGF	vascular endothelial growth factor
VSCC	voltage-sensitive calcium channel
WB	western blot

List of Figures

List of Tables

Chapter 1 Review of the Literature

1.1 Bone Composition and Structure

Bone is a highly organized tissue that has four major functions: maintain blood calcium levels, support skeletal haematopoiesis, provide mechanical support for soft tissue and provide protection to internal organs. It is important to understand the fundamental characteristics of bone composition and bone structure to develop and evaluate synthetic bone graft substitute (BGS) materials for clinical use.

1.1.1 Bone Cells

The bone cells make up 10% of the total volume of bone. There are three major types of cells: osteoblasts, osteocytes and osteoclasts in bone and they are responsible for the bone formation, bone maintenance and bone remodelling.

Osteoblasts originate from mesenchymal stem cells. Active osteoblasts have a cuboidal morphology and are found on the surface of new bone. Osteoblasts accomplish their bone formation function through three stages: synthesis of collagen, matrix maturation and matrix mineralization. During the proliferation of osteoblasts, matrix proteins, especially type I collagen are deposited onto the bone surface to form unmineralised matrix termed osteoid. This is followed by the precipitation of inorganic minerals forming the mineralized bone matrix. After the formation of bone matrix, some osteoblasts are entombed in the bone and subsequently differentiate into osteocytes or transform into resting, or quiescent osteoblasts and become bone-lining cells if not buried.

Osteocytes are the end cell phenotype in the osteoblastic lineage, constituting the most abundant cell type of bone. Although osteocytes lie within lacunae in mineralized tissue, they have long dendritic extensions through which they can communicate with other osteocytes or osteoblasts. It is the communication that enables osteocytes to perform the role of modulating the exchange of mineral ions, the supply of oxygen and nutrients throughout the bone. Another function of osteocytes is mechanotransduction, potentially because they are well placed to sense the magnitude and direction of mechanical forces within the tissue. It is well

documented that osteocytes are responsive to mechanical forces both *in vivo* and *in vitro* (Lanyon, 1993).

Osteoclasts are derived from the hematopoietic macrophage/monocyte lineage. The main function of osteoclasts is to resorb bone. The capacity of osteoclasts to resorb bone depends on their ability to synthesise a series of electrolytes and degradative enzymes (Teitelbaum, 2007). Once attached to bone, osteoclasts create an isolated microenvironment between itself and the bone surface. Osteoclasts secreted hydrogen ions via H^+-ATPase proton pumps and chloride channels to lower the pH to as low as 4.5 within the isolated environment. The acidity within the degradative space resorbs the mineral phase exposing the organic matrix of bone, which is subsequently degraded by cathepsin K (Saftig *et al.*, 1998).

1.1.2 Bone Matrix

Bone matrix consists of both an organic component and an inorganic component, resulting in a well-engineered composite structure which delivers the mechanical strength and toughness of bone with a relatively low density.

The organic component of bone matrix is primarily constituted of collagenous proteins (85 - 90%). Type I collagen is the major collagenous protein found in bone. Type I collagen is a unique triple helical molecule, which is made up of three parallel polypeptide chains. These triple helices assemble to form fibrils. Fibrils then combine with other molecules, such as proteoglycans, to form fibril bundles and fibres, which then assemble with each other and form bone tissue (Varma *et al.*, 2016).

The remain 10 - 15% of organic component consists of non-collagenous proteins. Several non-collagenous proteins, including osteonectin (ON), osteopontin (OPN), bone sialoprotein (BSP) and osteocalcin (OC), serve crucial functions in matrix organization and bone mineralization. Osteonectin plays a key role in bone by initiating formation of mineral, as it binds collagen I to form a complex, which in turn act as nucleator of hydroxyapatite formation (Termine *et al.*, 1981). Osteonectin was also found to support bone remodelling, regulate cell proliferation and cell-matrix interaction (Delany *et al.*, 2000). Osteopontin is a multifunctional protein. On one hand, as an extracellular matrix component, it can regulate mineral crystal formation

and growth. On the other hand, it is involved in physiological and pathological processes including cell proliferation, migration, survival and inflammation (Sodek *et al.*, 2000). Bone sialoprotein acts as a hydroxyapatite nucleator, and its secretion regulated precisely during the initiation of mineralization (Hunter and Goldberg, 1993). Because of its restricted secretion, bone sialoprotein provides a valuable marker for osteogenic differentiation and bone formation (Ganss *et al.*, 1999). Osteocalcin is the most abundant non-collagenous protein of bone extracellular matrix. Osteocalcin is known to limit bone formation by regulating mineral crystals' growth and controlling the size of growing crystals (Ducy *et al.*, 1996; Hoang *et al.*, 2003). Osteocalcin also plays a role in bone remodelling through cell signalling and the recruitment of osteoblasts and osteoclasts, which have active roles in bone deposition and resorption, respectively (Bodine and Komm, 1999; Chenu *et al.*, 1994). Apart from these bone extracellular matrix related proteins, another group of non-collagenous proteins are the growth factors, including the transforming growth factor-β family, insulin like growth factor-1, insulin like growth factor-2 and the bone morphogenic proteins. These growth factors play a crucial rule in cellular growth, differentiation, survival, and cell cycle progression (Lawrence, 1996; Jones and Clemmons, 1995; Bragdon *et al.*, 2011).

The inorganic component of bone, known as bone mineral, accounts for ~60-70% dry weight of bone (LeGeros, 2002). Bone mineral has a similar crystallographic structure to hydroxyapatite, $Ca_{10}(PO_4)_6(OH)_2$, but is a multi-substituted form, with cations such as Mg, Na, Mn, Zn substituted for Ca and ionic groups such as CO_3 substitute for PO_4 and OH. High resolution AFM studies find that the bone crystals are very small, with widths and lengths ranging from 30 to 200 nm (Hassenkam *et al.*, 2004). Non-stoichiometry and small size of the crystals were believed to give inorganic component the solubility needed for resorption of the bone by osteoclasts, which is compulsory for the continuous remodelling and repair of bone (Olszta *et al.*, 2007). The mineral phase of bone, as stiff and brittle reinforcement of the organic matrix, strongly influences the stiffness of bone. By comparing the moduli and fracture strain of the matrix component of bone (mineral: 135 GPa and 0.1%, collagen: 1 GPa and 10% respectively) with that of bone (10-25 GPa and 1- 1.5%), it can be seen that bone

achieves a compromise, making bone stiff (like mineral) but also tough (like collagen) (Wainwright *et al.*, 1982; Fratzl *et al.*, 2004).

1.1.3 Bone Structures

Bone exists mainly in two structural types, cortical bone and trabecular bone, on a macrostructure level depending on the location and function of the osseous tissue. Cortical bone and trabecular bone have the same matrix composition and ultra-structure, but they have different porosity and micro-structure which gives them different mechanical properties.

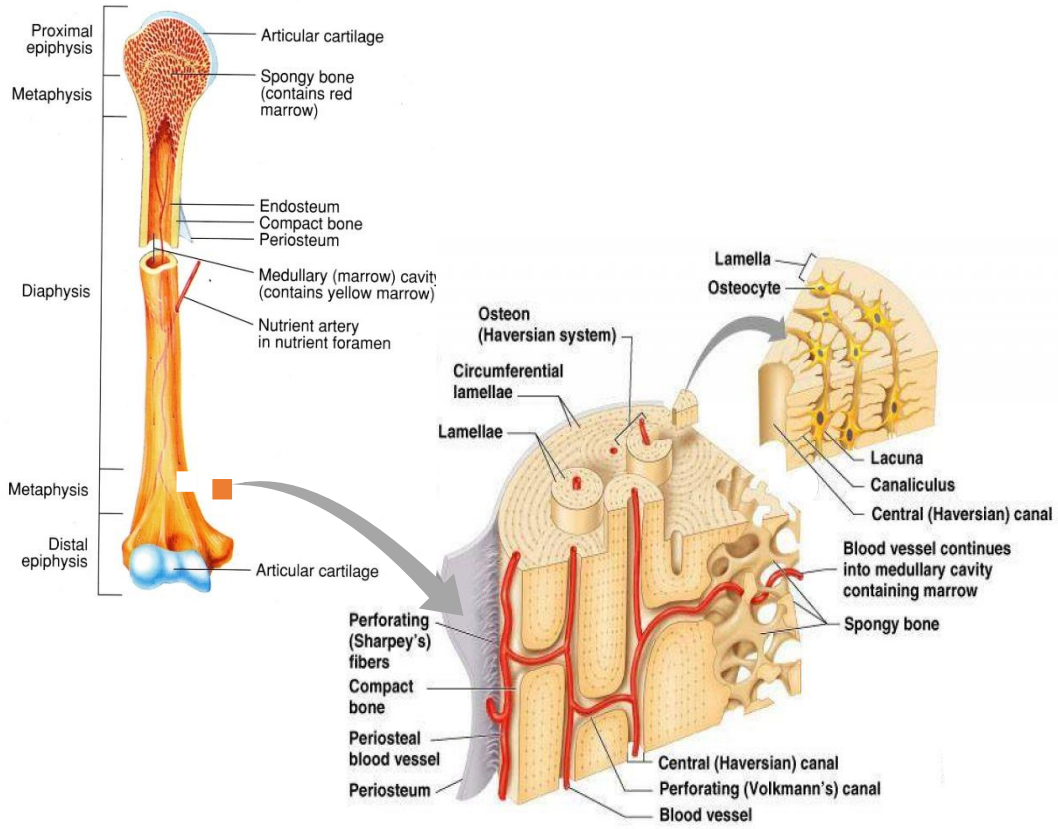

Figure 1-1 Bone structure diagram showing cortical osteons and trabeculae bone. (Marieb and Hoehn, 2007)

Cortical bone is dense (porosity 5-10%), constituting the diaphysis of adult long bones and the external surfaces of flat bones. It provides maximum resistance to torsion and bending. Cortical bone is composed of cortical osteons, also known as a Haversian system, which is the fundamental unit of compact bone (Figure 1-1). A

typical Haversian system is cylindrical in shape and runs parallel to the long axis of the diaphysis. At the centre of a Haversian system is the Haversian canal, which is surrounded by 4-20 concentric lamellae. The Haversian canal contains blood vessels, nerves, loose connective tissue and interstitial fluid. Each osteon connects with other osteons, the marrow cavity, and the periosteum through perpendicular or oblique canals namely the Volkmann's canal.

Cancellous bone or trabecular bone is the spongy, porous (porosity 50-90%) type of bone found at the ends of long bones, i.e epiphysis (Figure 1-1). The matrix forms struts called trabeculae which enclose a three-dimensional, interconnected porous space. The pores are filled with bone marrow which contains blood, and therefore the nutrients needed by the bone cells inside the trabeculae as well as on the surface of trabeculae. The trabecular macrostructure is typically oriented depends on the load distribution, which gives its anisotropy mechanical properties (Keaveny *et al.*, 2001).

1.2 Bone Mechanobiology

Cells in the human body are constantly exposed to a variety of mechanical forces through the actions of muscle forces, gravity, blood flow and other physical processes. It is well recognized that cells can sense and respond to mechanical forces, it can integrate and analyse this information and change its morphology, dynamics, behaviour and fate. The interactions between cells and mechanical forces are critical to the development and functionality of various tissues and organs of the body. For example, bone changes its shape, density and stiffness when its mechanical loading conditions are altered (Turner and Pavalko, 1998; Mullender *et al.*, 2004). Mechanobiology is a multi-disciplinary field that encompasses biology, biophysics and bioengineering, which focuses on how cells sense mechanical signals and translate mechanical signals into a cellular response.

1.2.1 Mechanically Responsive Bone Cells

The mechanical response of bone cells including osteocytes, osteoblasts, MSCs, osteoclasts, have all been documented. Osteocytes are pervasively distributed throughout bone and connected through a network of canaliculi, so they are well

placed to sense the magnitude and direction of mechanical force within the tissue (Rubin *et al.*, 2006). Osteocytes are indeed able to respond to a period of 6 min intermittent compressive load that varied sinusoidally from 0 to 600 N at 1 Hz *in vivo* as shown by increased number of cells displaying glucose 6-phosphate dehydrogenase (G6PD) activity (Skerry *et al.*, 1989). Forearm compression loading at 2.25 N, which represents a global strain of 2250 με for 100 cycles at 2 Hz, of mice showed the rapid activation of β-catenin through the early release of prostaglandin in osteocytes (Lara-Castillo *et al.*, 2015). It is likely that these signals that orchestrate bone homeostasis by regulating both bone-forming osteoblasts and bone-resorbing osteoclasts (Lanyon, 1992; Nakashima, 2011; Baron and Rawadi, 2007).

Many studies have demonstrated osteoblasts are mechanoresponsive both *in vitro* and *in vivo*. Osteoblasts respond to intermittent strain (majority of the cells on the plate received less than 5000 micro strain, three cycles per min for 1, 2, and 4 days) as shown by increased transcription and secretion of matrix proteins, including type I collagen, osteopontin, osteocalcin (Harter *et al.*, 1995). Osteoblastic like cells on polyurethane (PU) open cell foam BGS exposing to short bouts of cyclic compressive loading using a sine wave at 1 Hz, 5% strain also has a strong rise in mineralised matrix production (Sittichockechaiwut *et al.*, 2009). Osteoblasts in intact rat tibiae demonstrated the expression of cyclooxygenase (COX)-1 and COX-2 after subjected to 300 cycles of bending or sham loading at 2 Hz with an applied load of 65 N (Forwood *et al.*, 1998). Osteoblastic cell lines were observed to respond to cyclic strains (500 – 5000 με) at 1 Hz and produced nitric oxide (NO) and prostaglandin (Smalt *et al.*, 1997).

MSCs share the hematopoietic niche with blood stem cells and respond to the mechanical environment of the marrow by altering output of differentiated cell types (David et al., 2007; Sen et al., 2008). MSCs subjected to oscillatory fluid flow for 2 hours at 1 Hz with peak shear stress of 10 dyn/cm^2 exhibited increased proliferation and increased gene expression of osteogenic markers (Li *et al.*, 2004). It has been demonstrated that various forms of mechanical forces can regulate MSCs fate. For example, sinusoidal fluid flow for 1 hour at 1 Hz with peak shear stress of 10 dyn/cm^2 has been proved to upregulate the expression of transcription factors involved in

differentiation into osteogenic lineage (Arnsdorf *et al.*, 2009). While both sinusoidal compressive loading with 10% magnitude at 1 Hz for 4 hours and intermittent hydrostatic pressure of 0.1, 1 or 10 MPa at 1 Hz for 4 hour/day have been found to enhance chondrogenesis of MSCs as evidenced by increases in *sox9* expression, type II collagen and aggrecan gene expression (Huang, 2004; Miyanishi *et al.*, 2006).

Mechanical control of osteoclast function occurs typically through regulation of osteoclast recruitment, which is achieved by regulation of osteoclastogenesis via soluble signals. Rubin et.al have shown that dynamic mechanical strain can decrease osteoclast formation by around 50% in primary marrow cultures through a decrease in RANKL mRNA expression (Rubin *et al.*, 1999; Rubin *et al.*, 2002). Kim et al. also reported that oscillatory fluid flow induced decreased osteoclasts formation in a co-culture system of MSCs and osteoclast precursors by decreasing the RANKL/OPG mRNA ratio (Chi Hyun Kim *et al.*, 2006).

1.2.2 Candidate Mechanoreceptors

The ability of cells to sense the mechanical forces from the environment requires that mechanoreceptors either directly contact with the extracellular space, or that a mechanoreceptor can distinguish changes in a physical intermediary such as pressure or fluid shear on the plasma membrane (Thompson *et al.*, 2012).

1.2.2.1 Integrin

Integrins contain heterodimers of non-covalently associated α and β subunits. Each subunit has a large ECM domain, a single membrane-spanning helix, and usually a short unstructured cytoplasmic domain (Campbell and Humphries, 2011). On the ECM domain, integrins bind to a specific amino acid sequence (RGD ligand) found from ECM proteins like OPN and fibronectin. On the cytoplasmic domain, integrins associate with the peripheral domains of the cytoskeleton and a range of accessory proteins, including vinculin, paxillin, talin and α-actinin to form large, highly dynamic multiprotein complexes. The binding of extracellular ligands to integrins may initiate intracellular signalling events (outside-in signalling), while modification of intracellular domains also regulates the binding affinity of extracellular receptors (inside-out signalling).

Mechanical forces can alter the conformation of integrin-associated proteins, which could affect the exposure of binding sites, consequently modulating the recruitment of additional components. Integrins, together with a range of associated signalling proteins (for example kinases, phosphates), respond to mechanical forces by initiating a cascade of events. Such cascades include the activation of phosphorylation and G-protein mediated pathways, which result in local alterations in cytoskeletal dynamics. These, in turn, lead to alterations in cell shape, transcriptional regulation or other cellular behaviours (Geiger *et al.*, 2009).

Integrins have a primary role in sensing the environmental signals. Numerous studies that have been summarized in a series of reviews (Bershadsky *et al.*, 2006; Delon and Brown, 2007) show that integrin-based molecular complexes are involved in the sensing and processing of mechanical stimuli, such as fluid shear stress and substrate stretching. Integrins have been demonstrated as mechanoreceptors in a variety of cells including osteocytes, osteoblasts, mesenchymal stem cells and chondrocytes (Aderem, 1992; Mobasheri *et al.*, 2002; Klein-Nulend *et al.*, 2013; Liyue Liu *et al.*, 2012). For example, integrin β1 plays predominant roles in shear induced signalling and gene expression in osteoblast like cells (Lee *et al.*, 2008). *Integrin β1* play important roles in triggering the outside-in signalling and condensing precartilage during chondrogenesis of MSCs (Raghothaman *et al.*, 2014; Jin *et al.*, 2007; Zhang *et al.*, 2015). Mechanical stimulation and nanotopography led to significant upregulation of gene expression for *integrin α1*, as well as *runx2* in osteoblast like cells (Prodanov *et al.*, 2010).

1.2.2.2 Cell Cytoskeleton

The cell cytoskeleton is an interconnected network of filamentous polymers and regulatory proteins, by which cells can resist deformation, transport intracellular cargo and change shape during movement (Fletcher and Mullins, 2010). The interconnected and viscoelastic nature of the cytoskeleton together with its interaction with extracellular environment via receptor-ligand complexes is suited to the detection and transmission of mechanical signals to biochemical signals (Janmey, 1998). Fluid shear stress has been demonstrated to induce reorganization of actin filament into contractile stress fibres in osteoblasts (Pavalko *et al.*, 1998). While

inhibition of actin stress fibre development altered the response of osteoblasts to fluid shear stress (McGarry *et al.*, 2005).

1.2.2.3 Plasma Membrane Structure

The plasma membrane provides cells with a stable internal environment. Plasma membrane lipid rafts are known to have a significant role in the signalling facilitation system. Lipid rafts are highly organized and dynamic assemblies of cholesterol and sphingolipid. This structure creates a complex association of signalling molecules, including GTP-binding proteins, kinases, and calcium. The accumulation of these molecules in one location gives lipid rafts the capability to spread signals to downstream targets rapidly and specifically (Rizzo *et al.*, 1998). Lipid rafts have been demonstrated to be essential for responding to hydrostatic pressure and fluid shear stress and activation of ERK1/2 in osteoblasts (Ferraro *et al.*, 2004). Apart from lipid rafts, mechanical forces also have other effects on the plasma membrane, such as generating strong strain and inducing conformational changes, thus altering protein binding and cell structure.

1.2.2.4 Cell-Cell Connections

Cadherins are a family of integral membrane glycoproteins, composed of a long extracellular domain, a single-pass transmembrane domain, and a small, intracellular tail. A widespread view for many years was that cadherin-based adhesion involved a single binding interface between the cadherin extracellular domains. This adhesive connection intrinsically conveys mechanical information to cells by resisting mechanical forces. The intracellular domain anchors the cadherins to the cytoskeleton by associating with a variety of protein complexes, including β-catenin, α-catenin and vinculin. Therefore, cadherins act as mechanoreceptor that senses fluctuations in tensile force owing to dynamic cytoskeletal deformation. In osteoblasts, the intracellular domain of cadherins associates with β-catenin. Fluid shear stress decreased this association, which result in an increase in the cytoplasmic pool of β-catenin. The increase in unbound β-catenin in conjunction with the activation of glycogen synthase kinase 3 beta (GSK3β) induced by shear stress has been proposed as a potential upstream regulator of β-catenin nuclear translocation (Norvell *et al.*, 2004).

Gap junctions are membrane-spanning channels, composed of connexin subunits, that allow rapid and direct diffusion of small molecules (< 1 kDa), such as ionized calcium, from the one cell to another cell (Genetos *et al.*, 2007). Gap junction intercellular communication has been demonstrated as a mechanoreceptor in response to fluid flow (Alford *et al.*, 2003).

1.2.2.5 Primary Cilia

Primary cilia are microtubule-based organelles that project from the cell surface. As the cilia bends in response to fluid flow, increased tension on the membrane result in opening of mechanosensitive ion channels, such as an influx of intracellular Ca^{2+}, causing membrane depolarization and activation of auditory nerve fibres (Ingber, 2006). There is evidence that primary cilia deflection is required for fluid shear stress induced osteogenic responses (Malone *et al.*, 2007). Damage or removal of primary cilia of osteoblasts have been shown to inhibit oscillatory fluid flow(OFF)-induced PGE_2 release and mineral deposition (Delaine-Smith *et al.*, 2014).

1.2.2.6 Ion Channels

Bone cells express several different ion channels involved in mechanosensitive pathways, including stretch-active cation channels, voltage-sensitive calcium channels (VSCC), and transient receptor potential (TRP) channels. The application of different forms of mechanical forces have been shown to activate different mechanosensitive ion channels. Oscillatory fluid flow was shown to induce intracellular Ca^{2+} mobilization via the Inositol trisphosphate (IP3) pathway and the L-type VSCC (You *et al.*, 2001). Membrane stretch induced intracellular Ca^{2+} mobilization via T-type VSCC, which regulates downstream adenosine triphosphate (ATP) release and ERK1/2 activation (Thompson *et al.*, 2011). Fluid shear stress increased intracellular Ca^{2+} mobilization via mechanosensitive cation-selective channel and L-type VSCC, which together with a resultant release of ATP was found to activate the ERK1/2 phosphorylation (Liu *et al.*, 2008).

1.2.3 Intracellular Signalling Pathways

1.2.3.1 Kinase Activation

Mitogen activated protein kinase (MAPK) is a family of serine/threonine protein kinases including Extracellular Signal-regulated Kinase (ERK1/2), c-Jun N-terminal Kinase (JNK) and p38 kinase. Many studies have shown that ERK1/2 is activated by fluid shear in both osteoblasts and MSCs (Liu *et al.*, 2008; Glossop and Cartmell, 2009). The MAPK members have been demonstrated to be essential in cell growth, differentiation and apoptosis. For example, the activation of ERK1/2 is necessary for mechanical strain induced positive bone remodelling by inhibiting osteoclastic potential of bone marrow stromal cells (Rubin *et al.*, 2002).

Focal adhesion kinase (FAK) is a non-receptor cytoplasmic protein tyrosine kinase (PTK), which is concentrated near focal adhesions. FAK interacts with various signalling proteins, including Src family PTKs, phosphatidylinositol 3-kinases (PI3K), Shc, Grb2 and paxillin. This enables FAK to function within a network of integrin-stimulated signalling pathways resulting in the activation of downstream targets such as the MAPK cascades (Schlaepfer *et al.*, 1999). The fluid flow induced activation of FAK has been demonstrated to be critical for activation of ERK1/2 and JNK, and for the shear stress induced expression of c-fos, COX-2, OPN, and PGE2 release (Young *et al.*, 2009; Wang *et al.*, 2011).

1.2.3.2 β-Catenin

β-catenin plays a significant role in bone mass regulation (Case and Rubin, 2010). Studies have shown that loading activates the β-catenin signalling pathway both *in vitro* (Sunters *et al.*, 2010; Case *et al.*, 2011) and *in vivo* (Robinson *et al.*, 2006; Lara-Castillo *et al.*, 2015). Researchers have demonstrated that activation of β-catenin in response to load through the prostaglandin, and protein kinase (Akt) signalling pathways (Kamel *et al.*, 2010). It has been shown that uniform biaxial strain through focal adhesion induced mammalian target of rapamycin complex 2 (mTORC2) activation and phosphorylation of Akt, which caused the inactivation of GSK3β (Case *et al.*, 2011). The inactivation of GSK3β then resulted in the preservation of β-catenin by protecting it from degradation (Sen *et al.*, 2009). Preserved β-catenin is believed

to target genes like runt-related transcription factor 2 (*runx2*), osterix (*osx*) and *oc*, to promote osteoblast differentiation of MSCs (Day *et al.*, 2005).

1.2.3.3 GTPases

GTPases are a large family of enzymes that bind and hydrolyse guanosine triphosphate (GTP), in turn switching on a variety of physiological processes. Studies have indicated that Rho family of GTPases were activated in response to oscillatory fluid flow (Arnsdorf *et al.*, 2009), which in turn regulated cell shape via its effects on ROCK-mediated cytoskeletal tension, and guiding MSCs differentiation into the osteogenic lineage (McBeath *et al.*, 2004; Xu *et al.*, 2012).

1.2.3.4 Calcium Signalling

A rapid increase in intracellular calcium ($[Ca^{2+}]i$) levels is the earliest detected response in mechanically stimulated bone cells (Rawlinson *et al.*, 1996). Intracellular Ca^{2+} mobilization was initiated by variety of mechanical forces, including membrane stretch (Walker *et al.*, 2000), oscillatory flow (You *et al.*, 2001) and steady flow (Liu *et al.*, 2008). Intracellular Ca^{2+} mobilization subsequently initiated downstream signalling including ATP, prostaglandin (Genetos *et al.*, 2005), MAPK (You *et al.*, 2001; Katz *et al.*, 2006), c-fos, COX-2, (Chen *et al.*, 2000) and matrix protein production (Walker *et al.*, 2000). For example, it has been demonstrated that intracellular Ca^{2+} mobilization through the L-type VSCC in response to shear stress was compulsory for ATP release, which in turn mediated prostaglandin release (Genetos *et al.*, 2005).

Bone mechanobiology is a complicated area. A significant amount of research has been conducted to investigate bone mechanical signalling pathways. Bone grafts could potentially function through interacting with local mechanical environment, however, aside from the complexity of deconvolution of the multiple pathways involved, there are ethical considerations and high costs to study *in vivo*. Therefore, there is a clear need to develop an *in vitro* system to study mechano-biologic responses to changes in BGS structure and chemistry.

1.3 Bone Formation and Bone Healing

Intramembranous and endochondral ossification are two mechanisms through which bone formation occurs. Both processes start with stem cell proliferation and

condensation. During intramembranous ossification, condensed MSCs differentiate directly into osteoblasts and secrete organic matrix, after which the crystal apatite deposits. This process mainly forms flat bones, like craniofacial skeleton. Long bones are formed by endochondral ossification, during which MSCs first differentiate into chondrocytes and form the initial cartilage templates. Chondrocytes in the centre of these cartilage templates further differentiate into hypertrophic chondrocytes and form cartilage. The hypertrophic cartilage is then invaded by blood vessels and eventually replaced by bone and marrow.

Bone healing is a regenerative process that is initiated in response to injury. The process of bone healing can be divided into four overlapping stages: hematoma formation and inflammation, soft callus formation, hard callus formation, and bone remodelling (Figure 1-2).

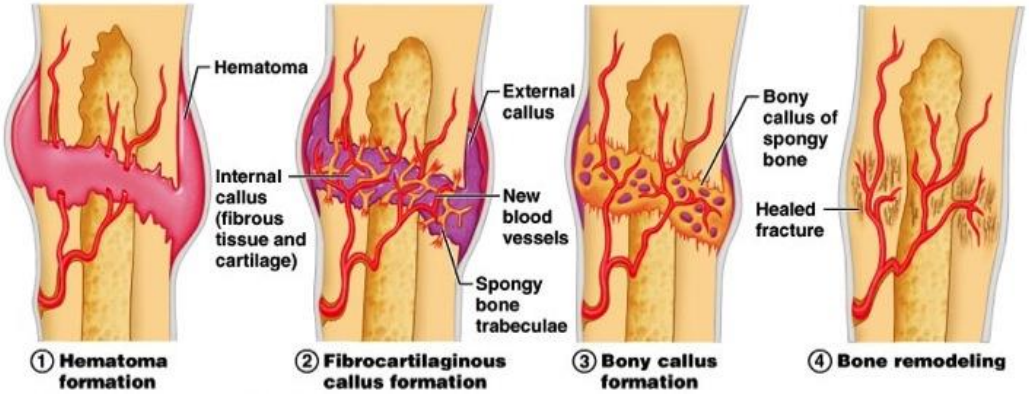

Figure 1-2 Diagram of bone healing process.

Following damage to the bone, disruption of local soft tissue integrity, blood vessels and marrow structure leads to the formation of a hematoma, which encloses the fracture area. Hematoma acts as the scaffold in which a callous is developed in the later stages of bone repair. Removal of the hematoma significantly attenuates bone repair (Grundnes and Reikerås, 1993). The correct inflammation response is also essential for bone repair. The inflammatory response is associated with the secretion of several cytokines and growth factors, including interleukin-1 (IL-1), interleukin-6 (IL-6), tumour necrosis factor-alpha (TNF-α), transforming growth factor-beta (TGF-β), platelet-derived growth factor (PDGF), vascular endothelial growth factor (VEGF)

and bone morphogenetic proteins (BMPs) (Mandracchia *et al.*, 2001; Gerstenfeld, Cullinane, *et al.*, 2003; Barnes *et al.*, 1999; Cho *et al.*, 2002). These cytokines and growth factors have important roles in bone healing. For example, TNF-α promotes the recruitment of mesenchymal stem cells (MSCs) and osteoclasts, and plays a regulatory role in bone healing (Gerstenfeld, Cho, *et al.*, 2003). VEGF promotes angiogenesis, which is crucial for blood supply to the injury site and bone healing (Street *et al.*, 2002).

The soft (cartilaginous) callus formation is an endochondral bone formation process. Release of the correct cytokines and growth factors aid the recruitment of mesenchymal stem cells (MSCs) from periosteum, endosteum, bone marrow and adjacent soft tissues, proliferation of MSCs and the their differentiation into chondrocytes (Bigham-Sadegh and Oryan, 2015). Chondrocytes proliferate and synthesise cartilaginous matrix and then undergo hypertrophy, mineralizing the cartilaginous matrix before undergoing apoptosis (Schindeler *et al.*, 2008). This cartilaginous callus provides initial stabilization of the fracture site. Meanwhile, the periosteum undergoes intramembranous ossification to create an external callus.

Hard callus formation represents the active period of osteogenesis process. The formation of new vascular structure is critical for formation of the hard callus, which increases oxygen tension in the local region necessary for osteoblasts differentiation (Schindeler *et al.*, 2008). Osteoblasts have prominent levels of activity at this stage and form mineralized bone matrix. Soft cartilaginous callus is gradually replaced by new formed hard callus of woven bone, which is typically irregular and under-remodelled.

Bone remodelling begins with an initiation phase that includes recruitment of osteoclast precursors, osteoclast differentiation, formation of sealing zones beneath osteoclasts and bone tissue resorption in these zones. After the resorption phase is completed, osteoclasts undergo apoptosis whilst osteoblasts are recruited and begin to lay down new bone.

Mechanical factors have been demonstrated to modulate bone healing. For example, in a controlled metaphyseal fracture model in sheep, low interfragmentary strain led

to intramembranous bone formation, whereas higher strains additionally provoked endochondral ossification (Claes *et al.*, 2011). The difference between remodelling in cortical bone and cancellous bone is that in cortical bone osteoclasts move along the length of a Haversian canal, progressively eroding away the whole osteon, whilst in cancellous bone, osteoclasts begin resorption at a designated surface of a piece of trabecular bone (Burr *et al.*, 1985; Huiskes *et al.*, 2000). Apart from fracture healing, healthy bone is also continuously remodelled, shaped and repaired, to maintain its structural integrity, strength and to fulfil its role in mineral homeostasis (Kular *et al.*, 2012). The presence of microcracks in bone and the osteocyte apoptosis in these areas is currently considered a crucial driver of the remodelling response (Cardoso *et al.*, 2009). Mechanical force is a key regulator of bone remodelling and therefore bone architecture (Carter, 1984; Lanyon, 1993; Jacobs *et al.*, 2010).

Spontaneous fracture healing is the natural way for bone to regenerate. However, for critical-sized defects, bone fails to self-repair which leads to musculoskeletal disorders. This is the situation where surgical intervention is required via application of graft materials or metal implants.

1.4 Bone Grafting and Evaluation of Synthetic BGS Performance

Bone grafting, a surgical procedure, involves transplantation of a bone tissue from patient's own body, bone tissue from another individual or species, a natural substitute or synthetic substitute to augment and regenerate bones that are lost due to a disease or injury. Although autograft accounts for the largest proportion of the global BGS market to date, its requirement of double incision and the post-surgery pain on both sites have drawn increasing interests of scientists and manufactures in synthetic BGS. The world market of BGS is expected to reach over $5031 million by the end of 2027, and this market is projected to grow at a compound annual growth rate of ~ 6.52% during the period of 2017 – 2027 due to aging population (IndustryToday, 2017). There are several types of BGS, including autologous graft, allogenous grafts and synthetic bone graft.

Autologous grafts, or autografts are bones harvested from the patient and transplanted to injured site. It is considered as the "gold standard" by clinicians and

accounts for the largest market of the global BGS so far. The advantage of autografts includes minimal risk of immunogenic response, osteoinductive and osteoconductive abilities (Cypher and Grossman, 1996; Giannoudis *et al.*, 2005). However, autografts can result in donor site morbidity (Silber *et al.*, 2003) and their availability is limited by the limited volume of bone that can be harvested from the donor site. Although autograft accounts for the largest market of the global BGS so far, its requirement of double incision and the post-surgery pain on both sites have drawn increasing interests of scientists and manufactures in synthetic BGS.

Allogenous grafts, or allografts, represents bone harvested from one individual and transplanted into another individual of the same species. Xenografts represents bone harvested from one individual and transplanted into another individual of a distinct species. Although allografts and xenografts are natural bone tissue, having risk of immunogenic response together with reduced osteoinductive ability make them less attractive choices.

Synthetic BGS have gained increasing interest in bone repair. They are available in different forms and materials, including calcium phosphates (Gauthier *et al.*, 1998), Bioglass (Jones, 2015), polymers (Thomson *et al.*, 1996) and their combination (Sang-Soo Kim *et al.*, 2006). The ideal BGS must satisfy a series of strict demands: appropriate surface chemistries encouraging cell adhesion, proliferation and differentiation; appropriate levels and sizes of porosity allow for cell migration; promoting biological processes such as the production of extracellular matrix and vascularisation; good mechanical properties; and a degradation rate that matches the regeneration rate of natural tissue (Lannutti *et al.*, 2007).

Porous hydroxyapatite (HA) has a close resemblance to the composition of bone mineral and has been suggested as promising BGS (Hing *et al.*, 2002). Silicon is crucial for bone growth and development because collagen and proteoglycans are crosslinked by it, and silicon has also been show to act in the bone mineralisation process (Pietak *et al.*, 2007). The incorporation of silicon into HA BGS induced several changes: release of soluble silica species, increased negative surface charge and higher solubility (Porter *et al.*, 2003; Hing *et al.*, 2006). These changes are important to enhance the osteoconductivity of hydroxyapatite by improving cell adhesion,

because the adhesion is highly dependent on composition, microstructure, wettability and surface charge of the material. Silicate substituted hydroxyapatite (SiHA) has demonstrated earlier organised collagen fibrils formation and more apatite crystallites at the bone-implant surface than pure HA *in vivo*, suggesting the promoted bone remodelling process (Porter *et al.*, 2004). Ovine defect model also showed significantly higher percentage of bone ingrowth and bone coverage for SiHA than pure HA, indicating the incorporation of silicon highly improves the bioactivity of hydroxyapatite (Patel *et al.*, 2005). Experiment results validated the response of healing response to Si level and suggest the optimal bone healing is obtained when SiHA is substituted with 0.8 wt% Si (Hing *et al.*, 2006).

Pore structure (such as macro-pore size, macro-porosity, interconnectivity of macro-pores, micro-porosity (the volume fraction of micro-pores in the struts of porous BGS)) has been demonstrated to have a strong impact on bone ingrowth *in vivo* (Mastrogiacomo *et al.*, 2006; Hing *et al.*, 2004; Hing *et al.*, 2005; Campion *et al.*, 2011; Coathup *et al.*, 2012). For example, *in vivo* study of hydroxyapatite (HA) BGS with different macro-pore structure has demonstrated that macro-porosity and pore interconnection of the BGS influenced the amount of deposited bone and kinetics of bone formation (Mastrogiacomo *et al.*, 2006). Increased levels of micro-porosity in HA BGS was found to facilitate earlier neovascularization (Hing *et al.*, 2004), thicker trabeculae of new bone (Hing *et al.*, 2005), and a greater volume of bone formation (Coathup *et al.*, 2012) *in vivo*. One explanation that micro-pore structure promoted BGS performance is micro-pores allow cellular infiltration, which increases biological fixation and thereby results in improved mechanical interlock between the cells and the surface of the substrate (Bignon *et al.*, 2003; Annaz *et al.*, 2004a). However, many *in vitro* studies were carried on BGS discs under static condition (Marra *et al.*, 1999; Liao *et al.*, 2004; Ghorbani *et al.*, 2015). Under these conditions, some BGS still perform quite good and it may be possible to screen for variation in chemistry or structure. But it is unknown that how/even if the cellular response to a BGS disc under static condition *in vitro* translates to the bone formation response to porous BGS *in vivo*.

1.4.1 Cells Used in Evaluation of Synthetic BGS Performance

Osteoblasts are an obvious choice for evaluation of synthetic BGS performance, because of their capacity to synthesise bone-specific proteins and deposit mineralized matrix. Many studies have used osteoblasts combined with various of BGS and demonstrated bone nodule formation *in vitro*, new bone formation *in vivo* and favourable healing efficacy (Xynos *et al.*, 2000; Wang *et al.*, 2014). However, the disadvantage associated with osteoblasts is that they have relatively limited proliferative capacity and short lifespans. Immortalized osteoblast cell lines, like MG63, SaOs2, MC3T3-E1, are often used in evaluating the performance of BGS because of their ease of access and repeatability. The osteoblast cell lines have some features of osteoblasts, however it is clear that these cells do not fully reflect the behaviour of primary osteoblasts and must be used with caution. For example, by characterizing osteosarcoma cell line MG-63, Saos-2 in comparison to primary human osteoblasts, Pautke found that no ALP activity could be detected in MG-63 cells (Pautke *et al.*, 2004). Czekanska also observed that the maximum level of ALP activity of MG-63 by day 28, was ~ 26 fold lower compared to human osteoblasts at the same point, while both SaOs2 and MG-63 cells demonstrated a higher proliferation rate than human osteoblasts (Czekanska *et al.*, 2014).

MSCs have been considered as attractive choice for evaluating BGS performance because of their high proliferation and multipotent differentiation capability. Bone repair process *in vivo* is initiated by MSCs recruitment, differentiation into chondrocytes and cartilaginous intermediate formation (Phinney and Prockop, 2007). The capacity of MSCs to repair skeletal defects has been proven in animal tests, and subsequently in human patients with osteogenesis imperfecta (Horwitz *et al.*, 2002). Minimal criteria for the characterization of MSCs were defined by the International Society of Cellular Therapy position statement: plastic-adherent; having the potential to differentiate into chondrogenic, osteogenic and adipogenic lineage *in vitro*; positive expression for CD105, CD73, CD90 surface markers; and negative expression for CD14, CD19, CD34, CD45 and HLA-DR surface markers (Dominici *et al.*, 2006). MSCs reside in a diverse host of tissues throughout the adult organism, including bone marrow, adipose tissue, periosteum, skeletal muscle, synovium membrane,

blood and dental pulp. Currently, bone marrow derived MSCs and adipose tissue derived MSCs are considered as the most accessible source of MSCs. Their bone regenerative capacity has been demonstrated *in vivo* (Cowan *et al.*, 2004; Karageorgiou and Kaplan, 2005).

1.5 Bioreactors

Mechanical forces are known to affect cellular behaviour, including morphology, proliferation, differentiation into specific lineages, and functions. Therefore, mechanical forces play important roles in bone healing (Lanyon and Rubin, 1984; Lanyon, 1993; Robling *et al.*, 2002; Boerckel *et al.*, 2012). However, studies of *in vitro* BGS efficacy evaluation and mechanism investigation have been traditionally carried out in a static environment which does not represent the mechanical environment that cells are exposed to *in vivo*. Researchers have designed a variety of bioreactors to apply mechanical force while evaluating the performance of BGS. The physiologic relevant mechanical forces are usually divided into three main categories: shear stress, compressive stress and strain. Several researchers hypothesized that flow of interstitial fluid is the most probable way of informing bone cells about mechanical loading (Knothe Tate *et al.*, 1998; Sikavitsas *et al.*, 2001). There are mainly three types of bioreactors: spinner flask bioreactor, rotating wall bioreactor and perfusion bioreactor that are used to apply mechanical forces to cell cultured on BGS.

1.5.1 Spinner Flask Bioreactor

Spinner flask bioreactor composes of a media reservoir, a stir bar or other stirring mechanism that stirs the media, side arms through which BGS and media can be removed and usually gas exchange system. BGS are typically suspended from the top of the flask using needle like apparatus. In spinner flask bioreactor, convective transport of nutrients to the BGS brings increased concentrations of oxygen to the BGS compared to diffusional transport of nutrients in static culture. Cells on the surface of the BGS are also exposed to shear stress which could enhance osteogenic differentiation.

One of the earliest studies using spinner flask reported that spinner flask demonstrated a 60% increased proliferation after 7 days, 2.4 times higher alkaline

phosphatase (ALP) activity after 14 days, 3.5 times OC secretion after 18 days of rat marrow stromal osteoblasts seeded on poly (D, L-lactic-co-glycolic acid) (PLGA) porous BGS compared to static culture. However cell growth and mineralization were limited to the outside of the BGS because of limited nutrient transport in internal BGS (Sikavitsas *et al.*, 2002). Another study also observed when human bone marrow MSCs were cultured on collagen BGS for 5 weeks in spinner flask, bone formation only happens in the peripheral region of the BGS (Meinel *et al.*, 2004). Research has demonstrated that spinner flask could reveal the influence of BGS structure on cellular behaviour. For example, 200 μm pore coralline hydroxyapatite exhibited faster rate of osteogenic differentiation than did the 500 μm pore, whereas 500 μm pore coralline hydroxyapatite BGS exhibited increased proliferation rate in spinner flask (Mygind *et al.*, 2007). A study reported that the extent of proliferation and osteogenic differentiation become higher at increased stir rate, which indicated increased shear stress affects the osteoblastic differentiation of rat MSCs in the study (Ichinohe *et al.*, 2008). Human adipose derived stem cells (ADSCs) cultured on cancellous BGS in spinner flask bioreactors showed enhanced osteogenic differentiation compared to static environment (Song *et al.*, 2014). Human ADSCs combined with cartilage biomimetic BGS, chitosan/gelatin hybrid hydrogel, in spinner flask bioreactors showed enhanced proliferation and chondrogenic differentiation compared to static environment (Song *et al.*, 2015).

1.5.2 Rotating Wall Bioreactor

Rotating wall bioreactors are composed of two concentric cylinders, an inner cylinder that is stationary and allows gas exchange and an outer cylinder that rotates. The space between the two cylinders is filled with culture media which hosts cell seeded BGS. BGS can move freely in the media, cells on the surface of the BGS are exposed to shear stress caused by the centrifugal forces of the outer cylinder balance with gravity (Godara *et al.*, 2008). It was first designed to aid high-density, three-dimensional cell cultures (Schwarz *et al.*, 1992). Many studies have used rotating wall bioreactor and achieved promoted cell behaviour *in vitro*. For example, osteoblasts in a rotating wall bioreactor have been reported to achieve rapid proliferation, increased ALP activity and differentiation (Song *et al.*, 2006). Co-culture MSCs with

MSC-derived endothelial cells (ECs) within a porous BGS using a rotating wall bioreactor generated bone tissue containing vascular-like structures (Nishi *et al.*, 2013). Primary articular chondrocytes cultured in rotating wall bioreactor were able to overcome the limited proliferation and their tendency to dedifferentiate in static culture (Mellor *et al.*, 2014). Other studies have showed rotating wall bioreactors to be relatively less effective. When rat primary calvarial cells were cultured on the BGS in rotating wall bioreactor for 7 days, osteoblasts showed significantly increased mineralized matrix formation, ALP activity, *oc* expression and *opn* expression but no influence on cell proliferation (Yu *et al.*, 2004). Rotating wall bioreactor culture yielded similar cell density, but had the lowest levels of ALP activity whereas those cultured in the perfusion system or in a spinner flask demonstrated enhanced ALP activity compared to those cultured statically (Goldstein *et al.*, 2001). Human mesenchymal stem cells and rat marrow stromal cells were also observed to have lower ALP activity and OC secretion in rotating wall bioreactor than in spinner flask bioreactor and static condition (Sikavitsas *et al.*, 2002; Tzu Wei Wang *et al.*, 2009). The limited cell proliferation in rotating wall bioreactors compared with spinner flask bioreactor could be due to collisions of BGS with the wall of bioreactor while moving or the low shear stresses on cells in the bioreactor.

1.5.3 Perfusion Bioreactor

Spinner flask bioreactor and rotating wall bioreactor have shown effectiveness in some instances; however, perfusion bioreactors have shown greater positive effects on osteoblastic differentiation due to direct perfusion of nutrients through BGS and ability to stimulate the cells with greater shear stresses (Yeatts and Fisher, 2011). Perfusion bioreactors typically comprises of a cartridge which houses the cell seeded BGS, a medium reservoir, a tubing system and a pump. Cartridge must be carefully designed to tightly fit the BGS which must be highly porous, so that medium can be perfused directly through the pores of the BGS, instead of around the BGS. Many perfusion bioreactors have been developed and used in *in vitro* studies (Table 1-1).

Table 1-1 showed that in a critical evaluation of 39 papers, it was clear that perfusion culture could promote cell expansion, differentiation to osteogenic phenotype, and mineralized matrix compared to static culture. Much of the work has been completed

to investigate how BGS materials, cell type, flow rate and flow mode used in a perfusion bioreactor system influence the outcome of cell expansion and development of phenotype. 48.7% of the studies (19/39) used polymer BGS and 30.8% of the studies (12/39) used calcium phosphate BGS in perfusion bioreactor. Apart from polymer and calcium phosphate, researchers also used titanium fibre mesh, composite and decellularized trabecular BGS in perfusion bioreactor.

Mainly MSCs or osteoblasts have been used in perfusion bioreactor studies. Most (66.7%) of the studies (26/39) used MSCs from different species, like human, rat and sheep in perfusion bioreactor. Osteoblasts or osteoblastic cells (11/39) were the second favourite choice (28.2%) of cells in perfusion bioreactor. Apart from MSCs and osteoblasts, there was one study that used human adipose stem cells and one study that used stromal vascular fraction cells in perfusion bioreactor.

Most of the perfusion rate (38/39) was from 0.01 ml/min to 4 ml/min, apart from one study that used 10 ml/min. However, shear stress is not only depending on flow rate, but also other parameters like BGS pore size, BGS diameter and BGS porosity. Flow rate should be used with caution when comparing the shear stress across different studies. Flow rate was demonstrated to have a dose effect on ALP activity, cell number and mineralized matrix, when rat MSCs were cultured on titanium fibre mesh BGS (Bancroft *et al.*, 2002). When hMSCs on decellularized bovine trabecular bone were cultured in perfusion bioreactor at 400 µm/s flow velocity, radically increased cell numbers and the amount of bone proteins and minerals compared to flow velocity of 100 µm/s (Grayson *et al.*, 2008). hMSCs on polylactic glycolic acid (PLGA) BGS showed induced osteogenic differentiation at 0.5 ml/min but not at 0.2 ml/min (Yang *et al.*, 2010).

Apart from flow rate, studies have compared the different influence of steady flow and dynamic flow on osteogenic differentiation. Oscillatory perfusion has demonstrated increased ALP activity of MC3T3-E1 (mouse osteoblastic cells) on β-TCP ceramic BGS compared with continuous unidirectional flow. Similarly, when MC3T3-E1 osteoblastic cells on collagen-glycosaminoglycan were subjected to continuous unidirectional flow, pulsatile flow or oscillatory flow, although all three types of flow configuration demonstrated increased cyclooxygenase-2 (COX-2),

prostaglandin E2 (PGE2) expression and OPN production, dynamic flow was found to be more stimulatory than continuous unidirectional flow (Jaasma and O'Brien, 2008).

Studies have demonstrated that perfusion bioreactor is a feasible *in vitro* system to mechanically stimulate cells cultured on 3D BGS, and cells are responsive to shear stress generated by flow in a perfusion bioreactor. However, studies focusing on cellular responses to BGS parameters such as porosity, pore size, stiffness were still conducted in a static environment which does not represent the mechanical environment that cells are exposed to *in vivo.* Therefore, the current study intends to investigate the cellular responses to SiHA BGS structure in a mechanical environment using perfusion bioreactor. Based on perfusion configurations from literatures, MSCs or osteoblast, and perfusion rate between 0.01 ml/min and 4 ml/min was used.

Table 1-1 *In vitro* studies utilizing perfusion bioreactors.

Reference	**BGS types**	**Cell types**	**Flow regimen**	**Observation (All observations were compared with static culture)**
(Goldstein *et al.*, 2001)	Poly (DL-lactic-co-glycolic acid) (PLGA) foam discs	Rat osteoblastic cells from marrow issue	Continuous unidirectional flow, 0.03 ml/s (0.34 dyn/cm^2)	No difference in cell number and OC activity; higher ALP activity
(Bancroft *et al.*, 2002)	Titanium fibre mesh	Rat MSCs	continuous unidirectional flow, 0.3, 1, 3 ml/min (< 1 dyn/cm^2)	Increased mineralized matrix, ALP activity, cell number; dose effect
(Sikavitsas *et al.*, 2003)	Titanium fibre mesh	Rat MSCs	Continuous unidirectional flow, 0.3 ml/min, culture medium has different viscosity	Increased mineralized matrix, ALP activity; dose effect
(Cartmell *et al.*, 2003)	Hydrated human trabecular bone	MC3T3-E1 osteoblastic cells	Continuous unidirectional flow, 0.01, 0.1, 0.2, and 1.0 mL/min	Increased cell proliferation at 0.01 mL/min; increased *runx2*, *oc*, *alp* expression at 0.2 ml/min

Table 1-1 cont.

Reference	**BGS types**	**Cell types**	**Flow regimen**	**Observation** **(All observations were compared with static culture)**
(Meinel *et al.*, 2004)	Collagen discs	hMSCs	Continuous unidirectional flow, 0.2 ml/min (35 µm/s)	Higher ALP activity, bone rods formation in the direction of flow distributed throughout the construct
(Wang *et al.*, 2003)	β-tricalcium phosphate	Rat MSCs	Continuous unidirectional flow, 2 ml/h	Higher ALP activity, OC content both *in vitro* and *in vivo*, increased bone formation *in vivo*
(Sikavitsas *et al.*, 2005)	Poly (L-lactic acid) (PLLA)	Rat MSCs	Continuous unidirectional flow, 0.6 ml/min	Increased matrix deposition, proliferation, ALP activity
(Fassina *et al.*, 2005)	Polyurethane foam	SAOS-2 osteoblastic cells	Continuous unidirectional flow, 3 ml/min	Increased proliferation, OPN, OC, decorin and COL I secretion, calcium deposition

Table 1-1 cont.

Reference	**BGS types**	**Cell types**	**Flow regimen**	**Observation (All observations were compared with static culture)**
(Vance *et al.*, 2005)	Silicon-stabilized tricalcium phosphate and hydroxyapatite	MC3T3-E1 osteoblastic cells	Continuous unidirectional flow, 0.025 ml/min; Oscillatory flow, 4 ml/min, 1 Hz, 30 min once daily	Enhanced PGE2 release; oscillatory flow further enhanced PGE2 release
(Zhao and Ma, 2005)	Poly(ethylene-terepthalate) (PET)	hMSCs	Continuous unidirectional flow, 0.2 ml/min	Higher cell number, more even cell distribution, maintained multipotential differentiation of hMSCs
(Porter *et al.*, 2007)	Polycaprolactone (PCL)	Rat MSCs	Continuous unidirectional flow, 0.2 ml/min	Increased mineralized matrix
(Manuela E Gomes *et al.*, 2006)	Corn starch and polycaprolactone (PCL)	Rat MSCs	Continuous unidirectional flow, 0.3 ml/min, 1 ml/min	Enhanced cell differentiation

Table 1-1 cont.

Reference	**BGS types**	**Cell types**	**Flow regimen**	**Observation (All observations were compared with static culture)**
(Janssen *et al.*, 2006)	Biphasic calcium phosphate (OsSatura™, IsoTis, The Netherlands), 10 cc of granules Ø 2 ~ 6 mm	Goat MSCs	Continuous unidirectional flow, 4 ml/min	Homogeneous and viable cell layer, dense layer of extracellular matrix, abundant de novo bone formation after 6 weeks implantation
(Holtorf, Jansen, *et al.*, 2005)	Titanium fibre mesh	Rat MSCs	Continuous unidirectional flow, 0.3 ml/min first day, then 1 ml/min	Increased mineralization, cellularity, ALP activity, OPN secretion even in the absence of dexamethasone; further enhanced by dexamethasone
(Holtorf, Sheffield, *et al.*, 2005)	60% hydroxyapatite/40% β-tricalcium phosphate	Rat MSCs	Continuous unidirectional flow, 0.3 ml/min first day, then 1 ml/min	Increased cell number, ALP activity, OPN secretion

Table 1-1 cont.

Reference	**BGS types**	**Cell types**	**Flow regimen**	**Observation** **(All observations were compared with static culture)**
(Zhao *et al.*, 2007)	Poly (ethylene terepthalate) (PET)	hMSCs	Continuous unidirectional flow, 0.1 ml/min, 1.5 ml/min	1.4 times higher proliferation, more fibronectin secretion at 0.1 ml/min; upregulated ALP activity and calcium matrix deposition at 1.5 ml/min
(Grayson *et al.*, 2008)	Decellularized bovine trabecular bone	hMSCs	Continuous unidirectional flow, 100 µm/s, 400 µm/s	Flow at 400 µm/s radically improved cell numbers, cell distribution, bone minerals and proteins
(Jaasma and O'Brien, 2008)	Collagen-glycosaminoglycan	MC3T3-E1 osteoblastic cells	Continuous unidirectional flow, 1 mL/min (~235 µm/s), 0.05 ml/min (~11.8 µm/s); Pulsatile flow, 0 - 1.0 mL/min (peak-to-peak), 2 Hz; Oscillatory flow, 1 mL/min (peak-to-peak), 1 Hz	All types of flow showed increased COX-2 expression, PGE2 expression, OPN production; dynamic fluid flow was more stimulatory than steady fluid flow during long term culture.

Table 1-1 cont.

Reference	**BGS types**	**Cell types**	**Flow regimen**	**Observation** **(All observations were compared with static culture)**
(Jaasma *et al.*, 2008)	Collagen-glycosaminoglycan GAG	MC3T3-E1 osteoblastic cells	Continuous unidirectional flow, 0.1 - 2 ml/min; Pulsatile flow, 0 - 1 mL/min (peak-to-peak), 2 Hz; Oscillatory flow, 1 mL/min (peak-to-peak), 1 Hz.	All types of flow showed decreased cell number and increased PGE2
(Du *et al.*, 2008)	β-tricalcium phosphate	MC3T3-E1 osteoblastic cells	Oscillatory perfusion, 0.5 ml/min (0.04 dyn/cm^2), 1/60 Hz	Higher seeding efficiency, homogeneous cell distribution, ALP activity, cellularity
(Du *et al.*, 2009)	β-tricalcium phosphate	MC3T3-E1 osteoblastic cells	Continuous unidirectional flow, 1 ml/min; Oscillatory perfusion, 0.5 ml/min, 1 ml/min	Increased cell number; oscillatory let to increased ALP activity

Table 1-1 cont.

Reference	**BGS types**	**Cell types**	**Flow regimen**	**Observation (All observations were compared with static culture)**
(Xu *et al.*, 2008)	β-tricalcium phosphate	Sheep MSCs	Continuous unidirectional flow, 3 ml/min (~0.0029-0.027 Pa)	Increased proliferation, non-homogenous cell proliferation rate and cell coverage
(Yang *et al.*, 2010)	Polylactic glycolic acid (PLGA)	hMSCs or hMSCs transduced with human telomerase catalytic subunit (hTERT) gene	Continuous unidirectional flow, 0.2 ml/min for 9 days and then 0.5 ml/min for 7, 14, 21, 28 days	Homogeneous seeding, Increased viability, proliferation, Induced osteogenic differentiation at 0.5 ml/min
(da Silva *et al.*, 2010)	Hydroxyapatite (HA) and silicate substituted HA (SiHA) dense tablets	SaOs-2 osteoblastic cells	Continuous unidirectional flow, through BGS surface, 2 ml/min	Increased cell number and ALP activity on both BGS; faster adhesion process, longer and thinner focal adhesions on SiHA

Table 1-1 cont.

Reference	**BGS types**	**Cell types**	**Flow regimen**	**Observation (All observations were compared with static culture)**
(Janssen *et al.*, 2010)	Biphasic calcium phosphate (OsSatura™, IsoTis, The Netherlands), 10 cc of granules Ø 2 ~ 6 mm	hMSCs	Continuous unidirectional flow, 4 ml/min (108 µm/s)	Homogeneous and viable cell layer, dense layer of extracellular matrix; no difference in osteogenic markers compared with static culture; abundant de novo bone formation but no difference compared with static culture
(Bjerre *et al.*, 2011)	HA Pro Osteon®	hMSCs	Continuous unidirectional flow, 0.1 ml/min	Decreased vitality, proliferation and differentiation
(Yu *et al.*, 2012)	Polycaprolactone (PCL) /hydrogel	Rat MSCs	Continuous unidirectional flow, 0.6 ml/min	Increased proliferation, *opn, oc*, and *bsp* expression

Table 1-1 cont.

Reference	**BGS types**	**Cell types**	**Flow regimen**	**Observation** **(All observations were compared with static culture)**
(Barron *et al.*, 2012)	Calcium phosphate	MC3T3-E1 osteoblastic cells coculture with mouse microvascular endothelial cells (EOMA)	Continuous bidirectional flow, 0.075 mL/min	Downregulated *vegf* and *opn* expression at early timepoints; Increased *alp* and *oc* expression at day 7; Increased cell number, cell/matrix area coverage, angiogenic activity at day 14
(Kim and Ma, 2012)	Poly (ethylene terepthalate) (PET)	hMSCs	Continuous unidirectional flow at BGS surface (PF), 0.2 ml/min; Continuous unidirectional flow through bone graft substitue (TF), 0.2 ml/min	PF: retained ECM protein, and mitogenic growth factors, preserve hMSCs proliferation TF: induced osteogenic differentiation, higher ALP, calcium deposition, osteogenic markers

Table 1-1 cont.

Reference	**BGS types**	**Cell types**	**Flow regimen**	**Observation** **(All observations were compared with static culture)**
(Pisanti *et al.*, 2012)	Poly (L-Lactic acid) (PLLA)	hMSCs	Continuous unidirectional flow, 0.3 ml/min	Increased ALP activity, *bmp2* expression
(Correia *et al.*, 2013)	Silk fibroin disk	Human adipose stem cells (hASC)	Steady perfusion, continuous unidirectional flow at 400 µm/s for 5 weeks; Dynamic perfusion, continuous unidirectional flow at 400 µm/s for 2 weeks, followed by 3 weeks pulsatile flow, velocity fluctuating between 400 and 1200 µm/s at 0.5 Hz	Dynamic perfusion group showed increased *opn* expression, PGE2 synthase expression, OPN, BSP, COL I protein deposition and mineral deposition compared with steady perfusion group

Table 1-1 cont.

Reference	**BGS types**	**Cell types**	**Flow regimen**	**Observation** **(All observations were compared with static culture)**
(Yeatts *et al.*, 2014)	Poly (lactic-co-glycolic acid)/polycaprolactone (PLGA/PCL)	hMSCs	Continuous unidirectional flow, 1 ml/min 10 days then *in vivo* implantation	Increased new bone area, bone regeneration
(Wang *et al.*, 2014)	β-tricalcium phosphate	Rabbit osteoblasts	Continuous unidirectional flow, 0.5 ml/min for day, followed by 2 ml/min	Increased cell viability, ALP activity; better bone formation, compression strength *in vivo*
(Filipowska *et al.*, 2016)	Gelatin-coated polyurethane (PU) disc	hMSCs	Continuous unidirectional flow, 2.5 ml/min	Increased *oc, opn, bsp* and *bmp2* expression
(Tang *et al.*, 2017)	polyurethane	Rat MSCs	Continuous unidirectional flow, 10 ml/min	Increased viability, proliferation, type I and III procollagen, equilibrium modulus

Table 1-1 cont.

Reference	**BGS types**	**Cell types**	**Flow regimen**	**Observation** **(All observations were compared with static culture)**
(Ismail *et al.*, 2017)	Porous HA (Engipore)	Stromal vascular fraction (SVF) cells	Oscillating perfusion, 1 ml/min	Accelerated initial vascularization, Increased bone formation
(Mitra *et al.*, 2017)	PLG/HA composite disk	hMSCs	Continuous bidirectional perfusion 3 ml/min	Increased proliferation, Ca, OC content, neovascularization globally. Great bone volume fraction, bone mineral density, tissue ingrowth, collagen density after perfusion culture 14 days than 1 or 7 days
(Chen *et al.*, 2017)	Collagen/HA	Rat MSCs	Oscillatory perfusion, 1 ml/min, 1/60 Hz	Increased viability, cell distribution uniformity, ECM, COL I secretion and mineral deposition, osteogenic differentiation
(Vetsch *et al.*, 2017)	Silk fibroin	hMSCs	Continuous unidirectional flow, 0.001 m/s, 0.061 m/s	Increased metabolic activity, DNA; Increased ECM formation, osteogenic differentiation at 0.061 m/s; decreased ECM formation, osteogenic differentiation at 0.001 m/s

1.6 Aims and Objectives

A substantial number of BGS materials have been developed for clinical use, and some of them claim to be osteoinductive. Various theories have been proposed to explain the claimed osteoinductivity, such as response to modulation of local mechanical environment, cells response to bone graft surface roughness, increased bone graft surface area, increased ion exchange, or increased nutrient transfer due to increased pore connectivity. Bone mechanosensitivity has been extensively acknowledged, and mechanical stimulus have been shown to significantly influence cellular behaviour. However, so far, studies of *in vitro* BGS efficacy evaluation and mechanism investigation were traditionally carried out in a static environment which does not represent the environment that cells are exposed to *in vivo*. Therefore, there is a clear need to develop a dynamic *in vitro* system, which includes mechanical perturbation, in order to investigate how BGS work and further develop smart BGS materials.

The hypothesis of this thesis is that synthetic bone graft architecture has an influence on osteogenic cell responses through its interaction with local mechanical environment. Therefore, to investigate the response of osteogenic cell responses to BGS macrostructure and microstructure, a test system should expose the cell seeded BGS to (i) direct strain and local fluid shear (ii) a local fluid shear in isolation (iii) a specific pattern/level of fluid shear.

The aims of this PhD research were to incorporate these mechanical forces in a 3D bioreactor system, examine the influence of BGS architecture on cell responses to probe the mechanism behind the excellent clinical performance of hierarchical porosity in SiHA BGS.

The flow diagram of this PhD research can be seen in Figure 1-3. This PhD thesis is composed of 7 chapters. Chapter 1 opens with studies in the literature about bone composition and structure, bone mechanobiology, bone healing, BGS and bioreactors. Chapter 2 describes the experimental procedures used in this PhD for the synthesis and characterization of SiHA BGS, cell culture model, 3D bioreactor

system and cellular response characterization. In Chapter 3, an *in vitro* 3D bioreactor system for application of direct strain and local fluid shear on cell-seeded SiHA BGS granules was validated. Parameters of seeding cells on SiHA BGS granules in the perfusion chamber were optimized. The response of osteoblastic-like MG63 cells to mechanical stimulation was investigated. In Chapter 4, SiHA granules consisting of equivalent levels of total porosity but various levels of micro-porosity, and SiHA granules consisting of equivalent levels of micro-porosity but various levels of total porosity were synthesised and characterised. The structural guidance of SiHA granules on human mesenchymal stem cells (hMSCs) proliferation and differentiation in static environment were examined. In Chapter 5, hMSCs were cultured on SiHA granules with defined micro-porosity in a static, basal perfusion rate (BPR) or a period of high perfusion rate (pHPR) environment. The synergistic effect of BGS micro-porosity and shear stress on responses of hMSCs was studied. In Chapter 6, the modulation of L-type voltage-sensitive calcium channels (VSCCs) on fluid shear stress induced differentiation of hMSCs cultured on 3D SiHA BGS was investigated. Chapter 7 describes the conclusions about the work in this PhD thesis, and future perspectives on BGS and 3D bioreactor systems.

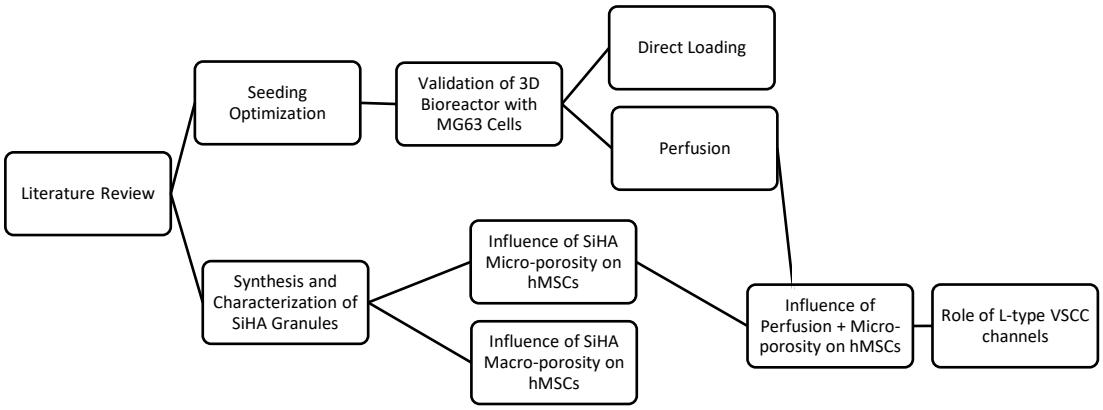

Figure 1-3 Flow diagram of the current PhD research.

Chapter 2 Materials and Methods

2.1 SiHA Granules Synthesis

SiHA has been successfully used as bone filler in clinic in the form of granules which are easy to shape to fit the defect size (Harshavardhana and Noordeen, 2015). Macro-porosity (the bulk of the pore fractions) and micro-porosity (fraction of porosity within the BGS body) (Hing *et al.*, 2005) of BGS play important roles in bioactivity of SiHA BGS. SiHA granules with different macro-porosities and micro-porosities were synthesised and their bioactivities were evaluated in *in vitro* experiments.

Dried silicate substituted hydroxyapatite (SiHA) precipitate cakes containing 0.8 wt% silicon were provided by Baxter Inc. They were crushed into small pieces, using a pestle and mortar and passed through a 1 cm sieve. The small pieces were disc-milled and then calcined at 700 ^{o}C for 4 hours to reduce any moisture.

Table 2-1 Parameters of foaming process to produce different SiHA granules.

	SiHA-14	SiHA-22	SiHA-28	SiHA70
SiHA powder (g)	560 ± 1	560 ± 1	490 ± 1	730 ± 1
Deionized water (g)	867 ± 2	867 ± 2	805 ± 2	1087 ± 2
Milling media (g)	4254 ± 5	4254 ± 5	4454 ± 5	5625 ± 5
First ball milling time (min)	90 ± 1	65 ± 1	10 ± 1	90 ± 1
PVA (g)	130 ± 1	130 ± 1	240 ± 1	170 ± 1

Calcined SiHA power was used to produce the different porous granules samples. Different amount of SiHA power, deionized water (Table 2-1) were added in a milling pot and mixed into a paste. Milling media (ceramic milling balls) were added to this paste (Table 2-1) and then the pot was sealed using nuts and bolts to avoid leaking. The whole container was ball milled firstly at a rate of 270 rpm onto a ball mill machine for the different time (Table 2-1). Polyvinyl alcohol (PVA) was dissolved in double distilled water and used as binder solution. When the first ball mill finished, the pot was opened and PVA (Table 2-1) was added into the pot, which was sealed,

and ball milled for a further 3 hours. After 3 hours, the foam was sieved to remove all milling media and then transferred to plastic moulds and dried at 40 - 50 °C for 48 hours (Genlab, drying cabinet). Once dried, the foam was demoulded and sintered at 1250 °C in a (Lenton, AWF) for 4 hours. Large pieces of sintered SiHA foam were collected for total porosity and micro-porosity quantification and the rest of sintered SiHA foam was gently crushed and sieved using 2 mm and 1 mm sieves to achieve 1-2 mm diameter SiHA granule fraction, which were used in cell culture experiments in the current thesis.

2.2 Materials Characterization

2.2.1 X-ray Diffraction (XRD)

XRD was used for determining the crystal structure of SiHA samples. The fundamental principle of XRD is that every crystal structure has unique atomic spacing and inter-planar spacing. Monochromatic X-ray is generated and directed toward the sample, when wavelength of the incident X-ray (λ), angle of incidence (θ) and crystal inter-planar spacing (d) satisfy Bragg's Law ($n\lambda = 2d\sin\theta$, n is the "order" of reflection), the interaction of the incident rays with the sample produces constructive interference and a diffracted ray (Figure 2-1). During scanning, sample and detector are rotated, so X-ray is irradiated with a range of 2θ angles, the intensity of reflected X-ray is recorded, converted to spectra and compared with reference patterns, in order to identify or verify the nature of the phases present in the sample.

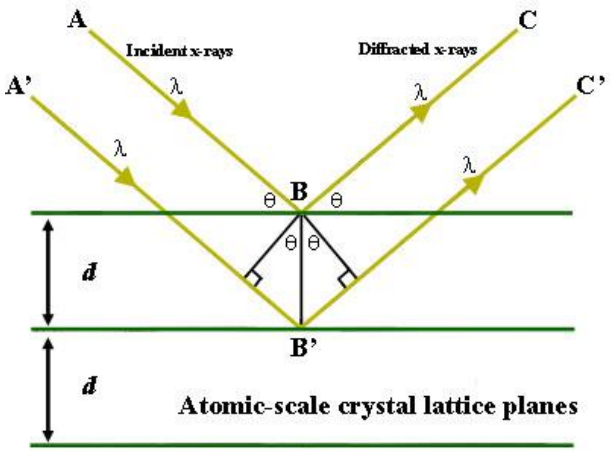

Figure 2-1 Schematic diagram of Bragg's Law.

Small SiHA granules (ϕ<1 mm) were used to obtain XRD patterns using a XPERT-Pro diffractometer (Philips). The monochromatic Cu-K_α radiation was operated at a voltage of 45 KV and 40 mA, and the data were acquired at a 2θ of 20° to 40° with a step size of 0.02° at 2.5 s per step. Phases were identified by comparing the obtained diffraction patterns with International Committee for Diffraction Data (ICDD) file cards 9-432, 37-1497, 25-1137, 9-348 and 9-169 for HA, calcium oxide (CaO), tetracalcium phosphate ($Ca_4(PO_4)_2O$), α and β-tricalcium phosphate ($Ca_3(PO_4)_2$) respectively.

2.2.2 Density and Total Porosity Measurement

The total porosity and apparent porosity were measured by water saturation method based on Archimedes' principle. SiHA pieces were weighed in a dry condition three times (Wdry), and then were placed in boiling deionised water for 60 mins to ensure all open pores were filled with water. Sample were allowed to cool before being weighed three times while submerged in deionised water at known temperature (Wsub). Then they were taken out of the water and weighed while saturated with water (Wsat). The apparent density (taking into account of both open pores and closed pores), the real density (taking into account only closed pores) and the total porosity can be calculated using the following equations, of which ρH_2O is the density of deionised water at the measurement temperature, and an accepted value(Akao *et al.*, 1981) of 3.156 g/cm^3 was used for the theoretical apatite density (ρ_{HA}).

$$\rho_{apparent} = \frac{Wdry}{Wsat-Wsub} * \rho H_2O \qquad \text{Equation 1.1}$$

$$\rho_{real} = \frac{Wdry}{Wdry-Wsub} * \rho H_2O \qquad \text{Equation 1.2}$$

$$Total\ Porosity = \left(1 - \frac{\rho_{apparent}}{\rho_{HA}}\right) * 100\% \qquad \text{Equation 1.3}$$

2.2.3 Micro-Porosity Measurement

Micro-porosity of SiHA BGS was analysed using quantitative metallography methods (Hing *et al.*, 1999). SiHA samples were embedded in resin (EpoFix, Struers), polished, coated with gold using sputter coater and imaged with secondary electron imaging

using scanning electron microscope (SEM) (FEI inspect F) at 300× magnification. Six images for each sample were taken and analysed to quantify the micro-porosity (number of pixels under and above an optically set threshold values of grey tones) in microporous regions by NIS element image analysis software (Nikon).

2.3 Cell Culture Models

Appendix 2 lists the supplier and CatLog number of all cell culture and molecular analysis chemicals used in this PhD study. Some key chemicals are also defined in the main body of the text.

2.3.1 MG-63 Osteoblast Cell Line Culture

Cryopreserved human MG-63 cells were seeded at a density of 4000 cells/cm^2 in T-75 flasks in basic cell culture medium (BM) (Table 2-2) at 37 ^oC in a humidified incubator with 5% CO_2.

Table 2-2 Components of basic cell culture medium (BM) for cell culture in T-75 flasks in CO_2 atmosphere.

Component	Supplier	CatLog number	Volume
High glucose Dulbecco's Modified Eagles Medium (DMEM) (contains $NaHCO_3$ buffer)	Sigma	D6429	15 ml
Fetal bovine serum (FBS)	Sigma	F9665	1.5 ml
Penicillin-Streptomycin	Sigma	P4333	150 µl

Culture medium was replaced every two to three days. 70% to 90% confluent cells were detached by trypsin-EDTA solution and were subcultured at a density of 4000 cells/cm^2 in T-75 flasks in 15 ml basic cell culture medium. Passage 4-5 of MG-63 cells were used in the study.

2.3.2 Human Bone Marrow Derived MSCs Culture

Cryopreserved human bone marrow derived mesenchymal stem cells (hMSCs) (PromoCell, Lot: 403Z003.2.) were seeded at a density of 4000 cells/cm^2 in T-75 flasks in 15 ml MSC growth medium 2 (PromoCell) at 37 ^oC in a humidified incubator with 5% CO_2. Culture medium was replaced every two to three days. 70% to 90% confluent

cells were detached by Accutase solution, which contains proteolytic and collagenolytic enzymes, and is a gentle alternative cell detachment solution to trypsin. hMSCs were then subcultured at a density of 4000 cells/cm^2 in T-75 flasks in 15 ml MSC growth medium 2. Passage 4-5 of hMSCs were used in the experiment.

2.4 Perfusion Bioreactor System

Cell seeded BGS were subjected to flow induced shear stress using an in-house 3D perfusion bioreactor system (Figure 2-2). The perfusion bioreactor system consists independent chambers and each chamber (diameter: 8 mm; height: 16 mm) accommodates one construct (i.e. cells were seeded on 0.47 ± 0.03 g of BGS granules packed in the chamber). Culture medium from the reservoir was perfused through the constructs vertically in a bottom-to-top direction using a peristaltic pump (IPC Iamatec, VWR). Experiments could be performed in both media flow to waste and recirculating configurations. The details of cell culture media used varied with cell type and experiment and are included in each chapter.

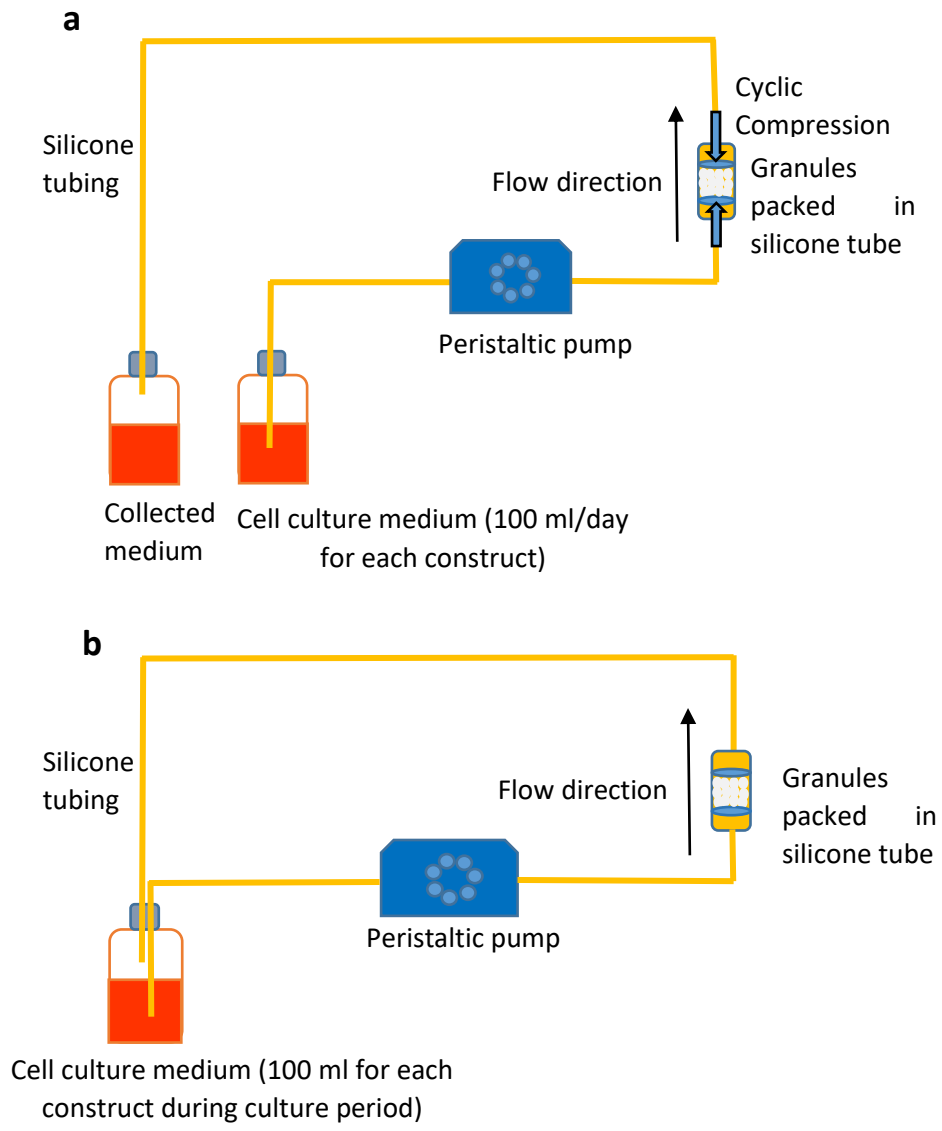

Figure 2-2 (a) Schematic diagram of flow to waste perfusion and compression system. (b) schematic diagram of recirculating perfusion bioreactor system.

2.5 DNA Quantification

Total DNA was quantified by using a Quant-iT PicoGreen dsDNA Assay kit (Invitrogen, UK). The PicoGreen dsDNA reagent is an ultrasensitive fluorescent nucleic acid stain for quantifying double-stranded DNA (dsDNA) in solution. Therefore, it is a very good indicator of DNA levels in specific samples.

Medium from each sample was aspirated and the BGS were then washed three times with phosphate buffered saline (PBS) and submerged into 1 ml of 0.05% Triton TX for cell lysis. Cell lysates were collected, frozen at -80 ^{o}C and then thawed for 3 cycles, sonicated for 5 minutes and centrifuged at 4 ^{o}C at 12000 rpm for 15 mins. The

resultant supernatant solutions from each construct were then collected for DNA quantification. The DNA quantification kit provided a 100 µg/ml lambda DNA solution which was diluted 50-fold in premade Tris-HCL EDTA (TE) buffer (1 ml 200 mM Tris-HCl, 20 mM EDTA, pH 7.5, mixed with 19 ml distilled DNAse-free water) to make a 2 µg/ml stock solution of dsDNA in TE buffer. The 2 µg/ml dsDNA stock solution was then 2-fold serial diluted for 8 times to make standards.

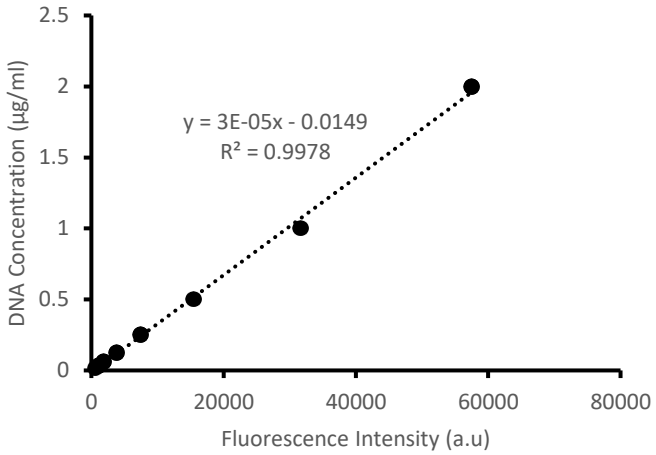

Figure 2-3 Calibration curve for DNA concentration.

100 µl of each standard or sample supernatant was then incubated with 100 µl of PicoGreen working solution (dilute concentrated PicoGreen DMSO solution 200-fold in TE buffer). Then the plate was incubated for 2 to 5 mins at room temperature and the fluorescence was read at excitation and emission wavelength of 480 nm and 592 nm respectively using plate reader (BMG LABTECH, FLUOstar OPTIMA). A standard curve of fluorescence versus DNA concentration was generated using standards, and DNA concentration from unknown samples was calculated from the DNA standard curve (Figure 2-3).

2.6 Specific ALP Activity Assay

ALP activity was quantified by using a highly sensitive colorimetric ALP Assay Kit (Abcam). The kit uses p-nitro phenyl phosphate (pNPP) as a phosphatase substrate which turns yellow (λmax = 405 nm) when dephosphorylated by ALP enzyme.

Medium from each sample was aspirated and BGS granules were then washed three times with ice cold PBS and submerged into 1 ml of ice-cold alkaline phosphatase

assay buffer from the kit for cell lysis. Cell lysates were frozen at -80 °C and then thawed for 3 cycles, sonicated for 5 minutes, centrifuged at 4 °C at 12000 rpm for 15 mins and the supernatant was used to test ALP activity. 10 mM 4-nitrophenol (4NP) (Sigma) was diluted 10 times to make 1 mM 4NP, and then 2-fold serial diluted for 8 times to make standards.

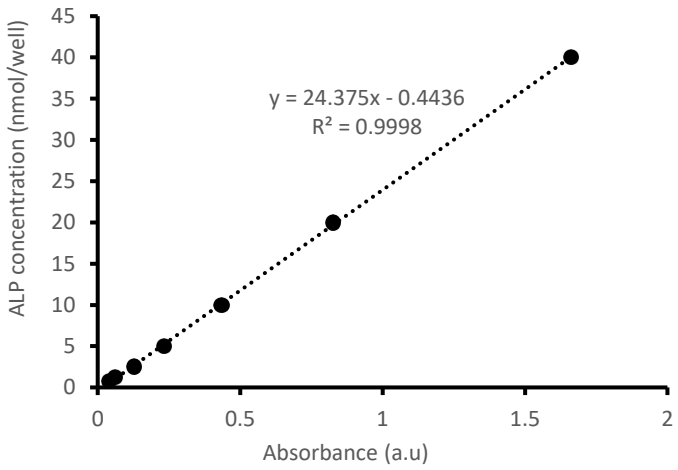

Figure 2-4 Calibration curve for ALP concentration.

80 µl of each standard or supernatant was then incubated with 50 µl of 5.4 mM pNPP buffer (2 p-nitro phenyl phosphate (pNPP) tablets dissolved in 5.4 ml of assay buffer) in clear 96 well-plate at 37 °C for 40 mins. The reaction was stopped using 20 µl of sodium hydroxide, and the final absorbance was read at 405 nm using a microplate reader (BMG LABTECH, SPECTROstar). A standard curve of absorbance versus 4NP concentration was generated using standards, and 4NP dephosphorylated by ALP from unknown samples were calculated from the standard curve (Figure 2-4). Specific ALP activity was calculated by the equation below.

$$Specific\ ALP\ activity = \frac{4NP\ dephosphorylated\ by\ ALP\ from\ unknow\ sample\ (nmol)}{sample\ supernatant\ volume(ml) * reaction\ time(\mathrm{min}) * DNA\ (\mu g)}$$

2.7 Alizarin Red S Staining

2 g Alizarin Red S (Sigma) was dissolved in 100 ml of ddH_2O and pH was adjusted to 4.1-4.3 with HCL or NH_4OH. The solution was then filtered through 0.22 µm membrane and stored at 4 °C in dark. Medium from each 24 wells was aspirated, and

cells were gently washed with 1 ml PBS. 1 ml 4% (w/v) formaldehyde in PBS was applied to the cells and incubated for 1 hour at room temperature. This was followed by aspirating formaldehyde solution and cells were washed with 1 ml of ddH_2O twice. 1 ml of freshly made Alizarin Red S solution was added to each well and incubated at room temperature for 45 mins in dark. After incubation, Alizarin Red S solution was removed and cells in each well were washed 5 times with 1 ml ddH_2O. 1 ml PBS was applied to each well after washing. Osteoblasts with extracellular calcium deposits are bright orange-red colour while undifferentiated osteoblasts without extracellular show slight red colour.

2.8 Immunofluorescence Methods

Prior to fixation, the cell culture medium was removed and the BGS granules with cells were briefly washed with PBS, and then cells on BGS were immediately fixed in 4% (w/v) paraformaldehyde in PBS solution at room temperature for 10 min. BGS granules with cells were washed three times for 5 min in PBS then cells on BGS were permeabilised with 100% methanol at -20 ^{o}C for 10 mins and rinsed with PBS. Cells on BGS were blocked in blocking buffer (PBS with 5% (v/v) fetal bovine serum and 0.3% triton) for 1 hour to reduce non-specific antibody interactions. The steps described above were all conducted at room temperature.

Cells on BGS were incubated with primary antibody at 4 ^{o}C overnight in staining buffer (PBS with 1% (w/v) bovine serum albumin (BSA) and 0.3% triton at a suitable concentration (Table 2-3). Cells on BGS were then washed three times for 5 min in PBS then incubated for 2 hours with species-specific fluorescent secondary antibodies at room temperature (Table 2-4). Following this, cells on BGS were incubated with 5 µl methanolic alexa fluor 488 phalloidin (Thermo Fisher Scientific, UK) stock solution into 500 µl PBS at room temperature for 30 min to label F-actin then washed three times for 5 min in PBS. Cells on BGS were further incubated with 1 µl of 1 mg/ml diamidino-2-phenylindole (DAPI) stock solution (Thermo Fisher Scientific) into 1 ml of PBS at room temperature for 5 min to label cell nuclei then washed three times for 5 min. Cells on BGS were imaged using a Zeiss LSM510 laser scanning confocal microscope, with 30-50 z-sections taken through the cells at 1.5 µm intervals. Maximum projections of z-stacks were processed by the Zeiss ZEN

software. Quantification of the nucleus and cellular size were performed using Image J software.

Table 2-3 Primary antibodies used in this thesis.

Target	Species	Supplier	Catalog number	Use	Dilution
RUNX2	Mouse	Abcam	ab76956	IF	1:100
ERK1/2	Rabbit	Cell Signalling Technology	mAb #4695	IF	1:500
pERK1/2	Rabbit	Cell Signalling Technology	mAb #4370	IF	1:200
ERK1/2	Rabbit	Cell Signalling Technology	mAb #4695	WB	1:1000
pERK1/2	Rabbit	Cell Signalling Technology	mAb #4370	WB	1:2000
GAPDH	Mouse	Abcam	ab9484	WB	1:2000

Table 2-4 Secondary antibodies used in this thesis.

Target	Supplier	Catalog number	Use	Dilution
Alexa Fluor 647 goat anti-mouse	Abcam	ab150119	IF	1:500
Alexa Fluor 594 donkey anti-rabbit	Abcam	ab150064	IF	1:200
IRDye® 680RD goat anti-mouse	Licor	P/N 925-68070	WB	1:15000
IRDye® 800CW donkey anti-rabbit	Licor	P/N 925-32213	WB	1:15000

2.9 Western Blotting

2.9.1 Cell Lysate Preparation

Prior to lysis, cells attached to BGS granules were washed three times with ice cold PBS. Cells from each sample were then lysed in ice cold 500 µl RIPA lysis extraction buffer supplemented with 1% (v/v) Halt protease and phosphatase inhibitor cocktail (Life Technology), incubated on ice for 15 min, sonicated for 30 s to increase the yield, and then centrifuged at 14000 rpm at 4 ^{o}C for 15 min. The supernatant was collected either immediately subjected to total protein quantification or stored at -20 ^{o}C for later use.

2.9.2 Total Protein Quantification

Total protein was quantified by using pierce BCA protein assay kit (Thermo Fisher Scientific). In an alkaline environment, Cu^{2+} in the reagent is reduced to Cu^{1+} which chelates with protein to form a light blue complex, then bicinchoninic acid (BCA) reacts with the Cu^{1+} and forms an intense purple-coloured complex which exhibits a strong linear absorbance at 562 nm. The intensity of absorbance at 562 nm increases with protein concentration. 2 mg/ml bovine serum albumin (BSA) stock from the kit and lysis buffer were used to make standards as listed in Table 2-5.

Table 2-5 BSA standard solution preparation.

Standard	BSA (µg/mL)	Vol 2 mg/mL BSA (µL)	Vol lysis buffer (µL)
Blank	0	0	100
STD1	20	1	99
STD2	100	5	95
STD3	250	12.5	87.5
STD4	500	25	75
STD5	900	45	55
STD6	1,400	70	30
STD7	2,000	100	0

10 µl of protein supernatant from each sample or each standard was incubated with 200 µl of working solution (made with 50 parts of reagent A and 1 part of reagent B) in triplicate in wells of a clear 96 well-plate. The plated was mixed thoroughly on a plate shaker for 30 s and then incubated at 37 ^{o}C for 30 min. After allowing the plate to cool down to room temperature, the absorbance was measured at 562 nm using a plate reader (BMG LABTECH, SPECTROstar). A standard curve of absorbance versus protein concentration was generated using standards, and protein concentration from unknown samples was determined from the protein standard curve.

2.9.3 Electrophoretic Separation of Proteins

Lysis buffer was used to dilute samples to get same protein concentration (20 µg/50 µl) for each, according to the protein concentration of each cell lysate as measured

using BCA. Loading buffer was made by mixing 900 µl of Leammli 4* concentrate and 100 µl of reduction reagent mercaptoethonal. 45 µl diluted protein sample was then mixed with 15 µl loading buffer, heat denatured by heating in a heat block at 100 ^{o}C for 5 min, and then chilled on ice.

Chilled samples were centrifuged down, mixed, and 50 µl cell lysate and loading buffer mix was loaded to each well and run on 4 - 20% Mini-PROTEAN® TGX™ Precast Protein Gels in tris/glycine/SDS running buffer at 150 mV for 1 hour. Pre-stained, strep-tagged recombinant proteins (10 - 250 kD) standards were run alongside the samples.

2.9.4 Immunoblotting and Band Quantification

Following electrophoresis, the gels were transferred to low-auto fluorescence PVDF membrane by semi-dry transfer method using a Trans-Blot Turbo transfer system and Trans-blot SD semi-dry transfer cell (Biorad, UK). A single gel was transferred at 2.5A, 25 V for 3 min for, but when two gels were transferred, the time was extended to 5 min.

Following transfer, membranes were blocked with 15 ml 5% (w/v) BSA in tris buffered saline (TBS) for 1 hr at room temperature. After blocking, membranes were incubated with the appropriate primary antibodies overnight at 4 ^{o}C (Table 2-3). Following this, membranes were washed three times for 5 min in TBS with 1% (v/v) tween20 (TBST), and then incubated with the appropriate species-specific infra-red secondary antibodies (Table 2-4) in 5% (w/v) BSA in TBS for 1 hr at room temperature. This was followed by two 5 min washes in TBST and one final wash in TBS. Membranes were imaged using the Licor Odyssey infrared scanner and densitometry was performed using Image J software to quantify band intensity.

2.10 Quantitative Gene Expression

2.10.1 RNA Isolation

BGS samples with attached cells were rinsed three times with ice cold PBS, and then lysed in 1 ml of tri-reagent (Life Technology). The cell lysate was collected and either immediately subjected to RNA isolation or stored at -80 ^{o}C for later use. 0.2 ml pure

chloroform was added to each sample, and then centrifuged to separate the upper aqueous RNA phase. The RNA phase was purified using RNeasy Mini Kit (QIAGEN). Briefly, total RNA binds to the column and the remaining lysate which passes through the column upon centrifugation (12000 rpm for 15 s) was discarded. Following this, the bound RNA was washed once with 700 µl RW1 buffer, twice with 500 µl buffer RPE, and then centrifuged in a fresh collection tube to remove any remaining RPE buffer. The column was then transferred to a clean collection tube and the RNA was eluted in 30 µl of RNAse free water.

The purity of RNA was determined using the Nanodrop ND-1000 spectrophotometer (LabTech). Pure RNA exhibits an A260/280 absorbance ratio of 2.0. Also RNA content of the sample can be quantified by measuring the absorbance of the samples at 260 nM, and an absorbance of 1 unit at 260 nm corresponds to 40 µg/ml of RNA.

2.10.2 cDNA Synthesis

The process comprises two steps 1) RNA denature: 1 µl of random primer was mixed with 4 µl of RNA template, denatured at 70 ^{o}C and then chilled on ice for 5 min. 2) Reverse transcription: reverse transcription reaction mix was prepared according to reaction 1, and then combined with 5 µl of denatured RNA and primer mix from step 1. Following this it was annealed in a heat block at 25 ^{o}C for 5 min, extended at 42 ^{o}C for 60 min and then reverse transcriptase was inactivated at 70 ^{o}C for 15 min.

Reaction 1:

GoScript 5* reaction buffer	4 µl
MgCl2 (25 mM)	2.4 µl
PCR Nucleotide Mix (10 mM)	1 µl
Recombinant RNasin ribonuclease inhibitor	1 µl
GoScript reverse transcriptase	1 µl
RNeasy free water	5.6 µl
Final Volume	**15 µl**

2.10.3 Primer Design

Primers were designed based on the sequences published in GenBank using Primer-BLAST tool and synthesised in Sigma. Sequence information for primers used in this thesis are shown in Table 2-6.

Table 2-6 Human primers for PCR.

Gene	Forward primer sequence (5'-3')	Reverse primer sequence (5'-3')
osx	F- GAGTGGAACAGGAGTGGAGC	R- GCTTGTAAAGGGGGCTGGAT
alp	F- CCGTGGCAACTCTATCTTTGG	R- GCCATACAGGATGGCAGTGA
bmp2	F- GACGGACTGCGGTCTCCTAAAG	R- CTGACCTGAGTGCCTGCGATAC
col i	F- CCCCGAGGCTCTGAAGGT	R- CACCAGCAATACCAGCAGCA
dmp1	F- AGCATCCTGCTCATGTTCCTTT	R- GAGCCAAATGACCCTTCCATT
runx2	F- AGGCAAGAGTTTCACCTTGA	R- CCTGGGGTCTGTAATCTGAC
sox9	F- AAAGGCTACGACTGGACGCT	R- AGATGTGCGTCTGCTCCGT
col ii	F- GTGTCACGGCCAGGATGTC	R- GCAGAGGACAGTCCCAGTGT
myoD	F- GGTCCCTCGCGCCCAAAAGAT	R- CAGTTCTCCCGCCTCTCCTAC
Integrin α1	F- CGCTGCTGCGTATCATTCAA	R- GGCCAACTAACGGAGAACCA
Integrin α5	F- CCTATGAGGCTGAGCTTCGG	R- GGTGCAGTTGAGTCCCGTAA
Integrin β1	F- GCCGCGCGGAAAAGATGAAT	R- TCGCAAAACCAACTGCTGTG
gapdh	F- GATCATCAGCAATGCCTCC	R- ATCACGCCACAGTTTCCC

2.10.4 Quantitative Real Time Polymerase Chain Reaction (qPCR)

Levels of gene expression were measured by qPCR and was conducted using SYBR Green dye-based assay. SYBR Green dye is a fluorescent DNA binding dye that preferentially binds to double-stranded DNA (dsDNA). It has an excitation and emission wavelength of 494 nm and 521 nm, respectively. Excitation of DNA-bound SYBR Green dye produces a much stronger fluorescent signal compared to unbound dye. The fluorescence signal (at 521 nm) of DNA-bound SYBR Green dye is monitored during the annealing and extension phases of the qPCR reaction. The threshold of the qPCR reaction is the level of the fluorescence signal that reflects a statistically significant increase over the calculated baseline signal. It is set to distinguish relevant

amplification signal from the background. The threshold cycle (Ct) is the cycle number at which the fluorescent signal of the reaction crosses the threshold.

qPCR was conducted on an Applied Biosystem Quantstudio 6 Flex Real-Time PCR system (Thermo Fisher Scientific) and analysed using Quantstudio Real-Time PCR software. Gene expression as quantified according to the comparative quantification algorithms $\Delta\Delta$Ct method, which compares the gene of interest (GOI) from experimental samples with both a calibrator (i.e. untreated or control sample) and glyceraldehyde 3-phosphate dehydrogenase (*gapdh*) as a house keeping (hk) gene. *gapdh* is one of the most commonly used housekeeping gene with the assumption that it remains constant in the cells. With this method, Ct_{GOI} in both experimental sample (s) and calibrator (c) are adjusted in relation to Ct_{hk} from the two samples. The resulting $\Delta\Delta$Ct value is incorporated to determine the fold change in expression.

Fold change = $2^{-\Delta\Delta Ct}$

$\Delta\Delta Ct = \Delta Ct^{\text{ sample}} - \Delta Ct^{\text{ calibrator}}$

$\Delta Ct_{\text{ sample}} = Ct_{GOI}{}^{s} - Ct_{hk}{}^{s}$

$\Delta Ct_{\text{ calibrator}} = Ct_{GOI}{}^{c} - Ct_{hk}{}^{c}$

The KAPA SYBR FAST Universal qPCR master mix (Sigma, UK) containing SYBR Green dye and passive reference dye ROX was used for qPCR. For QuantStudio System, low ROX from the kit was used to normalise for non-PCR-related fluctuations in fluorescence signal. PCR reactions were performed according to reaction 2. Reactions were performed on cDNA generated from 4 µg RNA and were diluted 1:10 so that each reaction contained at least 10 ng of the original RNA. A sample containing nuclease-free water instead of template cDNA, the 'no template control' (NTC) is also run for each GOI to distinguish between actual gene expression and background contamination. All samples are run in triplicate to minimise pipetting error and a mean Ct value is obtained for each experimental replicate.

Reaction 2:

cDNA	1 µl
Low ROX (100*)	0.1 µl
KAPA master mix	5 µl
Primer (10 µM)	1 µl
RNeasy free water	2.9 µl
Final Volume	**10 µl**

PCR reactions were performed according to the following process: firstly, the initial template was denatured into single-stranded DNA and polymerases were activated at 95 ^{o}C for 3 min. Secondly, there were 40 cycles of amplification which includes 3 steps: 1) dsDNA was denatured to single-strands DNA at 95 ^{o}C for 10 s. 2) Primers attach to the specific location of template cDNA at a lower temperature (3 to 5 degrees lower than melting temperature of primers) for 20 s. 3) A new strand of DNA was made by the KAPA SYBR DNA polymerase from the KAPA SYBR master mix at 72 ^{o}C for 30 s. At last, dissociation step was conducted by denaturing all the components at 95 ^{o}C for 1 min, annealing at 55 ^{o}C for 30 s and then gradually increasing temperature to 95 ^{o}C while monitoring the fluorescence to generate a dissociation curve.

While SYBR Green dye-based assay has the advantage of being more cost effective than other probe-based assays, its main drawback is less of specificity. Because SYBR Green dye binds to any amplified dsDNA product, regardless of target or non-target, and all such signals are summed, producing the amplification plot. It therefore requires primers to be accurately designed to only amplify the specific region of interest. Also, it is important to perform the dissociation analysis. By analysing the first derivative of the dissociation curve (a peak), homogeneity of the PCR product can be assessed, when combined with other information such as data from NTC sample, the specificity of the PCR reaction can be evaluated.

2.11 Cell Morphology Characterization Using SEM

Cell seeded BGS granules were chilled on ice for 30 min and then primarily fixed in 1 ml of 1.5% glutaraldehyde buffered in 0.1 M sodium cacodylate (PH 7.2 - PH 7.4) and

incubated overnight at 4 ^{o}C. The primarily fixed granules are stained in 1% osmium tetroxide buffered in 0.1 M sodium cacodylate and incubated for 1 h at room temperature. The samples were then washed (5 mins, 3 times) with 0.1 M sodium cacodylate, incubated in 1% tannic acid dissolved in 0.05 M sodium cacodylate for 30 mins at room temperature and then washed (5 mins, 3 times) with 0.1 M sodium cacodylate. The granules were then dehydrated by washing (5 mins, twice) in a graded series of ethanol (20%, 30%, 40%, 50%, 60%, 70%, 80%, 90%, 96%) and followed by a final wash in 100% ethanol (10 mins, twice). Samples were then immersed in hexamethyldisilazane (HMDS) for 10 mins and air-dried. Finally, the samples were mounted on SEM stubs, coated with gold using sputter coater and then observed with secondary electron imaging at an accelerating voltage of 5 KV and a working distance around 10 mm using field emission (FE) scanning electron microscope.

Chapter 3 Validation of an *in vitro* 3D Bioreactor for Application of Perfusion and Compression on Cells Cultured on SiHA BGS Granules

3.1 Introduction

Porous silicate substituted hydroxyapatite (SiHA) BGS have demonstrated excellent biocompatibility *in vivo* (Patel *et al.*, 2002; Hing *et al.*, 2006), particularly SiHA BGS granules which have the advantage of handling in clinic use. It has been shown that pore structure is critical to BGS performance *in vivo* (Hing *et al.*, 2004; Hing *et al.*, 2005; Campion *et al.*, 2011; Coathup *et al.*, 2012).

Cell seeding is generally performed under static conditions by inoculating cell suspensions onto BGS. Gravity action and capillary forces generated by porous BGS then encourage cell penetration within the BGS (Polak *et al.*, 2013). Seeding cells onto BGS determines the initial cell number in the BGS, as well as their spatial distribution throughout the matrix. Therefore, seeding cells onto a BGS represents a crucial step, which is known to influence cellular viability, proliferation, migration, phenotypic expression and functionality of engineered tissues (Holy *et al.*, 2000; Burg *et al.*, 2000; Qi *et al.*, 2004; Yang *et al.*, 2010). The first aim of the current study concerned investigation of the seeding parameters, include cell density, cell suspension volume and incubation period for SiHA BGS granules to achieve optimal seeding.

It is well known that mechanical loading plays an important role in bone remodelling and fracture healing (Lanyon and Rubin, 1984; Lanyon, 1993; Robling *et al.*, 2002; Boerckel *et al.*, 2012). Several researchers have hypothesized that flow of interstitial fluid is the most probable way of informing bone cells about mechanical loading (Knothe Tate *et al.*, 1998; Sikavitsas *et al.*, 2001). In BGS, fluid flow (shear stress) has been shown to enhance mineralized matrix deposition of marrow stromal osteoblasts (Bancroft *et al.*, 2002; Sikavitsas *et al.*, 2005; Porter *et al.*, 2007; Chen *et al.*, 2017), and benefit osteogenesis and bone formation *in vivo* (Wang *et al.*, 2003). While shear stress has been extensively used to mechanically stimulate cells in 3D

BGS, mechanically stimulation from compression should also be considered, as compression generated BGS deformations was sufficient to regulate gene expression of cells (Hazenbiller *et al.*, 2017). Several studies have used specially designed bioreactor systems to apply shear and compression at the same time (Bolgen *et al.*, 2008; Jagodzinski *et al.*, 2008; David *et al.*, 2008; Appelman *et al.*, 2009; Baas *et al.*, 2010; C X Liu *et al.*, 2012). Some of these bioreactors were developed and marketed by Bose®(Cartmell *et al.*, 2011) and Zetos® (Davies *et al.*, 2006; David *et al.*, 2008), which were initially developed for the culture of natural tissues like bone or cartilage, and were not fully adaptable to stimulate cells seeded on SiHA BGS granules. Therefore, the second aim of this study was to develop a bioreactor that enables cell-seeded SiHA BGS granules to be exposed to both shear stress and compression stress. Then cellular response to variation of BGS porosity can be investigated in the bioreactor.

3.2 Method

3.2.1 Seeding Investigation

Irregularly shaped SiHA granules (ϕ: 1-2 mm) were synthesised using a slip foaming technique, as described in Chapter 2.1, which enabled independent control of the level of total porosity and the level of micro-porosity (Hing and Bonfield, 2000). SiHA granules with total porosity of 80.9 ± 1.9% and micro-porosity of 21.5 ± 1.4% (SiHA-22) were used in all *in vitro* experiment in this chapter. A volume of 1 cm^3 (0.47 ± 0.03 g) of SiHA-22 BGS granules were gently packed in a silicone tube and sandwiched with a thin porous mesh, which retained granules in the tube and allowed cell culture medium to be perfused through the BGS. Two groups of cell suspension with different cell densities were prepared (Table 3-1):

Table 3-1 Cell number and suspension volume of seeding investigation experiment.

	1)				2)					
Cell Number (10^6 cells)	0.2				0.08	0.1	0.175	0.25	0.5	1
Suspension Volume (µl)	400	500	600	700	500					

1) 0.2 million of human osteoblast like cell line MG63 cells were suspended in 400, 500, 600 or 700 µl of basic cell culture medium (BM) (high glucose Dulbecco's modified Eagle Medium (DMEM) with 10% fetal bovine serum (FBS) and 1% penicillin-streptomycin, as per Table 2-2);

2) 0.08, 0.1, 0.175, 0.25, 0.5 or 1 million of MG63 cells were suspended in 500 µl of basic cell culture medium (BM, as per Table 2-2).

Prepared MG63 cell suspensions were divided into two equal volumes and each was pipetted onto each construct from both ends and allowed to attach for 2 hours under static condition at 37 ^{o}C in a humidified incubator with 5% CO_2 (Figure 3-1). After 2 hours of attachment, BGS granules were transferred from silicone tubes to 24 well-plates, rinsed three times with PBS to wash out the unattached cells and submerged into 1 ml of 0.05% Triton TX for cell lysis. Cell lysates were frozen at -80 ^{o}C and then thawed at room temperature for 3 cycles, sonicated for 5 minutes, centrifuged at 4 ^{o}C at 12000 rpm for 15 mins. The resultant supernatant solutions from each BGS were then collected for DNA quantification as described in Chapter 2.5.

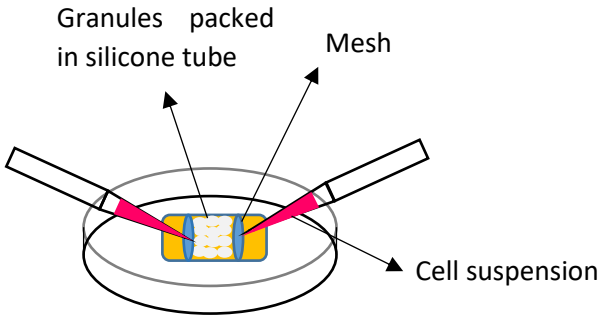

Figure 3-1 Diagram of seeding cells on to construct and incubate for 2 hours in incubator.

To visualize cell morphology on BGS with increasing lengths of time, BGS seeded with 0.5 and 1 million cells in 500 µl of cell suspension were incubated in cell culture medium for up to 7 days after 2 hours of attachment, media was changed every other day. After 1, 3, 5 and 7 days, 3 samples from each group were used to quantify DNA, another 2 samples from each group were used for Scanning Electron Microscopy (SEM) visualization. BGS were transferred from the silicon sample tubes to 24 well-

plates, chilled at 4 °C for 30 minutes, fixed, stained, dehydrated and visualized as described in Chapter 2.11.

3.2.2 MG63 Cell Differentiation

0.1 million MG63 cells in 1 ml basic cell culture medium were seeded in 24 well plates and incubated at 37 °C in a humidified incubator with 5% CO_2. After one day the culture medium was replaced with either basic cell culture medium (BM, as per Table 2-2) or BM enriched with osteogenic supplements (0.1 µM dexamethasone, 0.05 mM ascorbic acid and 10 mM β-glycerophosphate (Sigma-Aldrich)) (BMO). The medium was changed every 2 days thereafter. After 3, 7, 14, 25 and 38 days of incubation, total DNA amount and specific ALP activity of MG63 were quantified as described in Chapter 2.5 and 2.6. After 25 and 38 days of incubation, MG63 cells were fixed and extracellular calcium deposit was stained by using Alizarin Red S as described in Chapter 2.7.

3.2.3 Perfusion and Compression Bioreactor

Cell seeded BGS were subjected to mechanical stimulation using an in-house 3D perfusion bioreactor system (Figure 3-2). The perfusion bioreactor system consists of 6 independent chambers and each chamber (diameter: 8 mm; height: 16 mm) accommodates one construct (i.e. cells were seeded on 0.47 ± 0.03 g of BGS granules packed in the chamber). Perfusion culture medium (Table 3-2) from 6 individual reservoirs was perfused through the constructs vertically in a bottom-to-top direction using a multichannel peristaltic pump (IPC Iamatec, VWR). The bioreactor system was designed to be able to be incorporated into Bose ElectroForce 5500 Load Frame System to allow compression and perfusion at the same time. MG63 cell seeded SiHA-22 BGS granules were cultured under 3 different conditions:

1) Static culture in 24 well-plate;

2) continuous BASAL PERFUSION RATE (BPR) at 0.07 ml/min flow rate in flow to waste configuration as per Figure 3-2;

3) BASAL PERFUSION RATE + one hour daily cyclic COMPRESSION (BPR + C) of 5000 µε at 1 HZ rate in flow to waste configuration as per Figure 3-2.

After 3 days of culture, total DNA, specific ALP activity, and the gene expression of *runx2*, *col i* and *opn* of MG63 cells on the BGS were quantified as described in Chapter 2.5, 2.6, and 2.10. MG63 on BGS were visualized using Scanning Electron Microscopy (SEM) as described in Chapter 2.11, and RUNX2 distribution was visualized as described in Chapter 2.8.

Table 3-2 Components of perfusion culture medium in CO_2 atmosphere.

Component	Supplier	Catalog number	Volume
High glucose Dulbecco's Modified Eagles Medium (DMEM) (without $NaHCO_3$ buffer)	Sigma	D7777	1 g
Ultra-pure water	QMUL lab	N/A	870 ml
Fetal bovine serum (FBS)	Sigma	F9665	100 ml
HEPES Solution	Sigma	H0887	20 ml
Penicillin-Streptomycin	Sigma	P4333	10 ml

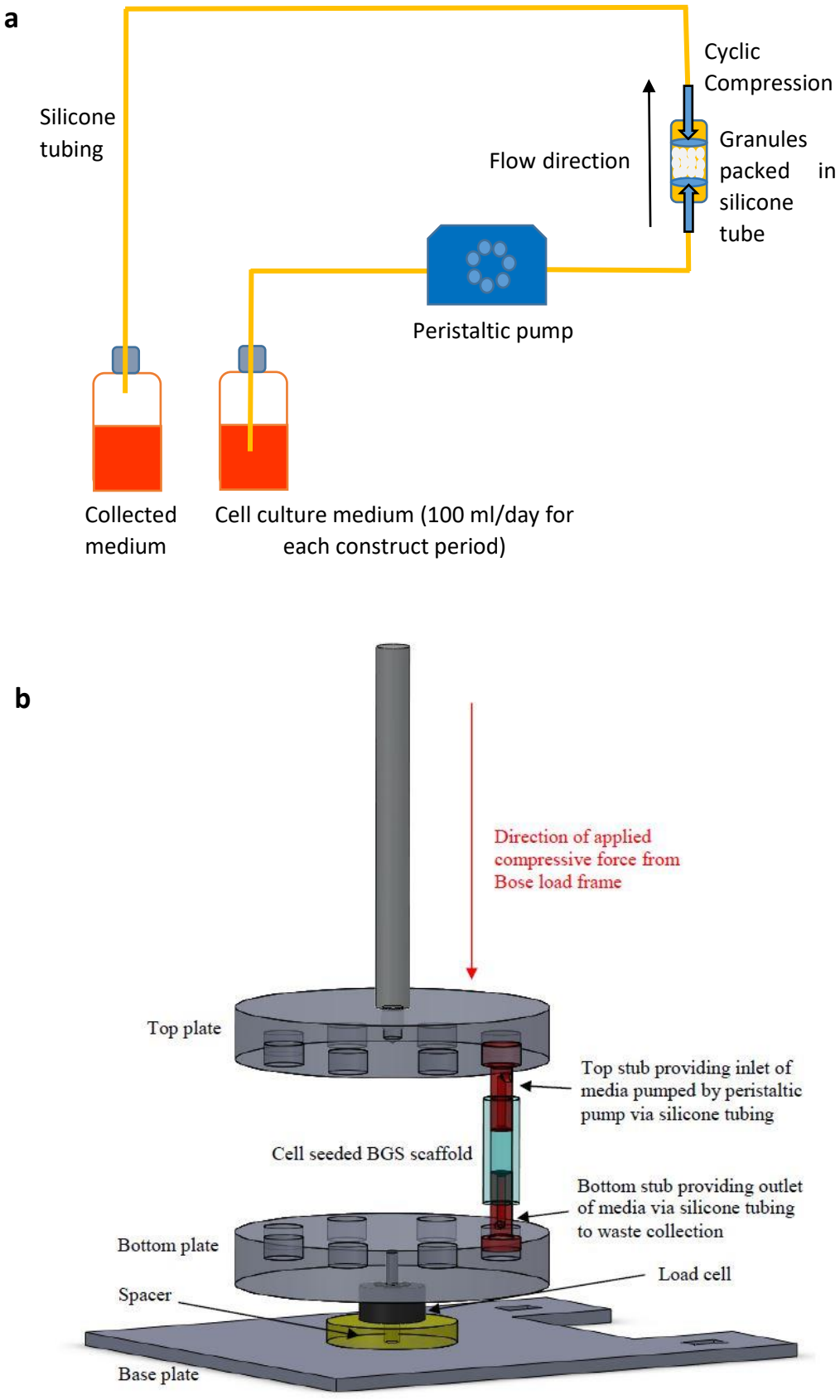

Figure 3-2 (a) Schematic diagram of flow to waste perfusion and compression system. (b) Schematic showing assembly parts of loading model (Chana, 2015)**.**

3.3 Results

3.3.1 Seeding Investigation

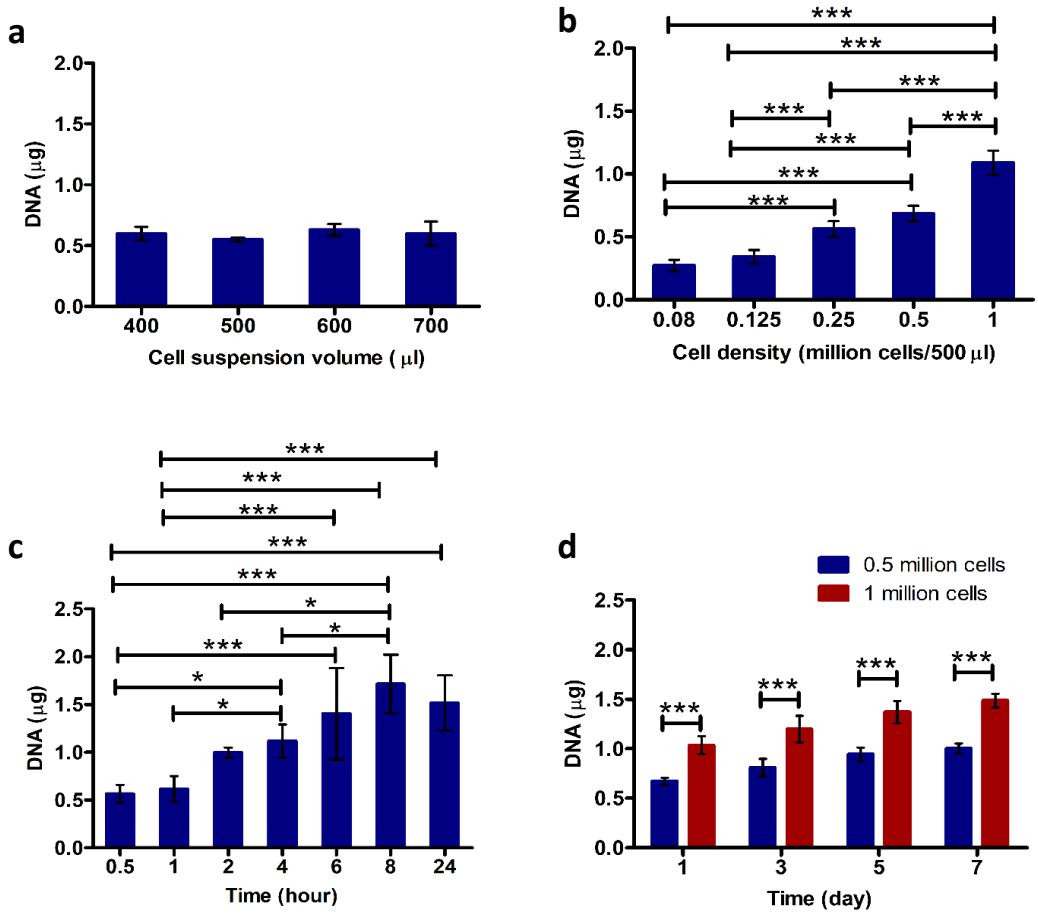

Figure 3-3 The effect of (a) volume and (b) cell density of cell suspension on DNA amount of attached MG63 cells on SiHA-22 after 2 hours. (c) The effect of attachment time on DNA amount of attached MG63 cells on SiHA-22 granules. (d) The effect of seeding density on DNA amount of attached MG 63 cells on SiHA-22 for 7 days. Results are presented as mean ± standard deviation (n>=3). Statistical analysis was performed by one-way ANOVA followed by Tukey's post-hoc multiple comparison with 95% confidence intervals (a, b, and c), or two-way ANOVA followed by Bonferroni post-tests(d). *p < 0.05, **p < 0.01 and ***p < 0.001.

The quantity of total DNA from the BGS was assumed to be proportional to the number of cells on the BGS. So total DNA production was quantified to evaluate the number of cells attached on the BGS. As can be seen in Figure 3-3(a), when 0.2 million MG63 cells were suspended into different volume of cell culture medium, seeded on BGS and incubated for 2 hours, the number of cells attached on BGS was not dependent on the volume of cell suspension. As can be seen in Figure 3-3(b), in 500 µl of cell suspension, the number of attached MG63 cells on BGS increased

significantly with increasing cell density and seeding 1 million MG63 cells generated the highest number of MG63 cells attached on BGS after 2 hours. As can be seen in Figure 3-3(c), attachment time had a positive effect on the attachment of MG63 cells on BGS. There was a trend that the number of attached cells increased with increasing attachment time until 8 hours then dropped after 8 hours. However, it was interesting to note that there was no significant difference in the number of attached cells from 2 - 4, 4 - 6 and 6 - 8 hours of attachment, and standard deviation were large at 6, 8 or 24 hours. There was no significant difference in the number of attached cells between 2 hours and 24 hours of attachment, while a significant difference was detected between 2 hours and 8 hours. As can be seen in Figure 3-3(d), when 1 million MG63 cells (500 µl cell suspension, at a concentration of 2×10^6 cells/ml) were seeded on SiHA-22 BGS and incubated for 7 days, MG63 cells attachment and proliferation on SiHA-22 BGS was significantly higher compared with 0.5 million MG63 cells (500 µl cell suspension, at a concentration of 1×10^6 cells/ml) seeded on BGS, irrespective of the time points. There was a trend that the number of MG63 cells on SiHA BGS increased with time, for both initial seeding number of 0.5 million and 1 million MG63 cells.

As can be seen in Figure 3-4, there were more cells observed on the BGS for initial seeding number of 1 million cells compared with initial seeding number of 0.5 million cells at any time point. There was a trend that the number of cells increased with time throughout 7 days of incubation, irrespective the initial number of cells seeded on the BGS. These observations were consistent with the result of DNA quantification.

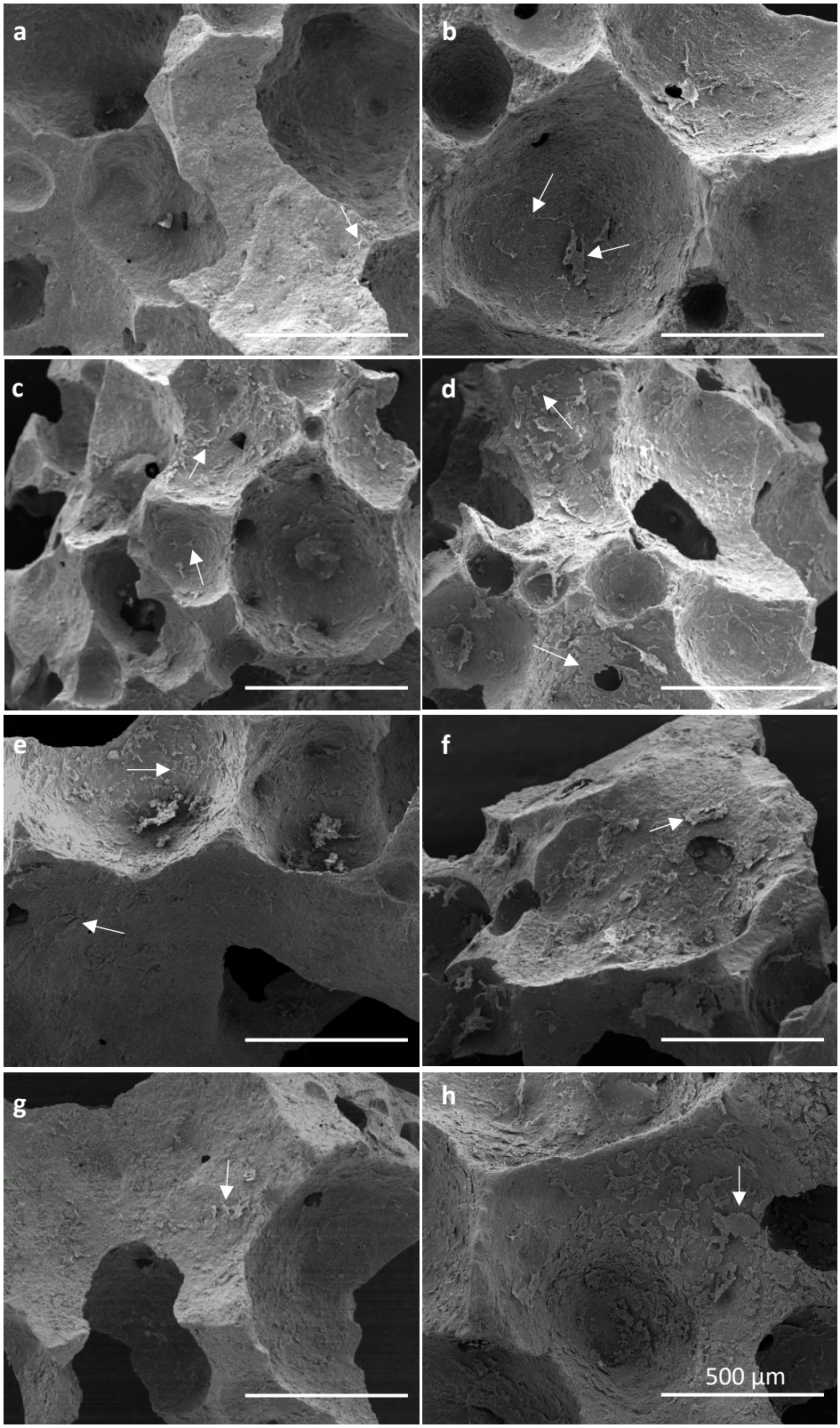

Figure 3-4 The effect of initial cell seeding number, i.e (a, c, e, g) 0.5 million of MG63 cells and (b, d, f, h) 1 million of MG63 cells on cell numbers and cell morphology (white arrow) on SiHA-22 BGS granules after (a, b) 1 day, (c, d) 3 days, (e, f) 5 days and (g, h) 7 days, visualized by SEM.

3.3.2 3D Bioreactor System

As can be seen in Figure 3-5, both continuous basal perfusion rate (BPR) and basal perfusion rate + compression (BPR + C) significantly increased the DNA amount of MG63 cells on the BGS compared with static condition. The specific ALP activity of MG63 cells was higher under static condition compared with BPR and BPR + C, however, there was no significant difference of specific ALP activity between culture conditions.

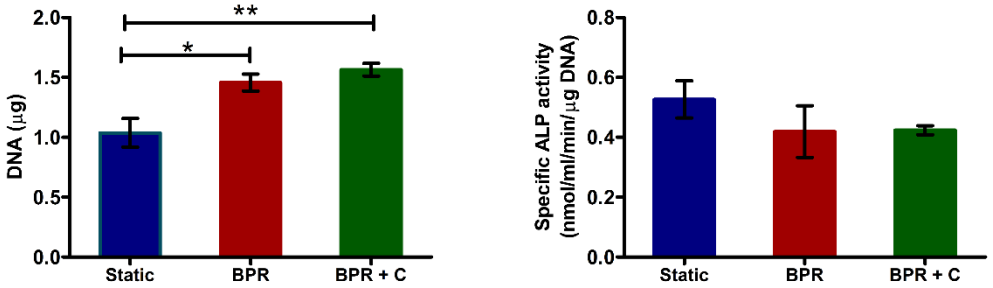

Figure 3-5 (a) DNA amount and (b) Specific ALP activity of MG63 cells cultured on SiHA-22 BGS under static condition, basal perfusion rate (BPR), basal perfusion rate with one hour daily cyclic compression (BPR + C) after 3 days. Statistical analysis was performed by one-way ANOVA followed by Tukey's post-hoc multiple comparison with 95% confidence intervals. *p < 0.05, **p < 0.01 and ***p < 0.001.

As can be seen in Figure 3-6, the expression of runt-related transcription factor 2 (*runx2*) was significantly increased by BPR + C compared with static culture. The expression of type I collagen (*col i*) was significantly higher under BPR than both static culture and BPR + C conditions. The expression of osteopontin (*opn*) was significantly higher under BPR + C than both static culture and BPR, with the expression of *opn* being significantly higher under static than BPR.

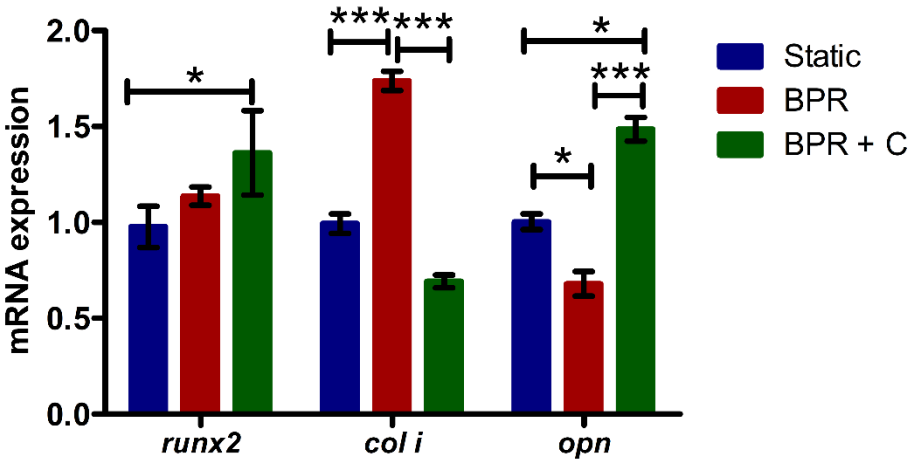

Figure 3-6 The gene expression of *runx2*, *col i* and *opn* of MG63 cells cultured on SiHA-22 BGS under static condition, basal perfusion rate (BPR), basal perfusion rate with one hour daily cyclic compression (BPR + C) after 3 days. Statistical analysis was performed by two-way ANOVA followed by Bonferroni post-tests. *p < 0.05, **p < 0.01 and ***p < 0.001.

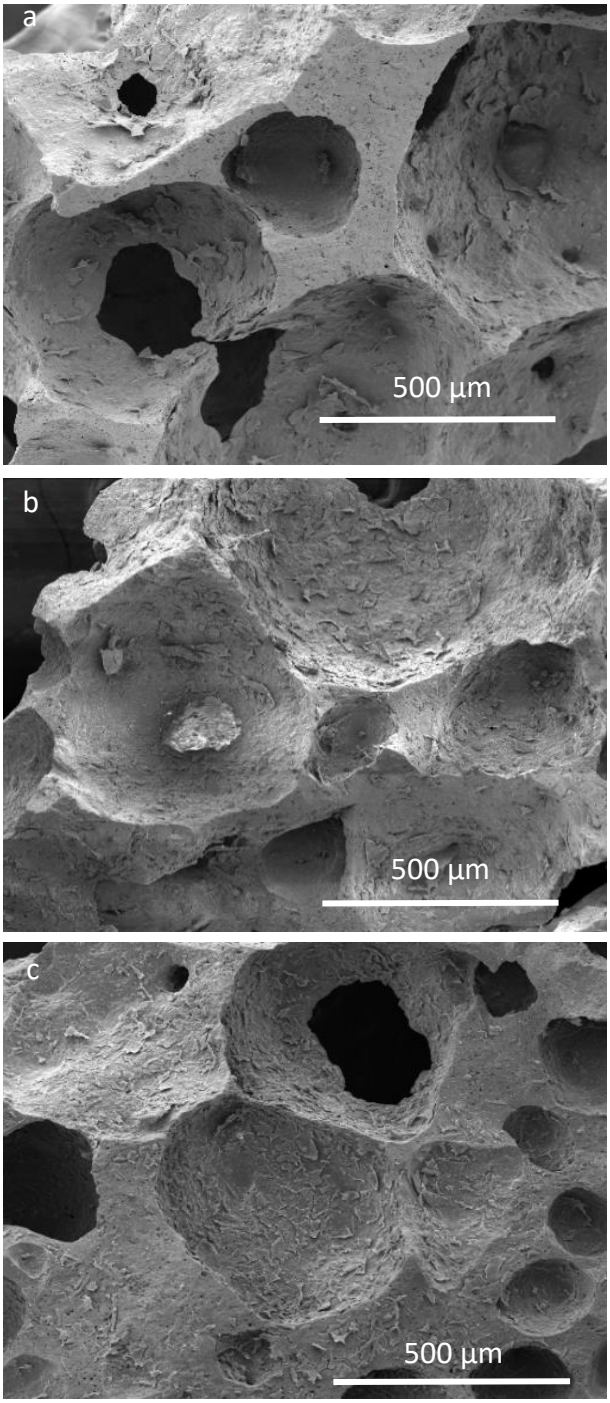

Figure 3-7 Cell populations under scanning electron microscopy (SEM). (a) 3 days of static culture, (b) 3 days of basal perfusion rate (BPR) culture, (c) 3 days of basal perfusion rate with one hour daily cyclic compression (BPR + C) culture.

From SEM images, the cell population was higher under basal perfusion rate (BPR) compared with static culture, with cell population being the highest under basal perfusion rate + compression (BPR + C), as can be seen in Figure 3-7.

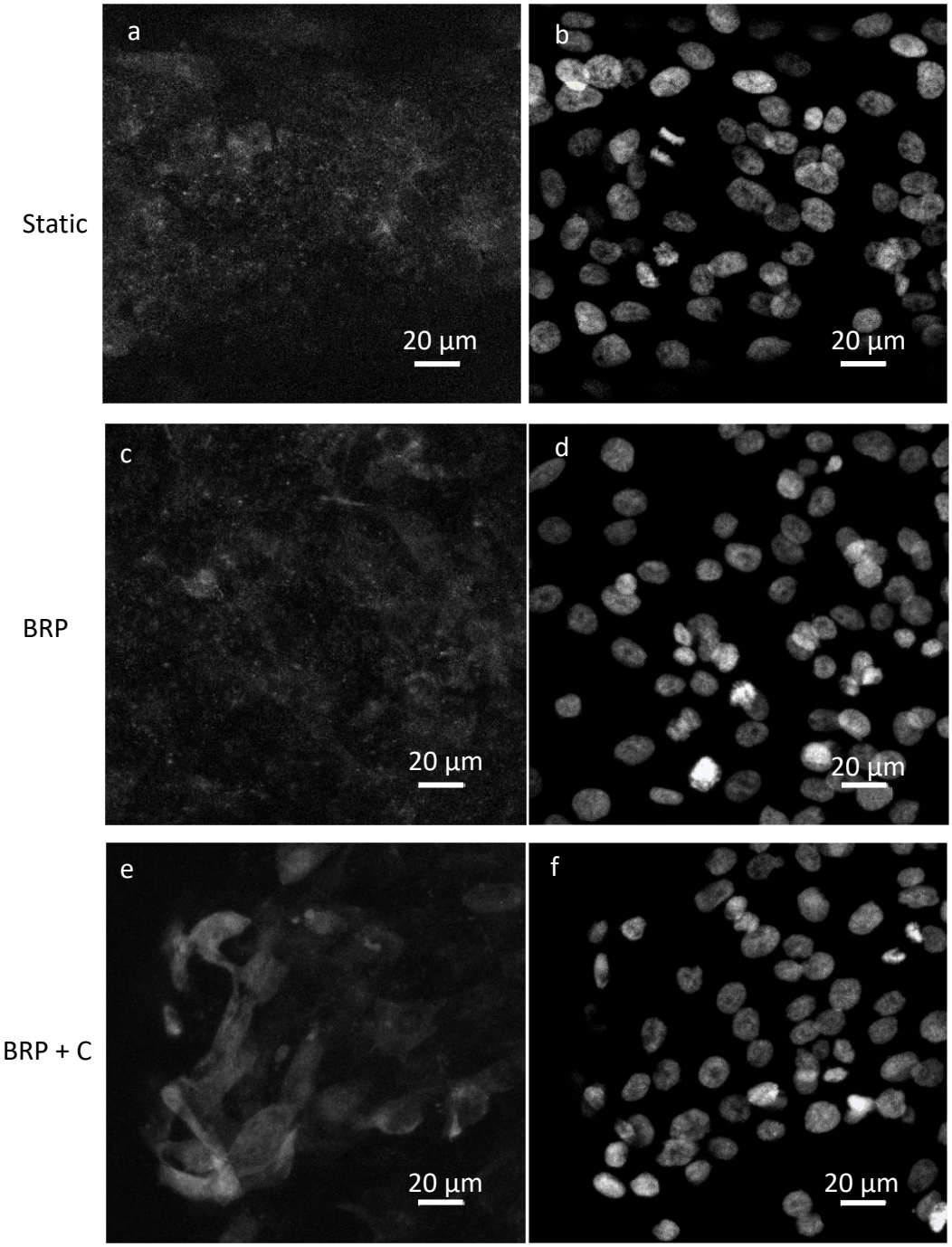

Figure 3-8 Runx2 expression (a, c, e) and nuclei (b, d, f) examined by immunofluorescence and confocal microscopy. (a, b) 3 days of static culture, (c, d) 3 days of basal perfusion rate (BPR) culture, (e, f) 3 days of basal perfusion rate with one hour daily cyclic compression (BPR + C) culture.

RUNX2 was observed to have a very faint expression, and BPR culture showed a stronger signal of RUNX2 than static culture (Figure 3-8(a, c)). RUNX2 was demonstrated to be more concentrated under BPR + C than BPR.

3.3.3 MG63 Cells Differentiation

As can be seen in Figure 3-9, the specific ALP activity of MG63 cells under static culture condition was very low between day 3 and day 14, and it increased significantly from day 25.

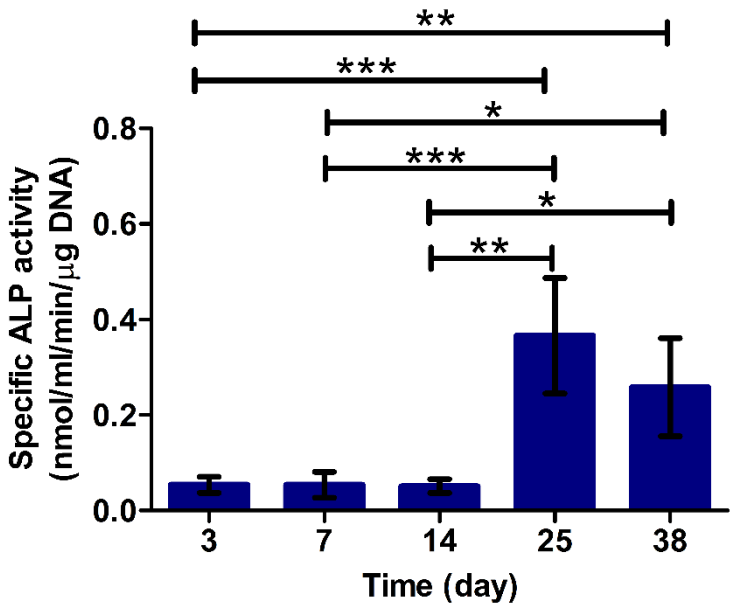

Figure 3-9 Specific ALP activity of MG63 cells (0.1 million cells/well in 24 well-plate) after 3, 7, 14, 25 and 38 days of incubation in 24 well plates in basic cell culture medium. Statistical analysis was performed by one-way ANOVA followed by Tukey's post-hoc multiple comparison with 95% confidence intervals. *p < 0.05, **p < 0.01 and ***p < 0.001.

The specific ALP activity of MG63 cells was not dependent on the supplement of osteogenic induction medium at both day 25 and day 38, which can be seen in Figure 3-10 (a). As can be seen in Figure 3-10 (b), there was small amount of extracellular calcium deposits after both 25 days and 38 days in basic cell culture medium. The extracellular calcium deposition was higher in osteogenic medium compared with basic medium.

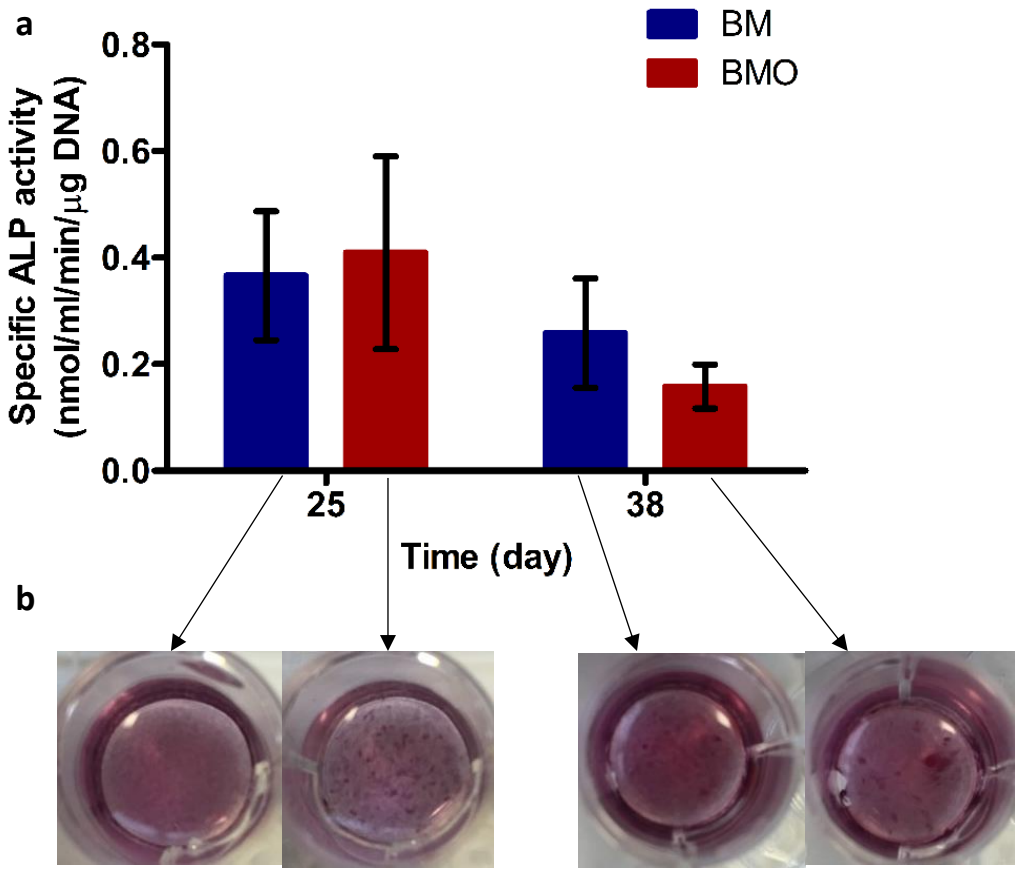

Figure 3-10 Specific ALP activity of MG63 cells (0.1 million cells/well in 24 well-plate) after 25 and 38 days of incubation in 24 well plates in basic cell culture medium (BM) or BM supplemented with osteogenic induction medium (BMO).

3.4 Discussion

It is important that enough cells are seeded onto a BGS, so cells can colonise the materials surface and interact with each other to proliferate and differentiate. Absolute cell number and ECM deposition have been shown to be significantly larger in high initial seeding density groups than their low initial seeding density control groups (Limin Wang *et al.*, 2009). However, high initial seeding densities might have negative repercussions on nutrient availability, cellular metabolism, and cell viability (Issa *et al.*, 2011). Therefore, it is crucial to optimize initial seeding density to achieve optimal cell attachment and growth. When conducting seeding investigation, it should also be borne in mind that once seeded the BGS granules need be compatible with a 3D bioreactor system.

A previous study has shown that seeding cells on to SiHA-22 BGS granules in a 24 well-plate first, allowing to attach for 2 hours and then transferring the granules into perfusion chamber was a very abrasive approach which led to a substantial degree of cell injury (Chana, 2015). However, seeding cells directly onto SiHA-22 BGS granules packed in the perfusion chamber and then allowing cells to attach for 2 hours was able to support cell proliferation, and the highest seeding cell number tested i.e. 0.112 million cells (700 µl of cell suspension at a concentration of 1.6×10^5 cells/ml) provided the most supportive environment for cell proliferation after 3 days (Chana, 2015). Considering the large specific surface (0.26 ± 0.05 m^2/g) area of the porous SiHA-22 BGS, it is worth investigating if increased initial seeding cell numbers could further increase cell attachment and proliferation. The experimental results demonstrated that increasing the initial number of seeding cells significantly increased absolute number of cells attached on the BGS. Initial seeding number of 1 million cells (500 µl of cell suspension at a concentration of 2×10^6 cells/ml) could continuously proliferate over 7 days. This suggests that porous SiHA-22 BGS was able to provide enough surface for cells to attach and the porous structure was beneficial for nutrient transfer and encourage cell colonisation. Seeding density in excess of 2×10^6 cells/ml may be suitable, however practical difficulties encountered in when working with cells at higher concentration prohibited this and a concentration of 2×10^6 cells/ml were used for each construct (0.47 ± 0.03 g of SiHA granules) for all of the further experiments.

The volume of cell suspension and attachment time should also be carefully considered when seeding cells directly onto BGS granules packed in the perfusion chamber. Limited volume of cell suspension cannot cover all BGS granules, while too much cell suspension cannot be held by the BGS granules, which makes the actual cell number seeding on the BGS uncontrollable. The results of the current study indicated when same number of cells were in cell suspension, the number of attached cells was not dependent on cell suspension volume. As handling 600 µl and 700 µl of cell suspension had a higher risk of overflowing the chamber when conducting the experiments, 500 µl of cell suspension was chosen for practical reasons. Interestingly, prolonging the attachment time (2 hours) for another 2 hours

or 4 hours did not significantly increase cell attachment, which indicated that 2 hours of attachment time was sufficient for cells to attach on SiHA-22 BGS granules. Although 8 hours of attachment time led to significantly higher number of attached cells compared with 2 hours of attachment, standard deviation was large suggesting a degree of variability. Moreover, it was not possible to finish the sample preparation and bioreactor construction continuously in a day. Therefore, it was decided that, for later experiments, 2 hours of attachment time would be used.

The response of osteoblastic cell to mechanical stimulation has been widely studied using various forms of load application. It is well established that a perfusion-based bioreactor is the most efficient culture system in terms of nutrient transport homogenization, waste elimination, cell distribution, cell growth and differentiation (Szpalski *et al.*, 2013). A great number of studies has proven that cell proliferation was stimulated by perfusion (Bancroft *et al.*, 2002; Sikavitsas *et al.*, 2005). Bioreactor systems for applying mechanical loading and shear stress at the same time have also shown beneficial effects of mechanical loading on proliferation, osteogenic differentiation and mineral matrix deposition (Table 3-3). In this current study, MG63 osteoblast-like cells seeded on 3D SiHA-22 BGS granules responded to changes in mechanical environment. Basal perfusion rate (BPR) was proven to promote MG63 cells proliferation compared with static culture. Basal perfusion rate + compression (BPR + C) further improved the proliferation compared with basal perfusion rate (BPR) condition. However, perfusion through BGS requires a tight fit between construct chamber and tubing, which creates friction resistance for compression and results in the compression force on BGS granules cannot be quantified.

It is well accepted that osteoblast differentiation can be characterized by specific ALP activity, osteogenic genes expression like *runx2*, *opn*, *oc* and *col i*, and *in vitro* mineralization capacity. RUNX2 transcription factor is a key regulator of osteoblast differentiation and bone formation (Harada and Rodan, 2003). OPN is a glycosylated bone phosphoprotein secreted during osteogenesis, before the onset of mineralization. BPR + C led to concentrated distribution of RUNX2, upregulated *runx2* expression and upregulated *opn* expression, agreeing with previous research that mechanical loading and shear stress supported osteogenic differentiation

(Jagodzinski *et al.*, 2008; David *et al.*, 2008). BPR upregulated *col i* expression, agreeing with previous research (Fassina *et al.*, 2005). While BPR downregulated the expression of *opn* after 3 days, which is contradictory to previous studies (Holtorf, Jansen, *et al.*, 2005; Jaasma and O'Brien, 2008). A Long-term study will need to be carried out to confirm the stimulatory effect of perfusion.

Table 3-3 Perfusion and mechanical loading of cell-seeded BGS: models and effects.

Reference	BGS	Cell type	Perfusion	Compression	Observation
(Bolgen *et al.*, 2008)	Cryogel, 2-hydroxyethyl methacrylate (HEMA)–lactate–dextran, cylindric (Ø = 8 mm, H = 4 mm)	MG63	Continuous 0.1 ml/min	1.5% strain, 1Hz 1 h daily for 2 weeks	Perfusion + compression: increased cell ingrowth, ECM, ALP activity
(Jagodzinski *et al.*, 2008)	bovine acellular matrix, Tutobone® discs, cylinder (Ø = 20 mm, H = 4mm)	hMSCs	Continuous 10 ml/min	10% strain, 0.5Hz, (24h, 1, 2, and 3 weeks)	Perfusion: increased proliferation, *runx2* expression, OC content; Perfusion + compression: increased proliferation, *runx2* expression Further increase OC content
(David *et al.*, 2008)	Bovine cancellous bone, cylinder (Ø = 10 mm, H = 5 mm)	Bone cells in bovine cancellous bone	Continuous 10 µl/min	0.4% strain, 1 Hz, 300 cycles daily for 3 weeks	Perfusion + compression: increased osteoblast differentiation, trabecula, Young's Modulus, ultimate force
(Appelman *et al.*, 2009)	PEG-Proteoglycan (PP), PEG-Fibrinogen (PF), PEG-Albumin (PA), and PEG BGS	Primary articular chondrocytes	Not mentioned	1 day of free swelling, then 15% strain, 1 Hz, 3 times for 1 hr on and 2 hrs off each day for 27 days stimulation	Increased BGS compressive modulus
(Baas *et al.*, 2010)	Poly (l-lactic acid) porous BGS, porosity: 90%	Primary rat bone cells	Continuous 0.1 ml/min	1.5% strain, 1 Hz, 3 times for 1 hr on and 2 hrs off per day for 28 days	Perfusion + compression: increased mineralized nodules, average of absolute principal strain at nodule sites

	pore size: 250 - 350 µm, cylinder (Ø = 9 mm, H = 4 mm)				
(C X Liu *et al.*, 2012)	polyurethane (PU)-based meniscus BGS (Actifit®), pore size 150 - 355 µm	hMSC	Continuous 10 ml/min	10% strain, 0.5 Hz, 4 times/day, 2 h/time with 4 hours of rest; 1 time/day, 8 h/time 24 h, 1 week and 2 weeks	Perfusion: increased proliferation, type III procollagen synthesis Perfusion + on-off compression: increased proliferation, equilibrium modulus, type I procollagen

In previous studies, most of *in vitro* mechanical stimulation has shown to increase ALP activity, however, there are studies report various effects of mechanical stimulation on ALP activity. For example, rat marrow stromal cells and osteoblastic cells stimulated by flow induced shear stress were observed to have significantly increased ALP activity compared with static culture (Goldstein *et al.*, 2001; Sikavitsas *et al.*, 2003; Sikavitsas *et al.*, 2005; Bancroft *et al.*, 2002; Holtorf, Sheffield, *et al.*, 2005). Du et al observed that the specific ALP activity of MC3T3-E1 cells did not differ significantly between the unidirectional perfusion culture and the static culture, and was significantly higher in the oscillatory flow perfusion group than in the unidirectional flow perfusion group (Du *et al.*, 2009). Rat calvarial osteoblasts subjected to fluid flow expressed lower *alp* mRNA especially under pulsatile fluid flow (Roelofsen *et al.*, 1995). In the current study, specific ALP activity was not dependent on perfusion or compression, and the specific ALP activity of MG63 cells on SiHA-22 BGS granules was several magnitude lower than the specific ALP activity of rat osteoblastic cells from marrow tissue or osteoblast-like MC3T3-E1 cells reported in previous studies (Goldstein et al., 2001; Du et al., 2008). Although MG63 osteosarcoma cells have some features of osteoblasts, they differ in proliferation kinetics and differentiation. The differentiation ability of MG63 cells, particularly specific ALP activity and mineralization were then investigated. The results of current study showed that the specific ALP activity of MG63 cells was very low and it did not increase until 25 days of culture. No extracellular calcium deposition by MG63 cells was observed.

By performing a systematic comparison of MG-63, HOS TE85 and human bone derived cells, Clover observed that the ALP activity of MG-63 cells was significantly lower than human bone derived cells after 4 days under both basal condition and 1,25-dihydroxyvitamin D_3 ($1,25(OH)_2D_3$) administration (Clover and Gowen, 1994). Pautke found that no ALP activity could be detected in MG-63 cells (Pautke *et al.*, 2004). Czekanska also observed that the maximum level of ALP activity of MG-63 by day 28, was ~ 26 fold lower compared to human osteoblasts at the same point (Czekanska *et al.*, 2014). MG63 cells formed a cell layer with evident nodules after 14 days of culture, however, no calcium deposition within the extracellular matrix was

seen during 28 days of culture. These results together indicated that cell lines could be useful for specific studies, but cell lines do not reflect the behaviour of primary cells and must be used with caution. MG63 cells were not a very good model in investigating the differentiation of cells induced by mechanical stimulation or osteoconductivity of BGS. Mesenchymal stem cells (MSCs) are mechanosensitive and mechanotransduction in MSCs has been proved to induce trabecular bone formation (Curtis *et al.*, 2018). Human bone marrow derived mesenchymal stem cells (hMSCs) have been widely used in investigating the cellular response to mechanical stimulation (Meinel *et al.*, 2004; Grayson *et al.*, 2008) , and hMSCs based therapy has emerged as a novel branch regenerative medicine, with more than 500 registered clinical trials worldwide in the last 10 years (Bunpetch *et al.*, 2017). Therefore, hMSCs were characterized and used in subsequent *in vitro* experiment.

3.5 Conclusion

The work in this chapter optimized the seeding parameters for seeding MG63 cells onto SiHA BGS granules in the perfusion chamber of a 3D bioreactor system, which is the first and crucial step for cells growth in a mechanical stimulation environment. A 3D bioreactor system which allow the application of shear stress and compression at the same time was built, and MG63 cells have been found to respond to both shear stress and mechanical loading in terms of proliferation and gene expression. However, a 3D bioreactor system that can precisely control compression force on BGS granules should be designed and used for future work. Cellular differentiation, particularly specific ALP activity is an important indicator in investigating the cellular response to mechanical stimulation. However, MG63 cells were found to have very low specific ALP activity, and it was not dependent on the environment such as mechanical stimulation, chemical stimulation and culture period. Therefore, hMSCs were used in subsequent *in vitro* experiment, considering their differentiation ability, response to the environment and potential clinical applications.

Chapter 4 Structural Guidance of 3D SiHA BGS on hMSCs Proliferation and Differentiation

4.1 Introduction

Using three dimensional BGS for the treatment of bone repair is a rapidly emerging field (Langer and Vacanti, 1993; Service, 2000; Hutmacher *et al.*, 2007; Shahrezaie *et al.*, 2018). So far, highly porous bioceramics represent the standard for generating osteoconductive BGS (Gauthier *et al.*, 1998; Boyde *et al.*, 1999; Chang *et al.*, 2000; Marcacci *et al.*, 2007; Sweedy *et al.*, 2018), as interconnected macro-pores (>100 μm) are necessary for blood vessels invasion and bone matrix deposition in empty space. Macro-pore size, macro-porosity (the volume fraction of macro-pores) and the interconnectivity of macro-pores have been demonstrated to have a strong impact on bone ingrowth. For example, an *in vivo* study of hydroxyapatite (HA) BGS with identical microstructure but different macro-pore structure has demonstrated that macro-porosity and pore interconnection of the BGS influenced the amount of deposited bone and kinetics of bone formation (Mastrogiacomo *et al.*, 2006). Based on early work (Hulbert *et al.*, 1970), it is widely believed that interconnected size of pores larger than 100 μm are necessary due to cell size, migration requirements and nutrient transport. The recommended macro-pore size is larger than 300 μm to achieve enhanced new bone formation (Gauthier *et al.*, 1998; Kuboki *et al.*, 2001; Karageorgiou and Kaplan, 2005). Although high macro-porosity BGS has the potential to facilitate bone ingrowth, it should be borne in mind that increasing porosity decreases mechanical properties, so the two have to be carefully balanced.

Incorporation of micro-pores (<30 μm), in the struts or walls of macro-porous BGS has been demonstrated to improve osteoblast anchorage and attachment on HA BGS surface at the early time points *in vitro* experiments (Annaz *et al.*, 2004b). Increased levels of micro-porosity (the volume fraction of micro-pores) in HA BGS was found to facilitate earlier neovascularization (Hing *et al.*, 2004), thicker trabeculae of new bone (Hing *et al.*, 2005), and a greater volume of bone formation (Coathup *et al.*, 2012) *in vivo*. One explanation that micro-pore structure promoted BGS performance is that micro-pores allow cellular infiltration, which increases biological fixation and

thereby results in improved mechanical interlock between the cells and the surface of the substrate (Bignon *et al.*, 2003; Annaz *et al.*, 2004a). Another mechanism that has been proposed recently is that micro-pores induced capillarity drive of cells, blood, or marrow components deep into the BGS pores and therefore enhance bone distribution *in vivo* (Rustom *et al.*, 2016). This is in line with the findings from literature that micro-porosity of calcium phosphate - based BGS can result in multiscale osteointegration, and thus a composite material (Lan Levengood *et al.*, 2010).

In the body, human mesenchymal stem cells (hMSCs) are known to migrate to a wound site and become incorporated into certain tissues and assist tissue repair or regeneration either through the secretion of chemokines or by differentiation into the mature native cell (Parekkadan and Milwid, 2010). hMSCs have the ability to differentiate towards the osteogenic lineage, so they have great potential for clinical applications for bone regeneration (Koç and Lazarus, 2001). The differentiation of hMSCs is likely to be initiated and directed by cues from the local microenvironment, such as soluble factors and topography of extracellular matrix. Therefore, the response of hMSCs to the geometric structure of a BGS is crucial to evaluate the osteoconductivity of that BGS. There are few studies investigating the effect of porosity on proliferation and osteogenic differentiation of hMSCs. Gomes found that a starch-based mesh BGS with 75% macro-porosity demonstrated significantly enhanced MSCs proliferation and higher specific ALP activity under perfusion condition compared with the BGS with 50% macro-porosity (Manuela E. Gomes *et al.*, 2006). Kasten found that specific ALP activity of hMSCs was not dependent on the macro-porosity (Kasten *et al.*, 2008). Presence of micro-pores in calcium phosphate BGS has been demonstrated to stimulate osteogenic differentiation of stem cells *in vitro* and bone formation *in vivo*, respectively (Yuan *et al.*, 2010). Enhanced micro-porosity in silicate-substituted calcium phosphate has proven stimulate osteogenic differentiation of hMSCs (De Godoy *et al.*, 2015)

Multiscale silicate substituted hydroxyapatite (SiHA) BGS, with both micro-pores and macro-pores, have excellent biocompatibility (Patel *et al.*, 2002; Hing *et al.*, 2006). However, the combined influence of micro-porosity and total porosity (the total

volume fraction of macro-pores and micro-pores) in SiHA BGS on hMSCs differentiation has not been investigated. The aim of this study was to synthesise and characterise a group of SiHA BGS with equivalent levels of total porosity, but different levels of micro-porosity and another group of SiHA BGS with equivalent levels of micro-porosity but different levels of total porosity. *In vitro* studies were performed to systematically investigate the influence of SiHA BGS structure on the proliferation and differentiation of hMSCs in different medium types and to choose the BGS structure and medium type in further perfusion study.

4.2 Materials and Methods

Irregularly shaped SiHA granules (ϕ: 1-2 mm) were synthesised using a slip foaming technique, as described in Chapter 2.1, which enabled independent control of the level of total porosity and the level of micro-porosity. 5 batches of SiHA granules were produced to enable investigation of changes in both total porosity and micro-porosity with designed porosity values as shown in Table 4-1.

Table 4-1 Designed total porosity and micro-porosity of SiHA BGS.

		Designed micro-porosity (%)		
		10	20	30
Designed total porosity (%)	60		✔	
	70		✔	
	80	✔	✔	✔

1 million of hMSCs in a 500 µl cell suspension (concentration: 2×10^6 cells/ml) were seeded per 1 cm^3 (0.47 ± 0.03 g) of SiHA BGS granules in 24 well-plates. After hMSCs had attached to BGS granules (2 hours), hMSCs were kept in static condition in 24 well-plates in 1.5 ml MSC growth medium 2 (PromoCell). After one day, the culture medium was replaced with one of 4 types of medium: 1) PM: MSC growth medium 2; 2) PMO: PM supplemented with osteogenic induction medium (0.1 µM dexamethasone, 0.05 mM ascorbic acid and 10 mM β-glycerophosphate (Sigma-Aldrich); 3) BM: basic cell culture medium (BM, as per Table 2-2) consisting of high glucose Dulbecco's modified Eagle Medium (DMEM) with 10% fetal bovine serum

(FBS) and 1% penicillin-streptomycin (Sigma-Aldrich); 4) BMO: BM supplemented with osteogenic induction medium. The medium was changed every 2 days thereafter. After 3, 7, and 10 days of culture, total DNA amount and specific ALP activity of hMSCs from each BGS were tested as described in Chapter 2.5 and Chapter 2.6.

4.3 Results

4.3.1 BGS Characterisation

In the group of SiHA BGS with equivalent amount of total porosity (80.9 ± 1.9%), their actual micro-porosities were listed in Table 4-2. As depicted in Figure 4-1 (a), (c) and (e), BGS SiHA-14, SiHA-22 and SiHA-28 was found to have similar macro-pore structure, while the micro-pore volume fraction was varied significantly that SiHA-14 has nominal micro-porosity of 14% (Figure 4-1 (b)), SiHA-22 has nominal micro-porosity of 22% (Figure 4-1 (d)), and SiHA-28 has nominal micro-porosity of 28% (Figure 4-1 (f)). Phase purity of SiHA-14, SiHA-22 and SiHA-28 after sintering were verified using X-ray diffractometry (Figure 4-2).

Table 4-2 The actual micro-porosity of BGS SiHA-14, SiHA-22 and SiHA-28.

	SiHA-14 (%)	SiHA-22 (%)	SiHA-28(%)
Micro-porosity	13.5 ± 0.7	22.4 ± 0.5	28.2 ± 2.7

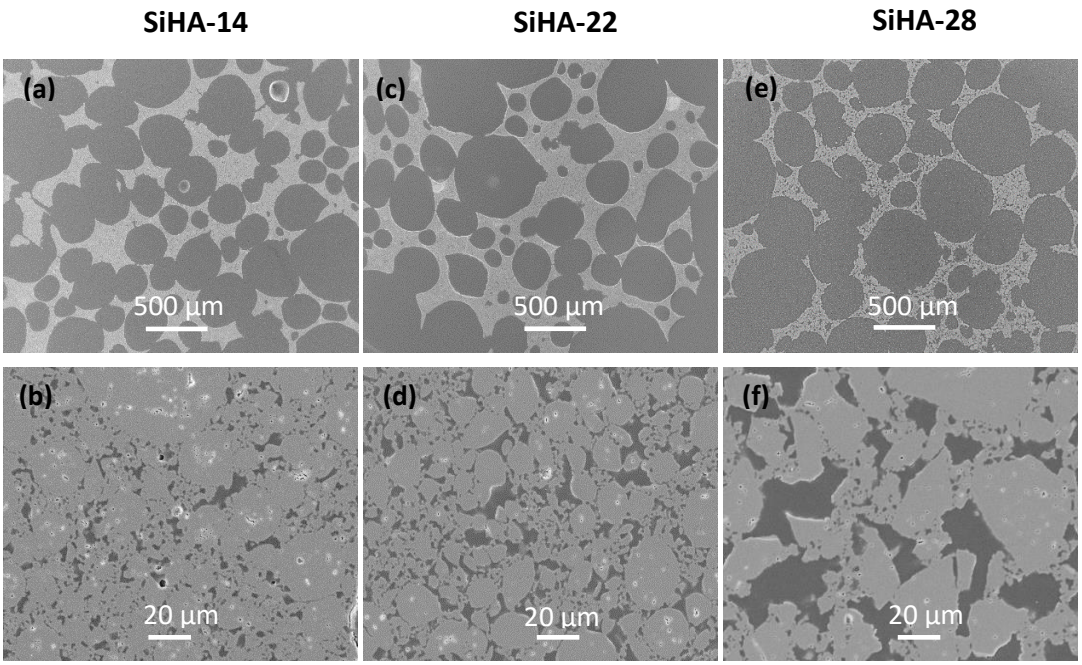

Figure 4-1 Macro-pore structure (a) and micro-pore structure (b) of SiHA-14; macro-pore structure (c) and micro-pore structure (d) of SiHA-22; macro-pore structure (e) and micro-pore structure (f) of SiHA-28.

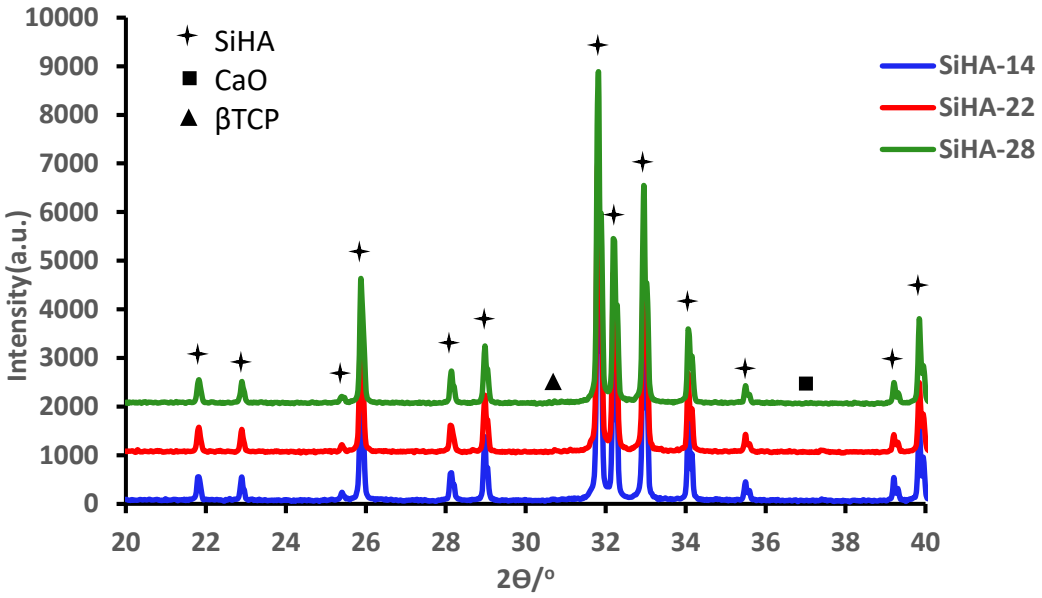

Figure 4-2 XRD patterns of SiHA-14, SiHA-22 and SiHA-28 BGS.

In the group of SiHA BGS with equivalent amount of micro-porosity (21.5 ± 1.4%), their total porosities were listed in Table 4-3. As can be seen in Figure 4-3 (b), (d) and (f), BGS SiHA60, SiHA70 and SiHA80 was found to have similar micro-pore structure, while the macro-pore volume fraction varied (Figure 4-3 (a), (c) and (e)), which results in the total porosity varied that SiHA60 has nominal total porosity of 60%, SiHA70 has nominal total porosity of 70% and SiHA80 has nominal total porosity of 80%. Phase purity of SiHA60, SiHA70 and SiHA80 after sintering were verified using X-ray diffractometry (Figure 4-4).

Table 4-3 The actual total porosity of BGS SiHA60, SiHA70 and SiHA80.

	SiHA60 (%)	SiHA70 (%)	SiHA80 (%)
Total porosity	61.8 ± 1.7	70.8 ± 0.4	80.4 ± 0.5

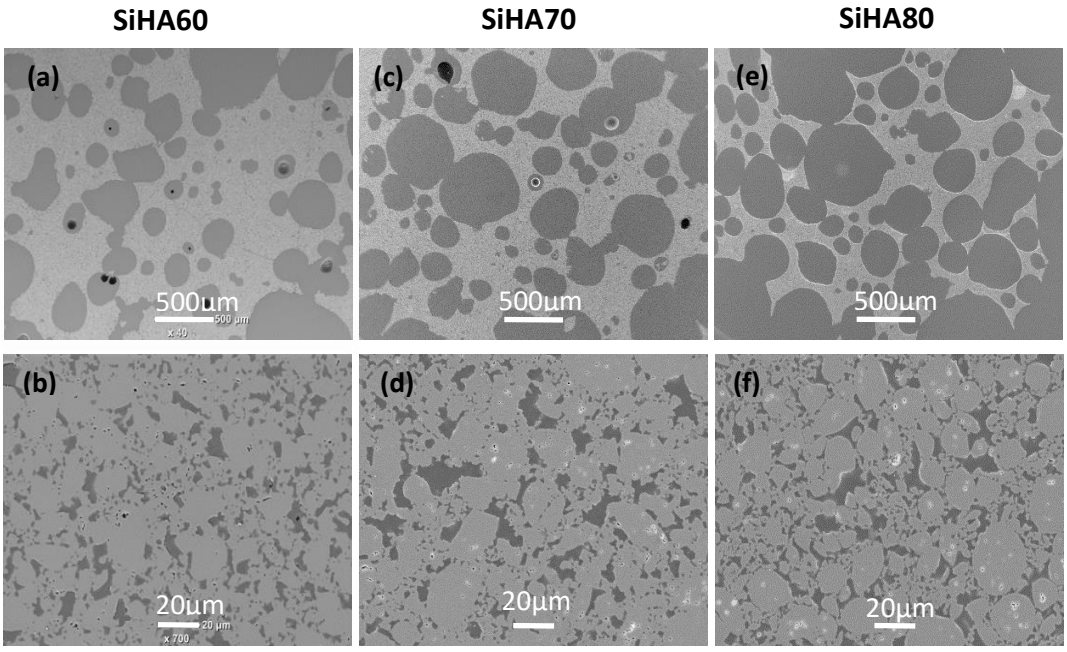

Figure 4-3 Macro-pore structure (a) and micro-pore structure (b) of SiHA60; macro-pore structure (c) and micro-pore structure (d) of SiHA70; macro-pore structure (e) and micro-pore structure (f) of SiHA80.

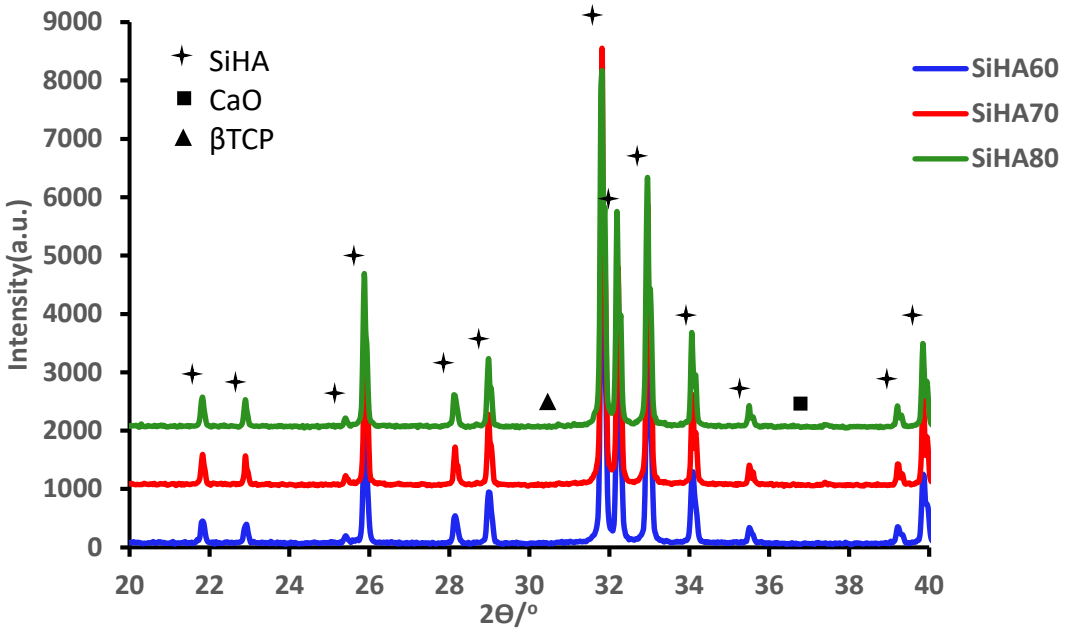

Figure 4-4 XRD patterns of SiHA60, SiHA70 and SiHA80 BGS.

4.3.2 DNA and specific ALP Activity of hMSCs on BGS with Equivalent Levels of Total Porosity and Different Micro-porosities in Different Culture Medium

To evaluate hMSCs proliferation on BGS with different micro-porosity, total DNA of hMSCs from cell lysate was quantified. As can be seen in Figure 4-5 (a), in PM medium, at day 3, the DNA content was significantly lower on SiHA-28 as compared to SiHA-14 and SiHA-22, while at day 7 and day 10, there was no significant difference in DNA content on all three types of BGS irrespective of micro-porosity. In PM medium, the DNA content of hMSCs increased significantly from day 3 to day 7 on SiHA-28 BGS, and there was no significant difference in DNA compared with day 7 to day 3 on both SiHA-14 and SiHA-22. In PM medium, at day 10, the DNA content of hMSCs was found to be significantly higher compared with day 3 on SiHA-22 and SiHA-28, but not SiHA-14 BGS.

As can be seen in Figure 4-5 (b), in PMO medium, at day 3, the DNA content was significantly lower on SiHA-28 compared with SiHA-14, while at day 7 and day 10, there was no significant difference in DNA content on all three types of BGS irrespective of micro-porosity. In PMO medium, there was no significant difference

in DNA content at day 7 compared with day 3 on all three types of BGS irrespective of BGS micro-porosity. In PMO medium, the DNA content of hMSCs increased significantly from day 7 to day 10 on both SiHA-22 and SiHA-28 BGS, but not SiHA-14 BGS. In PMO medium, at day 10, the DNA content of hMSCs was significantly higher compared with day 3 on SiHA-28 BGS, and there was no significant difference in DNA compared with day 10 to day 3 on SiHA-14 BGS and SiHA-22 BGS.

As can be seen in Figure 4-5 (c), in BM medium, at day 3, the DNA content was significantly lower on SiHA-28 compared with SiHA-14 and SiHA-22, while at day 7 and day 10, there was no significant difference in DNA content on all three types of BGS irrespective of micro-porosity. In BM medium, there was no significant difference in DNA content found at any of the time points, irrespective of BGS micro-porosity.

As can be seen in Figure 4-5 (d), in BMO medium, at day 3, the DNA content was significantly lower on SiHA-28 compared with SiHA-14 and SiHA-22, while at day 7 and day 10, there was no significant difference in DNA content on all three types of BGS irrespective of micro-porosity. In BMO medium, the DNA content of hMSCs on SiHA-14 BGS was found to be significantly decreased at both day 7 and day 10 compared with day 3. In contrast, in BMO medium, there was significant increase in DNA content from day 7 to day 10 on SiHA-28 BGS.

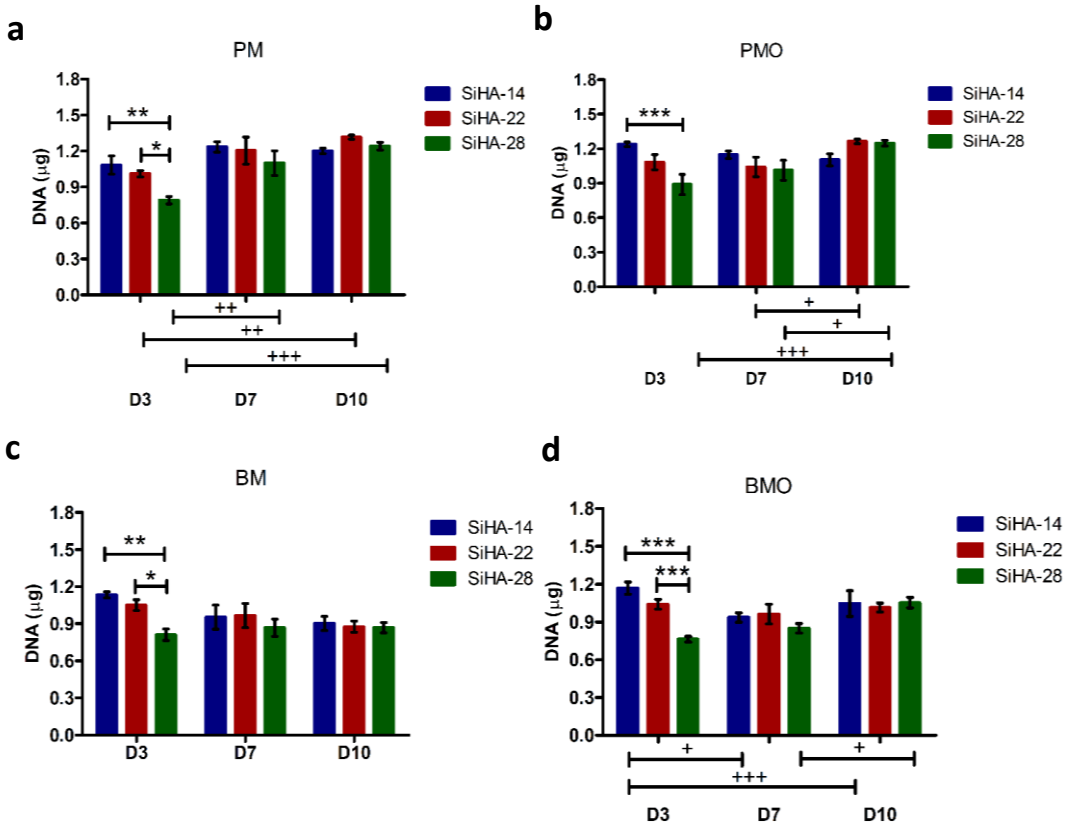

Figure 4-5 DNA content of hMSCs on different BGS cultured in (a) PM, (b) PMO, (c) BM and (d) BMO medium. Results are presented as mean ± standard deviation (n>=3). Statistical analysis was performed by two-way ANOVA followed by Bonferroni post-tests. *p < 0.05, **p < 0.01, ***p < 0.001, comparison between SiHA-14, SiHA-22 and SiHA-28. +p < 0. 05, ++p < 0.01, +++p < 0.001, comparison between D3, D7 and D10.

Specific ALP activity is an early marker of osteoblast differentiation towards osteoblastic phenotype. To investigate the response of hMSCs differentiation to BGS micro-porosity in different culture medium, specific ALP activity from cell lysate at day 3, day 7 and day 10 were tested and normalized by DNA content. As can be seen in Figure 4-6 (a), in PM medium, the specific ALP activity was not found to be responsive to BGS micro-porosity at any of the three time points. In PM medium, the specific ALP activity of hMSCs increased significantly from day 3 to day 7, and then further increased significantly from day 7 to day 10, with specific ALP activity being the highest at day 10 on any of the three types of BGS.

As can be seen in Figure 4-6 (b), in PMO medium, the specific ALP activity was not found to be responsive to BGS micro-porosity at both day 3 and day 7, whereas at day 10, specific ALP activity increased significantly with increasing BGS micro-porosity. In PMO medium, the specific ALP activity of hMSCs was found to be

significantly higher at both day 7 and day 10 compared with day 3, irrespective of the BGS micro-porosity. In PMO medium, the specific ALP activity of hMSCs was found to be significantly higher at day 10 compared with day 7 on both SiHA-22 and SiHA-28, but not SiHA-14 BGS.

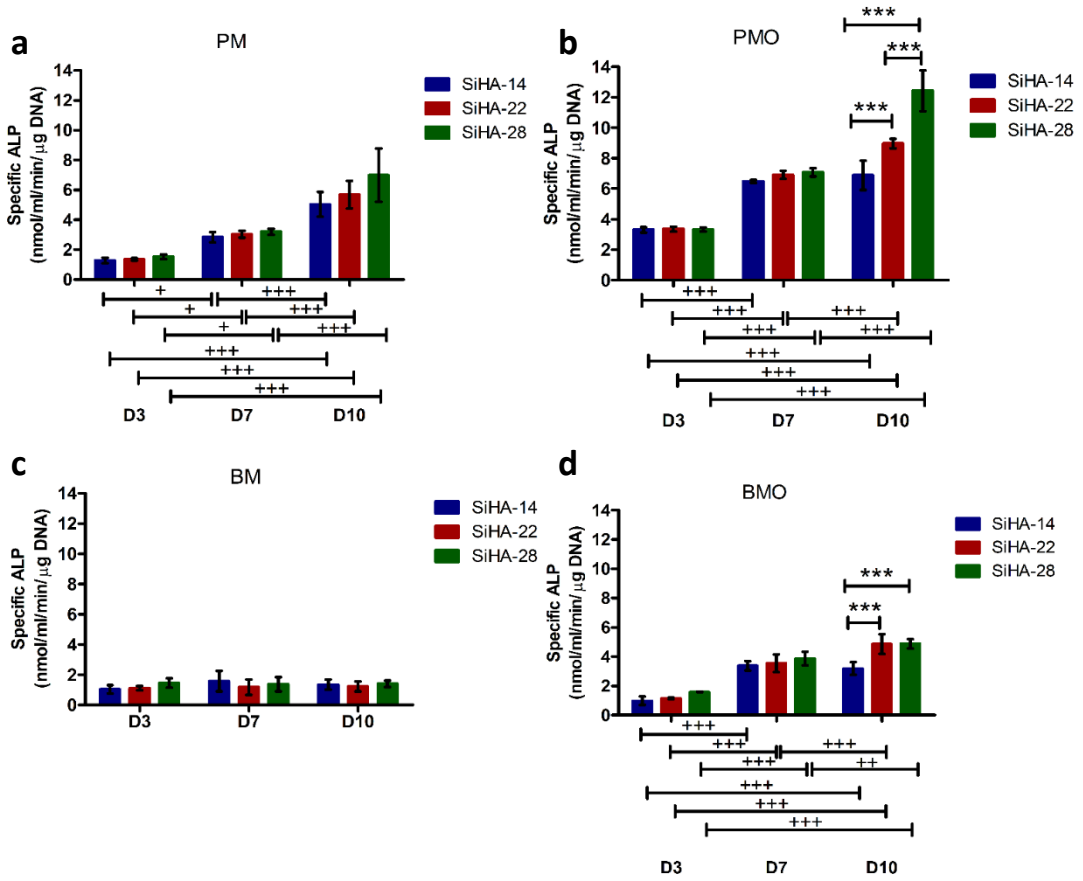

Figure 4-6 Specific ALP activity of hMSCs on BGS cultured in (a) PM, (b) PMO, (c) BM and (d) BMO medium. Results are presented as mean ± standard deviation (n>=3). Statistical analysis was performed by two-way ANOVA followed by Bonferroni post-tests. *p < 0.05, **p < 0.01, ***p < 0.001, comparison between SiHA-14, SiHA-22 and SiHA-28. +p < 0. 05, ++p < 0.01, +++p < 0.001, comparison between D3, D7 and D10.

As can be seen in Figure 4-6 (c), in BM medium, the specific ALP activity was not found to be dependent on BGS micro-porosity at any of the three time points. In BM medium, the specific ALP activity was also found not to be dependent on culture period on any of the three types of BGS.

As can be seen in Figure 4-6 (d), in BMO medium, the specific ALP activity was not found to be responsive to BGS micro-porosity at both day 3 and day 7, whereas at day 10, specific ALP activity was significantly higher on both SiHA-22 and SiHA-28 as

compared to SiHA-14 BGS. In BMO medium, the specific ALP activity of hMSCs was found to be significantly higher at both day 7 and day 10 compared with day 3 irrespective of the BGS micro-porosity. In BMO medium, the specific ALP activity of hMSCs was found to be significantly higher at day 10 compared with day 7 on both SiHA-22 and SiHA-28, but not SiHA-14 BGS.

4.3.3 DNA and specific ALP Activity of hMSCs on BGS with Equivalent Levels of Micro-porosity and Different Total Porosities in Different Culture Medium

In PM medium, at both day 3 and day 7, DNA content of hMSCs was not found to be dependent on BGS total porosity (i.e SiHA60, SiHA70 and SiHA80), whereas at day 10, the DNA content was significantly higher on SiHA80 BGS than SiHA60 BGS, as can be seen in Figure 4-7 (a). In PM medium, the DNA content of hMSCs increased significantly from day 3 to day 7 on SiHA70 and SiHA80, but not SiHA60 BGS. In PM medium, the DNA content of hMSCs was significantly higher at day 10 compared with day 3 on SiHA80 BGS, and there was no significant difference in DNA content at day 10 compared with day 3 on SiHA60 and SiHA70 BGS.

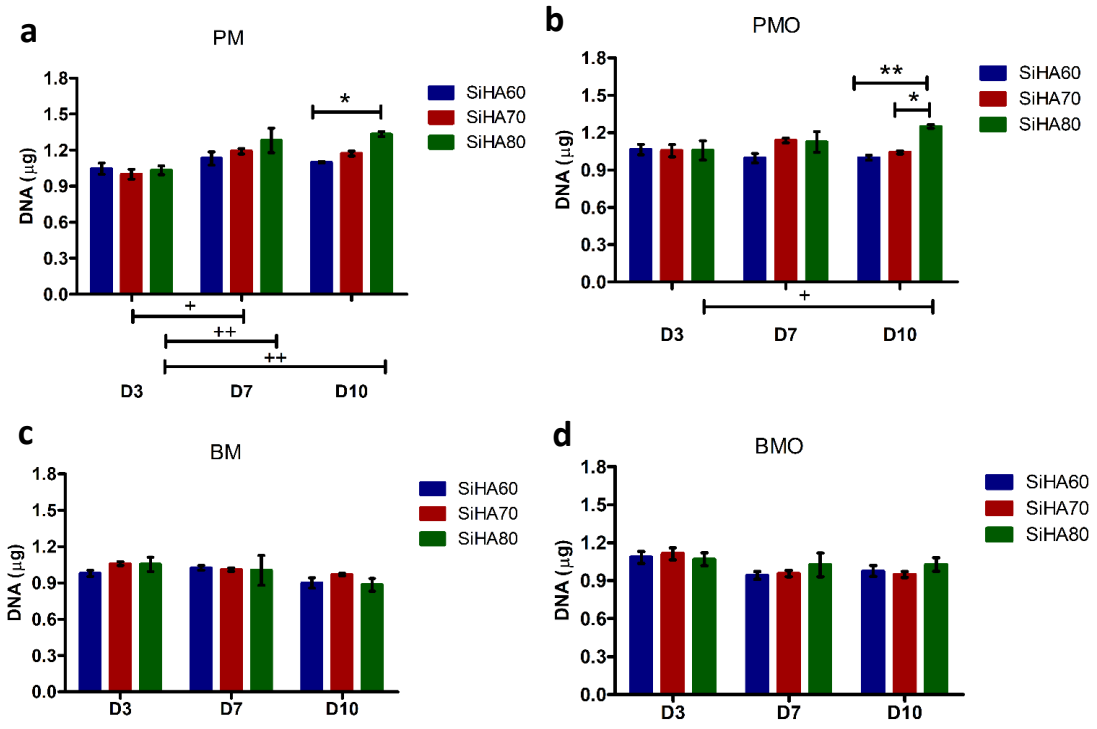

Figure 4-7 DNA content of hMSCs on BGS cultured in (a) PM, (b) PMO, (c) BM and (d) BMO medium. Results are presented as mean ± standard deviation (n>=3). Statistical analysis was performed by two-way ANOVA followed by Bonferroni post-tests. *p < 0.05, **p < 0.01, ***p < 0.001, comparison between SiHA60, SiHA70 and SiHA80. +p < 0. 05, ++p < 0.01, +++p < 0.001, comparison between D3, D7 and D10.

As can be seen in Figure 4-7 (b), in PMO medium, at both day 3 and day 7, DNA content of hMSCs was not found to be dependent on BGS total porosity, whereas at day 10, the DNA content was significantly higher on SiHA80 BGS than SiHA60 and SiHA70 BGS. In PMO medium, there was no significant difference in DNA content from day 3 to day 7, or from day 7 to day 10 irrespective of BGS total porosity. In PMO medium, the DNA content of hMSCs was significantly higher at day 10 compared with day 3 on SiHA80 BGS, however, DNA content of hMSCs was not significantly different at day 10 compared with day 3 on SiHA60 and SiHA70 BGS.

As can be seen in Figure 4-7 (c) and (d), in both BM and BMO medium, the DNA content of hMSCs was not dependent on BGS total porosity at any of the three time points.

As can be seen in Figure 4-8 (a), in PM medium, the specific ALP activity was not found to be dependent on BGS total porosity at any of the three time points. In PM medium, the specific ALP activity of hMSCs increased significantly from day 3 to day

7, and then further increased significantly from day 7 to day 10, with specific ALP activity being the highest at day 10 on any of the three types of BGS.

As can be seen in Figure 4-8 (b), in PMO medium, at day 3, the specific ALP activity was not found to be dependent on BGS total porosity, whereas at both day 7 and day 10, the specific ALP activity was significantly higher on SiHA80 compared with SiHA60 and SiHA70 BGS. In PMO medium, the specific ALP activity of hMSCs increased significantly from day 3 to day 7, and then further increased significantly from day 7 to day 10, with specific ALP activity being the highest at day 10 on any of the three types of BGS.

As can be seen in Figure 4-8 (c), in BM medium, the specific ALP activity was not found to be dependent on BGS total porosity at any of the three time points. In BM medium, the specific ALP activity of hMSCs increased significantly from day 3 to day 7, on SiHA60 and SiHA70, but not SiHA80 BGS. In BM medium, there was no significant difference in specific ALP activity at day 10 compared with day 7 irrespective BGS total porosity. In BM medium, the specific ALP activity of hMSCs was significantly higher at day 10 compared with day 3 on SiHA22 BGS, however, there was no significant difference in specific ALP activity of hMSCs at day 10 compared with day 3 on SiHA60 and SiHA70 BGS.

As can be seen in Figure 4-8 (d), in BMO medium, at both day 3 and day 7, the specific ALP activity was not found to be dependent on BGS total porosity, however at day 10, the specific ALP activity of hMSCs was significantly higher on SiHA-70 and SiHA80 BGS than SiHA60 BGS. In BMO medium, the specific ALP activity of hMSCs was found to be significantly higher at day 7 and day 10 compared with day 3 irrespective of the BGS total porosity. In BMO medium, the specific ALP activity of hMSCs was found to be significantly higher at day 10 compared with day 7 on both SiHA70 and SiHA80, but not SiHA60 BGS.

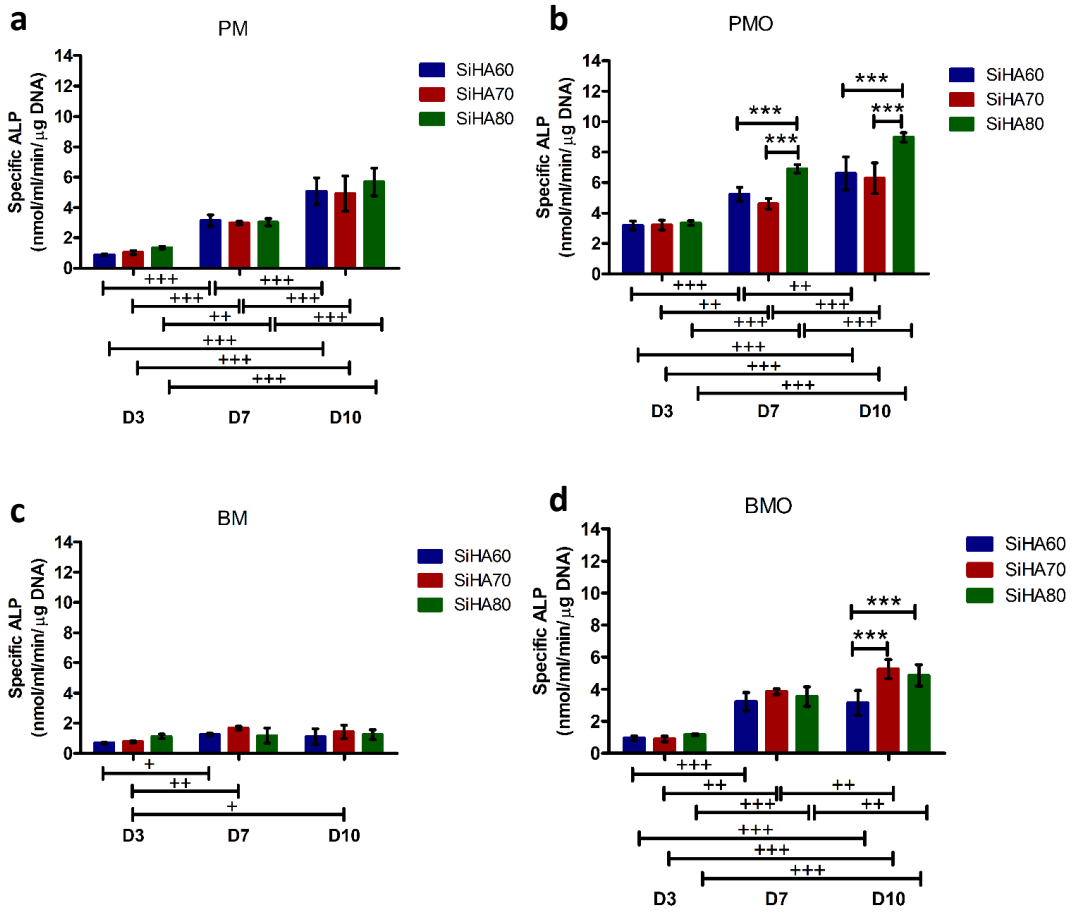

Figure 4-8 Specific ALP activity of hMSCs on BGS cultured in (a) PM, (b) PMO, (c) BM and (d) BMO medium. Results are presented as mean ± standard deviation (n>=3). Statistical analysis was performed by two-way ANOVA followed by Bonferroni post-tests. *p < 0.05, **p < 0.01, ***p < 0.001, comparison between SiHA60, SiHA70 and SiHA80. +p < 0. 05, ++p < 0.01, +++p < 0.001, comparison between D3, D7 and D10.

4.4 Discussion

Cell behaviour is directly affected by the BGS architecture, which provides cues that influence the specific integrin-ligand interactions between cells and the surroundings and thereby influence cell proliferation or direct cell differentiation (Murphy *et al.*, 2010; Loh and Choong, 2013). SiHA BGS with equivalent levels of total porosity, micro-porosity level altered hMSCs proliferation at day 3, where DNA content was significantly higher on SiHA-14 as compared to SiHA-28, in all of the four types of culture medium. Ma *et al.* also observed that the initial cell proliferation rate in the low porosity matrix was greater than those in the high porosity matrix (Ma *et al.*, 2000). One possible explanation is that SiHA-14 BGS has a greater number of small size of micro-pores (< 5 μm) compared with SiHA-28 BGS, which provided a more

suitable substrate for cell anchorage and attachment, leading to earlier hMSCs proliferation. This hypothesis is supported by previous study that an affinity was observed between the fidopillia of human osteoblasts-like cells and micro-pores *in vitro* (Annaz *et al.*, 2004b), and MC3TE-E1 cells were observed to attach and grow into micro-pores in the inner surface (Li *et al.*, 2005), respectively. However, at day 7 and day 10, hMSCs were not dependent on BGS with different micro-porosities, indicating that the micro-porosity level in SiHA BGS did not have an impact on late stage cell proliferation.

At both day 3 and day 7, the specific ALP activity of hMSCs was not altered by micro-porosity irrespective of the types of culture medium. However, at day 10, in PMO and BMO medium, BGS with high micro-porosity (SiHA-22 and SiHA-28) supported significantly increased levels of specific ALP activity in hMSCs as compared to the SiHA-14 BGS about 22%. This finding demonstrated that SiHA BGS with higher levels of micro-porosity had a greater potential to support hMSCs differentiation than those with lower levels of micro-porosity, but this needs a longer culture period and osteogenic supplements in the culture medium. It is possible that increasing the permeability of struts within the porous BGS increased physical accessibility of nutrients to support proliferation and differentiation. Higher surface area in SiHA BGS with higher levels of micro-porosity may also increase the osteogenic protein binding capacity and therefore increase the osteogenic differentiation capacity. It is worth mentioning that, in BM medium, the specific ALP activity of hMSCs did not increase significantly through the 10 days of culture, whereas in PM medium, the specific ALP activity of hMSCs increased significantly from day 3 to day 7 and from day 7 to day 10 irrespective of the levels of micro-porosity of SiHA BGS, which indicated that there might be some growth factors in PM medium that enhance hMSCs osteogenic differentiation. Unfortunately, the manufactures would not divulge the component of PM medium.

At both day 3 and day 7, DNA content of hMSCs was not found to be responsive to the total porosities of SiHA BGS irrespective the types of culture medium, whereas at day 10, in both PM and PMO medium, DNA content of hMSCs was significantly higher on SiHA80 BGS compared with SiHA60 BGS. This may be due to the fact that there

was greater number of macro-pores in SiHA80 BGS compared with SiHA60 BGS, also, macro-pores and pore interconnection in SiHA80 are likely to be bigger, which facilitated nutrient transportation and thereby increased hMSCs proliferation. This observation is in line with previous study that the absolute volume of bone ingrowth was consistently higher on HA BGS with higher total porosity (Hing *et al.*, 2002).

In both PM and BM medium, the specific ALP activity of hMSCs was not found to be responsive to BGS with different total porosities at any of the time points. However, in BMO medium, at day 10, the BGS with highest total porosity (SiHA80) was found to support significantly increased levels specific ALP activity in hMSCs compared with SiHA60, and in PMO medium, at both day 7 and day 10, SiHA80 was again found to support significantly increased levels of specific ALP activity of hMSCs as compared with SiHA60. The increased surface area or enhanced permeability due to greater levels of pore connectivity in SiHA80 BGS enhanced hMSCs proliferation and thereby advanced hMSCs proliferation and specific ALP activity.

4.5 Conclusion

Porosity influences cell spreading and cell ingrowth in BGS materials. SiHA BGS with equivalent level of total porosity but different levels of micro-porosities and SiHA BGS with equivalent level of micro-porosity but different levels of total porosities were synthesised, characterised and tested *in vitro*. All SiHA BGS types irrespective of micro-porosity and total porosity were found to be suitable for hMSCs to grow and differentiate. From all the combinations of micro-porosity and macro-porosity tested, it would appear that rapid cell attachment may be favoured on surfaces with lower levels of micro-porosity (SiHA-14). However, hMSCs growth and differentiation were supported by BGS with greater levels of micro-porosity (SiHA-22 and SiHA-28) and the highest levels of total porosity (SiHA80) in osteogenic supplemented culture medium. The response of hMSCs differentiation to BGS micro-porosity was found in osteogenic medium, especially PMO. To investigate the response of hMSCs differentiation to BGS structure and mechanical forces, hMSCs were cultured on BGS with different micro-porosity in PMO medium in perfusion bioreactor.

Chapter 5 Synergistic Effect of BGS Micro-porosity and Perfusion Culture on Differentiation of Human Mesenchymal Stem Cells (hMSCs)

5.1 Introduction

Synthetic hydroxyapatite (HA) bone substitutes have been increasingly used in bone repair due to their excellent biocompatibility (Bowen *et al.*, 1989; Yoshikawa *et al.*, 1996; Chu *et al.*, 2002; Woodard *et al.*, 2007; Tripathi and Basu, 2012; Xia *et al.*, 2016). Silicate substituted hydroxyapatite (SiHA) has proven to be particularly promising due to accelerated bone apposition, higher bone ingrowth and bone coverage on SiHA as compared to HA (Patel *et al.*, 2002; Hing *et al.*, 2006). There have been numerous studies conducted to investigate the effect of the parameters of geometric structure of BGS on bone repair, including pore size, total porosity, micro-porosity, and pore shape (Hing *et al.*, 2002; Mastrogiacomo *et al.*, 2006; Sweedy *et al.*, 2018). Specifically, increasing micro-porosity has been shown to support bone-like apatite precipitation, encourage early neovascularization and increase absolute new bone volume (Hing *et al.*, 2005; Campion *et al.*, 2013; Campion *et al.*, 2011; Coathup *et al.*, 2012).

It is well known that mechanical loading plays an important role in bone remodelling and fracture healing (Lanyon and Rubin, 1984; Lanyon, 1993; Robling *et al.*, 2002; Boerckel *et al.*, 2012). For example, compression loading of bone during walking results in non-uniform strains macroscopically. The associated pressure differences within the interconnected canalicular network cause interstitial fluid flow, which imparts shear stresses on the cells (Hillsley and Frangos, 1994). As a result, essential cellular functions and BGS properties that present *in vivo* are missing by using traditional static culture method. Perfusion culture that mimics the concept of mechanical loading has been widely used to improve viability, cell distribution, differentiation, matrix synthesis and functionality of tissue engineered constructs (Bancroft *et al.*, 2002; Wang *et al.*, 2003; Braccini *et al.*, 2005; Papadimitropoulos *et al.*, 2014). It also has the advantage of bridging the gap between static culture and *in*

vivo test with respect to evaluating the bioactivity of the BGS under more relevant physiological conditions.

The cylindrical pore model approach of Goldstein et al. (Goldstein *et al.*, 2001) has been widely used to estimate the shear stress (τ_w) on cells seeded on the BGS (μ: the viscosity of the culture medium, d: the mean pore size of the BGS, and Vm: mean velocity through the pores).

$$\tau_w = 8\mu V_m/d$$

Assuming flow was distributed uniformly across the BGS surface with diameter, the mean velocity (Vm) through the pores can be calculated based on flow rate Q, diameter of BGS D, and porosity of BGS Ø.

$$V_m = \frac{Q}{\emptyset\pi(\frac{D}{2})^2}$$

This model is a massive over simplification, but it is the best compromise that is available so far. Compatible shear stress values calculated based on this model (0.001 - 1 dyn/cm^2) have been reported and been demonstrated to activate osteogenic differentiation in 3D perfusion culture systems (Goldstein *et al.*, 2001; Bancroft *et al.*, 2002; Gomes *et al.*, 2003; Sikavitsas *et al.*, 2005; Li *et al.*, 2009; Vance *et al.*, 2005; McCoy and O'Brien, 2010) based on increased ALP activity (Goldstein *et al.*, 2001; Bancroft *et al.*, 2002; Sikavitsas *et al.*, 2005), PGE2 release (Vance *et al.*, 2005), or mineralized matrix deposition (Bancroft *et al.*, 2002; Gomes *et al.*, 2003; Sikavitsas *et al.*, 2005; Li *et al.*, 2009). The shear stress value calculated based on this model were also in line with shear stress estimated by computational fluid dynamics (CFD) models on the BGS surfaces, which was found to induce osteogenic differentiation (Zhao *et al.*, 2015; Stephens *et al.*, 2007; Vetsch *et al.*, 2017). In the current study, continuous BASAL PERFUSION RATE (BPR) at 0.07 ml/min flow rate was chosen to generate shear stress value of 0.0088 dyn/cm^2 (μ: 0.01 dyn * s/cm^2, d: 265 μm, D: 8 mm and Ø: 80%). BPR with a period of HIGH PERFUSION RATE (pHPR) every day at 2.5 ml/min flow rate was chosen to generate shear stress value of 0.31 dyn/cm^2 (μ: 0.01 dyn * s/cm^2, d: 265 μm, D: 8 mm and Ø: 80%).

Although both micro-porosity of BGS and shear stress are both involved in bone functional adaption and they have only been investigated independently. The combined effect of these two cues has not yet to be studied. The aim of this study here was to investigate the synergistic effects of micro-porosity and perfusion on hMSCs proliferation, cytoskeleton organisation, ERK1/2 signalling pathway activation and differentiation.

5.2 Materials and Methods

Irregularly shaped SiHA granules (ϕ: 1-2 mm) consisting of same total porosity (80.9 ± 1.9%), but different levels of micro-porosity: 13.5 ± 0.7% & 22.4 ± 0.5% & 28.4 ± 2.7% (SiHA-14 & SiHA-22 & SiHA-28) were synthesised as described in Chapter 2.1 in Baxter Inc (Elstree, London) and tested in *in vitro* experiments.

1 million of hMSCs in 500 µl cell suspension (concentration: 2×10^6 cells/ml) were seeded per 1 cm^3 (0.47 ± 0.03 g) of SiHA BGS granules. After hMSCs had attached to BGS granules (2 hours), granules were kept under static condition in 24 well-plates in 1.5 ml medium or moved to a recirculating perfusion bioreactor system consisting of 16 independent chambers (Figure 5-1) (as described in Chapter 2.4) for further incubation. MSC growth medium 2 (PromoCell) from the reservoir was perfused through the constructs vertically in a bottom-to-top direction using a peristaltic pump (IPC Iamatec, VWR). Two perfusion profiles were applied: 1) continuous BASAL PERFUSION RATE (BPR) at 0.7 ml/min flow rate; 2) BPR with a period (one hour daily) of HIGH PERFUSION RATE (pHPR) at 2.5 ml/min flow rate in recirculating configuration as in Figure 5-1.

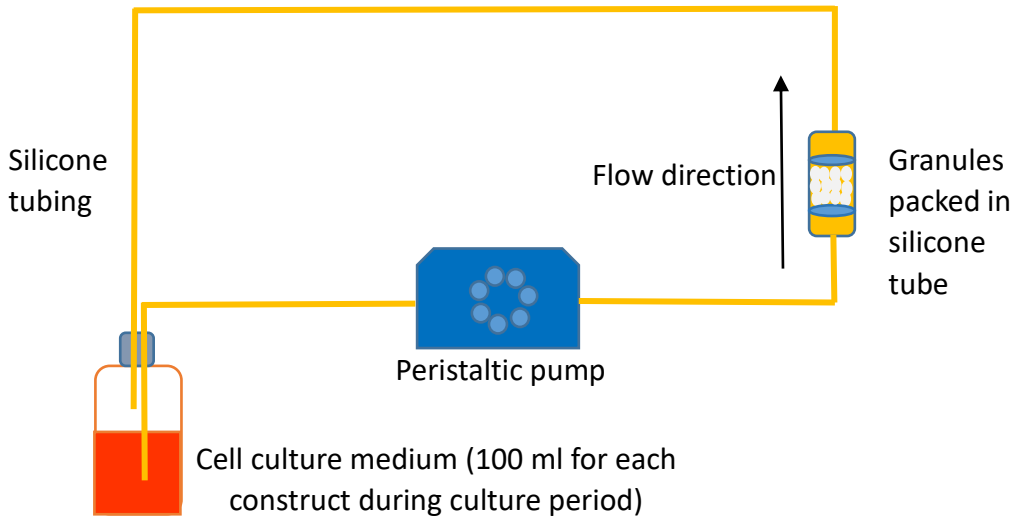

Figure 5-1 Schematic diagram of recirculating perfusion bioreactor system.

In Chapter 4, the response of hMSCs differentiation to BGS micro-porosity was found in osteogenic medium, but not basic cell culture medium. Previous study also proved that flow perfusion culture alone induces osteogenic differentiation of MSCs, while osteogenic medium enhanced its response to perfusion (Holtorf, Jansen, *et al.*, 2005). To clearly show the response of hMSCs differentiation to BGS micro-porosity and perfusion, and to better understand the synergistic effect of BGS micro-porosity and perfusion culture, in this study, after cells attached on BGS for a short period (24 hours), the MSC growth medium 2 was supplemented with osteogenic medium (0.1 µM dexamethasone, 0.05 mM ascorbic acid and 10 mM β-glycerophosphate) (Sigma-Aldrich). 1.5 ml medium was used for each BGS under static condition and culture medium was exchanged every 2 days thereafter. 100 ml medium was recirculated for each BGS during 7 days of perfusion culture, and the bottle of medium was vented in normoxic atmosphere.

After 3 or 7 days, hMSCs on the BGS were fixed, cytoskeleton organization was made visible as described in Chapter 2.8. hMSCs on the BGS were lysised, DNA and specific ALP activity, ERK1/2 and phosphorylated ERK (pERK1/2) distribution and production, gene expression for osteogenic differentiation markers (*osx*, *alp*, *bmp2*, *col i*, *dmp1*), chondrogenic differentiation markers (*sox9*, *runx2*, *col ii*), myogenic differentiation markers (*myoD*) and integrin subunits (*integrin α1*, *integrin α5*, *integrin β1*) were tested as described in Chapter 2.10.

5.3 Results

5.3.1 Cytoskeleton Organisation

Actin cytoskeleton was made visible to determine if the presence or absence of fluid shear stress results in cytoskeletal reorganisation after culturing for 3 days (Figure 5-2 (a)) and 7 days (Figure 5-3 (a)) on different BGS. At both day 3 and day 7, there was no observable difference in cytoskeleton organisation of hMSCs irrespective of whether they were cultured on SiHA-14, SiHA-22 or SiHA-28 BGS in static environment. Under basal perfusion rate (BPR) and a period of high perfusion rate (pHPR) culture conditions, there were also no significant difference in actin organisation with different BGS types. However, significant difference in actin organisation was observed to respond to change in culture condition from static to dynamic culture.

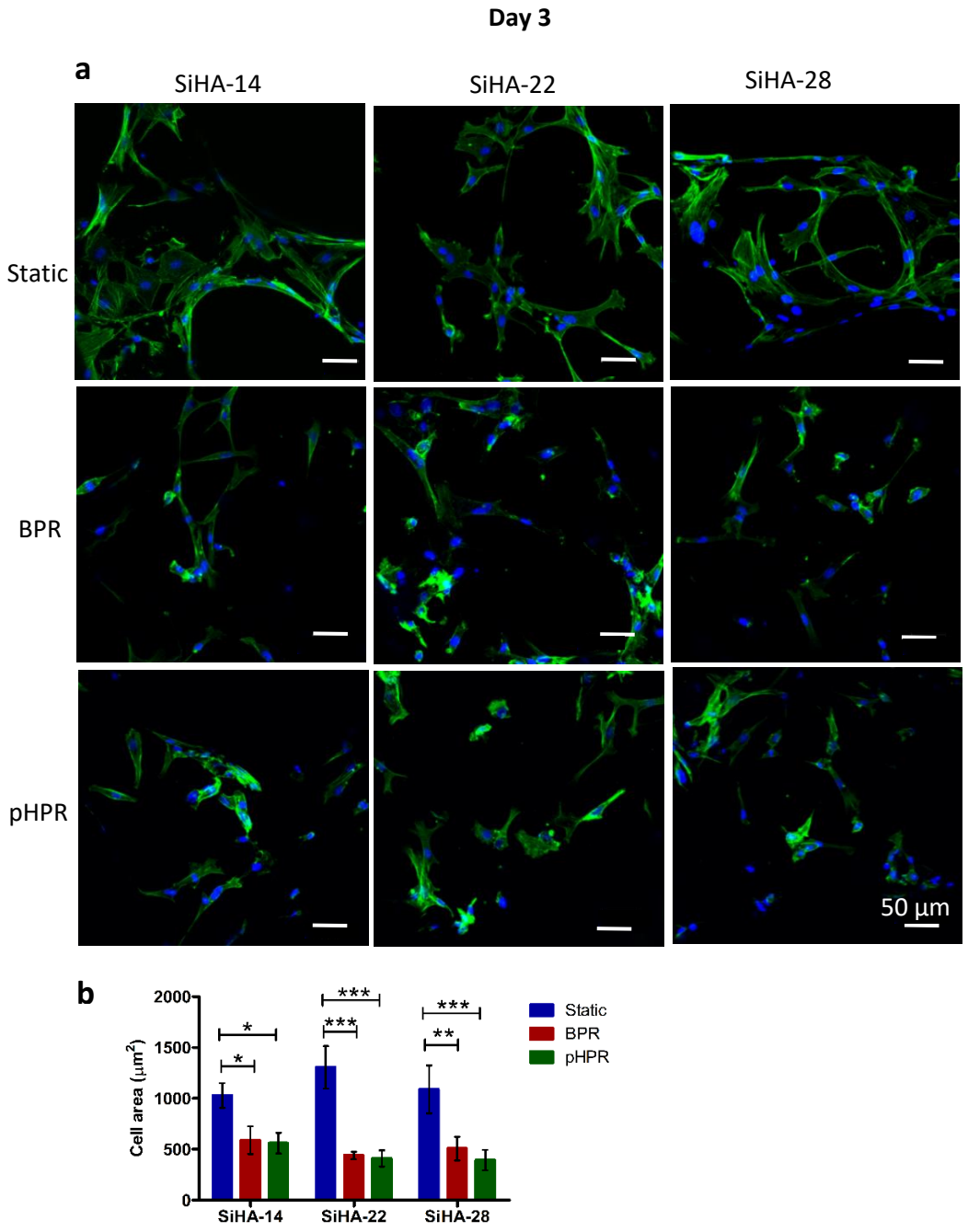

Figure 5-2 At day 3, actin organisation in hMSCs on SiHA-14, SiHA-22 and SiHA-28 BGS under static, basal perfusion rate (BPR) and a period of high perfusion rate (pHPR) conditions. (a) The actin cytoskeleton was labelled with Alexa 488 conjugated phalloidin (green) and nuclei were counterstained with DAPI (blue). Scale bar represents 50 µm. (b) Quantitative analysis of cell area by Image J. Results are presented as mean ± standard deviation (n=3). Statistical analysis was performed by two-way ANOVA followed by Bonferroni post-tests. *p < 0.05, **p < 0.01, ***p < 0.001, comparison between static, basal perfusion rate (BPR) and a period of high perfusion rate (pHPR) for each BGS.

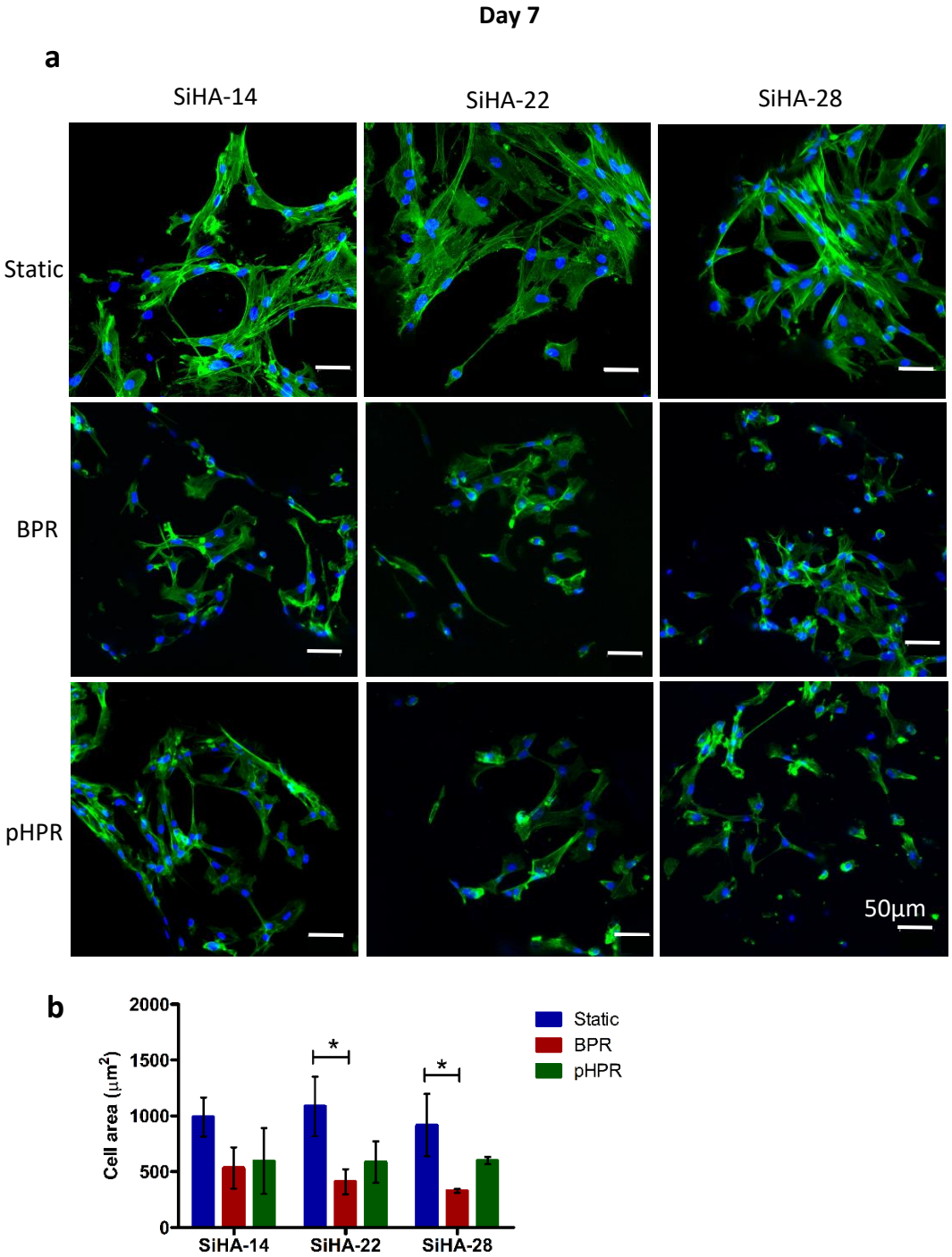

Figure 5-3 At day 7, actin organisation in hMSCs on SiHA-14, SiHA-22 and SiHA-28 BGS under static, basal perfusion rate (BPR) and a period of high perfusion rate (pHPR) conditions. (a) The actin cytoskeleton was labelled with Alexa 488 conjugated phalloidin (green) and nuclei were counterstained with DAPI (blue). Scale bar represents 50 µm. (b) Quantitative analysis of cell area by Image J. Results are presented as mean ± standard deviation (n=3). Statistical analysis was performed by two-way ANOVA followed by Bonferroni post-tests. *p < 0.05, comparison between static, basal perfusion rate (BPR) and a period of high perfusion rate (pHPR) for each BGS.

It is noticeable that majority hMSCs were spread on BGS under static culture condition, while most hMSCs were found to have relatively less spread cytoskeleton under basal perfusion rate (BPR) and a period of high perfusion rate (pHPR) conditions. This is confirmed by the quantification of the average cellular size, as shown in Figure 5-2 (b), which demonstrated that at day 3, cell area was significantly larger when cultured in a static environment than cultured in basal perfusion rate (BPR) or a period of high perfusion rate (pHPR) environment irrespective of BGS types. At day 7, cell area was larger when cultured in a static environment than cultured in basal perfusion rate (BPR) or a period of high perfusion rate (pHPR) environment on SiHA-14, whereas cell area was significantly larger when cultured in a static environment than cultured in basal perfusion rate (BPR) or a period of high perfusion rate (pHPR) environment on SiHA-22 and SiHA-28. There was no significant difference in cell area irrespective of whether they were cultured under basal perfusion rate (BPR) condition or a period of high perfusion rate (pHPR) condition irrespective of BGS types.

5.3.2 Total DNA Quantity

The quantity of total DNA from the BGS was assumed to be proportional to the number of cells on the BGS. So total increases in DNA was quantified to reflect cellular proliferation. As can be seen in Figure 5-4 (a), at day 3, cell proliferation was not dependent on culture conditions on any of the 3 BGS types. Also, total DNA production was not responsive to the BGS micro-porosity under any of the culture conditions.

Total DNA production did not change with time in static environment, whereas, at day 7, it was around 1.2 times higher in basal perfusion rate (BPR) and 1.4 times higher in a period of high perfusion rate (pHPR) environment respectively (Figure 5-4 (b)) compared with day 3. As a result, the DNA content of BGS cultured under perfusion conditions was significantly higher than under static culture condition at day 7. A period of high perfusion rate (pHPR) increased cell proliferation to a greater extent than basal perfusion rate (BPR), although there was no significant difference in total DNA quantity when culturing under basal perfusion rate (BPR) or a period of high perfusion rate (pHPR).

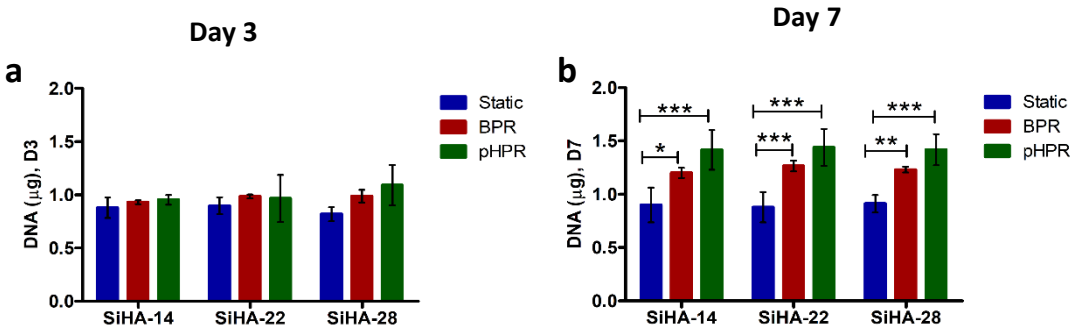

Figure 5-4 Total DNA production of hMSCs on SiHA-14, SiHA-22 and SiHA-28 BGS under static, basal perfusion rate (BPR) and a period of high perfusion rate (pHPR) conditions at (a) day 3 and (b) day 7. Results are presented as mean ± standard deviation (n=3). Statistical analysis was performed by two-way ANOVA followed by Bonferroni post-tests. *p < 0.05, **p < 0.01, ***p < 0.001, comparison between static, basal perfusion rate (BPR) and a period of high perfusion rate (pHPR) for each BGS.

5.3.3 Specific ALP Activity

Specific ALP activity is an early marker of bone marrow stromal cells differentiating towards the osteoblastic phenotype. So, ALP activity normalized by µg DNA (specific ALP activity) was measured to evaluate osteogenic differentiation of hMSCs on different samples after 3 and 7 days. In Figure 5-5 (a), at day 3, specific ALP activity of hMSCs was significantly greater under static culture condition than under basal perfusion rate (BPR) condition on SiHA-14 BGS. The specific ALP activity of hMSCs was significantly lower under a period of high perfusion rate (pHPR) than both static and basal perfusion rate (BPR) conditions on SiHA-28 BGS. The specific ALP activity was not found to be dependent on BGS micro-porosity under both static and a period of high perfusion rate (pHPR) conditions. However, under basal perfusion rate (BPR) condition, the specific ALP activity of hMSCs was significantly higher on SiHA-22 and SiHA-28 than SiHA-14 BGS.

After 7 days, specific ALP activity of hMSCs was significantly lower under basal perfusion rate (BPR) than both static and a period of high perfusion rate (pHPR) conditions irrespective of BGS types, as shown in Figure 5-5 (b). At day 7, on both SiHA-22 and SiHA-28 BGS, specific ALP activity was significantly higher under a period of high perfusion rate (pHPR) than static condition. The specific ALP activity was not dependent on BGS micro-porosity under both static and basal perfusion rate (BPR) conditions. However, under a period of high perfusion rate (pHPR) condition, specific

ALP activity of hMSCs was significantly lower on SiHA-14 compared with on both SiHA-22 and SiHA-28 BGS.

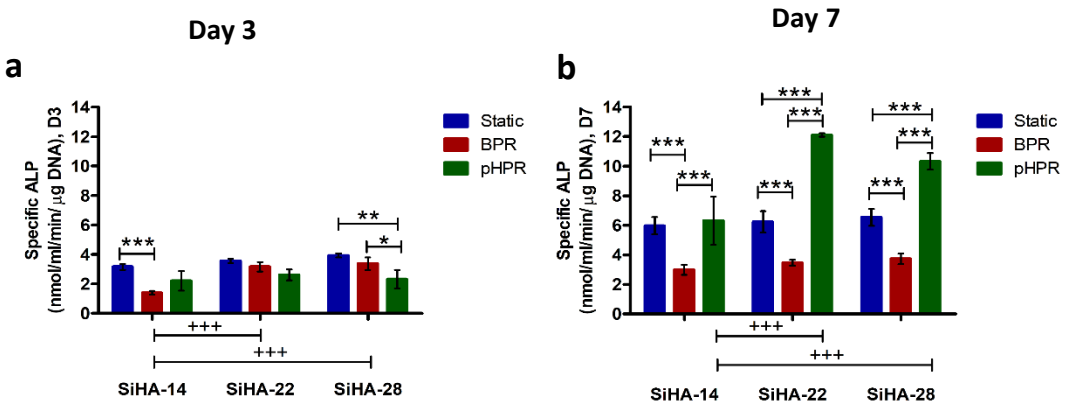

Figure 5-5 Specific ALP activity of hMSCs on SiHA-14, SiHA-22 and SiHA-28 BGS under static, basal perfusion rate (BPR) and a period of high perfusion rate (pHPR) conditions at (a) day 3 and (b) day 7. Results are presented as mean ± standard deviation (n=3). Statistical analysis was performed by two-way ANOVA followed by Bonferroni post-tests. *p < 0.05, **p < 0.01, ***p < 0.001, comparison between static, basal perfusion rate (BPR) and a period of high perfusion rate (pHPR) for each BGS. +++p < 0.001, comparison between SiHA-14, SiHA-22 and SiHA-28 under each culture condition.

5.3.4 ERK and pERK Nuclear Translocation

When hMSCs seeded BGS were cultured under static condition for 3 days, in some of hMSCs, ERK1/2 localised exclusively in the cytoplasm, while for other hMSCs, ERK1/2 homogeneously distributed in both cytoplasm and nucleus, as can be seen in Figure 5-6. However, when hMSCs seeded BGS were cultured under basal perfusion rate (BPR) or a period of high perfusion rate (pHPR) conditions, strong nuclear accumulation of ERK1/2 was detected, as can be seen in Figure 5-7. Under each isolated culture condition of static, basal perfusion rate (BPR) or a period of high perfusion rate (pHPR), ERK1/2 distribution did not appear to vary on the three types of BGS. Interestingly, pERK was found to have the same pattern with ERK, as can be seen in Figure 5-8 and Figure 5-9, i.e. pERK also located at nucleus when hMSCs seeded BGS were cultured in the basal perfusion rate (BPR) or a period of high perfusion rate (pHPR) environment rather than in static environment.

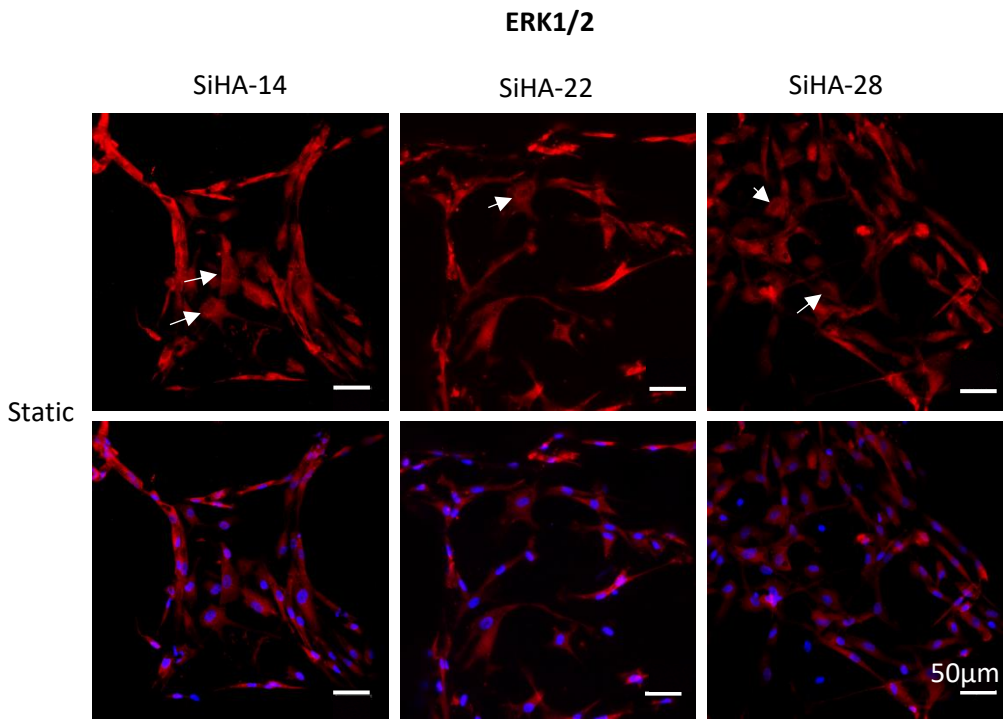

Figure 5-6 ERK1/2 distribution in hMSCs on SiHA-14, SiHA-22 and SiHA-28 BGS under static condition after 3 days. ERK1/2 was labelled using an antibody against at ERK1/2 (red), and nuclei were counterstained with DAPI (blue), scale bar represents 50 µm. White arrow showed ERK1/2 localised exclusively in the cytoplasm.

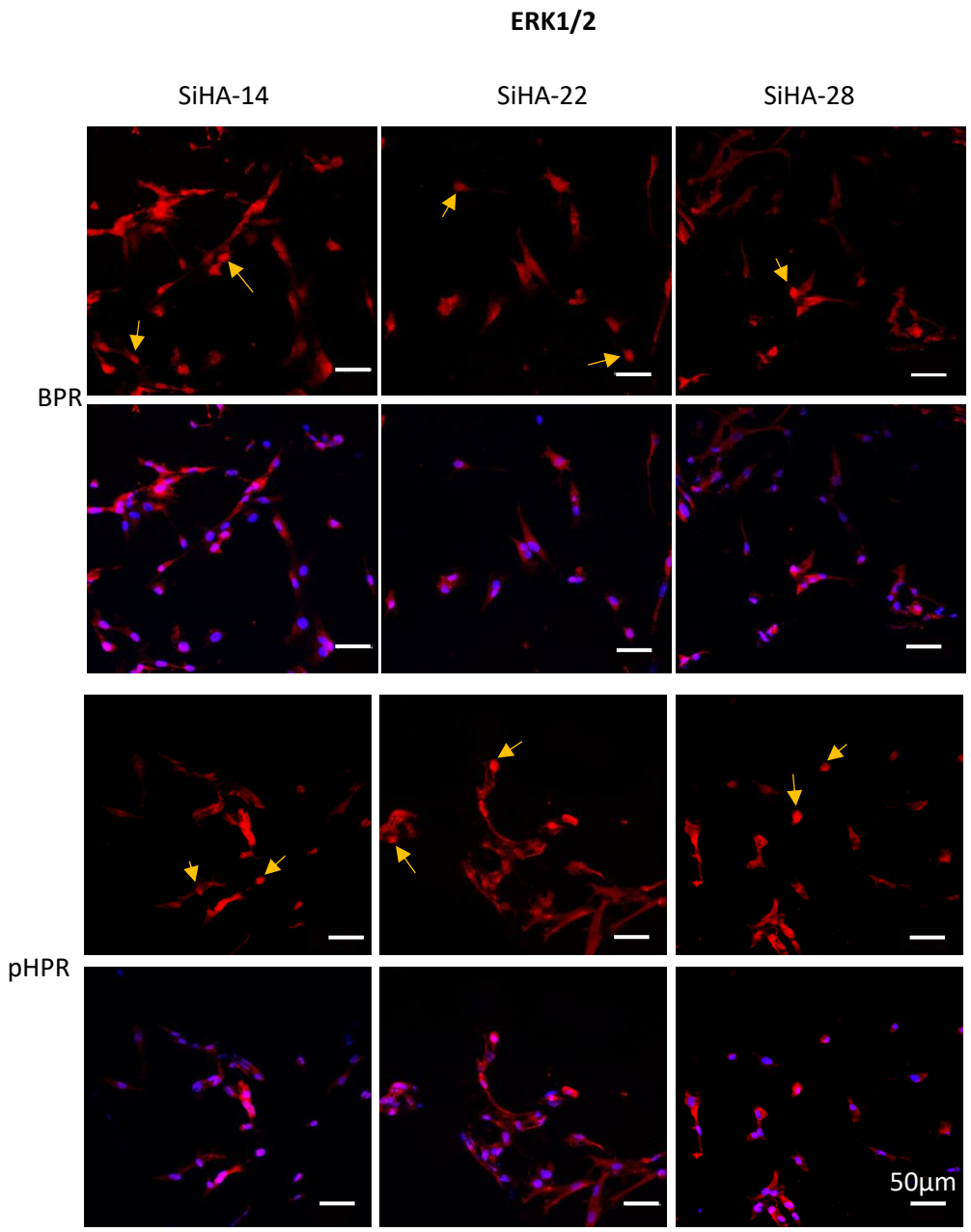

Figure 5-7 ERK1/2 distribution in hMSCs on SiHA-14, SiHA-22 and SiHA-28 BGS under basal perfusion rate (BPR) and a period of high perfusion rate (pHPR) conditions after 3 days. ERK1/2 was labelled using an antibody against at ERK1/2 (red), and nuclei were counterstained with DAPI (blue), scale bar represents 50 µm. Yellow arrow showed ERK1/2 was accumulated in nuclear.

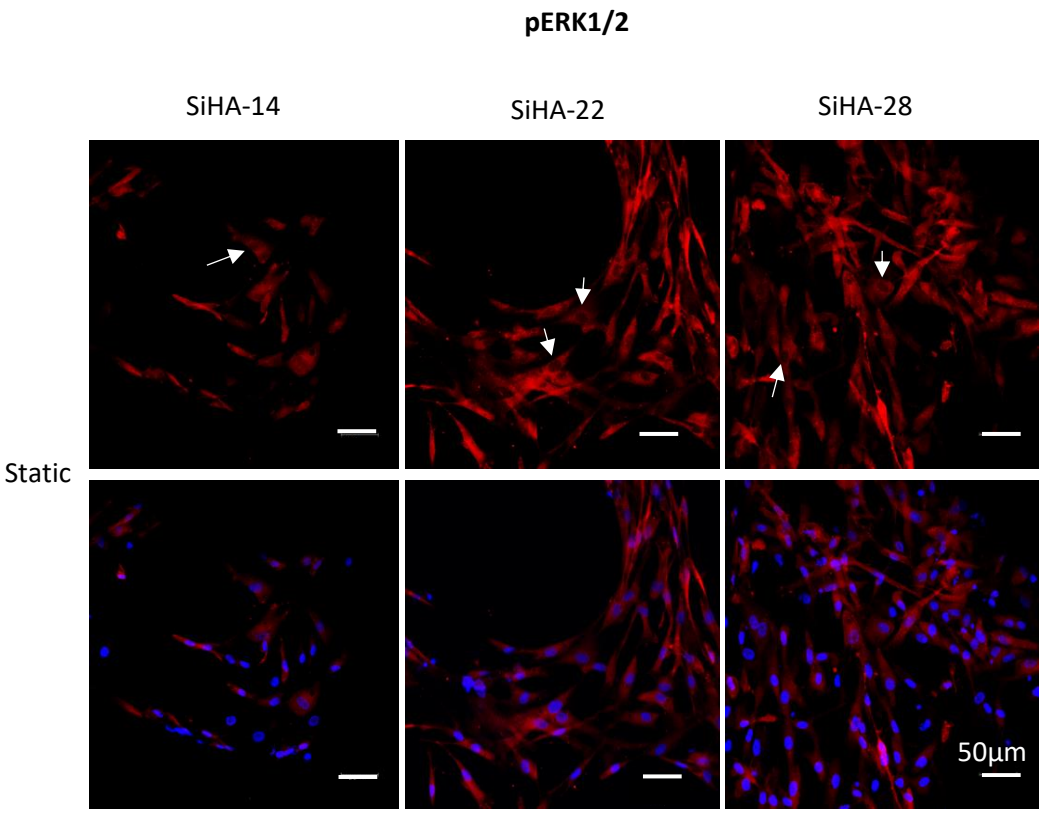

Figure 5-8 pERK1/2 distribution in hMSCs on SiHA-14, SiHA-22 and SiHA-28 BGS under static condition after 3 days. pERK1/2 was labelled using an antibody against at pERK1/2 (red), and nuclei were counterstained with DAPI (blue), scale bar represents 50 µm. White arrow showed ERK1/2 localised exclusively in the cytoplasm.

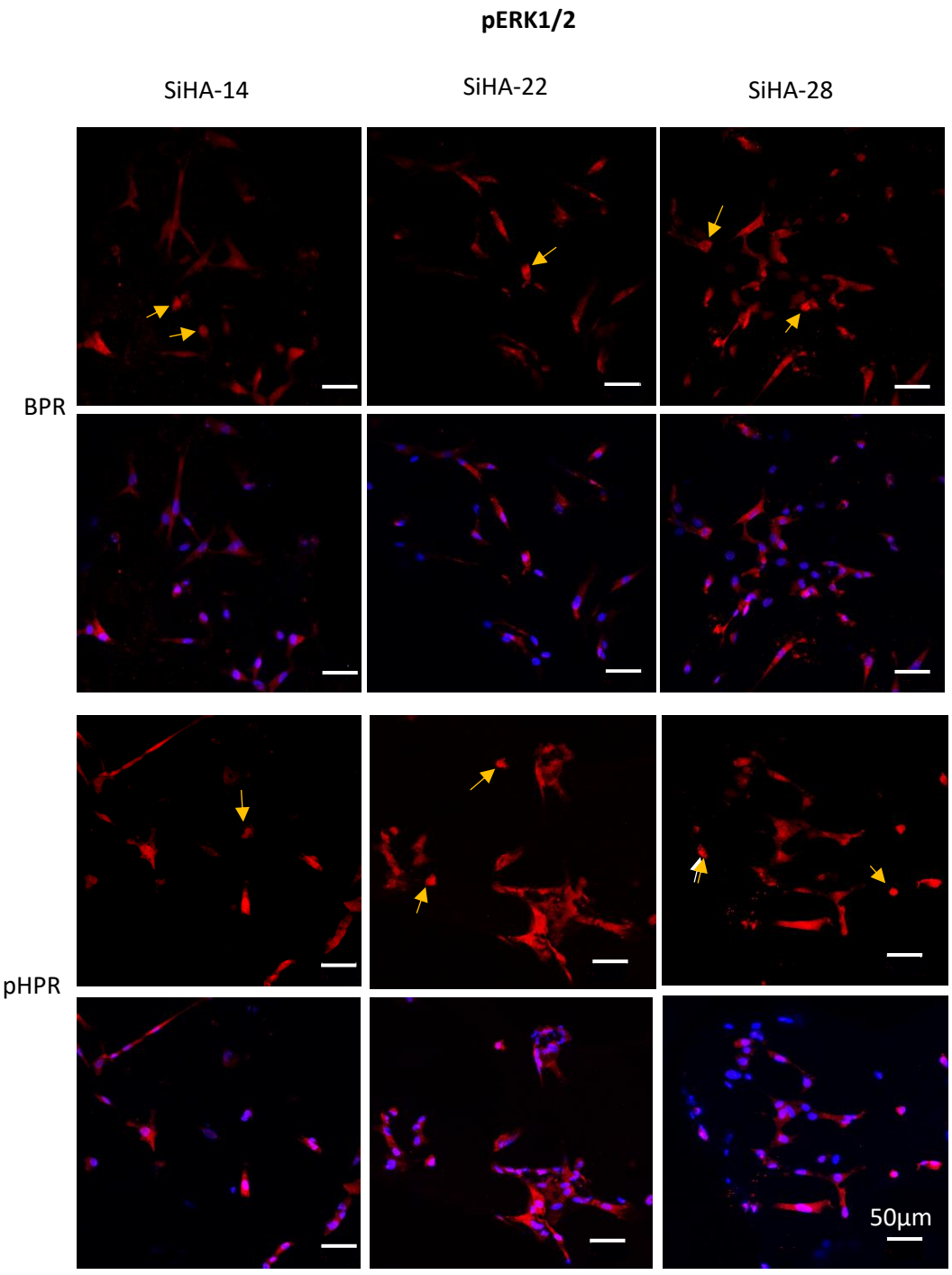

Figure 5-9 pERK1/2 distribution in hMSCs on SiHA-14, SiHA-22 and SiHA-28 BGS under basal perfusion rate (BPR) and a period of high perfusion rate (pHPR) conditions after 3 days. pERK1/2 was labelled using an antibody against at pERK1/2 (red), and nuclei were counterstained with DAPI (blue), scale bar represents 50 µm. Yellow arrow showed pERK1/2 was accumulated in nuclear.

5.3.5 ERK Phosphorylation Levels

The phosphorylation status of ERK1/2 was examined by Western blot and normalised by total ERK1/2 expression. As can be seen in Figure 5-10(b), at day 3, on SiHA-14 and SiHA-22, pERK1/2 in hMSCs was found to be significantly lower under basal perfusion rate (BPR), compared with both static condition and a period of high perfusion rate (pHPR) condition. On SiHA-28, the phosphorylation of ERK1/2 in hMSCs was significantly higher under a period of high perfusion rate (pHPR) compared with both static and basal perfusion rate (BPR) conditions. The phosphorylation of EKR1/2 at day 3 has the similar pattern of the specific ALP activity at day 7, which implies EKR1/2 is part of the upstream signalling of hMSCs differentiation.

After 7 days, the phosphorylation of ERK1/2 in hMSCs was significantly higher under static culture than basal perfusion rate (BPR) and a period of high perfusion rate (pHPR) on SiHA-14, as shown in Figure 5-11 (b). On BGS SiHA-28, the phosphorylation of ERK1/2 in hMSCs was not dependent on culture conditions. It is worth mentioning that the phosphorylation of ERK1/2 in hMSCs was significantly higher on SiHA-14 than on SiHA-22 and SiHA-28 under static condition, while it increased with increasing in BGS micro-porosity under basal perfusion rate (BPR) condition.

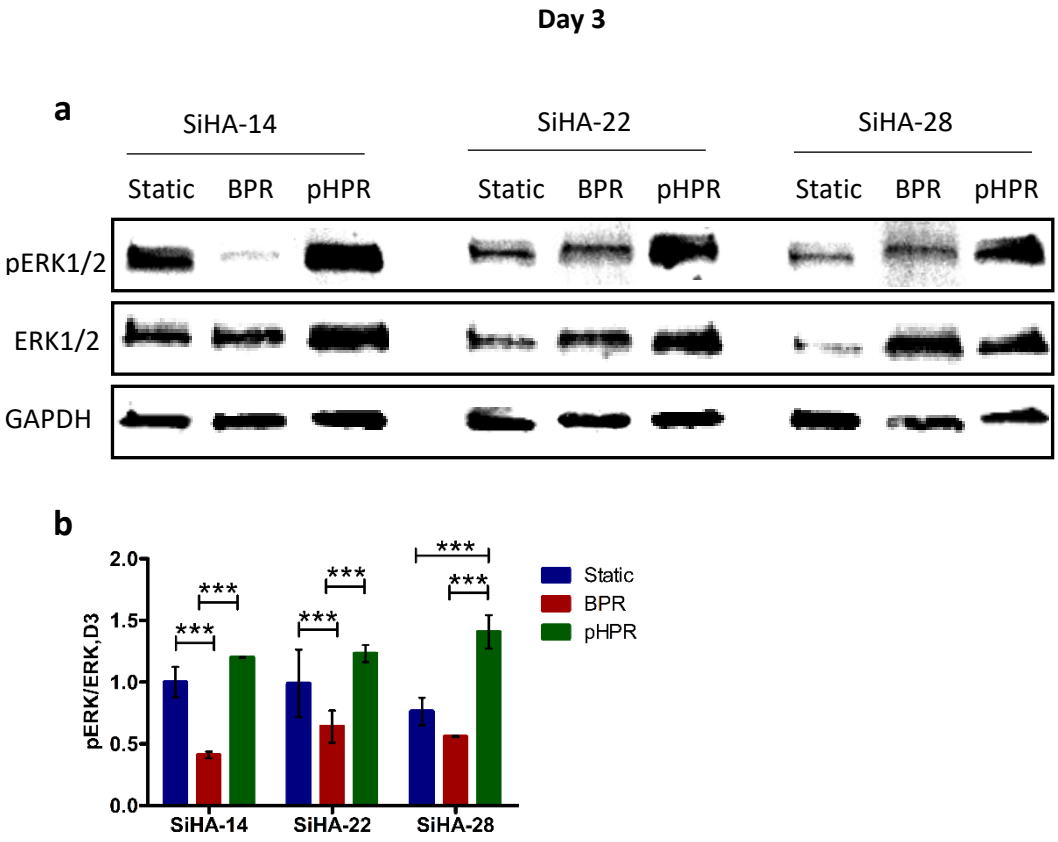

Figure 5-10 (a) At day 3, the phosphorylation of ERK1/2 (pERK1/2) and ERK protein expression on SiHA-14, SiHA-22 and SiHA-28 under static, basal perfusion rate (BPR) and a period of high perfusion rate (pHPR) conditions. (b) Quantitative analysis of pERK1/2 expression. Results are presented as mean ± standard deviation (n=3). Statistical analysis was performed by two-way ANOVA followed by Bonferroni post-tests. *p < 0.05, **p < 0.01, ***p < 0.001, comparison between static, basal perfusion rate (BPR) and a period of high perfusion rate (pHPR) for each BGS.

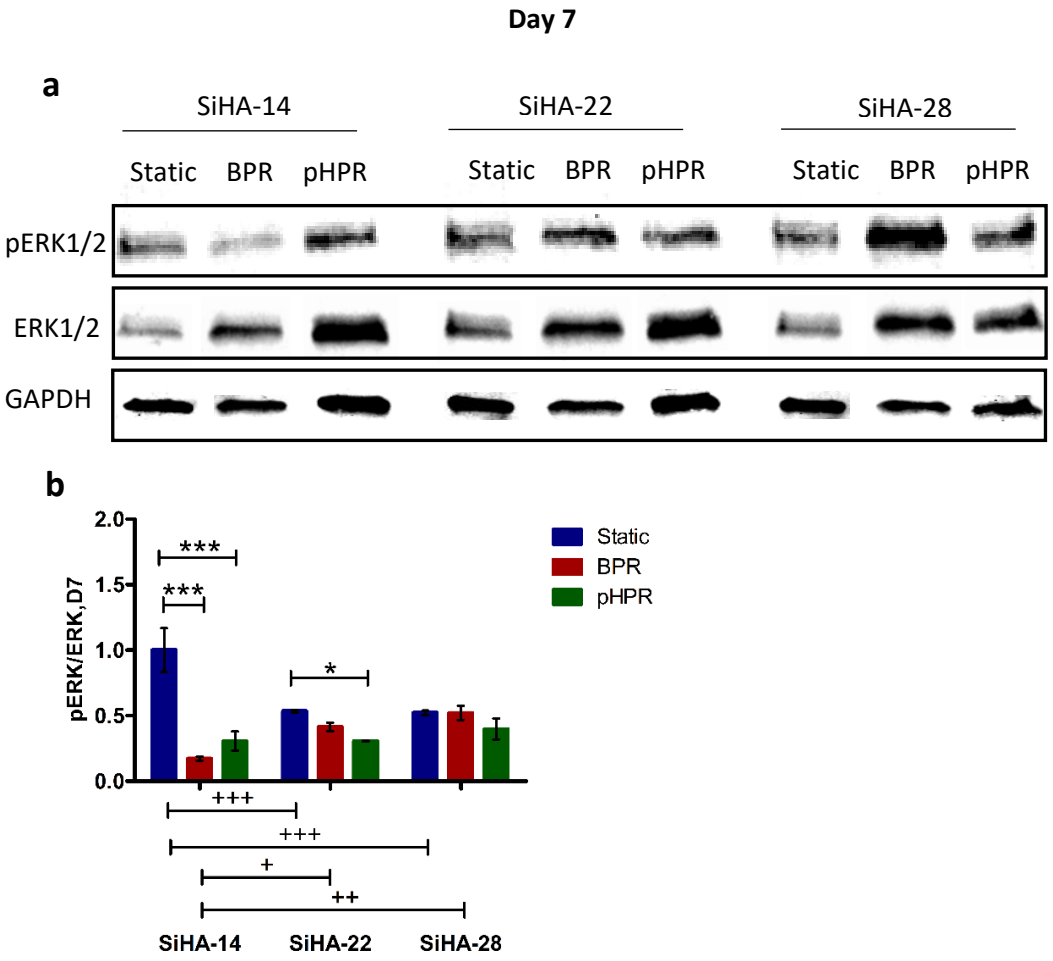

Figure 5-11 (a) At day 7, the phosphorylation of ERK1/2 (pERK1/2) and ERK protein expression on SiHA-14, SiHA-22 and SiHA-28 under static, basal perfusion rate (BPR) and a period of high perfusion rate (pHPR) conditions. (b) Quantitative analysis of pERK1/2 expression. Results are presented as mean ± standard deviation (n=3). Statistical analysis was performed by two-way ANOVA followed by Bonferroni post-tests. *p < 0.05, **p < 0.01, ***p < 0.001, comparison between static, basal perfusion rate (BPR) and a period of high perfusion rate (pHPR) for each BGS. +p < 0.05, ++p < 0.01, +++p < 0.001, comparison between SiHA-14, SiHA-22 and SiHA-28 under each culture condition.

5.3.6 Relative Gene Expression

5.3.6.1 Expression of Osteogenic Gene Markers

mRNA levels of osteogenic markers: osterix (*osx*), alkaline phosphatase (*alp*), bone morphogenetic protein 2 (*bmp2*), collagen I (*col i*) and dentin matrix acidic phosphoprotein (*dmp1*) of hMSCs were measured by quantitative real-time PCR to evaluate how BGS micro-porosity and shear stress influences the expression of markers of osteogenic differentiation. *osx* is a transcription factor that has been demonstrated to be critical for osteoblast differentiation and bone formation (Nakashima *et al.*, 2002; Tu *et al.*, 2006). At day 3, the expression of *osx* was

significantly higher when BGS were cultured under basal perfusion rate (BPR) than both a period of high perfusion rate (pHPR) and static conditions, with *osx* expression under static condition being significantly lower than under a period of high perfusion rate (pHPR) condition, irrespective of BGS types (Figure 5-12 (a)). At day 3, under basal perfusion rate (BPR) condition, *osx* gene expression increased significantly with increasing in BGS micro-porosity. At day 7, there was no significant difference in *osx* gene expression with time under static condition irrespective of BGS types, whereas there was a significant decrease in *osx* expression under basal perfusion rate (BPR) and a period of high perfusion rate (pHPR) conditions, compared with day 3 (Figure 5-12 (a) and (b)). The decrease under basal perfusion rate (BPR) condition was more prominent on SiHA-22 and SiHA-28 than on SiHA-14. However, at day 7, the expression of *osx* was still significantly higher under basal perfusion rate (BPR) than both static and a period of high perfusion rate (pHPR) conditions on any of the 3 BGS types.

ALP is a transient early marker of bone marrow stromal cells differentiating towards the osteoblastic phenotype (Datta *et al.*, 2005). At day 3, on both SiHA-14 and SiHA-28, *alp* gene expression was significantly higher under static condition than either type of perfusion conditions, while on SiHA-22, *alp* gene expression was significantly higher under basal perfusion rate (BPR) than both static and a period of high perfusion rate (pHPR) conditions (Figure 5-12(c)). At day 3, *alp* gene expression was significantly higher on SiHA-22 BGS than SiHA-14 and SiHA-28 BGS under basal perfusion rate (BPR) condition. *alp* gene expression tended to increase with time from day 3 to day 7 under all conditions. At day 7, *alp* gene expression was significantly higher under static condition compared with basal perfusion rate (BPR) condition on SiHA-14 BGS, whereas it was significantly higher under basal perfusion rate (BPR) than both static and a period of high perfusion rate (pHPR) conditions on SiHA-22 BGS, as can be seen in Figure 5-12 (d). At day 7, under basal perfusion rate (BPR), *alp* gene expression was found to be significantly higher on SiHA-22 BGS than both SiHA-14 and SiHA-28 BGS. Specific ALP activity at day 7 (in section 5.3.3) did not match with gene expression of *alp* at day 7. One possible explanation is that specific ALP activity reaches the highest levels under a period of high perfusion rate (pHPR)

at day 7, but it is ready to decrease after day 7 according its gene expression levels at day 7. Arpornmaeklong also found that ALP activity increased to reach the highest levels then decreased during osteogenic differentiation (Arpornmaeklong *et al.*, 2009).

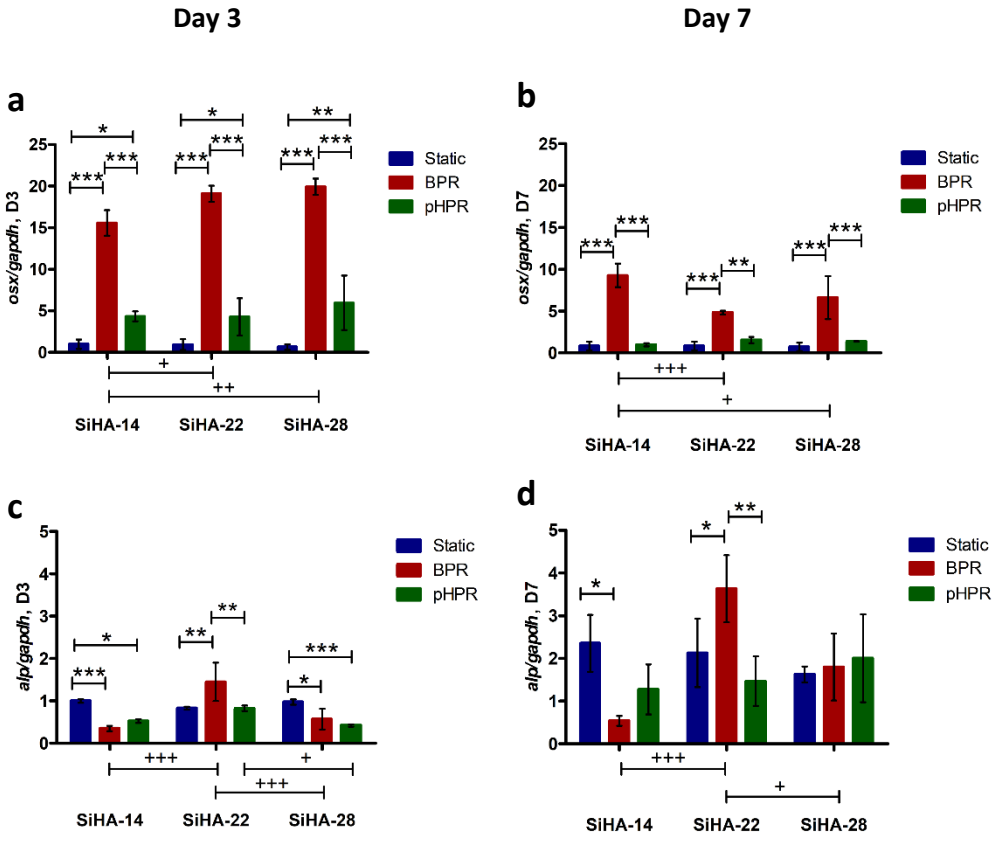

Figure 5-12 Expression of *osx* and *alp* genes in hMSCs cultured on SiHA-14, SiHA-22 and SiHA-28 BGS under static, basal perfusion rate (BPR) and a period of high perfusion rate (pHPR) conditions after 3 and 7 days. Results are presented as mean ± standard deviation (n=3). Statistical analysis was performed by two-way ANOVA followed by Bonferroni post-tests. *p < 0.05, **p < 0.01, ***p < 0.001, comparison between static, basal perfusion rate (BPR) and a period of high perfusion rate (pHPR) for each BGS. +p < 0.05, ++p < 0.01, +++p < 0.001, comparison between SiHA-14, SiHA-22 and SiHA-28 under each culture condition.

BMP2 plays a critical role in bone formation and regeneration (Reddi, 1998). The short-term expression of *bmp2* was demonstrated to be necessary and sufficient for osteochondral differentiation of MSCs *in vivo* (Noel *et al.*, 2008). At day 3, both basal perfusion rate (BPR) and a period of high perfusion rate (pHPR) facilitated the expression of *bmp2*, as compared to static culture on SiHA-22 and SiHA-28 BGS (Figure 5-13 (a)). With increasing in BGS micro-porosity, expression of *bmp2* decreased irrespective of culture conditions. Interestingly, expression of *bmp2*

decreased with time from day 3 to day 7 irrespective of culture conditions, as shown in Figure 5-13 (b). The decrease in *bmp2* expression was less marked under basal perfusion rate (BPR), with *bmp2* expression under basal perfusion rate (BPR) condition being consistently the highest at day 7, and there no longer being any response in *bmp2* expression to BGS micro-porosity under any of 3 culture conditions used in this study.

col i has been reported to be expressed early during the commitment to the osteoblastic phenotype (Rodan and Noda, 1991). At day 3, the gene expression of *col i* was significantly higher under basal perfusion rate (BPR) than both static and a period of high perfusion rate (pHPR) conditions for both SiHA-14 and SiHA-22 BGS, while it was the highest under a period of high perfusion rate (pHPR) on SiHA-28 BGS. At day 3, *col i* gene expression was found to be significantly lower on SiHA-28 than on SiHA-14 and SiHA-22 under basal perfusion rate (BPR), as can be seen in Figure 5-13 (c). The expression of *col i* was found to have an obvious decrease with time from day 3 to day 7 under a period of high perfusion rate (pHPR) condition irrespective of BGS types. At day 7, expression of *col i* (Figure 5-13 (d)) was the highest under basal perfusion rate (BPR) than static and a period of high perfusion rate (pHPR) irrespective of BGS types. At day 7, the pattern of *col i* expression was similar to day 3, with the expression of *col i* was found to be significantly lower on SiHA-28 than on SiHA-14 under basal perfusion rate (BPR).

dmp1 has been found to be highly expressed in osteocytes and can be classed as a pro-osteogenic factor (Kalajzic *et al.*, 2004). At both day 3 and day 7, the expression of *dmp1* was significantly higher under basal perfusion rate (BPR) than both static and a period of high perfusion rate (pHPR) conditions irrespective of BGS types, as can be seen in Figure 5-13 (e) and (f). *dmp1* expression was not found to be responsive to micro-porosity of BGS at either time point or under any of 3 culture conditions used in this study.

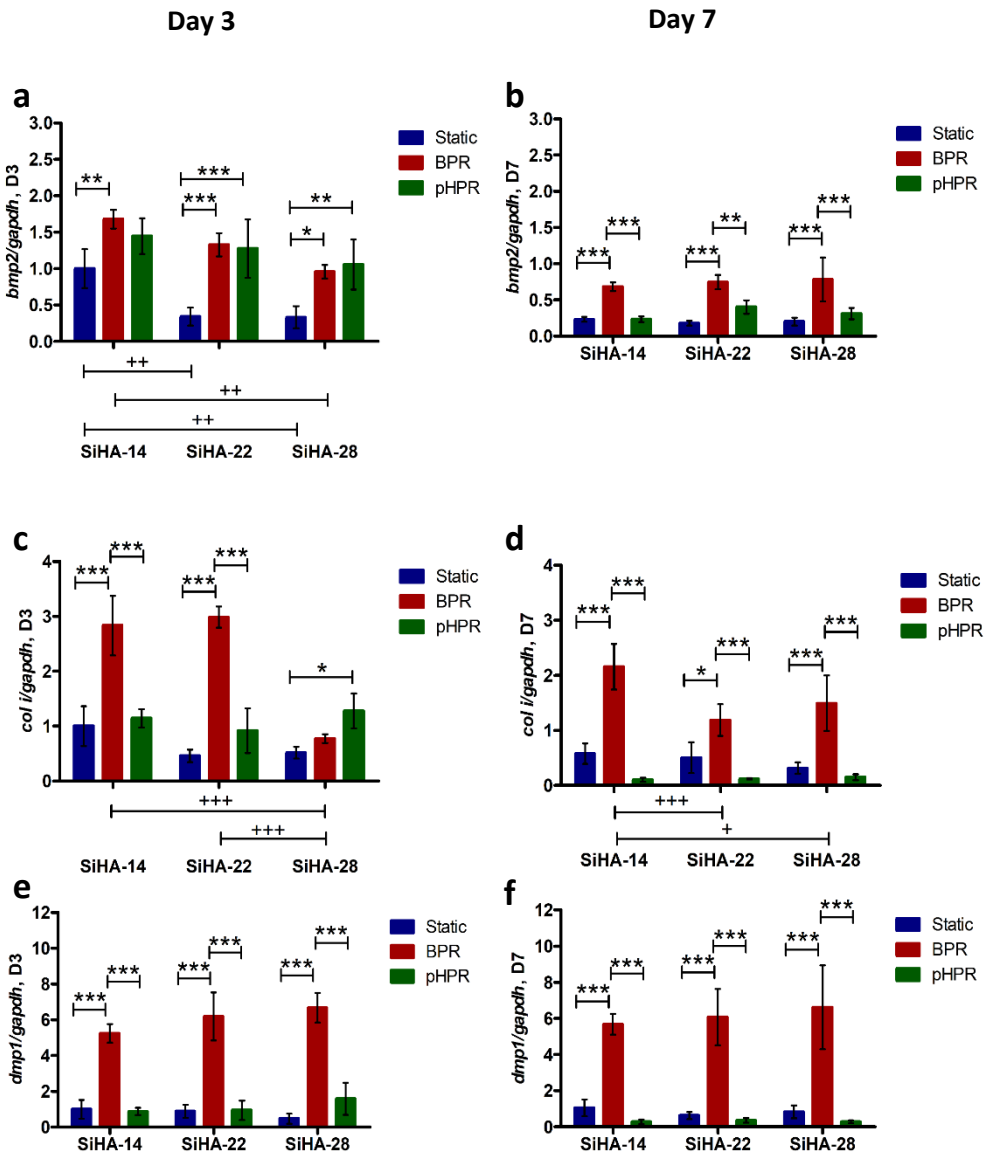

Figure 5-13 Expression of *bmp2*, *col i* and *dmp1* genes in hMSCs cultured on SiHA-14, SiHA-22 and SiHA-28 BGS under static, basal perfusion rate (BPR) and a period of high perfusion rate (pHPR) conditions after 3 and 7 days. Results are presented as mean ± standard deviation (n=3). Statistical analysis was performed by two-way ANOVA followed by Bonferroni post-tests. *p < 0.05, **p < 0.01, ***p < 0.001, comparison between static, basal perfusion rate (BPR) and a period of high perfusion rate (pHPR) for each BGS. +p < 0.05, ++p < 0.01, +++p < 0.001, comparison between SiHA-14, SiHA-22 and SiHA-28 under each culture condition.

5.3.6.2 Expression of Chondrogenic Gene Markers

SRY-box 9 (*sox9*) and runt-related transcription factor 2 (*runx2*) have been identified as important transcriptional regulators of early and late chondrogenic differentiation, respectively (Karsenty, 2008). At day 3, basal perfusion rate (BPR) significantly increased the expression of *sox9* compared with static culture, and a period of high

perfusion rate (pHPR) increased it even further irrespective of BGS types, as can be seen in Figure 5-14 (a). At day 3, *sox9* expression was significantly lower on SiHA-28 than on SiHA-22 under a period of high perfusion rate (pHPR) condition. From day 3 to day 7, the expression of *sox9* increased under basal perfusion rate (BPR) condition, while it decreased under static and a period of high perfusion rate (pHPR) conditions. At day 7, *sox9* expression was found to be significantly higher under either type of perfusion culture conditions than under static condition irrespective of BGS types. At day 7, expression of *sox9* was not found to be responsive to micro-porosity of BGS irrespective of culture conditions.

At day 3, there was no significant difference in *runx2* expression when culturing under static or basal perfusion rate (BPR), while in comparison with static and basal perfusion rate (BPR), a period of high perfusion rate (pHPR) enhanced expression of *runx2* significantly irrespective of BGS types, as can be seen in Figure 5-14 (c). At day 3, under a period of high perfusion rate (pHPR), *runx2* expression was significantly lower on SiHA-28 than both on SiHA-14 and SiHA-22. But there was no response of *runx2* expression to BGS micro-porosity under static or basal perfusion rate (BPR) conditions. Under static condition there was no significant difference in expression of *runx2* with time, in contrast, under either type of perfusion conditions, it increased significantly from day 3 to day 7 (Figure 5-14 (d)). As a result, at day 7, *runx2* expression was significantly higher under a period of high perfusion rate (pHPR) as compared to static and basal perfusion rate (BPR) conditions, with *runx2* expression under basal perfusion rate (BPR) being higher than static condition. At day 7, under a period of high perfusion rate (pHPR) condition, the expression of *runx2* was higher on SiHA-22 BGS than on SiHA-14 and SiHA-28 at day 7.

Collagen II (COL II) is the major structural component of cartilage, so it is one of the commonly used markers of chondrogenesis (Ng *et al.*, 1997). At day 3, there was no significant difference between static and basal perfusion rate (BPR) on any of the three BGS types. At day 3, there was significant increase in the expression of *col ii* under a period of high perfusion rate (pHPR) as compared static condition on SiHA-14, SiHA-22 and SiHA-28, Figure 5-14 (e). At day 3, *col ii* expression was found to be higher under a period of high perfusion rate (pHPR) as compared to basal perfusion

rate (BPR) on SiHA-14 and SiHA-22 BGS. At day 3, under a period of high perfusion rate (pHPR), the expression of *col ii* was found to be significantly lower on SiHA-28 than on either SiHA-14 or SiHA-22. At day 7, *col ii* expression was found to be significantly higher under a period of high perfusion rate (pHPR) condition as compared to static condition on any of the three BGS types. At day 7, *col ii* expression was found to be significantly higher under a period of high perfusion rate (pHPR) as compared to basal perfusion rate (BPR) on SiHA-14 and SiHA-28. *col ii* expression was not found to be responsive to micro-porosity of BGS at day 7 under any of 3 culture conditions used in this study.

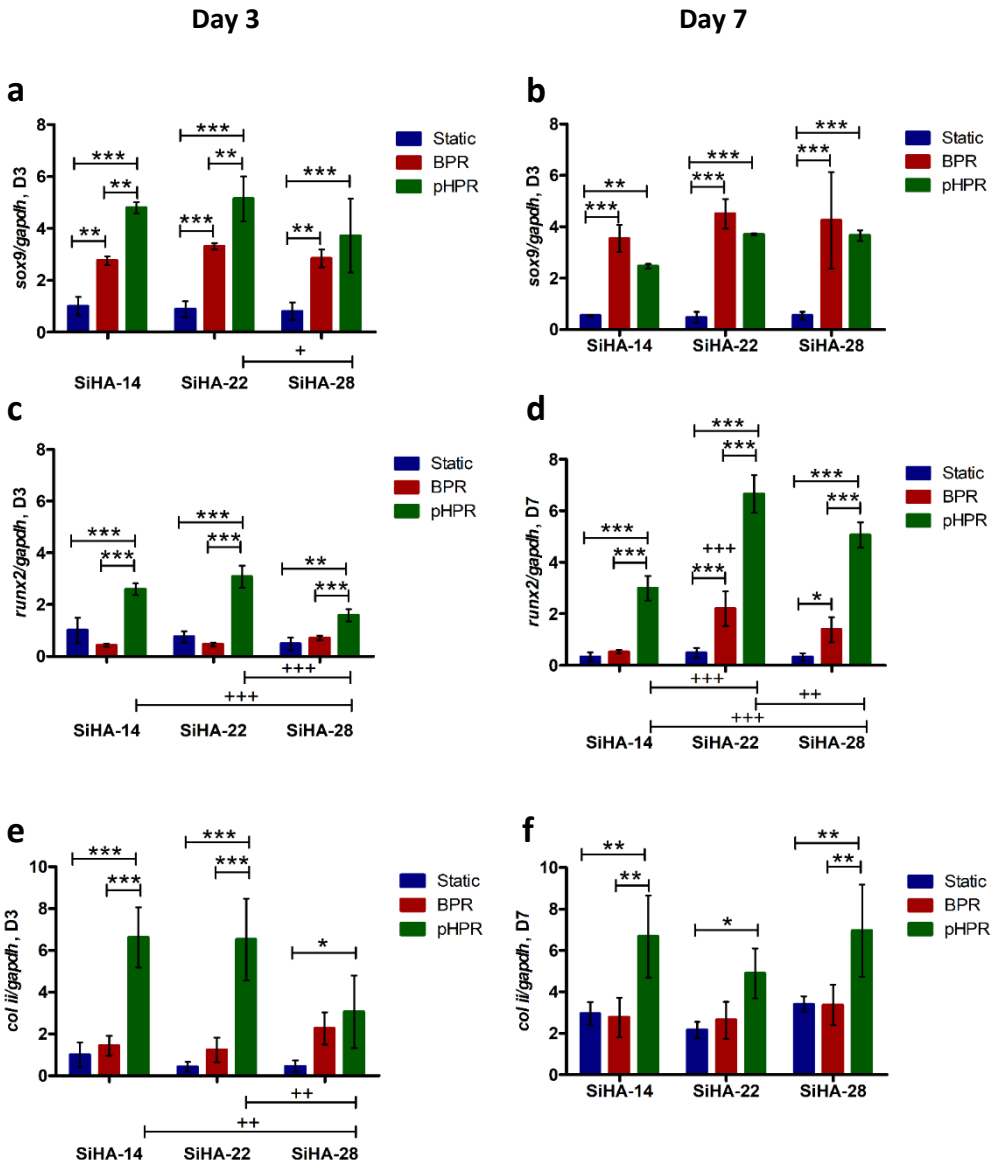

Figure 5-14 Expression of *sox9*, *runx2* and *col ii* genes in hMSCs cultured on SiHA-14, SiHA-22 and SiHA-28 BGS under static, basal perfusion rate (BPR) and a period of high perfusion rate (pHPR) conditions after 3 and 7 days. Results are presented as mean ± standard deviation (n=3). Statistical analysis was performed by two-way ANOVA followed by Bonferroni post-tests. *p < 0.05, **p < 0.01, ***p < 0.001, comparison between static, basal perfusion rate (BPR) and a period of high perfusion rate (pHPR) for each BGS. +p < 0.05, ++p < 0.01, +++p < 0.001, comparison between SiHA-14, SiHA-22 and SiHA-28 under each culture condition.

5.3.6.3 Expression of Myogenic Gene Marker

Myoblast determination protein (*myoD*) is a myogenic transcriptional regulatory factor that activate a number of muscle-specific structural genes and transcription factors to drive myogenesis (Rao *et al.*, 2006). On day 3, there was no significant difference in *myoD* expression under basal perfusion rate (BPR) compared with static

culture irrespective of BGS types. At day 3, the expression of *myoD* was found to be significantly lower under a period of high perfusion rate (pHPR) than under either static or basal perfusion rate (BPR) conditions on SiHA-14 and SiHA-22, Figure 5-15 (a). At day 3, under both static and basal perfusion rate (BPR) conditions, the expression of *myoD* was significantly lower on SiHA-28 than on SiHA-14.

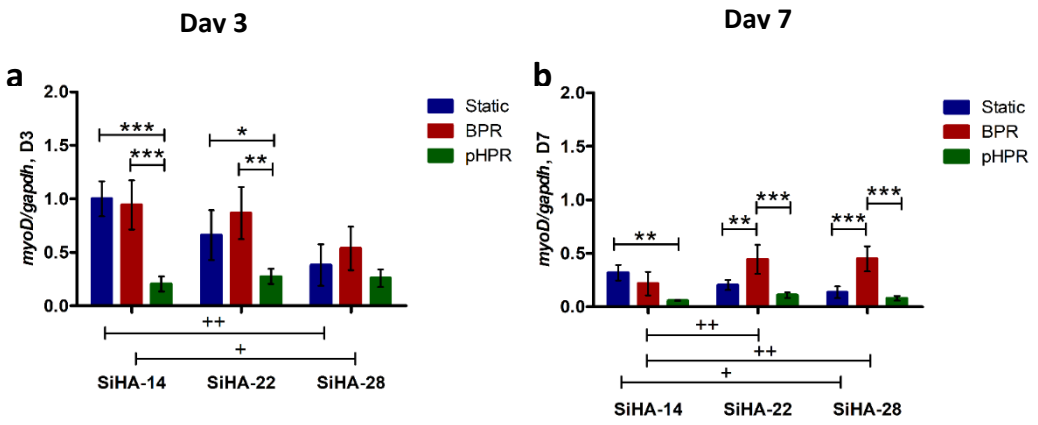

Figure 5-15 The gene expression of *myoD* in hMSCs cultured on SiHA-14, SiHA-22 and SiHA-28 BGS under static, basal perfusion rate (BPR) and a period of high perfusion rate (pHPR) conditions after 3 and 7 days. Results are presented as mean ± standard deviation (n=3). Statistical analysis was performed by two-way ANOVA followed by Bonferroni post-tests. *p < 0.05, **p < 0.01, ***p < 0.001, comparison between static, basal perfusion rate (BPR) and a period of high perfusion rate (pHPR) for each BGS. +p < 0.05, ++p < 0.01, comparison between SiHA-14, SiHA-22 and SiHA-28 under each culture condition.

By day 7, the expression of *myoD* was found to be significantly decreased (Figure 5-15 (b)) compared with day 3, regardless of BGS micro-porosity and culture condition. At day 7, *myoD* expression was found to be significantly lower under a period of high perfusion rate (pHPR) as compared to static condition on SiHA-14. At day 7, the expression of *myoD* was significantly higher under basal perfusion rate (BPR) condition than either static or a period of high perfusion rate (pHPR) conditions on SiHA-22 and SiHA-28. At day 7, under static condition, *myoD* expression was significantly higher under on SiHA-14 than on SiHA-28. At day 7, under basal perfusion rate (BPR), there was a significant increase in *myoD* expression when hMSCs were cultured on either SiHA-22 or SiHA-28 compared with SiHA-14.

5.3.6.4 Expression of Integrin Subunits

At day 3, either type of perfusion culture significantly increased *integrin α1* expression compared with static culture when hMSCs were cultured on SiHA-22 and

SiHA-28 BGS, Figure 5-16 (a). For SiHA-14 BGS, basal perfusion rate (BPR) significantly increased the *integrin α1* expression as compared to static culture and a period of high perfusion rate (pHPR). At day 3, under static condition, higher micro porosity (SiHA-22 or SiHA-28) suppressed *integrin α1* expression compared with SiHA-14, whereas under either type of perfusion conditions, there was no obvious difference in expression of *integrin α1* with respect to BGS micro-porosity. By day 7, *integrin α1* expression under basal perfusion rate (BPR) condition was significantly higher as compared to static and a period of high perfusion rate (pHPR) on SiHA-14 and SiHA-28 BGS, as can be seen in Figure 5-16 (b). At day 7, on BGS SiHA-22, *integrin α1* expression was significantly higher on either type of perfusion conditions than static condition. At day 7, under basal perfusion rate (BPR) condition, the expression of *integrin α1* was found to be significantly higher on SiHA-28 than on SiHA-14, whereas, under a period of high perfusion rate (pHPR), the expression of integrinα1 was significantly higher on SiHA-22 compared with on SiHA-14.

At day 3, basal perfusion rate (BPR) significantly increased *integrin α5* expression compared with static culture, and a period of high perfusion rate (pHPR) further increased *integrin α5* expression significantly irrespective of BGS types, Figure 5-16 (c). At day 3, under basal perfusion rate (BPR) condition, the expression of *integrin α5* was significantly higher on SiHA-28 than on SiHA-14, however, under a period of high perfusion rate (pHPR) condition, *integrin α5* expression was found to be significantly lower on SiHA-28 than SiHA-14 and SiHA-22. By day 7, the expression of *integrin α5* significantly decreased (Figure 5-16 (d)) under a period of high perfusion rate (pHPR) compared with day 3 on SiHA-14 and SiHA-22. At day 7, under a period of high perfusion rate (pHPR) condition, the expression of *integrin α5* was significantly higher compared with static condition on any of the three BGS types, and the expression of *integrin α5* was also significantly higher compared with basal perfusion rate (BPR) on SiHA-28. At day 7, under a period of high perfusion rate (pHPR), the expression of *integrin α5* increased significantly on SiHA-28 compared with both SiHA-14 and SiHA-22. At day 3, there was no significant difference in the expression of *integrin β1* when comparing basal perfusion rate (BPR) with static culture condition, while a period of high perfusion rate (pHPR) significantly increased

integrin β1 expression compared with static culture irrespective of BGS types, as shown in Figure 5-16 (e). At day 3, *integrin β1* expression was significantly higher under a period of high perfusion rate (pHPR) than basal perfusion rate (BPR) condition on both SiHA-14 and SiHA-22 BGS. At day 3, under static and basal perfusion rate (BPR) conditions, there was no response to BGS type in expression of *integrin β1*, however, under a period of high perfusion rate (pHPR) condition, expression of *integrin β1* was downregulated on SiHA-28 than on SiHA-14 and SiHA-22. By day 7, the expression of *integrin β1* did not vary significantly compared with day 3 under static and basal perfusion rate (BPR) conditions, while it increased significantly under a period of high perfusion rate (pHPR) on SiHA-22 and SiHA-22 compared with day 3 (Figure 5-16 (f)). At day 7, under static and basal perfusion rate (BPR) conditions, the expression of *integrin β1* was not dependent on BGS micro-porosity, while under a period of high perfusion rate (pHPR), the expression of *integrin β1* was significantly higher on SiHA-22 than SiHA-28, which is in turn significantly higher than on SiHA-14.

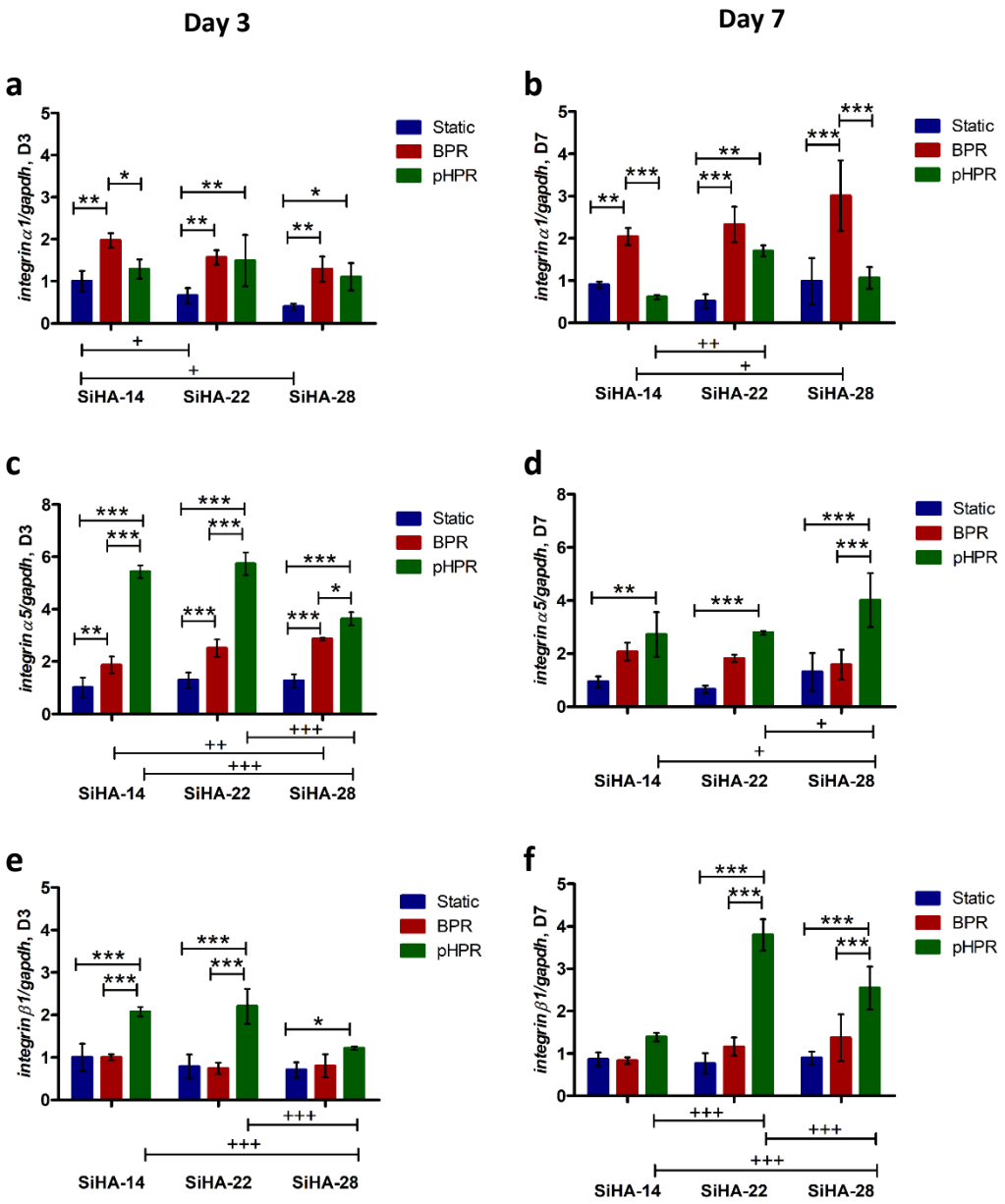

Figure 5-16 Expression of *integrin α1*, *integrin α5* and *integrin β1* genes in hMSCs cultured on SiHA-14, SiHA-22 and SiHA-28 BGS under static, basal perfusion rate (BPR) and a period of high perfusion rate (pHPR) conditions after 3 and 7 days. Results are presented as mean ± standard deviation (n=3). Statistical analysis was performed by two-way ANOVA followed by Bonferroni post-tests. *p < 0.05, **p < 0.01, ***p < 0.001, comparison between static, basal perfusion rate (BPR) and a period of high perfusion rate (pHPR) for each BGS. +p < 0.05, ++p < 0.01, +++p < 0.001, comparison between SiHA-14, SiHA-22 and SiHA-28 under each culture condition.

5.4 Discussion

In this study, SiHA BGS granules with different micro-porosities were seeded with hMSCs then cultured in static, basal perfusion rate (BPR) or a period of high perfusion rate (pHPR) environment. Responses of hMSCs, for example proliferation,

cytoskeleton organisation, integrin activation and differentiation, were analysed to investigate the synergistic effect of BGS geometry (micro-porosity) and perfusion.

The cytoskeleton is composed of a network of microfilaments and microtubules that link extracellular matrix to the cell nucleus and could play an important role in sensing mechanical forces and transforming mechanical forces into biochemical signals. Actin filamentous network is highly dynamic, and it can rearrange in response to mechanical stimulation, substrate stiffness or topography (Pavalko *et al.*, 1998; Lee *et al.*, 2015; Park *et al.*, 2011). To investigate the synergistic effect of micro-structure of BGS and shear stress on cytoskeleton organisation, F-actin of hMSCs cultured on SiHA-14, SiHA-22 and SiHA-28 BGS at different condition was studied *in vitro* and shown in Figure 5-2 (a). Cytoskeleton responded to both basal perfusion rate (BPR) and a period of high perfusion rate (pHPR) culture. Cytoskeleton was found to be less spread under both basal perfusion rate (BPR) and a period of high perfusion rate (pHPR) conditions, i.e. when cells differentiate to osteogenic lineage or chondrogenic lineage, compared with under static condition. Similar findings were also reported in the literature that cells become more rounded, when the expression of chondrogenic markers (*sox9* and *col ii*) are upregulated (Zhang *et al.*, 2006). Under *In vivo* condition, osteoblasts were also found to adopt a cuboidal morphology when actively secreting matrix (Franz-Odendaal *et al.*, 2006).

Cell proliferation is crucial for bone tissue regeneration. However, traditional static culture may lead to the death of seeded cells on 3D BGS, due to limited nutrients and oxygen transport (Volkmer *et al.*, 2008; Yeatts and Fisher, 2011). This can be overcome by using dynamic 3D perfusion bioreactors with constant replacement of fresh medium. In this study, at day 3, there was no significant difference in hMSCs proliferation irrespective of culture conditions on any of the three types of BGS. However, at day 7, either type of perfusion conditions was found to significantly increase hMSCs proliferation, especially a period of high perfusion rate (pHPR), which provides more efficient nutrients and oxygen exchange as well as increased shear stress.

The mitogen-activated protein kinase (MAPK) pathways have been found to respond to various extracellular stimuli and control a large number of fundamental cellular

processes including cell survival, growth, proliferation, differentiation, motility, stress response and apoptosis. ERK1/2 is one of the members of MAP Kinase, which has been widely recognised as a latent integrin-related pathway and can facilitate osteogenic differentiation of hMSCs in response to mechanical stimulation (Liu *et al.*, 2011; Ward Jr. *et al.*, 2007; Liu *et al.*, 2009). However, the role of ERK appears to be more complex in chondrogenesis. Some researchers reported that ERK signalling represses chondrogenesis (Yoon *et al.*, 2000; Appleton *et al.*, 2010), whereas others demonstrated the requirement of ERK activation for induction of the chondrogenic master gene *sox9* or precartilage condensation in the early stage of chondrogenesis (Zhang *et al.*, 2014; Li *et al.*, 2010; Murakami *et al.*, 2000).

In order to execute its functions, MAP kinase was required to translocate into the nucleus, where MAP kinase phosphorylates a large number of substrates (Roskoski, 2012; Plotnikov *et al.*, 2011; Brunet *et al.*, 1999). Studies have demonstrated that ERK1/2 was localized in the cytoplasm of resting cells due to interaction with anchoring proteins. Following stimulation, most ERK1/2 molecules were observed to enter the nucleus rapidly (in 15 min), and remain there persistently (Lenormand *et al.*, 1993). The main activity of ERK1/2 in the nucleus is to regulate transcription factors, which can in turn induce various physiological processes. In this study, both ERK1/2 and pEKR1/2 were mostly located in the nucleus under both basal perfusion rate (BPR) and a period of high perfusion rate (pHPR). One explanation may be that ERK1/2 translocated from the cytoplasm to nucleus in response to shear stress and phosphorylated in nucleus. It is worth mentioning that, at day 3, the phosphorylated ERK1/2 amount was significantly lower under basal perfusion rate (BPR) condition compared with under static condition. However, pERK1/2 was mostly observed in the nucleus, indicating that it could regulate transcription factors more efficiently than static culture.

The significant upregulation of *osx* expression under basal perfusion rate (BPR) suggested that it can induce osteogenic differentiation of hMSCs. The enhancement of *alp*, *bmp2*, *dmp1* and *col i* expression under basal perfusion rate (BPR) condition consolidated the differentiation towards the osteogenic lineage. In this study, when hMSCs seeded BGS were subjected to a period of high perfusion rate (pHPR), the

expression of osteogenic markers was lower compared with basal perfusion rate (BPR). This demonstrated that a period of high perfusion rate (pHPR) diminished the advantage of basal perfusion rate (BPR) in terms of osteogenic differentiation. However, the expression of certain osteogenic genes, like *osx* and *bmp2*, and specific ALP activity were higher compared with static culture. This demonstrated that a period of high perfusion rate (pHPR) could still support osteogenic differentiation to some extent. Taken together, these findings agree with previous research that, in 3D perfusion culture bioreactor, shear stress in the range of 0.001 – 1 dyn/cm^2 generated by flow induces osteogenic differentiation (Bancroft *et al.*, 2002; Gomes *et al.*, 2003; Sikavitsas *et al.*, 2005; Li *et al.*, 2009; Vance *et al.*, 2005; McCoy and O'Brien, 2010). In this study, although hMSCs seeded BGS were cultured in osteogenic medium, it is surprising to notice that a period of high perfusion rate (pHPR) significantly increased the expression of chondrogenic markers, like *sox9*, *runx2* and *col ii*, throughout 7 days of culture compared with static condition. Interestingly, cyclic tensile strain was also proved to play a role in directing both intramembranous and endochondral ossification of mesenchymal stem cells (Carroll *et al.*, 2017).

In a previous study, continuous flow rate of 0.1 ml/min was demonstrated to favour chondrogenic potential of goat MSCs on 3D biodegradable polymeric BGS (Gonçalves *et al.*, 2011). Another study showed decreased chondrogenic gene expression and matrix production of pellet hMSCs mounted in porous BGS that were exposed to a 1.22 ml/min flow (Kock *et al.*, 2014). Although the flow rate of 1.22 ml/min is more than 10 times higher compared to flow rate of 0.1 ml/min, shear stress is affected by the dimension of flow chamber and structure of the BGS, as well as flow rate. So, the interference of shear stress level and chondrogenic differentiation cannot be concluded by comparing directly the levels of flow rate between previous studies using different experimental setups. Basal perfusion rate (BPR) culture also elevated the expression of chondrogenic gene markers compared static condition. This finding suggested that in a 3D perfusion environment, higher shear stress enhanced chondrogenic differentiation, and this finding is in line with a previous study that, rabbit chondrocytes cultured in a 3D bioreactor at increased flow rate (0.8 ml/min)

were found to have significantly higher production of chondrogenic markers, like glycosaminoglycan (GAG) and matrix deposition, compared with chondrocytes that were cultured at low flow rate (0.05 ml/min) (Dror *et al.*, 1996). The models that are used in shear stress evaluation in 3D perfusion culture were different from that are used in monolayer cell culture models. The quantified shear stress value in monolayer cell culture is usually 2 to 4 orders of magnitude higher. For example, in monolayer cell culture model, Yourek et al. and Juhasz et al. found that the shear stresses of 9 dyn/cm^2 and 50 dyn/cm^2 could enhance osteogenic and chondrogenic differentiation, respectively (Yourek *et al.*, 2010; Juhász *et al.*, 2014). The evidence of higher shear stress induced chondrogenic differentiation from previous studies was in chondrogenic media. The current study showed that higher shear stress induced chondrogenic differentiation in osteogenic medium for the first time. It is widely accepted that hypoxia can promote chondrogenesis. However, it is unlikely that the perfusion conditions in the current study cause or change hypoxia, because the bottle of medium was vented in normoxic atmosphere.

The findings in this study reveal a clear dependence of hMSCs response on perfusion flow rate: hMSCs cultured in basal perfusion rate (BPR) environment differentiate towards the osteogenic lineage, while a period of high perfusion rate (pHPR) induces hMSCs differentiate towards the chondrogenic lineage. This may explain the results that low strain led to the intramembranous bone formation, whereas higher strain additionally provoked endochondral ossification with respect to fracture healing in trabecular metaphyseal bone (Claes *et al.*, 2011). The first stage of endochondral ossification is the aggregation of MSCs to form cellular aggregates, after which the cells undergo chondrogenic differentiation to form the cartilaginous template (Mackie *et al.*, 2008), and mechanical stimuli have been found to have an important effect on the rate of endochondral ossification during this early stage (Lacroix and Prendergast, 2002; Isaksson *et al.*, 2006; Lacroix *et al.*, 2002). In a SiCaP bone substitute graft materials used in an *in vivo* ectopic model, bone formation were observed by both intramembranous and endochondral ossification, often within close proximity to one another, illustrated differences in the local mechanical environment (Chan *et al.*, 2012). The findings in this study may explain the possible

mechanism for this observation, with the different pathways of bone formation potentially illustrating differences in the local mechanical environment. Mechanical stimulus was distributed differently in BGS, and areas that receive low level of stimulus form bone by intramembranous ossification, while areas that receive excessive mechanical stimulus form bone by endochondral ossification. Rough surface causes a higher shear pressure gradient and leads to the early transition from laminar to turbulent flow, therefore SiHA-28 has a higher possibility to create turbulent flow. However, its unknown whether micro-porosity creates local turbulent flow and how micro-porosity affects shear stress, as the transition from laminar to turbulent flow also depends on flow rate, friction factor of the surface and dimension of the micro-pores. A previous study demonstrated that chondrogenic priming of hMSCs could improve vessel invasion within bioengineered constructs (Farrell *et al.*, 2009). Therefore, this finding also demonstrated a possible approach in tissue engineering in terms of controlling shear stress to optimize hMSCs chondrogenic differentiation and achieve bone regeneration.

It has been postulated that MSCs commit to myogenic lineage when cultured on relatively soft muscle-like substrates, and to osteogenic lineage when cultured on rigid bone-like substrates (Engler *et al.*, 2006; Pek *et al.*, 2010). The expression of *myoD* on SiHA BGS under static culture decreased with time significantly possibly due to the high stiffness of SiHA dominantly induce osteogenic differentiation over myogenic differentiation. The effect of perfusion on myogenesis was also investigated in this study. At day 3, there was no significant difference in myogenic differentiation of hMSCs under basal perfusion rate (BPR) compared with static culture. At both day 3 and day 7, a period of high perfusion rate (pHPR) significantly suppressed myogenic differentiation of hMSCs compared with static culture, as demonstrated by the downregulation of *myoD* expression.

Integrins play important roles in adhesion, cell survival, regulating matrix metabolism and responding to mechanical stimuli (Desgrosellier and Cheresh, 2010; Kasten *et al.*, 2010; Lee *et al.*, 2015). Previous study demonstrated that integrin β1 plays predominant roles in shear induced signalling and gene expression in osteoblast like cells (Lee *et al.*, 2008). Yan also showed that the knockdown of integrin β1 led to the

inhibition of ERK activity and cell proliferation (Yan *et al.*, 2012). The mechanism proposed was that integrin β1 in hMSCs acts as mechanoreceptors, which can activate signalling proteins such as focal adhesion kinase (FAK), and then activate the MAP kinase pathway (Friedland *et al.*, 2009; Young *et al.*, 2009; Lal *et al.*, 2007; Pommerenke *et al.*, 2002; Yang *et al.*, 2014). On the other hand, fluid shear stress has been demonstrated to upregulate the expression of *integrin β1* and this upregulation depended on FSS activated ERK1/2 (Liyue Liu *et al.*, 2012). In this study, the gene expression of *integrin β1* was upregulated up to 4 times during "chondrogenesis" under a period of high perfusion rate (pHPR). This finding strengthened previous research that β1 integrins play important roles in triggering the outside-in signalling and condensing precartilage during chondrogenesis of MSCs (Raghothaman *et al.*, 2014; Jin *et al.*, 2007; Zhang *et al.*, 2015), and blocking β1 integrins with blocking antibodies abolished proteoglycan synthesis response to mechanical stimuli (Chai *et al.*, 2010).

α integrins were widely recognised to be involved in stem cell lineage specification. This study demonstrated that *integrin α5* increased significantly while chondrogenic gene markers were upregulated under a period of high perfusion rate (pHPR), which is in line with previous research showing that the level of *integrin α5* increased during the early stage of chondrogenic differentiation (Jin *et al.*, 2007; Chang *et al.*, 2009). Combing the upregulation of *integrin β1* under a period of high perfusion rate (pHPR) condition, these results agreeing with previous research that the fibronectin receptor (integrin α5β1) was expressed and rose during chondrogenic differentiation of MSCs (Goessler *et al.*, 2008). Results from this study also indicate that the expression of *integrin α5* was upregulated significantly while the expression of osteogenic markers was enhanced under basal perfusion rate (BPR). However, there are conflicting results in the literature regarding the role of integrin α5 in osteogenesis. Some studies have reported that *integrin α5* was downregulated during osteogenesis (Chen *et al.*, 2016; Lu and Zreiqat, 2010); whereas others have suggested that *integrin α5* was upregulated during osteogenesis (Frith *et al.*, 2012) and downregulated with shRNA blocking osteogenic differentiation (Hamidouche *et al.*, 2009).

The expression profile of *integrin α1* was different to *integrin α5*, i.e. it was upregulated to a great extent during osteogenesis under basal perfusion rate (BPR). This is in line with findings from previous research that combined effects of mechanical stimulation and nanotopography led to significant upregulation of gene expression for *integrin α1*, as well as *runx2* in osteoblast like cells (Prodanov *et al.*, 2010). Previous research also demonstrated that COL I receptor *integrin α1*β1 played important roles in promoting osteogenesis, and it was consistently enhanced following BMP-2 treatment induced osteoblast differentiation (Jikko *et al.*, 1999; Salasznyk *et al.*, 2004).

Under static condition, hMSCs proliferation, cytoskeleton reorganisation, specific ALP activity, and most of the differentiation markers like *osx*, *alp*, *col i*, *dmp1*, *sox9*, *runx2* and *col ii* were not found to be responsive to BGS with different micro-porosities. On the contrary, when basal perfusion rate (BPR) was introduced to cell culture, at day 3, specific ALP activity and expression of *osx* were found to be significantly higher on BGS with higher micro-porosities like SiHA-22 and SiHA-28, compared with SiHA-14. At day 7, the phosphorylation of ERK1/2, and the expression of *myoD* were also significantly higher on BGS SiHA-22 and SiHA-28, compared with SiHA-14 under basal perfusion rate (BPR). At both day 3 and day 7, the expression of *alp* was found to be significantly higher on BGS SiHA-22 than both BGS SiHA-14 and SiHA-28 under basal perfusion rate (BPR).

Under a period of high perfusion rate (pHPR), the expression of markers and integrin subunits related to chondrogenic differentiation were also found to be responsive to micro-porosity of BGS. For example, at day 3, the expression of *runx2*, *col ii*, *integrin α5* and *integrin β1* were found to be significantly higher on SiHA-14 and SiHA-22, compared with SiHA-28 under a period of high perfusion rate (pHPR). At day D7, the expression of *runx2* and *integrin β1* was significantly higher on SiHA-22, compared with SiHA-14 and SiHA-28 under a period of high perfusion rate (pHPR). This demonstrates that traditional static culture is not enough to screen BGS with different micro-porosities. Basal perfusion rate (BPR) was not only able to induce osteogenic differentiation, but also screen the osteoconduction capability of BGS with different micro-porosities. A period of high perfusion rate (pHPR) was not only

able to induce chondrogenic differentiation, but also screen the chondroconduction capability of BGS with different micro-porosities.

5.5 Conclusion

In summary, results in this study have demonstrated a strong interaction between perfusion shear stress and BGS micro-porosity, with perfusion culture facilitated proliferation, activated signalling pathways and being able to differentiate the bioactivity of BGS *in vitro* even with a small geometric difference. Furthermore, this study showed a clear dependence of hMSCs fate on the perfusion flow rate applied. Basal perfusion rate (BPR) led to upregulation of osteogenic differentiation markers, whereas a period of high perfusion rate (pHPR) induced upregulation of chondrogenic differentiation markers. Therefore, these findings provide valuable guidance for the future research and design of testing protocols in terms of investigating the behaviour of hMSCs towards different lineage commitment in combination with different BGS structures and chemistries.

Chapter 6 L-type Voltage Sensitive Calcium Channels (VSCCs) Modulate Fluid Shear Stress Induced Differentiation of hMSCs Cultured on 3D SiHA BGS

6.1 Introduction

Mechanical stimuli have been reported to produce a variety of biological signals in bone cells, and one of the earliest events was the activation of calcium channels. Under physiological conditions, Ca^{2+} concentrations are reported to be 20,000 - 100,000 times higher in the extracellular space than in the cell cytoplasm (around 100 nM) (Clapham, 2007; Matta *et al.*, 2015; Demaurex and Nunes, 2016). With the activation of calcium channels, intracellular calcium ($[Ca^{2+}]i$) levels increase rapidly. For example, rat calvarial bone cells subjected to a hydrostatic pressure (6.9 x 10^4 dyn/cm^2, 1 Hz) were observed to have a significant increase in the concentration of $[Ca^{2+}]i$ after 25 s from the onset of mechanical strain (Brighton *et al.*, 1996). By monitoring flow induced $[Ca^{2+}]i$ changes in intact bone of embryonic chicks, researchers have also proved that the percentage of responsive cells was increased in both osteoblasts and osteocytes under flow compared with static condition (Ishihara *et al.*, 2013).

L-type voltage-sensitive calcium channels (VSCCs) are one of the best characterized type of calcium channel. Much study has been conducted investigating the participation of L-type VSCCs in responding to mechanical load by using L-type VSCCs inhibitor, like nifedipine. For example, researchers have reported L-type VSCCs mediate load-induced bone formation *in vivo* (Li *et al.*, 2002; Li *et al.*, 2003), and they are critical components actively involved in the early long bone skeletal development (Shao *et al.*, 2005).

The early response of rat osteoblasts to bone loading was found to be associated with L-type VSCCs (Rawlinson *et al.*, 1996). Whereas the responsiveness of L-type VSCCs to loading is conflicting in osteocytes. Rawlinson reported osteocytes' response to bone loading did not involve ion channels dependent on nifedipine (Rawlinson *et al.*, 1996), however, Miyauchi found that hypotonic stretch induced

rapid $[Ca^{2+}]i$ increase in isolated osteocytes, which required the expression of L-type Ca^{2+} channel subunit α1C (Miyauchi *et al.*, 2000). One possible reason of these conflicting results is that osteocytes were cultured in different environments, i.e. in situ in bone loading experiment (Rawlinson *et al.*, 1996), or isolated osteocytes stimulated by hypotonic stretch (Miyauchi *et al.*, 2000). This suggests that experiment should be carefully evaluated when conducting comparison between different findings. Only a few studies have been conducted to investigate the presence or function of L-type VSCCs in MSCs. Li demonstrated that L-type VSCCs were presented in a small portion of undifferentiated rat MSCs (Li *et al.*, 2006). Wen reported that L-type VSCCs play a crucial role in the proliferation, expression of osteogenic markers in rat MSCs (Wen *et al.*, 2012). Kearney demonstrated that L-type VSCCs coupled tensile strains of 7.5% or greater activated calpain and JNK, which lead to apoptosis of rat MSCs through DNA fragmentation (Kearney *et al.*, 2008).

Application of stretch via an expandable membrane resulted in immediate increase in $[Ca^{2+}]i$ in rat femur-derived osteoblast cells, which in turn modulated the increased production of OPN and OC proteins. Presence of nifedipine, L-type VSCCs blocker, blocked increases in $[Ca^{2+}]i$ and these matrix proteins production (Walker *et al.*, 2000). However, there are conflicting results in the literature regarding involvement of L-type VSCCs in response to fluid flow. Oscillatory fluid flow (20 to -20 dyn/cm^2, 1 Hz, 2 h) was found to induce $[Ca^{2+}]i$ mobilization within 1 min, then p38 and ERK1/2 activation and *opn* mRNA upregulation in MC3T3-E1 cells, with L-type VSCCs playing an important role in this process (You *et al.*, 2001). Liu reported that steady fluid flow (12 dyn/cm^2, 30 min) also induced ERK1/2 phosphorylation in MC3T3-E1 cells, which was dependent on L-type VSCCs activation and ATP release (Liu *et al.*, 2008). However, Chen demonstrated that MC3T3-E1 cells responded to steady fluid flow (12 dyn/cm^2, 1 h) by showing $[Ca^{2+}]i$ increase within 20 s of onset, cytoskeletal reorganisation and c-fos and COX-2 activation, but these responses were independent of L-type VSCCs (Chen *et al.*, 2000). This may indicate that steady flow (12 dyn/cm^2) or oscillatory fluid flow (20 to -20 dyn/cm^2) induced L-type VSCCs play an important role in MAP kinase activation, but L-type VSCCs were not involved in steady flow (12 dyn/cm^2) induced cytoskeletal reorganisation. Ryder found that

steady fluid shear (12 dyn/cm^2 or 25 dyn/cm^2, 3 min) induced [Ca^{2+}]i increase in MC3T3-E1 cells, but it was independent of L-type VSCCs, although in the same study, L-type VSCCs were found to be involved in parathyroid hormone (PTH) enhanced the [Ca^{2+}]i response to shear (Ryder and Duncan, 2001). It should be borne in mind that all of these studies investigating the involvement of L-type VSCCs in response to fluid flow were conducted in monolayer cell culture model, and shear stress in these studies (12 - 25 dyn/cm^2) are several magnitudes higher than the shear stress (0.001 - 1 dyn/cm^2) in 3D bioreactor system that have been reported to be able to activate signalling pathways and osteogenic differentiation (Goldstein *et al.*, 2001; Bancroft *et al.*, 2002; Gomes *et al.*, 2003; Sikavitsas *et al.*, 2005; Li *et al.*, 2009; Vance *et al.*, 2005; McCoy and O'Brien, 2010). It has not been investigated how L-type VSCCs regulate shear stress induced biological signals in a 3D perfusion culture model.

Findings in a previous chapter (Chapter 5) demonstrated that fluid flow induced expression of osteogenic differentiation or chondrogenic differentiation markers of hMSCs cultured on SiHA BGS was dependent on the flow profile and micro-porosity of SiHA BGS. The aim of this study was to investigate the role of L-type VSCCs in these processes.

6.2 Materials and Methods

hMSCs seeded on either SiHA-14 or SiHA-28 BGS granules were cultured under static condition, basal perfusion rate (BPR) or a period of high perfusion rate (pHPR) as described in Chapter 5.2, hereafter cited as "control group", or in control medium supplemented with 10 μM nifedipine for 3 days, hereafter cited as "nifedipine group". 100 ml medium was recirculated for each BGS during 3 days of perfusion culture, and the bottle of medium was vented in normoxic atmosphere. Composition of cell culture medium can be seen in Table 6-1. All analytical methods are same for control group and nifedipine group, which can be seen in Chapter 5, and all data are from 3 days of culture.

Table 6-1 Cell culture medium in control group and nifedipine group in CO_2 atmosphere.

	Control group	Nifedipine group
Day 1	PM	PM + 10 μM nifedipine
Day 2 - Day 3	PMO	PMO + 10 μM nifedipine

* PM and PMO are defined in Chapter 4.2.

6.3 Results

6.3.1 Cytoskeleton Organisation

Changes in actin cytoskeleton were monitored to determine if L-type VSCCs mediated the shear stress induced cytoskeletal organisation on SiHA-14 (Figure 6-1) and SiHA-28 (Figure 6-2) BGS. The presence of nifedipine was not found to change the cytoskeleton of hMSCs noticeably compared with control group on both SiHA-14 and SiHA-28 BGS, irrespective the culture conditions. This was confirmed by the quantification of the average cellular size, as shown in Figure 6-3, which demonstrated that the presence of nifedipine did not change cellular size significantly compared with control group on both SiHA-14 (Figure 6-3 (a)) and SiHA-28 BGS (Figure 6-3 (b)), irrespective of culture conditions. On SiHA-14, cell area was significantly larger when cultured in a static environment compared with cultured in a period of high perfusion rate (pHPR) environment in control group. However, there was no significant difference in cell area on SiHA-14 in nifedipine group, irrespective the culture conditions. On SiHA-28, cell area was significantly larger when cultured in

a static environment than cultured in basal perfusion rate (BPR) or a period of high perfusion rate (pHPR) environment in both control group and nifedipine group.

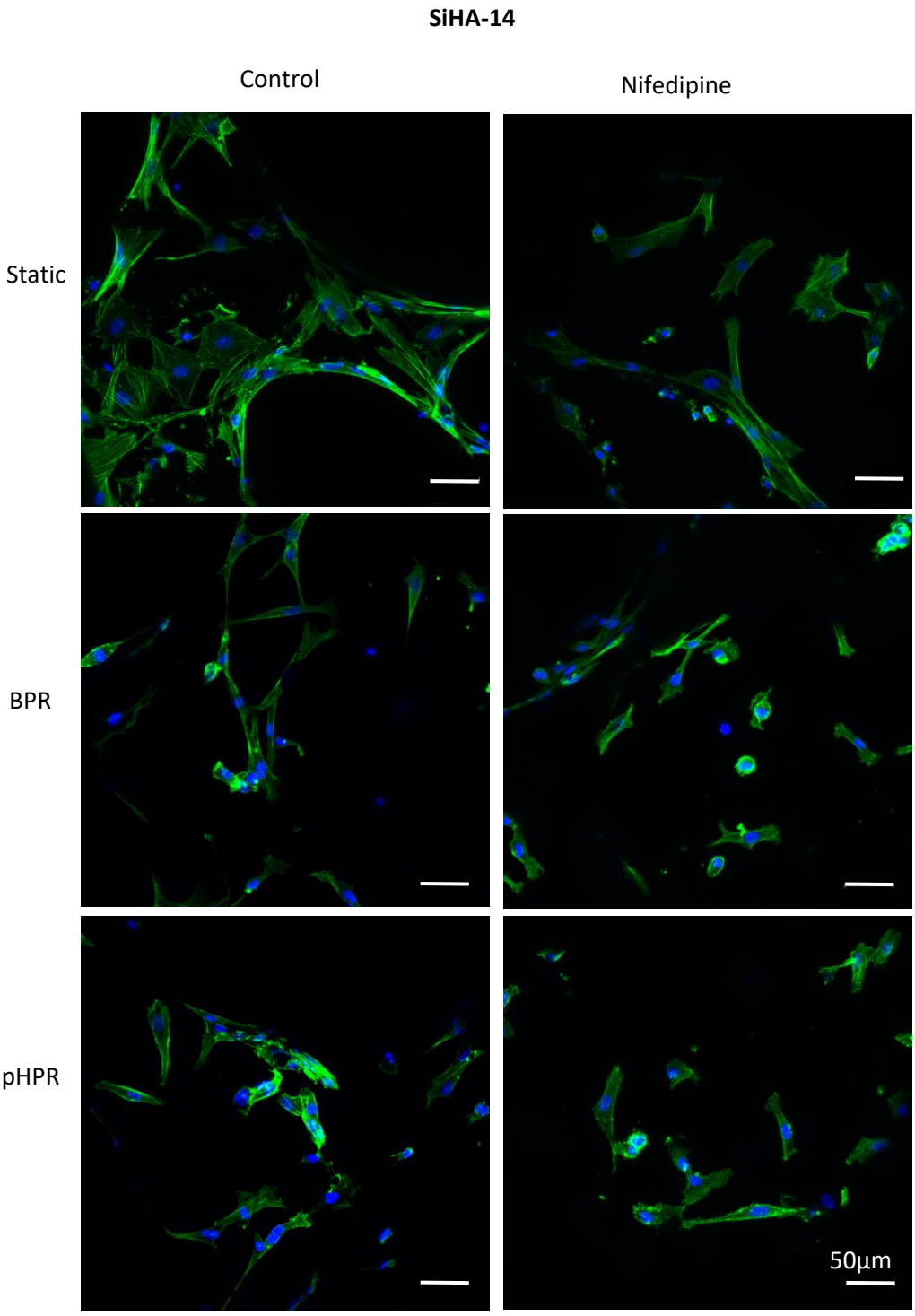

Figure 6-1 Influence of nifedipine on actin organisation in hMSCs on SiHA-14 under static, basal perfusion rate (BPR) and a period of high perfusion rate (pHPR) conditions. The actin cytoskeleton was labelled with Alexa 488 conjugated phalloidin (green) and nuclei were counterstained with DAPI (blue). Scale bar represents 50 µm.

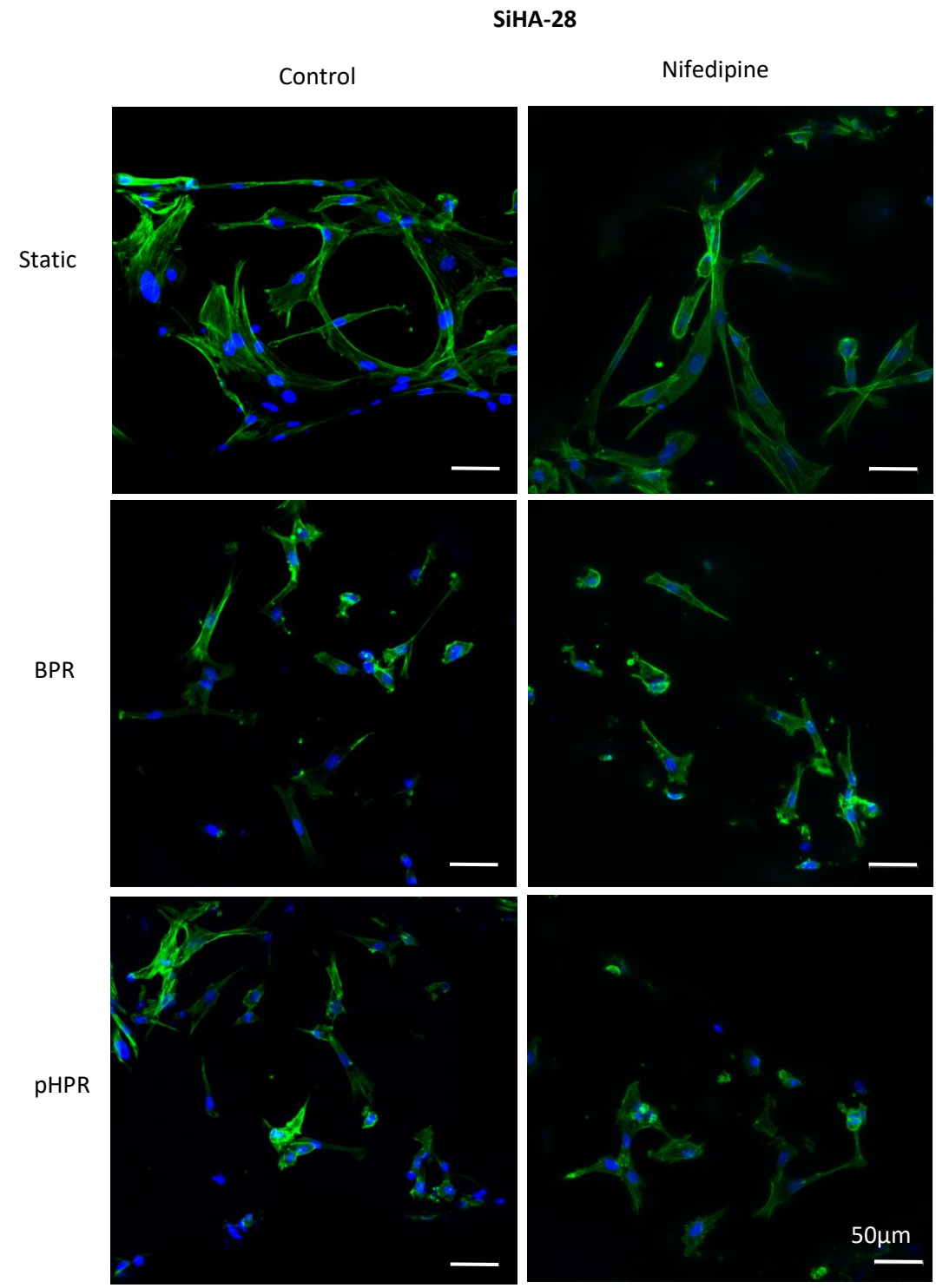

Figure 6-2 Influence of nifedipine on actin organisation in hMSCs on SiHA-28 under static basal perfusion rate (BPR) and a period of high perfusion rate (pHPR) conditions. The actin cytoskeleton was labelled with Alexa 488 conjugated phalloidin (green) and nuclei were counterstained with DAPI (blue). Scale bar represents 50 µm.

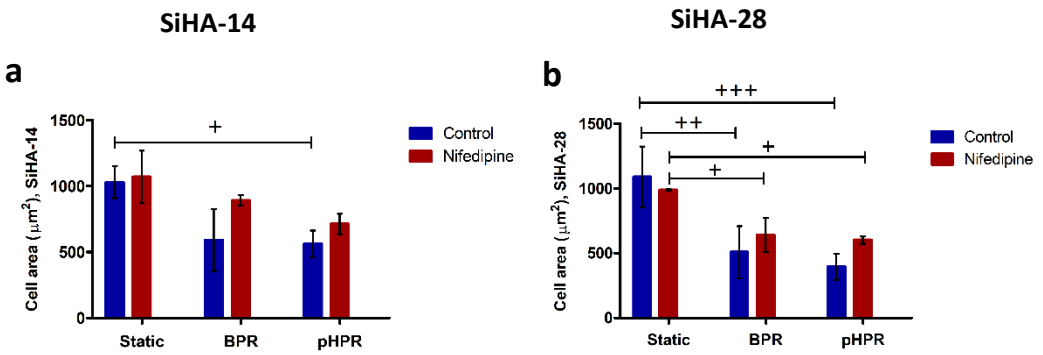

Figure 6-3 Influence of nifedipine on cellular size of hMSCs on (a) SiHA-14 and (b) SiHA-28 BGS under static, basal perfusion rate (BPR) and a period of high perfusion rate (pHPR) conditions. Results are presented as mean ± standard deviation (n=3). Statistical analysis was performed by two-way ANOVA followed by Bonferroni post-tests. +p < 0. 05, ++p < 0.01, +++p < 0.001, comparison between static, basal perfusion rate (BPR) and a period of high perfusion rate (pHPR).

6.3.2 Total DNA and Specific ALP Activity

Total DNA was quantified to determine whether L-type VSCCs modulated cellular proliferation on SiHA BGS. As can be seen in Figure 6-4 (a), on SiHA-14, under static culture and basal perfusion rate (BPR) conditions, total DNA production was not significantly influenced by adding nifedipine into medium, however, under a period of high perfusion rate (pHPR) condition, total DNA production increased significantly with the presence of nifedipine compared with control group. On BGS SiHA-14, total DNA production was not responsive to culture conditions in control group. However, with the presence of nifedipine, total DNA production was significantly higher when BGS were cultured under a period of high perfusion rate (pHPR) condition compared with under basal perfusion rate (BPR) and static condition, with total DNA production under basal perfusion rate (BPR) condition being significantly higher than under static condition. Figure 6-4 (b) showed adding nifedipine into medium did not affect total DNA on SiHA-28 BGS under any culture conditions. On SiHA-28, total DNA production was found to be significantly higher under both basal perfusion rate (BPR) and a period of high perfusion rate (pHPR) conditions compared with static condition, irrespective whether nifedipine was added into medium. In both control group and nifedipine group, total DNA production was not found to be dependent on BGS micro-porosity, irrespective of culture condition.

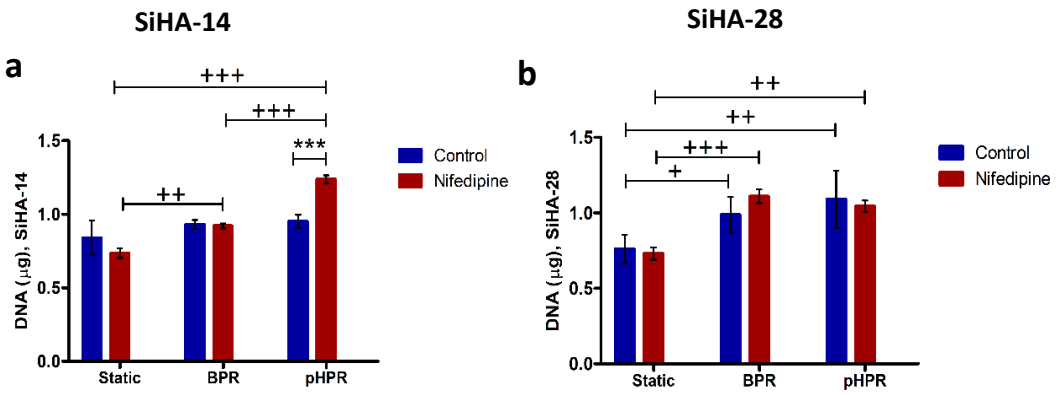

Figure 6-4 Total DNA content of hMSCs on (a) SiHA-14 and (b) SiHA-28 BGS under static, basal perfusion rate (BPR) and a period of high perfusion rate (pHPR) conditions. Results are presented as mean ± standard deviation (n=3). Statistical analysis was performed by two-way ANOVA followed by Bonferroni post-tests. ***p < 0.001, the comparison between control group and nifedipine group. +p < 0.05, ++p < 0.01, +++p < 0.001, comparison between static, basal perfusion rate (BPR) and a period of high perfusion rate (pHPR).

ALP activity was measured and normalized by total DNA content (i.e. specific ALP activity) to examine how L-type VSCCs mediated the specific ALP activity of hMSCs on SiHA BGS. As can be seen in Figure 6-5 (a), on SiHA-14 BGS, specific ALP activity was not found to be dependent on the presence of nifedipine irrespective of culture conditions. On SiHA-14 BGS, specific ALP activity was found to be significantly higher under static condition than both basal perfusion rate (BPR) and a period of high perfusion rate (pHPR) conditions, irrespective whether nifedipine was added into medium.

As can be seen in Figure 6-5 (b), on SiHA-28, under basal perfusion rate (BPR) condition, specific ALP activity was significantly decreased by adding nifedipine into medium compared with control group. On SiHA-28, under static and a period of high perfusion rate (pHPR) conditions, specific ALP activity was reduced with the presence of nifedipine in medium compared with control group. When SiHA-28 BGS was incubated in control medium, specific ALP activity was significantly lower under a period of high perfusion rate (pHPR) condition than static condition, however, with the presence of nifedipine, specific ALP activity was not found to be dependent on culture conditions.

As can be seen in Figure 6-5, in control medium, under basal perfusion rate (BPR) condition, specific ALP activity increased significantly on SiHA-28 compared with

SiHA-14, whereas under static condition and a period of high perfusion rate (pHPR) condition, specific ALP activity was not responsive to BGS type. When nifedipine was added into medium, specific ALP activity was not found to be responsive to BGS micro-porosity irrespective of culture conditions.

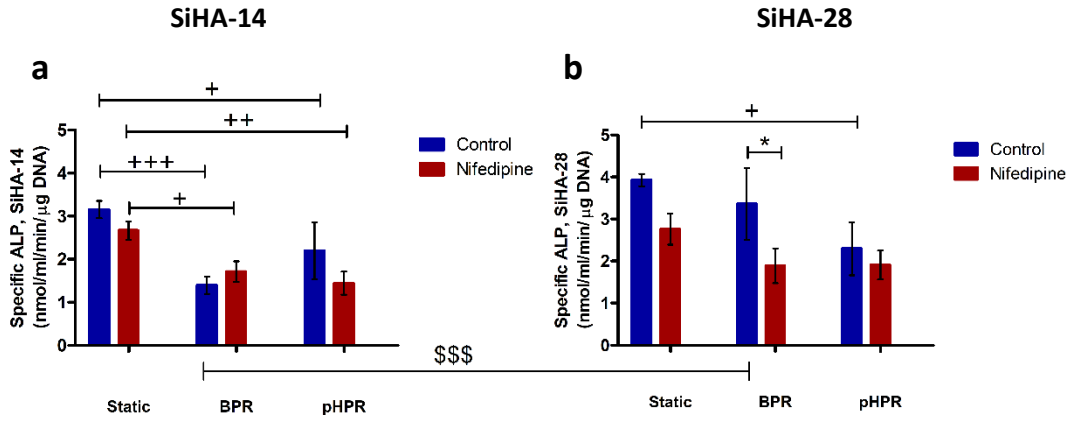

Figure 6-5 Specific ALP activity of hMSCs on (a) SiHA-14 and (b) SiHA-28 BGS under static, basal perfusion rate (BPR) and a period of high perfusion rate (pHPR) conditions. Results are presented as mean ± standard deviation (n=3). Results are presented as mean ± standard deviation (n=3). Statistical analysis was performed by two-way ANOVA followed by Bonferroni post-tests. *p < 0.05, comparison between control group and nifedipine group. +p < 0.05, ++p < 0.01, +++p < 0.001, comparison between static, basal perfusion rate (BPR) and a period of high perfusion rate (pHPR). $$$p < 0.001, comparison between SiHA-14 and SiHA-28.

6.3.3 ERK Distribution

ERK1/2 distribution followed similar pattern on SiHA-14 (Figure 6-6) and SiHA-28 (Figure 6-7) BGS. In control medium, ERK1/2 localised mostly in the cytoplasm (showed by white arrows in Figure 6-6 and Figure 6-7) under static condition, whereas strong nuclear accumulation of ERK1/2 was detected under both basal perfusion rate (BPR) and a period of high perfusion rate (pHPR) conditions (showed by yellow arrows in Figure 6-6 and Figure 6-7). However, with the addition of L-type VSCCs blocker nifedipine in medium, ERK1/2 was found to be homogeneously distributed in both cytoplasm and nucleus, irrespective of culture conditions (showed by green arrows in Figure 6-6 and Figure 6-7).

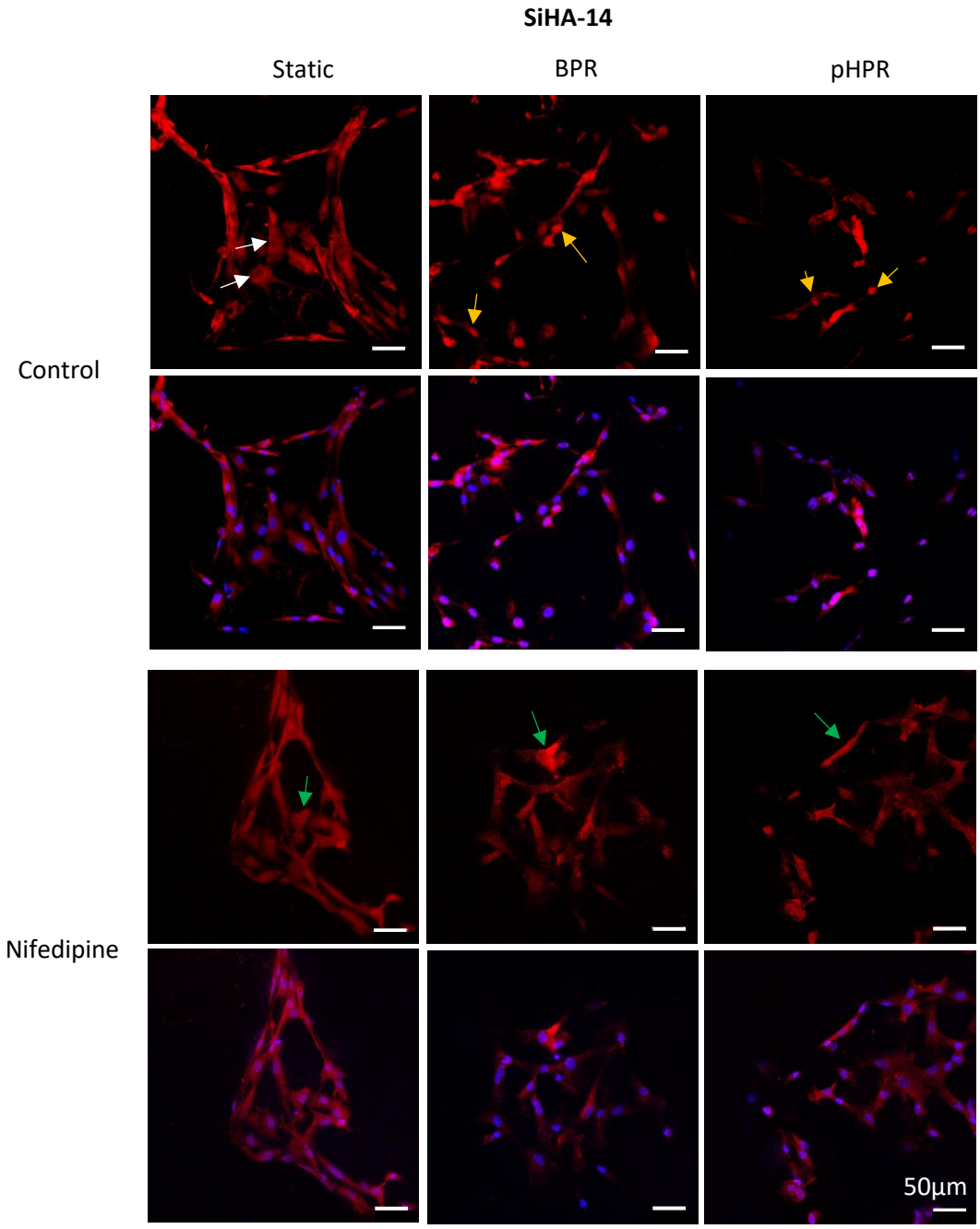

Figure 6-6 Influence of nifedipine on ERK1/2 distribution in hMSCs on SiHA-14 under static, basal perfusion rate (BPR) and a period of high perfusion rate (pHPR) conditions. ERK1/2 was labelled using an antibody against at ERK1/2 (red), and nuclei were counterstained with DAPI (blue), scale bar represents 50 µm. White arrow showed ERK1/2 localised exclusively in the cytoplasm, yellow arrow showed ERK1/2 was accumulated in nuclear, green arrow showed ERK1/2 was homogeneously distributed in both cytoplasm and nuclear.

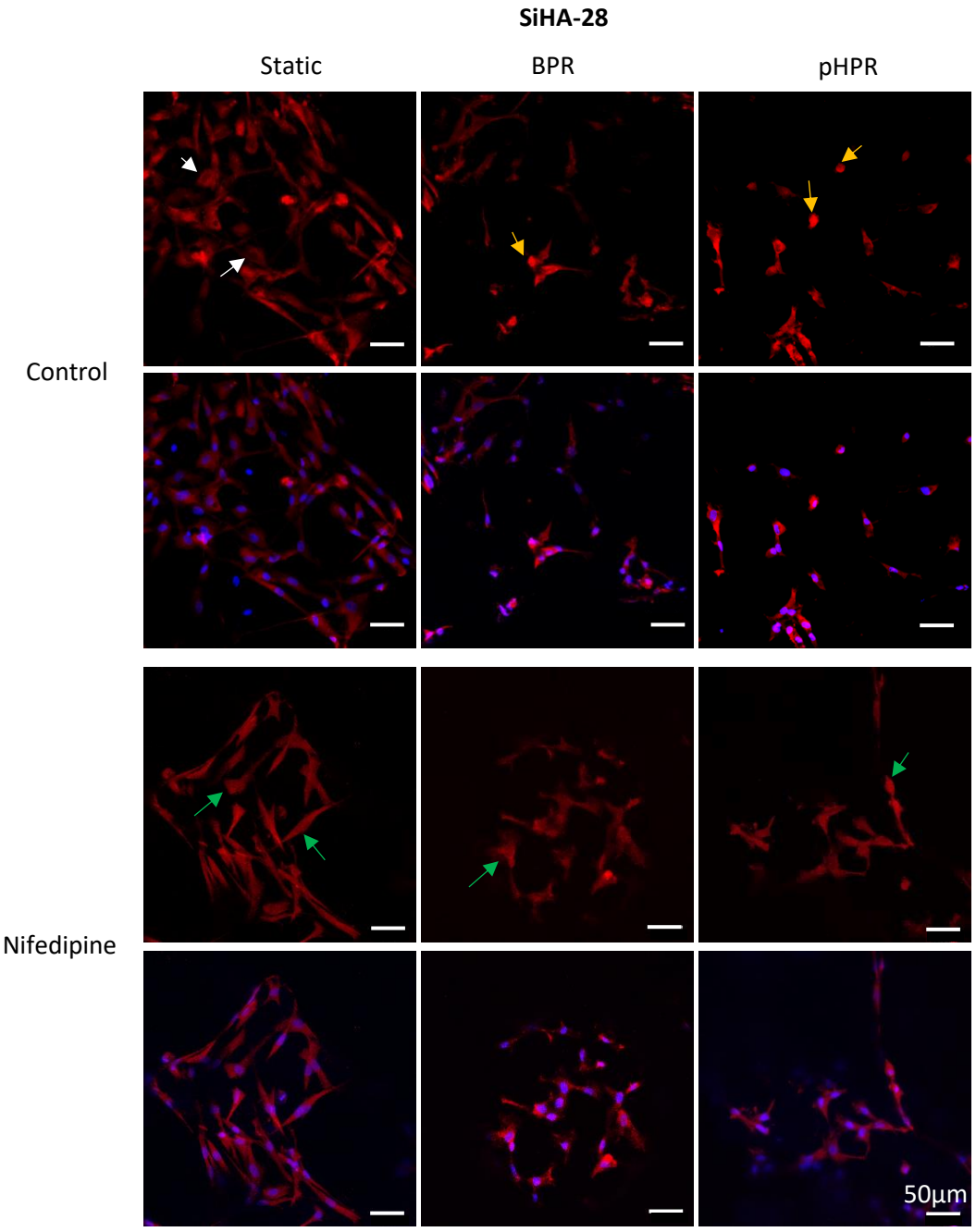

Figure 6-7 Influence of nifedipine on ERK1/2 distribution in hMSCs on SiHA-28 under static, basal perfusion rate (BPR) and a period of high perfusion rate (pHPR) conditions. ERK1/2 was labelled using an antibody against at ERK1/2 (red), and nuclei were counterstained with DAPI (blue), scale bar represents 50 µm. White arrow showed ERK1/2 localised exclusively in the cytoplasm, yellow arrow showed ERK1/2 was accumulated in nuclear, green arrow showed ERK1/2 was homogeneously distributed in both cytoplasm and nuclear.

6.3.4 Western Blot

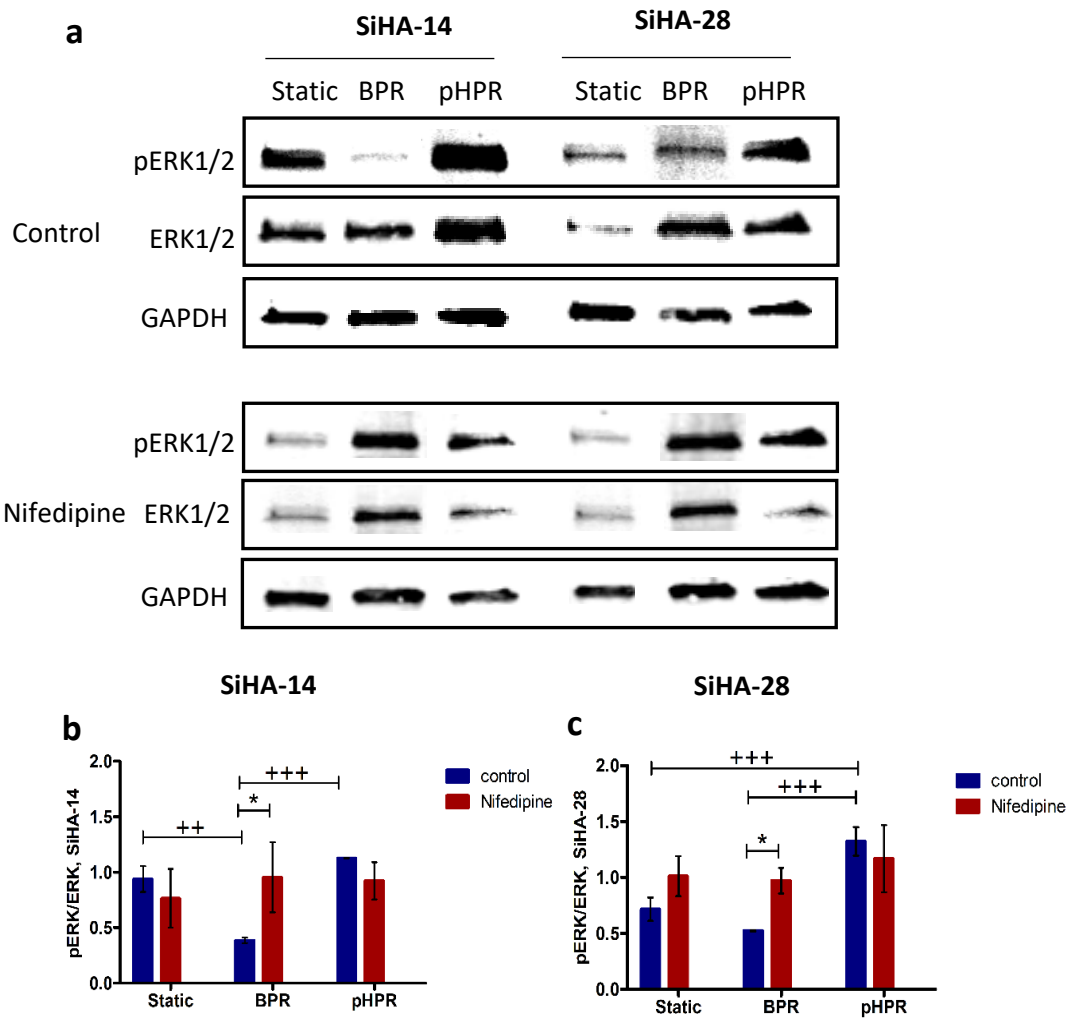

Figure 6-8 (a) Influence of nifedipine on pERK1/2 protein expression on SiHA-14 and SiHA-28 under static, basal perfusion rate (BPR) and a period of high perfusion rate (pHPR) conditions. (b)(c) Quantitative analysis of pERK1/2 expression. Results are presented as mean ± standard deviation (n=3). Statistical analysis was performed by two-way ANOVA followed by Bonferroni post-tests. *p < 0.05 comparison between control group and nifedipine. ++p < 0.01, +++p < 0.001, comparison between static, basal perfusion rate (BPR) and a period of high perfusion rate (pHPR).

The phosphorylated ERK1/2 was tested and normalised by total ERK1/2 to evaluate if L-type VSCCs mediated ERK1/2 activation. As can be seen in Figure 6-8 (b), on BGS SiHA-14, under basal perfusion rate (BPR), the presence of nifedipine significantly increased phosphorylation of ERK1/2 compared with control group. On BGS SiHA-14, in control medium, the phosphorylation of ERK1/2 was found to be significantly lower under basal perfusion rate (BPR) condition than both static and a period of high perfusion rate (pHPR) conditions, however, with the presence of nifedipine in

medium, the phosphorylation of ERK1/2 was not found to be dependent on the culture conditions.

As can be seen in Figure 6-8 (c), on BGS SiHA-28, under basal perfusion rate (BPR) condition, the presence of nifedipine significantly increased phosphorylation of ERK1/2 compared with control group. On BGS SiHA-28, in control medium, the phosphorylation of ERK1/2 was found to be significantly higher under a period of high perfusion rate (pHPR) condition than both static and basal perfusion rate (BPR) conditions, however, with the addition of nifedipine into medium, the phosphorylation of ERK1/2 was not found to be dependent on the culture conditions. In both control group and nifedipine group, the phosphorylation of ERK1/2 was not found to be responsive to BGS micro-porosity irrespective of culture conditions.

6.3.5 Relative Gene Expression

6.3.5.1 Expression of Osteogenic Gene Markers

hMSCs seeded BGS were cultured in static, basal perfusion rate (BPR) or a period of high perfusion rate (pHPR) environment in control medium or in medium supplemented with nifedipine for 3 days, and mRNA levels of osterix (*osx*), alkaline phosphatase (*alp*), bone morphogenetic protein 2 (*bmp2*), type I collagen (*col i*) and dentin matrix acidic phosphoprotein (*dmp1*) were measured by quantitative real-time PCR. *osx* is a transcription factor that has been demonstrated to be critical for osteoblast differentiation and bone formation (Nakashima *et al.*, 2002; Tu *et al.*, 2006). As can be seen from Figure 6-9 (a) and (b), on both BGS SiHA-14 and BGS SiHA-28, blocking L-type VSCCs with nifedipine significantly downregulated the expression of *osx* under basal perfusion rate (BPR) condition compared with control group, while significantly upregulated the expression of *osx* under a period of high perfusion rate (pHPR) condition, compared with control group. On BGS SiHA-14, in control medium, the expression of *osx* was significantly higher under basal perfusion rate (BPR) condition compared with static and a period of high perfusion rate (pHPR) conditions, with the expression of *osx* under a period of high perfusion rate (pHPR) condition being significantly higher than static condition. On BGS SiHA-14, with the addition of nifedipine in medium, the expression of *osx* was significantly higher under either type of perfusion conditions compared with static condition. On BGS SiHA-28, in control

medium, the expression of *osx* was significantly higher under basal perfusion rate (BPR) condition than both static and a period of high perfusion rate (pHPR) conditions, with the expression of *osx* under a period of high perfusion rate (pHPR) condition being significantly higher than static condition. On BGS SiHA-28, when nifedipine was added into medium, the expression of *osx* was significantly higher under a period of high perfusion rate (pHPR) condition than both basal perfusion rate (BPR) and static conditions, with the expression of *osx* under basal perfusion rate (BPR) condition being significantly higher than static condition. In control medium, under basal perfusion rate (BPR) condition, the expression of *osx* was significantly upregulated on SiHA-28 compared with SiHA-14, whereas, the expression of *osx* was not found responsive to BGS micro-porosity under static and a period of high perfusion rate (pHPR) condition. With the presence of nifedipine, the expression of *osx* was not found to be responsive to BGS micro-porosity irrespective of culture conditions.

ALP is a transient early marker of bone marrow stromal cells differentiating towards the osteoblastic phenotype (Datta *et al.*, 2005). On BGS SiHA-14, the addition of nifedipine into medium did not alter the expression of *alp* compared with control group, irrespective of culture conditions, as can be seen in Figure 6-9 (c). On BGS SiHA-14, the expression of *alp* was significantly higher under static condition than either type of perfusion conditions, irrespective whether nifedipine was added into medium. As can be seen in Figure 6-9 (d), on BGS SiHA-28, the expression of *alp* was significantly downregulated with the presence of nifedipine in the medium compared with control group under both static and basal perfusion rate (BPR) conditions, but not a period of high perfusion rate (pHPR) condition. On BGS SiHA-28, in control medium, the expression of *alp* was significantly higher under static condition than both basal perfusion rate (BPR) and a period of high perfusion rate (pHPR) conditions, whereas with the addition of nifedipine into medium, the expression of *alp* was significantly higher under both static and a period of high perfusion rate (pHPR) conditions compared with basal perfusion rate (BPR) condition. In control medium, the expression of *alp* was not found to be dependent on BGS micro-porosity irrespective of culture conditions. When medium was supplemented with nifedipine, under static condition, the expression of *alp* was found to be significantly

downregulated on SiHA-28 compared with SiHA-14, while under both basal perfusion rate (BPR) and a period of high perfusion rate (pHPR) conditions, the expression of *alp* was not found to be dependent on BGS micro-porosity.

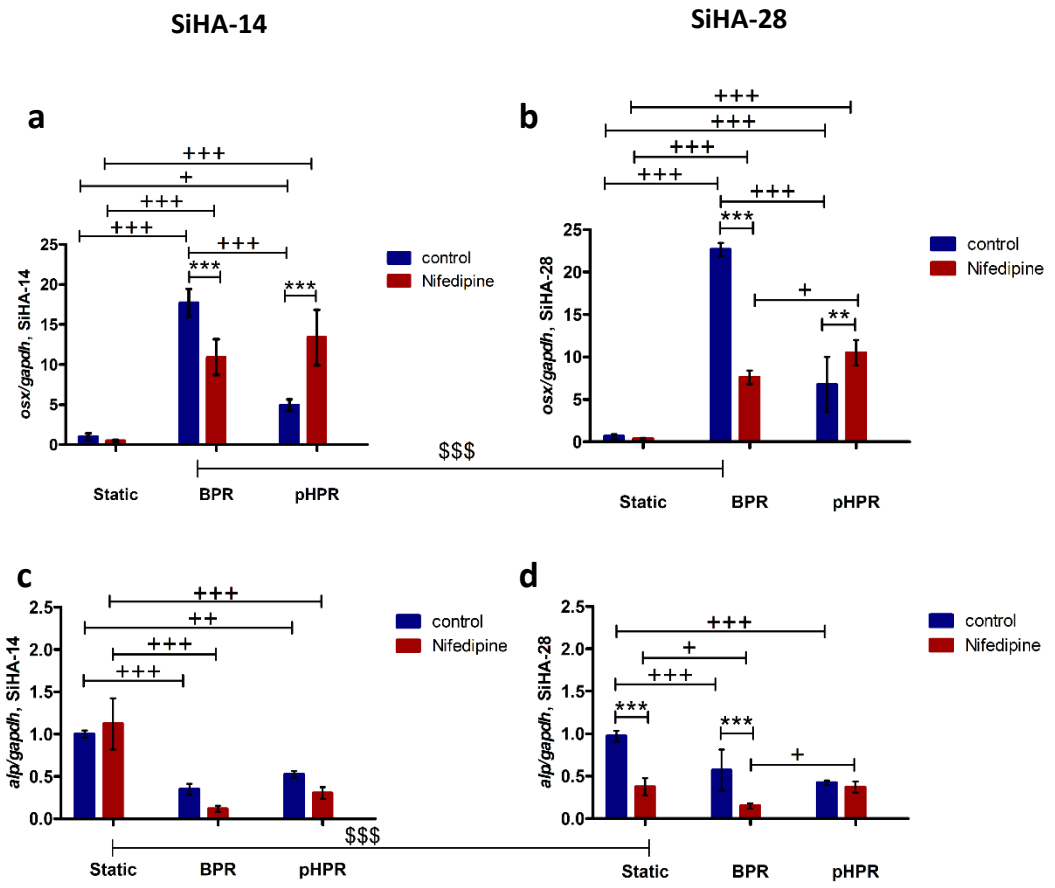

Figure 6-9 Influence of nifedipine on expression of *osx* and *alp* genes in hMSCs cultured on SiHA-14 and SiHA-28 under static, basal perfusion rate (BPR) and a period of high perfusion rate (pHPR) conditions. Results are presented as mean ± standard deviation (n=3). Statistical analysis was performed by two-way ANOVA followed by Bonferroni post-tests. **p < 0.01, ***p < 0.001, comparison between control group and nifedipine group. +p < 0.05, ++p < 0.01, +++p < 0.001, comparison between static, basal perfusion rate (BPR) and a period of high perfusion rate (pHPR). $$$p < 0.001, comparison between SiHA-14 and SiHA-28.

BMP2 plays a critical role in bone formation and regeneration (Reddi, 1998). On both BGS SiHA-14 and BGS SiHA-28, under a period of high perfusion rate (pHPR) condition, the expression of *bmp2* was significantly upregulated with the presence of nifedipine compared with control group, whereas under both static and basal perfusion rate (BPR) conditions, the expression of *bmp2* was not responsive to the addition of nifedipine into medium compared with control group, as can be seen in Figure 6-10

(a) and (b). On BGS SiHA-14, in control medium, the expression of *bmp2* was significantly higher under either type of perfusion conditions compared with under static condition. On BGS SiHA-14, with the addition of nifedipine into medium, the expression of *bmp2* under a period of high perfusion rate (pHPR) condition was significantly higher than both static and basal perfusion rate (BPR) conditions. On BGS SiHA-28, in control medium, the expression of *bmp2* was not found to be dependent on culture conditions, whereas when adding nifedipine into medium, the expression of *bmp2* was significantly higher under a period of high perfusion rate (pHPR) condition compared with both static and basal perfusion rate (BPR) conditions. In both control group and nifedipine group, under static condition, the expression of *bmp2* was significantly downregulated on SiHA-28 compared with SiHA-14, however, under either type of perfusion conditions, the expression of *bmp2* was not found to be responsive to BGS micro-porosity.

col i has been reported to be expressed early during the commitment to the osteoblastic phenotype (Rodan and Noda, 1991). On BGS SiHA-14, under basal perfusion rate (BPR) condition, the expression of *col i* was significantly downregulated with the presence of nifedipine in medium compared with control group, whereas under both static and a period of high perfusion rate (pHPR) conditions, the expression of *col i* was not dependent on the addition of nifedipine into medium compared with control group, as can be seen in Figure 6-10 (c). On BGS SiHA-14, in control medium, the expression of *col i* was significantly higher under basal perfusion rate (BPR) condition compared with both a period of high perfusion rate (pHPR) and static conditions, with the expression of *col i* under a period of high perfusion rate (pHPR) condition being significantly higher than under static condition. In medium supplemented with nifedipine, the expression of *col i* was not found to be dependent on culture conditions. On BGS SiHA-28, the expression of *col i* was not dependent on the presence of nifedipine compared with control group irrespective the culture conditions. On BGS SiHA-28, in control medium, the expression of *col i* was significantly higher under a period of high perfusion rate (pHPR) condition, compared with both basal perfusion rate (BPR) and static conditions, with the expression of *col i* under basal perfusion rate (BPR) being significantly higher than

static condition. On BGS SiHA-28, in medium supplemented with nifedipine, the expression of *col i* was significantly higher under either type of perfusion conditions compared with static condition. In control medium, under basal perfusion rate (BPR) condition, the expression of *col i* was significantly downregulated on SiHA-28 compared with SiHA-14, whereas under static and a period of high perfusion rate (pHPR) conditions, the expression of *col i* was not responsive to BGS micro-porosity. With the addition of nifedipine into medium, the expression of *col i* was not found to be responsive to BGS micro-porosity, irrespective of culture conditions.

dmp1 has been found to be highly expressed in osteocytes and can be classed as a pro-osteogenic factor (Kalajzic *et al.*, 2004). On both BGS SiHA-14 and BGS SiHA-28, under basal perfusion rate (BPR) condition, the expression of *dmp1* was significantly downregulated with the presence of nifedipine in medium compared with control group, whereas under both static and a period of high perfusion rate (pHPR) conditions, the expression of *dmp1* was not responsive to the addition of nifedipine into medium compared with control group, as can be seen in Figure 6-10 (e) and (f). On BGS SiHA-14, the expression of *dmp1* was found to be significantly higher under basal perfusion rate (BPR) condition than both static and a period of high perfusion rate (pHPR) conditions, irrespective whether nifedipine was added into culture medium. On BGS SiHA-28, in control medium, the expression of *dmp1* was found to be significantly higher under basal perfusion rate (BPR) condition than both static and a period of high perfusion rate (pHPR) conditions, with the expression of *dmp1* under a period of high perfusion rate (pHPR) being significantly higher than under static condition. On BGS SiHA-28, with the addition of nifedipine into medium, the expression of *dmp1* was significantly higher under a period of high perfusion rate (pHPR) condition than under static condition. In control medium, the expression of *dmp1* was not found to be dependent on BGS micro-porosity, irrespective of culture conditions. With the presence of nifedipine in medium, under basal perfusion rate (BPR) condition, the expression of *dmp1* was significantly downregulated on SiHA-28 compared with SiHA-14, whereas under a period of high perfusion rate (pHPR) condition, the expression of *dmp1* was significantly upregulated on SiHA-28 compared with SiHA-14.

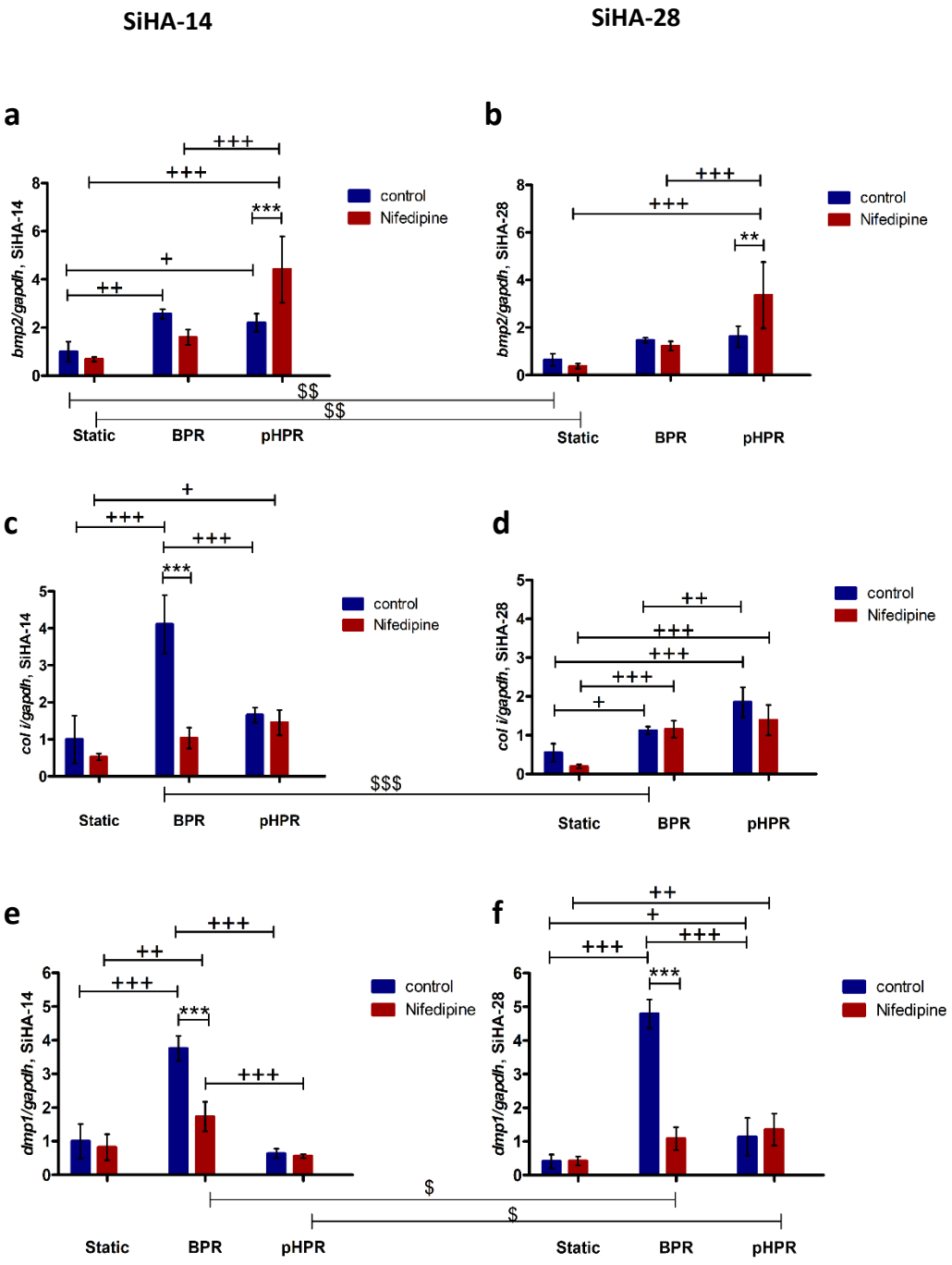

Figure 6-10 Influence of nifedipine on expression of *bmp2*, *col i* and *dmp1* in hMSCs cultured on SiHA-14 and SiHA-28 under static, basal perfusion rate (BPR) and a period of high perfusion rate (pHPR) conditions. Results are presented as mean ± standard deviation (n=3). Statistical analysis was performed by two-way ANOVA followed by Bonferroni post-tests. **p < 0.01, ***p < 0.001, comparison between control group and nifedipine group. +p < 0.05, ++p < 0.01, +++p < 0.001, comparison between static, basal perfusion rate (BPR) and a period of high perfusion rate (pHPR). $$p < 0.01, $$$p < 0.001, comparison between SiHA-14 and SiHA-28.

6.3.5.2 Expression of Chondrogenic Gene Markers

SRY-box 9 (*sox9*) and runt-related transcription factor 2 (*runx2*) have been identified as important transcriptional regulators of early and late stage chondrogenic differentiation, respectively (Karsenty, 2008). On BGS SiHA-14, the expression of *sox9* was not dependent on the addition of nifedipine into medium, irrespective of culture conditions, as can be seen in Figure 6-11 (a). On BGS SiHA-14, in both control medium and medium with the presence of nifedipine, the expression of *sox9* was significantly higher under a period of high perfusion rate (pHPR) condition compared with both basal perfusion rate (BPR) and static conditions, with the expression of *sox9* under basal perfusion rate (BPR) being significantly higher than under static condition. On BGS SiHA-28, under a period of high perfusion rate (pHPR) condition, *sox9* expression was significantly upregulated by the presence of nifedipine compared with control medium, whereas under both static and basal perfusion rate (BPR) conditions, *sox9* expression was not dependent on the presence of nifedipine in medium compared with control medium, as can be seen in Figure 6-11 (b). On BGS SiHA-28, in control medium, *sox9* expression was significantly higher under either type of perfusion conditions compared with under static condition. On BGS SiHA-28, in medium supplemented with nifedipine, *sox9* expression was significantly higher under a period of high perfusion rate (pHPR) condition compared with both basal perfusion rate (BPR) and static conditions, with *sox9* expression under basal perfusion rate (BPR) condition being significantly higher than under static condition. In both control medium and medium supplemented with nifedipine, *sox9* expression was not found to be dependent on BGS micro-porosity, irrespective of culture conditions.

On BGS SiHA-14, *runx2* expression was significantly upregulated with the presence of nifedipine in medium compared with control medium under both basal perfusion rate (BPR) and a period of high perfusion rate (pHPR) conditions, but not static condition, as can be seen in Figure 6-11 (c). On BGS SiHA-14, in control medium, *runx2* expression was significantly higher under a period of high perfusion rate (pHPR) condition than both basal perfusion rate (BPR) and static conditions. On BGS SiHA-14, with the addition of nifedipine into medium, *runx2* expression was significantly higher under a period of high perfusion rate (pHPR) condition than both basal

perfusion rate (BPR) and static conditions, with *runx2* expression under basal perfusion rate (BPR) being significantly higher than static condition. On BGS SiHA-28, under static and basal perfusion rate (BPR) conditions, the expression of *runx2* was not dependent on the presence of nifedipine in medium, whereas under a period of high perfusion rate (pHPR), the expression of was significantly upregulated by the addition of nifedipine into medium compared with control medium, as can be seen in Figure 6-11 (d). On BGS SiHA-28, in control medium, the expression of *runx2* was not dependent on culture conditions. On BGS SiHA-28, in medium supplemented with nifedipine, the expression of *runx2* was significantly higher under a period of high perfusion rate (pHPR) condition than both basal perfusion rate (BPR) and static conditions, with the expression of *runx2* under basal perfusion rate (BPR) condition being significantly higher than static condition. In control medium, under a period of high perfusion rate (pHPR) condition, *runx2* expression was significantly downregulated on SiHA-28 compared with on SiHA-14, whereas under basal perfusion rate (BPR) and static conditions, *runx2* expression was not responsive to the BGS micro-porosity. In medium supplemented with nifedipine, the expression of *runx2* was not found to be dependent on BGS micro-porosity irrespective of culture conditions.

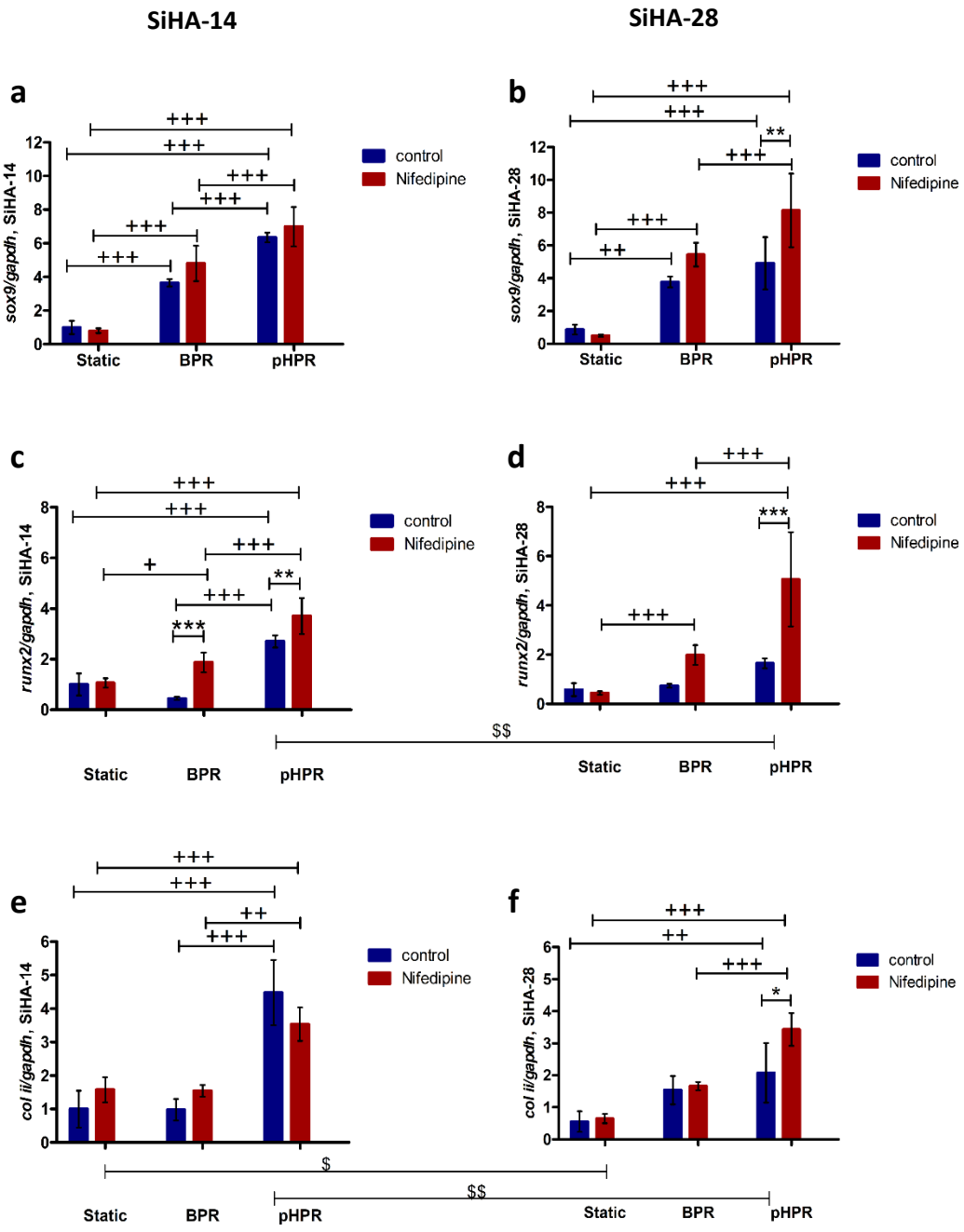

Figure 6-11 Influence of nifedipine on expression of chondrogenic gene markers in hMSCs cultured on SiHA-14 and SiHA-28 under static, basal perfusion rate (BPR) and a period of high perfusion rate (pHPR) conditions. Results are presented as mean ± standard deviation (n=3). Statistical analysis was performed by two-way ANOVA followed by Bonferroni post-tests. *p < 0.05, **p < 0.01, ***p < 0.001, comparison between control group and nifedipine group. +p < 0.05, ++p < 0.01, +++p < 0.001, comparison between static, basal perfusion rate (BPR) and a period of high perfusion rate (pHPR). $p <0.05, $$p < 0.01, comparison between SiHA-14 and SiHA-28.

Type II collagen (COI II) is the major structural component of cartilage, so it is one of the commonly used markers of chondrogenesis (Ng *et al.*, 1997). On BGS SiHA-14, *col ii* expression was not responsive to the presence of nifedipine in medium irrespective

of culture conditions (Figure 6-11 (e)). On BGS SiHA-14, in both control medium and medium with the addition of nifedipine, the expression of *col ii* was significantly higher under a period of high perfusion rate (pHPR) condition than both static and basal perfusion rate (BPR) conditions. On BGS SiHA-28, under both static and basal perfusion rate (BPR) conditions, *col ii* expression was not responsive to the presence of nifedipine in medium, whereas under a period of high perfusion rate (pHPR) condition, *col ii* expression was significantly upregulated with the presence of nifedipine in medium compared with control medium (Figure 6-11 (f)). On BGS SiHA-28, in control medium, *col ii* expression was significantly higher under a period of high perfusion rate (pHPR) condition than under static condition, whereas in medium with the addition of nifedipine, *col ii* expression was significantly higher under a period of high perfusion rate (pHPR) condition than both basal perfusion rate (BPR) and static conditions. In control medium, under both static and a period of high perfusion rate (pHPR) conditions, the expression of *col ii* was significantly downregulated on SiHA-28 compared with on SiHA-14. In medium with the presence of nifedipine, the expression of *col ii* was not dependent on BGS micro-porosity irrespective of culture conditions.

6.3.5.3 Expression of Myogenic Gene Marker

Myoblast determination protein (*myoD*) is a myogenic transcriptional regulatory factor that activates a number of muscle-specific structural genes and transcription factors to drive myogenesis (Rao *et al.*, 2006). As shown in Figure 6-12 (a), on SiHA-14 BGS, blocking L-type VSCCs with nifedipine significantly downregulated the gene expression of *myoD* compared with in control medium under both static and basal perfusion rate (BPR) conditions, but not under a period of high perfusion rate (pHPR) condition. On BGS SiHA-14, in control medium, the expression of *myoD* was significantly higher under both static and basal perfusion rate (BPR) conditions compared with under a period of high perfusion rate (pHPR) condition. On BGS SiHA-14, in medium supplemented with nifedipine, *myoD* expression was significantly higher under static condition than both basal perfusion rate (BPR) and a period of high perfusion rate (pHPR) conditions. On BGS SiHA-28, under basal perfusion rate (BPR) condition, the expression of *myoD* was significantly downregulated by the

presence of nifedipine in the medium compared with control medium, whereas under both static and a period of high perfusion rate (pHPR) conditions, the expression of *myoD* was not dependent on the addition of nifedipine into medium, as can be seen in Figure 6-12 (b). On BGS SiHA-28, in control medium, *myoD* expression was significantly higher under basal perfusion rate (BPR) condition compared with under a period of high perfusion rate (pHPR) condition. On BGS SiHA-28, in medium with the addition of nifedipine, *myoD* expression was significantly higher under static condition compared than both basal perfusion rate (BPR) and a period of high perfusion rate (pHPR) conditions. In control medium, the expression of *myoD* was significantly downregulated on BGS SiHA-28 than SiHA-14 under both static and basal perfusion rate (BPR) conditions, but not a period of high perfusion rate (pHPR) condition. In medium with the addition of nifedipine, the expression of *myoD* was not found to be dependent on BGS micro-porosity irrespective of culture conditions.

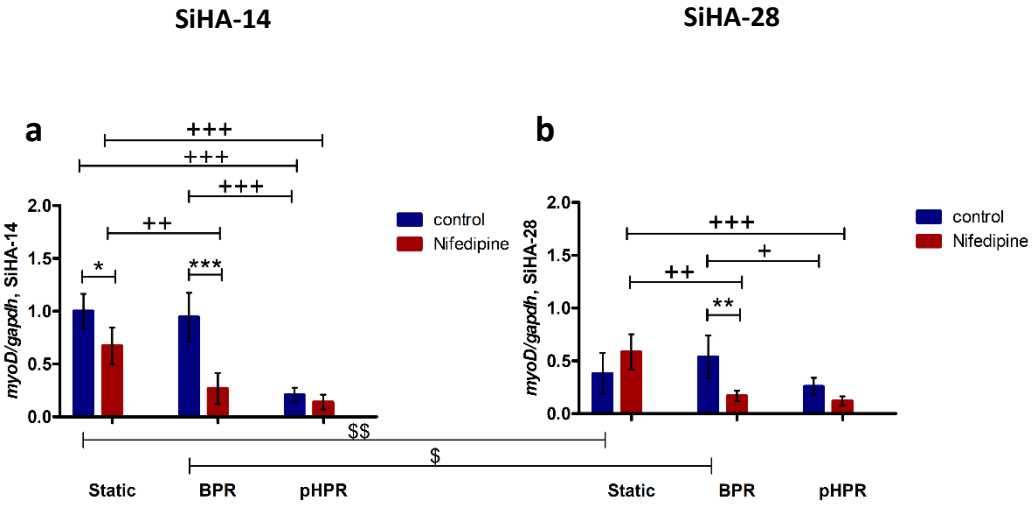

Figure 6-12 Influence of nifedipine on gene expression of *myoD* in hMSCs cultured on SiHA-14 and SiHA-28 under static, basal perfusion rate (BPR) and a period of high perfusion rate (pHPR) conditions. Results are presented as mean ± standard deviation (n=3). Statistical analysis was performed by two-way ANOVA followed by Bonferroni post-tests. ***p < 0.001, comparison between control group and nifedipine group. ++p < 0.01, +++p < 0.01, comparison between static, basal perfusion rate (BPR) and a period of high perfusion rate (pHPR). $p <0.05, $$p < 0.01, comparison between SiHA-14 and SiHA-28.

6.3.5.4 Expression of Integrin Subunits

On BGS SiHA-14, the expression of *integrin α1* was significantly downregulated under either type of perfusion conditions (Figure 6-13 (a)) by the presence of nifedipine in

culture medium compared with control medium. On BGS SiHA-14, in control medium, the expression of *integrin α1* was significantly higher under basal perfusion rate (BPR) condition than both static and a period of high perfusion rate (pHPR) conditions, with *integrin α1* expression under a period of high perfusion rate (pHPR) being significantly higher than under static condition. On BGS SiHA-14, with the presence of nifedipine in the medium, the expression of *integrin α1* was significantly higher under a period of high perfusion rate (pHPR) than basal perfusion rate (BPR) condition. On BGS SiHA-28, under basal perfusion rate (BPR) condition, the expression of *integrin α1* was significantly downregulated by the addition of nifedipine into medium, whereas under both static and a period of high perfusion rate (pHPR) conditions, the expression of *integrin α1* was not responsive to the presence of nifedipine in the medium compared with control medium, as can be seen in Figure 6-13 (b). On BGS SiHA-28, in control medium, the expression of *integrin α1* was significantly higher under either type of perfusion condition compared with under static condition. On BGS SiHA-28, in medium supplemented with nifedipine, the expression of *integrin α1* was significantly higher under a period of high perfusion rate (pHPR) condition than both static and basal perfusion rate (BPR) conditions. In control medium, the expression of *integrin α1* was significantly downregulated on SiHA-28 than SiHA-14 under static condition, but not either type of perfusion culture conditions. With the addition of nifedipine into medium, the expression of *integrin α1* was not dependent on BGS micro-porosity irrespective of culture conditions.

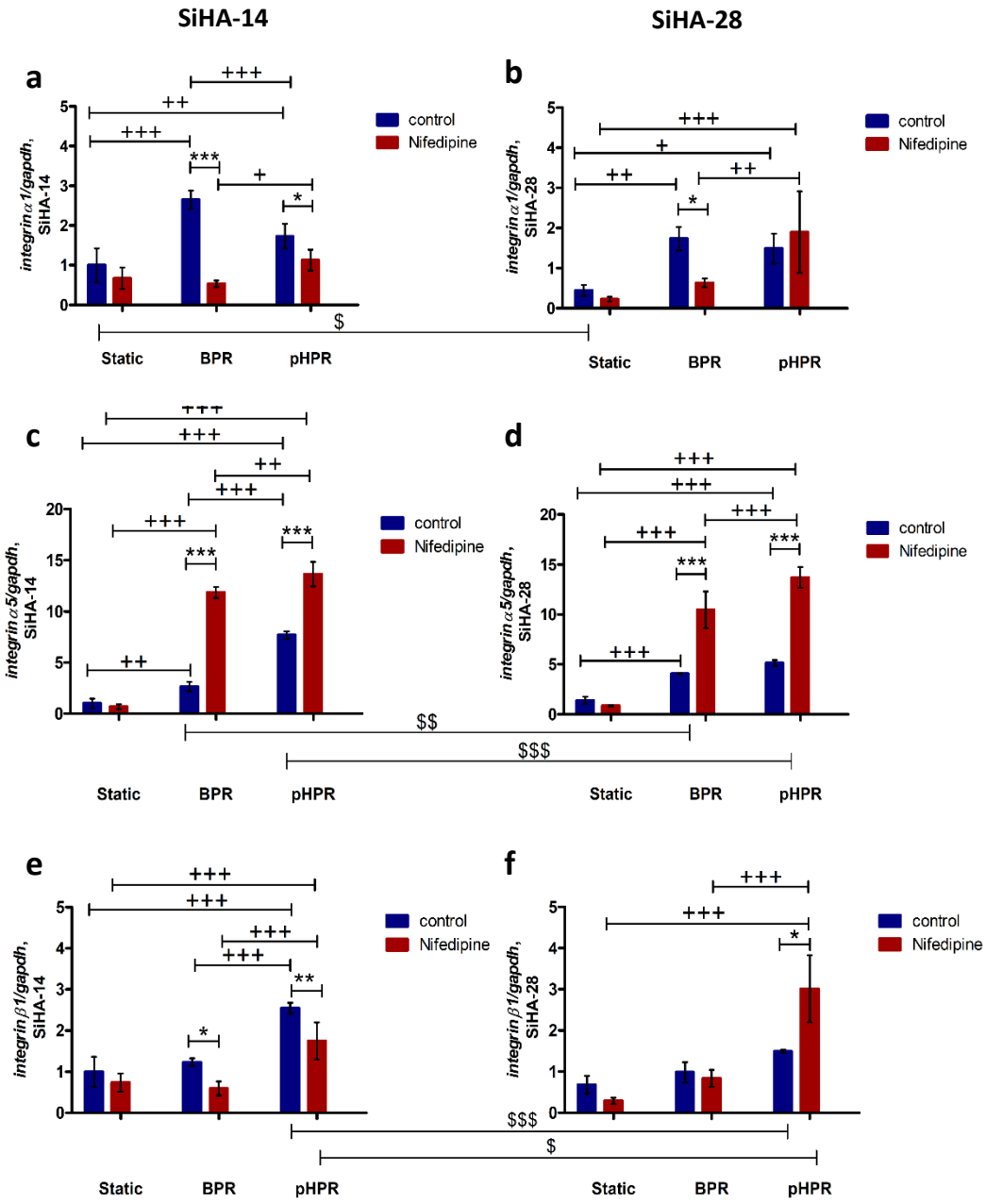

Figure 6-13 Influence of nifedipine on gene expression of integrin subunits in hMSCs cultured on SiHA-14 and SiHA-28 under static, basal perfusion rate (BPR) and a period of high perfusion rate (pHPR) conditions. Results are presented as mean ± standard deviation (n=3). Statistical analysis was performed by two-way ANOVA followed by Bonferroni post-tests. *p < 0.05, **p < 0.01, ***p < 0.001, comparison between control group and nifedipine group. +p < 0.05, ++p < 0.01, +++p < 0.001, comparison between static, basal perfusion rate (BPR) and a period of high perfusion rate (pHPR). $p <0.05, $$p < 0.01, $$$p < 0.001, comparison between SiHA-14 and SiHA-28.

On both BGS SiHA-14 and SiHA-28, the expression of *integrin α5* increased significantly with the addition of nifedipine into medium compared with control medium under either type of perfusion culture conditions, as shown in Figure 6-13

(c) and (d). On BGS SiHA-14, in both control medium and medium supplemented with nifedipine, the expression of *integrin α5* was significantly higher under a period of high perfusion rate (pHPR) condition than both basal perfusion rate (BPR) and static conditions, with *integrin α5* expression under basal perfusion rate (BPR) being significantly higher than under static condition. On BGS SiHA-28, in control medium, the expression of *integrin α5* was significantly higher under either type of perfusion culture conditions compared with under static condition. On BGS SiHA-28, in medium supplemented with nifedipine, the expression of *integrin α5* was significantly higher under a period of high perfusion rate (pHPR) condition than both basal perfusion rate (BPR) and static conditions, with *integrin α5* expression under basal perfusion rate (BPR) being significantly higher than under static condition. In control medium, under basal perfusion rate (BPR) condition, the expression of *integrin α5* was significantly upregulated on SiHA-28 compared with SiHA-14, whereas under a period of high perfusion rate (pHPR) condition, the expression of *integrin α5* was significantly downregulated on SiHA-28 compared with SiHA-14. In medium with the presence of nifedipine, the expression of *integrin α5* was not found to be dependent on BGS micro-porosity irrespective of culture conditions.

On BGS SiHA-14, presence of nifedipine in the medium downregulated the expression of *integrin β1* compared with control medium under either type of perfusion conditions, but not static condition (Figure 6-13 (e)). On BGS SiHA-14, in both control medium and medium supplemented with nifedipine, the expression of *integrin β1* was significantly higher under a period of high perfusion rate (pHPR) than both basal perfusion rate (BPR) and static conditions. On BGS SiHA-28, under a period of high perfusion rate (pHPR) condition, presence of nifedipine in the medium significantly upregulated the expression of *integrin β1* compared with control medium, whereas under static and basal perfusion rate (BPR) conditions, the expression of *integrin β1* was not dependent on the presence of nifedipine in the medium, as can be seen in Figure 6-13 (f). On BGS SiHA-28, in control medium, the expression of *integrin β1* was not dependent on the culture conditions. On BGS SiHA-28, with the addition of nifedipine into medium, the expression of *integrin β1* was significantly higher under a period of high perfusion rate (pHPR) condition than both

static and basal perfusion rate (BPR) conditions. In both control medium and medium with the presence of nifedipine, *integrin β1* expression was not s responsive to BGS micro-porosity under both static and basal perfusion rate (BPR) conditions. Under a period of high perfusion rate (pHPR) condition, in control medium, the expression of *integrin β1* was downregulated on SiHA-28 than on SiHA-14, whereas in medium supplemented with nifedipine, the expression of *integrin β1* was upregulated on SiHA-28 than on SiHA-14.

6.4 Discussion

In this study, SiHA BGS granules were seeded with hMSCs then cultured under static, basal perfusion rate (BPR) or a period of high perfusion rate (pHPR) conditions in control medium or medium supplemented with the L-type VSCCs blocker, nifedipine. Responses of hMSCs, i.e. cytoskeleton organisation, proliferation, specific ALP activity, ERK1/2 activation and expression of gene markers for differentiation were analysed to investigate the modulation by L-type VSCCs on shear stress induced differentiation of hMSCs.

The cytoskeleton has been well-recognised as a responder to mechanical stimuli, such as stretch (Xu *et al.*, 2012), shear stress (Ajubi *et al.*, 1996), hydrostatic pressure (Knight *et al.*, 2006) and compression (Zhang *et al.*, 2015). Current research agrees with previous results showing that, with the stimulation of fluid shear stress, cytoskeleton exhibited a less spread morphology and smaller cellular size compared with static culture. However, this process was independent of L-type VSCCs. This result agrees with previous findings demonstrating that flow activated stress fibre formation was dependent on $[Ca^{2+}]i$ release, not extracellular Ca^{2+} entry (Chen *et al.*, 2000).

Proliferation and specific ALP activity of rat MSCs were reported to be significantly decreased after nifedipine treatment (Wen *et al.*, 2012). However, in the current study, treatment with nifedipine was not observed to decrease either proliferation or specific ALP activity under static culture on both SiHA-14 and SiHA-28 BGS. One possible explanation is that hMSCs were cultured on SiHA BGS, instead of well-plates, in osteogenic medium, which maintained hMSCs proliferation and specific ALP

activity robustly and they were not dependent on L-type VSCCs. Previous research has reported that any enhanced proliferation by stretch in chicken chondrocytes was blocked by nifedipine treatment (Wu and Chen, 2000). In the current study, enhanced proliferation by shear stress was not observed to be blocked by nifedipine treatment, indicating that shear stress induced proliferation on SiHA BGS was independent of L-type VSCCs.

Interestingly, L-type VSCCs were demonstrated to be involved in the distribution of ERK1/2 in response to shear stress. Distribution of ERK1/2 was dependent on culture conditions and this dependence was blocked by adding nifedipine into culture medium. On both BGS SiHA-14 and SiHA-28, the production of pERK was significantly different under basal perfusion rate (BPR) compared with a period of high perfusion rate (pHPR) condition in control medium, and treatment with nifedipine inhibited this difference. This inhibition of response to different perfusion culture conditions by nifedipine treatment was also observed in the expression of genes like *osx*, *col i* and *myoD*. Previous studies also reported that L-type VSCCs were involved in the activation of the ERK phosphorylation (Dolmetsch *et al.*, 2001; Nakayama *et al.*, 2008). Findings in the current study agreed with previous research, indicating that L-type VSCCs play a role in modulating shear stress induced activation of ERK pathway of hMSCs on SiHA BGS.

Ca^{2+} is the most widely used second messenger in cell biology and calcium channels fulfil a lot of essential cell functions. One such function is the involvement in the regulation of gene expression (Barbado *et al.*, 2009). The regulation of L-type VSCCs blocker, nifedipine, on the expression of osteogenic genes was similar on SiHA-14 and SiHA-28 BGS. Osteogenic gene makers like *osx*, *bmp2*, *col i* and *dmp1* were significantly upregulated under basal perfusion rate (BPR) compared with under static condition. This upregulation was diminished by L-type VSCCs blocker, nifedipine, indicating that L-type VSCCs were compulsory in osteogenic differentiation induced by basal perfusion rate (BPR). This agreed with previous research reported that L-type VSCCs mediate load-induced bone formation (Li *et al.*, 2003). Under a period of high perfusion rate (pHPR), the expression of some osteogenic genes, like *alp*, *col i* and *dmp1* was not affected by the presence of

nifedipine in the medium, however, the expression of *osx* and *bmp2* was upregulated by nifedipine treatment. These findings demonstrated that under a period of high perfusion rate (pHPR) condition, the regulation of L-type VSCCs on osteogenic differentiation was more complicated compared with under basal perfusion rate (BPR) condition, and different pathways might be involved in the regulation process. It is interesting to notice that *integrin α1* expression followed the same pattern with osteogenic gene expression, i.e it was upregulated under basal perfusion rate (BPR), and this upregulation was dependent on L-type VSCCs. Under a period of high perfusion rate (pHPR), the expression of *integrin α1* was downregulated by nifedipine treatment on SiHA-14 but not SiHA-28, indicating that BGS SiHA-28 protected against the downregulation effect by the addition of nifedipine in medium.

The expression of chondrogenic gene markers like *sox9*, *runx2* and *col ii* was not dependent on the blocking of L-type VSCCs by nifedipine under static condition. This finding was confirmed by previous research, in a high density chondrifying MSCs culture model, blocking L-type VSCCs did not interfere with the mRNA expression of *sox9* (Fodor *et al.*, 2013). Basal perfusion rate (BPR) upregulated chondrogenic gene markers as compared to static condition, and a period of high perfusion rate (pHPR) further increased their expression significantly. Under either type of perfusion culture conditions, the expression level of chondrogenic markers was further increased with the addition of nifedipine into medium, indicating that active L-type VSCCs regulates the extent of perfusion induced chondrogenic differentiation. It is unknown how silica enters hMSCs and whether blocking L-type VSCCs affects silica entering hMSCs. It is also unknown whether silica has a pro-chondrogenic effect when calcium is deficient. Shear stress induced chondrogenic differentiation and its regulation by L-type VSCCs has received little attention to date. The upregulation of an endochondral bone formation mediator (parathyroid hormone (PTH) related peptide) in rat chondrocyte by cyclic mechanical strain was found to be dependent on L-type VSCCs activation (Tanaka *et al.*, 2005). It is understandable that the role of L-type VSCCs in shear stress induced chondrogenic differentiation was distinct from in cyclic mechanical strain induced chondrogenic differentiation. *Integrin α5* was upregulated significantly while chondrogenic markers were upregulated significantly

under a period of high perfusion rate (pHPR). Adding nifedipine into medium further enhanced expression of *integrin α5*, as well as chondrogenic markers under either type of perfusion culture conditions. These results indicated that integrin α5 was closely related to chondrogenesis process.

Under basal perfusion rate (BPR) condition, the expression of *osx*, *col i* and *myoD* was responsive to BGS micro-porosity. Under a period of high perfusion rate (pHPR) culture condition, the expression of *runx2*, *col ii* and *integrin α5* was dependent on BGS micro-porosity. The response of these gene expression to BGS micro-porosity was blocked by adding L-type VSCCs nifedipine into medium, indicating that fully functional L-type VSCCs were necessary when evaluating BGS performance.

6.5 Conclusion

In summary, current research results have demonstrated that L-type VSCCs play important roles in activating ERK pathway and regulating flow activated hMSCs differentiation. Basal perfusion rate (BPR) induced osteogenic differentiation was dependent on L-type VSCCs. L-type VSCCs also regulated shear stress activated chondrogenic differentiation. Integrin subunits showed a strong preference in stem cell lineage specification. Integrin α1 was proved to be closely related to osteogenesis process, whereas integrin α5 was demonstrated to be more involved in chondrogenesis process.

Chapter 7 Conclusions and Future Work

7.1 Conclusions

Cells in the human body are exposed to shear stress and other mechanical forces, which are known to influence cellular response, bone regeneration and bone remodelling (Lanyon and Rubin, 1984; Boerckel *et al.*, 2012). The evaluation of how cells response to BGS in a static environment usually cannot be translated to subsequent *in vivo* studies and clinical trials. Therefore, a 3D bioreactor that allows cell-seeded SiHA BGS granules to be applied with both shear stress and compression was built. A specific perfusion chamber which hosts BGS granules and can be fitted into the 3D bioreactor was designed, and parameters of seeding MG63 cells on BGS granules in this chamber were optimized. Results demonstrated that osteoblast-like cells on BGS was dependent on both shear stress and mechanical loading, showing different proliferation and gene expression profiles, which is in line with previous studies (Bancroft *et al.*, 2002; Chen *et al.*, 2017; Bolgen *et al.*, 2008; David *et al.*, 2008; C X Liu *et al.*, 2012). However, after careful characterization, MG63 cells were found to lack the capacity to reflect the pattern of specific ALP activity demonstrated primary osteoblast cells, which is an important indicator in investigating the cellular response to mechanical stimulation. hMSCs were then characterized and used for the rest of the study. Perfusing cell culture medium through BGS requires tight fit between construct chamber and tubing, which creates friction resistance for compression and results in the compression force on BGS granules becoming unquantifiable. Therefore, perfusion in isolation with two different perfusion profiles was employed for the rest of the study.

The structure of BGS has been demonstrated to have a strong impact on cellular response and bone regeneration *in vivo* (Manuela E. Gomes *et al.*, 2006; Hing *et al.*, 2005; Campion *et al.*, 2011; Coathup *et al.*, 2012). SiHA BGS with defined total porosity and micro-porosity were synthesised and characterised. The proliferation and osteogenic differentiation of hMSCs on different BGS were preliminarily tested in a static environment. The composition and hierarchical structure of SiHA were found to be beneficial for the growth of hMSCs, however under static conditions the

structural differences between BGS did not have a significant influence on hMSCs at day 3. However, in culture medium with osteogenic supplements, SiHA BGS with high micro-porosity (SiHA-28) was demonstrated to be more beneficial in enhancing hMSCs proliferation and differentiation after 7 days. Therefore, it was decided to further investigate the response of hMSCs to variation in micro-porosity under perfusion conditions.

Two perfusion patterns were employed in the study, as perfusion parameters including flow type, magnitude, duration, insertion of rest periods were found to influence cell responses (Bancroft *et al.*, 2002; Grayson *et al.*, 2008; Yang *et al.*, 2010; Jaasma and O'Brien, 2008). Results demonstrated that hMSCs on SiHA BGS were dependent on basal perfusion rate (BPR), showing significantly increased proliferation and osteogenic differentiation compared with static culture, with the involvement of cytoskeleton and ERK1/2 signalling pathway. The response of hMSCs was not consistently dependent on BGS micro-porosity under static condition. While basal perfusion rate (BPR) revealed the response of hMSCs to BGS micro-porosity, with the expression of osteogenic marker *osx* increased significantly with increasing BGS micro-porosity. On the other hand, a period of high perfusion rate (pHPR) significantly increased the gene expression of chondrogenic markers, and SiHA-22 was demonstrated to be more supportive in terms of chondrogenic markers expression compared with SiHA-14 and SiHA-28. Since perfusion condition is more relevant to physiological *in vivo* situation, the future evaluation of porous BGS bioactivity should be conducted under carefully selected perfusion conditions, and the results of this thesis suggest that chondrogenic markers should also be used as one of the indicators for BGS performance in addition to conventional osteogenic markers, as early chondrogenic activity may denote the onset of osteochondral bone formation. This would also argue for longer term culture to further monitor cell fate and the development of any ECM produced.

Many studies have demonstrated that L-type voltage-sensitive calcium channels (VSCCs) were activated in response to mechanical stimulation, which then initiate a variety of biological signals in bone cells and also mediate bone formation (Rawlinson *et al.*, 1996; Li *et al.*, 2002). The regulation of L-type VSCCs on shear stress induced

hMSCs response were also examined in this study. Results demonstrated that shear stress induced osteogenic and chondrogenic differentiation of hMSCs on SiHA BGS was modulated by L-type VSCCs, possibly through ERK1/2 signalling pathways. The results of this study underline the importance of evaluating BGS performance especially when investigating the mechanisms behind response to variation in BGS structure and chemistry under well understood perfusion conditions.

7.2 Future Work

Although it is encouraging that perfusion culture can result in improved differentiation and disclose the cellular response to small BGS architectural differences, this is only a small step towards a physiological-mimicking bioreactor system.

- Future work is required to prolong culturing period and investigate the effect of SiHA BGS micro-porosity on cell proliferation and differentiation under perfusion conditions at 14 days, 21 days and 28 days.
- Future work is required to investigate the effect of SiHA BGS macro-porosity on cell proliferation and differentiation under mechanical stimulated conditions.
- Inhibitors of ERK1/2 and cytoskeletal drugs can be used in the experiment to examine their role in the synergistic effect of perfusion and BGS structure on hMSCs response.
- Future work is required to simulate/investigate how micro-porosity affects type of flow, shear stress and strain field, which could contribute to explain the response of hMSCs to SiHA with different micro-porosity under perfusion condition.
- Future work is required to investigate the cellular response to HA and SiHA with equivalent structure under perfusion condition to study the role of silica on osteogenic and chondrogenic effect. Cellular response to HA and SiHA when L-type VSCC channels are blocked should also be investigated to examine the role of silica on osteogenic and chondrogenic effect when calcium is deficient.

- A more advanced bioreactor which can apply both compression and perfusion in an accurate manner should be developed.
- The final goal of bioreactor system is carrying out real time monitored, automated control over relevant parameters during the cultivation. Also, studies using bioreactor system should be preferably completed in conjunction with μCT scan and computational fluid dynamics (CFD) to characterise the fluid shear stress field. Then the fluid shear stress from studies using different BGS or flow with different configurations can be compared. A thorough network of studies of using bioreactors can be built, which will provide valuable guidance for tissue engineering in clinical practice.

Appendix 1: DNA and specific ALP activity of hMSCs in 24 well-plates (5000 cells/well) after 7 days

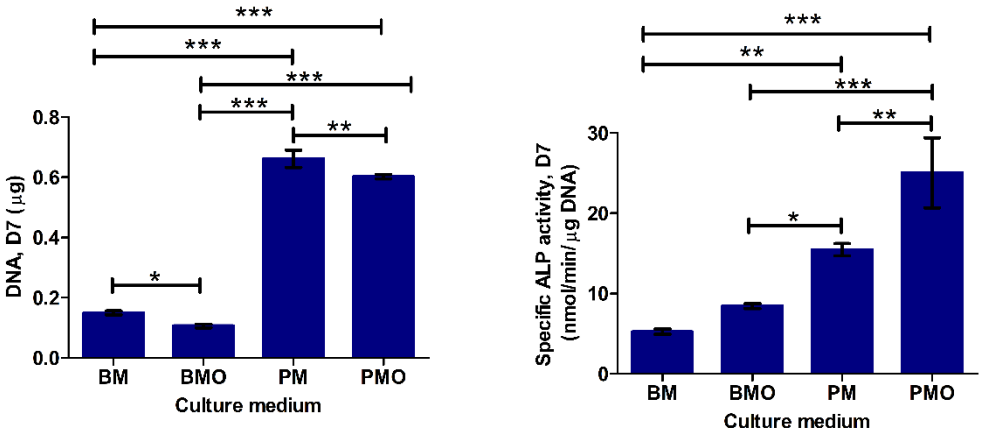

Appendix 2: Cell culture and molecular analysis chemicals used in this PhD research.

Chemicals	Supplier	CatLog number
MG-63 cell line human	Sigma	86051601
Dulbecco's Phosphate Buffered Saline (PBS)	Sigma	D8537
Trypsin-EDTA solution	Sigma	T3824
High glucose Dulbecco's Modified Eagles Medium (DMEM) (contains $NaHCO_3$ buffer)	Sigma	D6429
High glucose Dulbecco's Modified Eagle's Medium (DMEM) (without $NaHCO_3$ buffer)	Sigma	D7777
Fetal bovine serum (FBS)	Sigma	F9665
HEPES solution	Sigma	H0887
Penicillin-Streptomycin	Sigma	P4333
Human Mesenchymal Stem Cells from Bone Marrow (hMSC-BM), Lot: 403Z003.2.	PromoCell	C-12974
Mesenchymal Stem Cell (MSC) Growth Medium 2	PromoCell	C-28009
Accutase-Solution	PromoCell	C-41310

Dexamethasone	Sigma	D4902
β-Glycerophosphate disodium salt hydrate	Sigma	G9422
L-Ascorbic acid 2-phosphate sesquimagnesium salt hydrate	Sigma	A8960
Bovine Serum Albumin	Sigma	A2058
Triton® X-100 (Polyethylene glycol tert-octylphenyl ether)	VWR	437002A
Quant iT PicoGreen dsDNA Assay Kit	Life Technologies	P11496
UltraPure™ DNase/RNase-Free Distilled Water	Life Technologies	10977035
Alkaline Phosphatase Assay Kit	Abcam	ab83369
4-Nitrophenol solution	Sigma	N7660
Alizarin Red S	Sigma	A5533
Paraformaldehyde solution, 4%(w/v) in PBS	Thermo Fisher Scientific	J19943
RIPA Lysis and Extraction Buffer	Life Technologies	89900
Halt™ Protease and Phosphatase Inhibitor Cocktail (100X)	Life Technologies	78440
Pierce™ BCA Protein Assay Kit	Thermo Fisher Scientific	23227
4x Laemmli Sample Buffer	Bio Rad	1610747
2-Mercaptoethanol	Sigma	M6250
Precision Plus Protein™ WesternC™ Blotting Standards	Bio Rad	1610376
4–20% Mini-PROTEAN® TGX™ Precast Protein Gels	Bio Rad	4561094
Tris/Glycine/SDS	Bio Rad	1610732
Trans-Blot® Turbo™ RTA Mini LF PVDF Transfer Kit	Bio Rad	1704274
Tris Buffered Saline	Bio Rad	1706435
TWEEN® 20	Sigma	P2287
TRI Reagent® Solution	Life Technologies	AM9738
Chloroform, pure	Acros Organics	38376025
RNeasy Mini Kit	Qiagen	74104

GoScript™ Reverse Transcription System	Promega	A5000
KAPA SYBR® FAST	Sigma	KK4618
Nifedipine	Sigma	N7634
Glutaraldehyde	Agar Scientific	AGR1011
Sodium cacodylate	Sigma	C0250
Osmium tetroxide	TAAB	O015/1
Tannic acid	Sigma	T0125
Ethyl alcohol	Sigma	459836
Hexamethyldisilazane	Sigma	52619

References

Aderem, A. (1992) Signal transduction and the actin cytoskeleton: the roles of MARCKS and profilin. *Trends in Biochemical Sciences*. **17**(10), 438–443.

Ajubi, N.E., Klein-Nulend, J., Nijweide, P.J., Vrijheid-Lammers, T., Alblas, M.J., Burger, E.H. (1996) Pulsating fluid flow increases prostaglandin production by cultured chicken osteocytes -- a cytoskeleton-dependent process. *Biochemical and biophysical research communications*. **225**(1), 62–8.

Akao, M., Aoki, H., Kato, K. (1981) Mechanical properties of sintered hydroxyapatite for prosthetic applications. *Journal of Materials Science*. **16**(3), 809–812.

Alford, A.., Jacobs, C.., Donahue, H.. (2003) Oscillating fluid flow regulates gap junction communication in osteocytic MLO-Y4 cells by an ERK1/2 MAP kinase-dependent mechanism☆. *Bone*. **33**(1), 64–70.

Annaz, B., Hing, K.., Kayser, M., Buckland, T., Di Silvio, L. (2004a) An ultrastructural study of cellular response to variation in porosity in phase-pure hydroxyapatite. *Journal of Microscopy*. **216**(2), 97–109.

Annaz, B., Hing, K.., Kayser, M., Buckland, T., Di Silvio, L. (2004b) Porosity variation in hydroxyapatite and osteoblast morphology: a scanning electron microscopy study. *Journal of Microscopy*. **215**(1), 100–110.

Appelman, T.P., Mizrahi, J., Elisseeff, J.H., Seliktar, D. (2009) The differential effect of scaffold composition and architecture on chondrocyte response to mechanical stimulation. *Biomaterials*. **30**(4), 518–525.

Appleton, C.T.G., Usmani, S.E., Mort, J.S., Beier, F. (2010) Rho/ROCK and MEK/ERK activation by transforming growth factor-alpha induces articular cartilage degradation. *Laboratory investigation; a journal of technical methods and pathology*. **90**(1), 20–30.

Arnsdorf, E.J., Tummala, P., Kwon, R.Y., Jacobs, C.R. (2009) Mechanically induced osteogenic differentiation--the role of RhoA, ROCKII and cytoskeletal dynamics. *Journal of cell science*. **122**(Pt 4), 546–53.

Arpornmaeklong, P., Brown, S.E., Wang, Z., Krebsbach, P.H. (2009) Phenotypic characterization, osteoblastic differentiation, and bone regeneration capacity of human embryonic stem cell-derived mesenchymal stem cells. *Stem cells and development*. **18**(7), 955–68.

Baas, E., Kuiper, J.H., Yang, Y., Wood, M.A., El Haj, A.J. (2010) In vitro bone growth responds to local mechanical strain in three-dimensional polymer scaffolds. *Journal of Biomechanics*. **43**(4), 733–739.

Bancroft, G.N., Sikavitsas, V.I., van den Dolder, J., Sheffield, T.L., Ambrose, C.G., Jansen, J.A., Mikos, A.G. (2002) Fluid flow increases mineralized matrix deposition in 3D perfusion culture of marrow stromal osteoblasts in a dose-dependent manner. *Proceedings of the National Academy of Sciences of the United States of America*. **99**(20), 12600–5.

Barbado, M., Fablet, K., Ronjat, M., De Waard, M. (2009) Gene regulation by voltage-dependent calcium channels. *Biochimica et Biophysica Acta (BBA) - Molecular Cell Research*. **1793**(6), 1096–1104.

Barnes, G.L., Kostenuik, P.J., Gerstenfeld, L.C., Einhorn, T.A. (1999) Growth factor regulation of fracture repair. *Journal of Bone and Mineral Research*. **14**(11), 1805–1815.

Baron, R., Rawadi, G. (2007) Targeting the Wnt/β-Catenin pathway to regulate bone

formation in the adult skeleton. *Endocrinology*. **148**(6), 2635–2643.

Barron, M.J., Goldman, J., Tsai, C.J., Donahue, S.W. (2012) Perfusion flow enhances osteogenic gene expression and the infiltration of osteoblasts and endothelial cells into three-dimensional calcium phosphate scaffolds. *International Journal of Biomaterials*. **2012**, 17–20.

Bershadsky, A., Kozlov, M., Geiger, B. (2006) Adhesion-mediated mechanosensitivity: a time to experiment, and a time to theorize. *Current Opinion in Cell Biology*. **18**(5), 472–481.

Bigham-Sadegh, A., Oryan, A. (2015) Basic concepts regarding fracture healing and the current options and future directions in managing bone fractures. *International Wound Journal*. **12**(3), 238–247.

Bignon, A., Chouteau, J., Chevalier, J., Fantozzi, G., Carret, J.-P., Chavassieux, P., Boivin, G., Melin, M., Hartmann, D. (2003) Effect of micro- and macroporosity of bone substitutes on their mechanical properties and cellular response. *Journal of Materials Science: Materials in Medicine*. **14**(12), 1089–1097.

Bjerre, L., Bünger, C., Baatrup, A., Kassem, M., Mygind, T. (2011) Flow perfusion culture of human mesenchymal stem cells on coralline hydroxyapatite scaffolds with various pore sizes. *Journal of Biomedical Materials Research Part A*. **97A**(3), 251–263.

Bodine, P.V.., Komm, B.. (1999) Evidence that conditionally immortalized human osteoblasts express an osteocalcin receptor. *Bone*. **25**(5), 535–543.

Boerckel, J.D., Kolambkar, Y.M., Stevens, H.Y., Lin, A.S.P., Dupont, K.M., Guldberg, R.E. (2012) Effects of in vivo mechanical loading on large bone defect regeneration. *Journal of Orthopaedic Research*. **30**(7), 1067–1075.

Bolgen, N., Yang, Y., Korkusuz, P., Guzel, E., El Haj, A.J., Piskin, E. (2008) Three-dimensional ingrowth of bone cells within biodegradable cryogel scaffolds in bioreactors at different regimes. *Tissue Engineering Part A*. **14**(10), 1743–1750.

Bowen, J.A., Mellonig, J.T., Gray, J.L., Towle, H.T. (1989) Comparison of decalcified freeze-dried bone allograft and porous particulate hydroxyapatite in human periodontal osseous defects. *Journal of Periodontology*. **60**(12), 647–654.

Boyde, A., Corsi, A., Quarto, R., Cancedda, R., Bianco, P. (1999) Osteoconduction in large macroporous hydroxyapatite ceramic implants: Evidence for a complementary integration and disintegration mechanism. *Bone*. **24**(6), 579–589.

Braccini, A., Wendt, D., Jaquiery, C., Jakob, M., Heberer, M., Kenins, L., Wodnar-Filipowicz, A., Quarto, R., Martin, I. (2005) Three-dimensional perfusion culture of human bone marrow cells and generation of osteoinductive grafts. *Stem Cells*. **23**(8), 1066–1072.

Bragdon, B., Moseychuk, O., Saldanha, S., King, D., Julian, J., Nohe, A. (2011) Bone morphogenetic proteins: a critical review. *Cellular Signalling*. **23**(4), 609–620.

Brighton, C.T., Fisher, J.R.S., Levine, S.E., Corsetti, J.R., Landsman, A.S., Williams, J.L., Thibault, L.E. (1996) The biochemical pathway mediating the proliferative response of bone cells to a mechanical stimulus. *The Journal of Bone and Joint Surgery*. **78**–**A**(9).

Brunet, A., Le Roux, D., Lenormand, P., Dowd, S., Keyse, S., Pouyssé Gur, J. (1999) Nuclear translocation of p42/p44 mitogen-activated protein kinase is required for growth factor-induced gene expression and cell cycle entry. *The EMBO Journal*. **18**(3), 664–674.

Bunpetch, V., Zhang, Z.-Y., Zhang, X., Han, S., Zongyou, P., Wu, H., Hongwei, O. (2017) Strategies for MSC expansion and MSC-based microtissue for bone regeneration. *Biomaterials*.

Burg, K.J., Holder, W.D., Culberson, C.R., Beiler, R.J., Greene, K.G., Loebsack, A.B., Roland, W.D., Eiselt, P., Mooney, D.J., Halberstadt, C.R. (2000) Comparative study of seeding methods for three-dimensional polymeric scaffolds. *Journal of biomedical materials research*. **51**(4), 642–9.

Burr, D.B., Martin, R.B., Schaffler, M.B., Radin, E.L. (1985) Bone remodeling in response to in vivo fatigue microdamage. *Journal of Biomechanics*. **18**(3), 189–200.

Campbell, I.D., Humphries, M.J. (2011) Integrin structure, activation, and interactions. *Cold Spring Harbor perspectives in biology*. **3**(3), a004994.

Campion, C.R., Ball, S.L., Clarke, D.L., Hing, K.A. (2013) Microstructure and chemistry affects apatite nucleation on calcium phosphate bone graft substitutes. *J Mater Sci Mater Med*. **24**(3), 597–610.

Campion, C.R., Chander, C., Buckland, T., Hing, K. (2011) Increasing strut porosity in silicate-substituted calcium-phosphate bone graft substitutes enhances osteogenesis. *J Biomed Mater Res B Appl Biomater*. **97**(2), 245–254.

Cardoso, L., Herman, B.C., Verborgt, O., Laudier, D., Majeska, R.J., Schaffler, M.B. (2009) Osteocyte apoptosis controls activation of intracortical resorption in response to bone fatigue. *Journal of Bone and Mineral Research*. **24**(4), 597–605.

Carroll, S.F., Buckley, C.T., Kelly, D.J. (2017) Cyclic tensile strain can play a role in directing both intramembranous and endochondral ossification of mesenchymal stem cells. *Frontiers in Bioengineering and Biotechnology*. **5**(November), 1–12.

Carter, D.R. (1984) Mechanical loading histories and cortical bone remodeling. *Calcified Tissue International*. **36**(S1), S19–S24.

Cartmell, S.H., Porter, B.D., García, A.J., Guldberg, R.E. (2003) Effects of medium perfusion rate on cell-seeded three-dimensional bone constructs in vitro. *Tissue engineering*. **9**(6), 1197–1203.

Cartmell, S.H., Rathbone, S., Jones, G., Hidalgo-Bastida, L.A. (2011) 3D sample preparation for orthopaedic tissue engineering bioreactors. *Methods Mol Biol*. **695**, 61–76.

Case, N., Rubin, J. (2010) β-Catenin-A supporting role in the skeleton. *Journal of Cellular Biochemistry*. **110**(3), 545–553.

Case, N., Thomas, J., Sen, B., Styner, M., Xie, Z., Galior, K., Rubin, J. (2011) Mechanical regulation of glycogen synthase kinase 3β (GSK3β) in mesenchymal stem cells is dependent on Akt protein serine 473 phosphorylation via mTORC2 protein. *The Journal of biological chemistry*. **286**(45), 39450–6.

Chai, D.H., Arner, E.C., Griggs, D.W., Grodzinsky, A.J. (2010) αv and β1 integrins regulate dynamic compression-induced proteoglycan synthesis in 3D gel culture by distinct complementary pathways. *Osteoarthritis and Cartilage*. **18**(2), 249–256.

Chan, O., Coathup, M.J., Nesbitt, A., Ho, C.Y., Hing, K.A., Buckland, T., Campion, C., Blunn, G.W. (2012) The effects of microporosity on osteoinduction of calcium phosphate bone graft substitute biomaterials. *Acta Biomaterialia*. **8**(7), 2788–2794.

Chana, N.K. (2015) Development of a 3D perfusion system to monitor behaviour of synthetic bone graft substitute granules and osteoblast-like cell response under physio-mimetic conditions. *PhD Thesis*.

Chang, B.S., Lee, C.K., Hong, K.S., Youn, H.J., Ryu, H.S., Chung, S.S., Park, K.W. (2000) Osteoconduction at porous hydroxyapatite with various pore configurations. *Biomaterials*. **21**(12), 1291–1298.

Chang, J.C., Hsu, S. hui, Chen, D.C. (2009) The promotion of chondrogenesis in adipose-derived adult stem cells by an RGD-chimeric protein in 3D alginate culture. *Biomaterials*. **30**(31), 6265–6275.

Chen, G., Xu, R., Zhang, C., Lv, Y. (2017) Responses of MSCs to 3D scaffold matrix mechanical properties under oscillatory perfusion culture. *ACS Applied Materials & Interfaces*. **9**(2), 1207–1218.

Chen, N.X., Ryder, K.D., Pavalko, F.M., Turner, C.H., Burr, D.B., Qiu, J., Duncan, R.L. (2000) Ca(2+) regulates fluid shear-induced cytoskeletal reorganization and gene expression in osteoblasts. *American journal of physiology. Cell physiology*. **278**(5), C989-97.

Chen, X., Wang, J., Chen, Y., Cai, H., Yang, X., Zhu, X., Fan, Y., Zhang, X. (2016) Roles of calcium phosphate-mediated integrin expression and MAPK signaling pathways in the osteoblastic differentiation of mesenchymal stem cells. *J. Mater. Chem. B*. **4**(13), 2280–2289.

Chenu, C., Colucci, S., Grano, M., Zigrino, P., Barattolo, R., Zambonin, G., Baldini, N., Vergnaud, P., Delmas, P.D., Zallone, A.Z. (1994) Osteocalcin induces chemotaxis, secretion of matrix proteins, and calcium-mediated intracellular signaling in human osteoclast-like cells. *The Journal of cell biology*. **127**(4), 1149–58.

Cho, T.-J., Gerstenfeld, L.C., Einhorn, T.A. (2002) Differential temporal expression of members of the transforming growth factor β superfamily during murine fracture healing. *Journal of Bone and Mineral Research*. **17**(3), 513–520.

Chu, T.M.G., Orton, D.G., Hollister, S.J., Feinberg, S.E., Halloran, J.W. (2002) Mechanical and in vivo performance of hydroxyapatite implants with controlled architectures. *Biomaterials*. **23**(5), 1283–1293.

Claes, L., Reusch, M., Gockelmann, M., Ohnmacht, M., Wehner, T., Amling, M., Beil, F.T., Ignatius, A. (2011) Metaphyseal fracture healing follows similar biomechanical rules as diaphyseal healing. *Journal of Orthopaedic Research*. **29**(3), 425–432.

Clapham, D.E. (2007) Calcium signaling. *Cell*. **131**(6), 1047–58.

Clover, J., Gowen, M. (1994) Are MG-63 and HOS TE85 human osteosarcoma cell lines representative models of the osteoblastic phenotype? *Bone*. **15**(6), 585–591.

Coathup, M.J., Hing, K.A., Samizadeh, S., Chan, O., Fang, Y.S., Campion, C., Buckland, T., Blunn, G.W. (2012) Effect of increased strut porosity of calcium phosphate bone graft substitute biomaterials on osteoinduction. *Journal of Biomedical Materials Research Part A*. **100**(6), 1550–1555.

Correia, C., Bhumiratana, S., Sousa, R.A., Reis, R.L., Vunjak-Novakovic, G. (2013) Sequential application of steady and pulsatile medium perfusion enhanced the formation of engineered bone. *Tissue Engineering Part A*. **19**(9–10), 1244–1254.

Cowan, C.M., Shi, Y.-Y., Aalami, O.O., Chou, Y.-F., Mari, C., Thomas, R., Quarto, N., Contag, C.H., Wu, B., Longaker, M.T. (2004) Adipose-derived adult stromal cells heal critical-size mouse calvarial defects. *Nature Biotechnology*. **22**(5), 560–567.

Curtis, K.J., Coughlin, T.R., Mason, D.E., Boerckel, J.D., Niebur, G.L. (2018) Bone marrow mechanotransduction in porcine explants alters kinase activation and enhances trabecular bone formation in the absence of osteocyte signaling. *Bone*. **107**, 78–87.

Cypher, T.J., Grossman, J.P. (1996) Biological principles of bone graft healing. *The Journal of Foot and Ankle Surgery*. **35**(5), 413–417.

Czekanska, E.M., Stoddart, M.J., Ralphs, J.R., Richards, R.G., Hayes, J.S. (2014) A phenotypic comparison of osteoblast cell lines versus human primary osteoblasts for biomaterials

testing. *Journal of Biomedical Materials Research Part A*. **102**(8), 2636–2643.

Datta, N., Holtorf, H.L., Sikavitsas, V.I., Jansen, J.A., Mikos, A.G. (2005) Effect of bone extracellular matrix synthesized in vitro on the osteoblastic differentiation of marrow stromal cells. *Biomaterials*. **26**(9), 971–977.

David, V., Guignandon, A., Martin, A., Malaval, L., Lafage-Proust, M.H., Rattner, A., Mann, V., Noble, B., Jones, D.B., Vico, L. (2008) Ex vivo bone formation in bovine trabecular bone cultured in a dynamic 3D bioreactor is enhanced by compressive mechanical strain. *Tissue Engineering Part A*. **14**(1), 117–126.

Davies, C.M., Jones, D.B., Stoddart, M.J., Koller, K., Smith, E., Archer, C.W., Richards, R.G. (2006) Mechanically loaded ex vivo bone culture system 'Zetos': Systems and culture preparation. *European Cells and Materials*. **11**, 57–75.

Day, T.F., Guo, X., Garrett-Beal, L., Yang, Y. (2005) Wnt/β-catenin signaling in mesenchymal progenitors controls osteoblast and chondrocyte differentiation during vertebrate skeletogenesis. *Developmental Cell*. **8**(5), 739–750.

Delaine-Smith, R.M., Sittichokechaiwut, A., Reilly, G.C. (2014) Primary cilia respond to fluid shear stress and mediate flow-induced calcium deposition in osteoblasts. *Faseb Journal*. **28**(1), 430–439.

Delany, A.M., Amling, M., Priemel, M., Howe, C., Baron, R., Canalis, E. (2000) Osteopenia and decreased bone formation in osteonectin-deficient mice. *The Journal of clinical investigation*. **105**(7), 915–23.

Delon, I., Brown, N.H. (2007) Integrins and the actin cytoskeleton. *Current Opinion in Cell Biology*. **19**(1), 43–50.

Demaurex, N., Nunes, P. (2016) The role of STIM and ORAI proteins in phagocytic immune cells. *American journal of physiology. Cell physiology*. **310**(7), C496-508.

Desgrosellier, J.S., Cheresh, D.A. (2010) Integrins in cancer: biological implications and therapeutic opportunities. *Nature Reviews Cancer*. **10**(1), 9–22.

Dolmetsch, R.E., Pajvani, U., Fife, K., Spotts, J.M., Greenberg, M.E. (2001) Signaling to the nucleus by an L-type calcium channel-calmodulin complex through the MAP kinase pathway. *Science*. **294**(5541), 333–9.

Dominici, M., Le Blanc, K., Mueller, I., Slaper-Cortenbach, I., Marini, F.., Krause, D.S., Deans, R.J., Keating, A., Prockop, D.J., Horwitz, E.M. (2006) Minimal criteria for defining multipotent mesenchymal stromal cells. The International Society for Cellular Therapy position statement. *Cytotherapy*. **8**(4), 315–317.

Dror, S., Noushin, D., Alvin, E.P., Ronda, E.S., Willoughby, Gail, K.N. (1996) Application of shear flow stress to chondrocytes or chondrocyte stem cells to produce cartilage. *US Grant*.

Du, D., Furukawa, K., Ushida, T. (2008) Oscillatory perfusion seeding and culturing of osteoblast-like cells on porous beta-tricalcium phosphate scaffolds. *Journal of Biomedical Materials Research Part A*. **86A**(3), 796–803.

Du, D., Furukawa, K.S., Ushida, T. (2009) 3D culture of osteoblast-like cells by unidirectional or oscillatory flow for bone tissue engineering. *Biotechnology and Bioengineering*. **102**(6), 1670–1678.

Ducy, P., Desbois, C., Boyce, B., Pinero, G., Story, B., Dunstan, C., Smith, E., Bonadio, J., Goldstein, S., Gundberg, C., Bradley, A., Karsenty, G. (1996) Increased bone formation in osteocalcin-deficient mice. *Nature*. **382**(6590), 448–452.

Engler, A.J., Sen, S., Sweeney, H.L., Discher, D.E. (2006) Matrix elasticity directs stem cell lineage specification. *Cell*. **126**(4), 677–689.

Farrell, E., van der Jagt, O.P., Koevoet, W., Kops, N., Van Manen, C.J., Hellingman, C.A., Jahr, H., O'Brien, F.J., Verhaar, J.A.N., Weinans, H., van Osch, G.J.V.M. (2009) Chondrogenic priming of human bone marrow stromal cells: a better route to bone repair? *Tissue Engineering Part C: Methods*. **15**(2), 285–295.

Fassina, L., Visai, L., Asti, L., Benazzo, F., Speziale, P., Tanzi, M.C., Magenes, G. (2005) Calcified matrix production by SAOS-2 cells inside a polyurethane porous scaffold, using a perfusion bioreactor. *Tissue Engineering*. **11**(5–6), 685–700.

Ferraro, J.T., Daneshmand, M., Bizios, R., Rizzo, V. (2004) Depletion of plasma membrane cholesterol dampens hydrostatic pressure and shear stress-induced mechanotransduction pathways in osteoblast cultures. *American Journal of Physiology-Cell Physiology*. **286**(4), C831–C839.

Filipowska, J., Reilly, G.C., Osyczka, A.M. (2016) A single short session of media perfusion induces osteogenesis in hBMSCs cultured in porous scaffolds, dependent on cell differentiation stage. *Biotechnology and Bioengineering*. **113**(8), 1814–1824.

Fletcher, D.A., Mullins, R.D. (2010) Cell mechanics and the cytoskeleton. *Nature*. **463**(7280), 485–492.

Fodor, J., Matta, C., Oláh, T., Juhász, T., Takács, R., Tóth, A., Dienes, B., Csernoch, L., Zákány, R. (2013) Store-operated calcium entry and calcium influx via voltage-operated calcium channels regulate intracellular calcium oscillations in chondrogenic cells. *Cell Calcium*. **54**(1), 1–16.

Forwood, M.R., Kelly, W.L., Worth, N.F. (1998) Localization of prostaglandin endoperoxide H synthase (PGHS)-1 and PGHS- 2 in bone following mechanical loading in vivo. *Anatomical Record*. **252**(4), 580–586.

Franz-Odendaal, T.A., Hall, B.K., Witten, P.E. (2006) Buried alive: How osteoblasts become osteocytes. *Developmental Dynamics*. **235**(1), 176–190.

Fratzl, P., Gupta, H.S., Paschalis, E.P., Roschger, P. (2004) Structure and mechanical quality of the collagen–mineral nano-composite in bone. *J. Mater. Chem.*. **14**(14), 2115–2123.

Friedland, J.C., Lee, M.H., Boettiger, D. (2009) Mechanically activated integrin switch controls α5β1 function. *Science*. **323**(5914), 642–644.

Frith, J.E., Mills, R.J., Hudson, J.E., Cooper-White, J.J. (2012) Tailored integrin-extracellular matrix interactions to direct human mesenchymal stem cell differentiation. *Stem Cells and Development*. **21**(13), 2442–2456.

Ganss, B., Kim, R.H., Sodek, J. (1999) Bone sialoprotein. *Critical Reviews in Oral Biology and Medicine*. **10**(1), 79–98.

Gauthier, O., Bouler, J.M., Aguado, E., Pilet, P., Daculsi, G. (1998) Macroporous biphasic calcium phosphate ceramics: Influence of macropore diameter and macroporosity percentage on bone ingrowth. *Biomaterials*. **19**(1–3), 133–139.

Geiger, B., Spatz, J.P., Bershadsky, A.D. (2009) Environmental sensing through focal adhesions. *Nature Reviews Molecular Cell Biology*. **10**(1), 21–33.

Genetos, D.C., Geist, D.J., Liu, D., Donahue, H.J., Duncan, R.L. (2005) Fluid shear-induced ATP secretion mediates prostaglandin release in MC3T3-E1 osteoblasts. *Journal of Bone and Mineral Research*. **20**(1), 41–49.

Genetos, D.C., Kephart, C.J., Zhang, Y., Yellowley, C.E., Donahue, H.J. (2007) Oscillating fluid flow activation of gap junction hemichannels induces ATP release from MLO-Y4 osteocytes. *Journal of cellular physiology*. **212**(1), 207–14.

Gerstenfeld, L.C., Cho, T.J., Kon, T., Aizawa, T., Tsay, A., Fitch, J., Barnes, G.L., Graves, D.T., Einhorn, T.A. (2003) Impaired fracture healing in the absence of TNF-α signaling: The role of TNF-α in endochondral cartilage resorption. *Journal of Bone and Mineral Research*. **18**(9), 1584–1592.

Gerstenfeld, L.C., Cullinane, D.M., Barnes, G.L., Graves, D.T., Einhorn, T.A. (2003) Fracture healing as a post-natal developmental process: Molecular, spatial, and temporal aspects of its regulation. *Journal of Cellular Biochemistry*. **88**(5), 873–884.

Ghorbani, F.M., Kaffashi, B., Shokrollahi, P., Seyedjafari, E., Ardeshirylajimi, A. (2015) PCL/chitosan/Zn-doped nHA electrospun nanocomposite scaffold promotes adipose derived stem cells adhesion and proliferation. *Carbohydrate Polymers*. **118**, 133–142.

Giannoudis, P. V., Dinopoulos, H., Tsiridis, E. (2005) Bone substitutes: An update. *Injury*. **36**(3), S20–S27.

Glossop, J.R., Cartmell, S.H. (2009) Effect of fluid flow-induced shear stress on human mesenchymal stem cells: Differential gene expression of IL1B and MAP3K8 in MAPK signaling. *Gene Expression Patterns*. **9**(5), 381–388.

Godara, P., McFarland, C.D., Nordon, R.E. (2008) Design of bioreactors for mesenchymal stem cell tissue engineering. *Journal of Chemical Technology & Biotechnology*. **83**(4), 408–420.

De Godoy, R.F., Hutchens, S., Campion, C., Blunn, G. (2015) Silicate-substituted calcium phosphate with enhanced strut porosity stimulates osteogenic differentiation of human mesenchymal stem cells. *Journal of Materials Science: Materials in Medicine*. **26**(1), 54.

Goessler, U.R., Bugert, P., Bieback, K., Stern-Straeter, J., Bran, G., Hormann, K., Riedel, F. (2008) Integrin expression in stem cells from bone marrow and adipose tissue during chondrogenic differentiation. *International Journal of Molecular Medicine*. **21**(3), 271–279.

Goldstein, A.S., Juarez, T.M., Helmke, C.D., Gustin, M.C., Mikos, A.G. (2001) Effect of convection on osteoblastic cell growth and function in biodegradable polymer foam scaffolds. *Biomaterials*. **22**(11), 1279–1288.

Gomes, M.E., Bossano, C.M., Johnston, C.M., Reis, R.L., Mikos, A.G. (2006) In Vitro Localization of Bone Growth Factors in Constructs of Biodegradable Scaffolds Seeded with Marrow Stromal Cells and Cultured in a Flow Perfusion Bioreactor. *Tissue Engineering*. **12**(1), 177–188.

Gomes, M.E., Holtorf, H.L., Reis, R.L., Mikos, A.G. (2006) Influence of the porosity of starch-based fiber mesh scaffolds on the proliferation and osteogenic differentiation of bone marrow stromal cells cultured in a flow perfusion bioreactor. *Tissue Engineering*. **12**(4), 801–809.

Gomes, M.E., Sikavitsas, V.I., Behravesh, E., Reis, R.L., Mikos, A.G. (2003) Effect of flow perfusion on the osteogenic differentiation of bone marrow stromal cells cultured on starch-based three-dimensional scaffolds. *Journal of Biomedical Materials Research*. **67A**(1), 87–95.

Gonçalves, A., Costa, P., Rodrigues, M.T., Dias, I.R., Reis, R.L., Gomes, M.E. (2011) Effect of flow perfusion conditions in the chondrogenic differentiation of bone marrow stromal cells cultured onto starch based biodegradable scaffolds. *Acta Biomaterialia*. **7**(4), 1644–1652.

Grayson, W.L., Bhumiratana, S., Cannizzaro, C., Chao, P.-H.G., Lennon, D.P., Caplan, A.I.,

Vunjak-Novakovic, G. (2008) Effects of initial seeding density and fluid perfusion rate on formation of tissue-engineered bone. *Tissue Engineering Part A*. **14**(11), 1809–1820.

Grundnes, O., Reikerås, O. (1993) The importance of the hematoma for fracture healing in rats. *Acta Orthopaedica Scandinavica*. **64**(3), 340–342.

Hamidouche, Z., Fromigué, O., Ringe, J., Häupl, T., Vaudin, P., Pagès, J.-C., Srouji, S., Livne, E., Marie, P.J. (2009) Priming integrin alpha5 promotes human mesenchymal stromal cell osteoblast differentiation and osteogenesis. *Proceedings of the National Academy of Sciences of the United States of America*. **106**(44), 18587–91.

Harada, S., Rodan, G.A. (2003) Control of osteoblast function and regulation of bone mass. *Nature*. **423**(6937), 349–355.

Harshavardhana, N.S., Noordeen, M.H.H. (2015) Surgical results with the use of Silicated Calcium Phosphate (SiCaP) as bone graft substitute in Posterior Spinal Fusion (PSF) for Adolescent Idiopathic Scoliosis (AIS). *Scoliosis*. **10**(1), 27.

Harter, L. V, Hruska, K.A., Duncan, R.L. (1995) Human osteoblast-like cells respond to mechanical strain with increased bone matrix protein production independent of hormonal regulation. *Endocrinology*. **136**(2), 528–535.

Hassenkam, T., Fantner, G.E., Cutroni, J.A., Weaver, J.C., Morse, D.E., Hansma, P.K. (2004) High-resolution AFM imaging of intact and fractured trabecular bone. *Bone*. **35**(1), 4–10.

Hazenbiller, O., Nasr, S., Krawetz, R.J., Duncan, N.A. (2017) Effect of mechanical strain on the pluripotency of murine embryonic stem cells seeded in a collagen-I scaffold. *Journal of Orthopaedic Research*. **36**(2), 799–807.

Hillsley, M. V., Frangos, J.A. (1994) Review: Bone tissue engineering: The role of interstitial fluid flow. *Biotechnology and Bioengineering*. **43**(7), 573–581.

Hing, K.A., Annaz, B., Saeed, S., Revell, P.A., Buckland, T. (2005) Microporosity enhances bioactivity of synthetic bone graft substitutes. *Journal of Materials Science: Materials in Medicine*. **16**(5), 467–475.

Hing, K.A., Best, S.M., Bonfield, W. (1999) Characterization of porous hydroxyapatite. *Journal of materials science.Materials in medicine*. **10**(3), 135–145.

Hing, K.A., Best, S.M., Tanner, K.E., Bonfield, W., Revell, P.A. (2002) Mediation of bone ingrowth in porous hydroxyapatite bone graft substitutes. *Journal of biomedical materials research. Part A*. **68**(1), 187–200.

Hing, K.A., Bonfield, W. (2000) WO2000020353A1 - Foamed ceramics.

Hing, K.A., Revell, P.A., Smith, N., Buckland, T. (2006) Effect of silicon level on rate, quality and progression of bone healing within silicate-substituted porous hydroxyapatite scaffolds. *Biomaterials*. **27**(29), 5014–5026.

Hing, K.A., Saeed, S., Annaz, B., Buckland, T., Revell, P. (2004) Microporosity affects bioactivity of macroporous hydroxyapatite bone graft substitutes. *Key Engineering Materials*. **256**, 273–276.

Hoang, Q.Q., Sicheri, F., Howard, A.J., Yang, D.S.C. (2003) Bone recognition mechanism of porcine osteocalcin from crystal structure. *Nature*. **425**(6961), 977–980.

Holtorf, H.L., Jansen, J.A., Mikos, A.G. (2005) Flow perfusion culture induces the osteoblastic differentiation of marrow stromal cell-scaffold constructs in the absence of dexamethasone. *Journal of Biomedical Materials Research Part A*. **72A**(3), 326–334.

Holtorf, H.L., Sheffield, T.L., Ambrose, C.G., Jansen, J.A., Mikos, A.G. (2005) Flow perfusion

culture of marrow stromal cells seeded on porous biphasic calcium phosphate ceramics. *Annals of Biomedical Engineering*. **33**(9), 1238–1248.

Holy, C.E., Shoichet, M.S., Davies, J.E. (2000) Engineering three-dimensional bone tissue in vitro using biodegradable scaffolds: Investigating initial cell-seeding density and culture period. *J Biomed Mater Res*. **51**, 376–382.

Horwitz, E.M., Gordon, P.L., Koo, W.K.K., Marx, J.C., Neel, M.D., McNall, R.Y., Muul, L., Hofmann, T. (2002) Isolated allogeneic bone marrow-derived mesenchymal cells engraft and stimulate growth in children with osteogenesis imperfecta: Implications for cell therapy of bone. *Proceedings of the National Academy of Sciences of the United States of America*. **99**(13), 8932–7.

Huang, C.-Y.C. (2004) Effects of cyclic compressive loading on chondrogenesis of rabbit bone-marrow derived mesenchymal stem cells. *Stem Cells*. **22**(3), 313–323.

Huiskes, R., Ruimerman, R., van Lenthe, G.H., Janssen, J.D. (2000) Effects of mechanical forces on maintenance and adaptation of form in trabecular bone. *Nature*. **405**(6787), 704–706.

Hulbert, S.F., Young, F.A., Mathews, R.S., Klawitter, J.J., Talbert, C.D., Stelling, F.H. (1970) Potential of ceramic materials as permanently implantable skeletal prostheses. *Journal of Biomedical Materials Research*. **4**(3), 433–456.

Hunter, G.K., Goldberg, H.A. (1993) Nucleation of hydroxyapatite by bone sialoprotein. . **90**, 8562–8565.

Hutmacher, D.W., Schantz, J.T., Lam, C.X.F., Tan, K.C., Lim, T.C. (2007) State of the art and future directions of scaffold-based bone engineering from a biomaterials perspective. *Journal of Tissue Engineering and Regenerative Medicine*. **1**(4), 245–260.

Ichinohe, N., Takamoto, T., Tabata, Y. (2008) Proliferation, osteogenic differentiation, and distribution of rat bone marrow stromal cells in nonwoven fabrics by different culture methods. *Tissue engineering. Part A*. **14**(1), 107–16.

IndustryToday (2017) Bone graft substitute market ultimate analysis & global forecast to 2027. *Industry Today*.

Ingber, D.E. (2006) Cellular mechanotransduction: putting all the pieces together again. *Faseb Journal*. **20**(7), 811–827.

Isaksson, H., Wilson, W., van Donkelaar, C.C., Huiskes, R., Ito, K. (2006) Comparison of biophysical stimuli for mechano-regulation of tissue differentiation during fracture healing. *Journal of Biomechanics*. **39**(8), 1507–1516.

Ishihara, Y., Sugawara, Y., Kamioka, H., Kawanabe, N., Hayano, S., Balam, T.A., Naruse, K., Yamashiro, T. (2013) Ex vivo real-time observation of Ca2+ signaling in living bone in response to shear stress applied on the bone surface. *Bone*. **53**(1), 204–215.

Ismail, T., Osinga, R., Todorov, A., Haumer, A., Tchang, L.A., Epple, C., Allafi, N., Menzi, N., Largo, R.D., Kaempfen, A., Martin, I., Schaefer, D.J., Scherberich, A. (2017) Engineered, axially-vascularized osteogenic grafts from human adipose-derived cells to treat avascular necrosis of bone in a rat model. *Acta Biomaterialia*. **63**, 236–245.

Issa, R.I., Engebretson, B., Rustom, L., McFetridge, P.S., Sikavitsas, V.I. (2011) The effect of cell seeding density on the cellular and mechanical properties of a mechanostimulated tissue-engineered tendon. *Tissue Engineering Part A*. **17**(11–12), 1479–1487.

Jaasma, M.J., O'Brien, F.J. (2008) Mechanical stimulation of osteoblasts using steady and dynamic fluid flow. *Tissue Engineering Part A*. **14**(7), 1213–1223.

Jaasma, M.J., Plunkett, N.A., O'Brien, F.J. (2008) Design and validation of a dynamic flow perfusion bioreactor for use with compliant tissue engineering scaffolds. *Journal of Biotechnology*. **133**(4), 490–496.

Jacobs, C.R., Temiyasathit, S., Castillo, A.B. (2010) Osteocyte mechanobiology and pericellular mechanics. *Annual Review of Biomedical Engineering*. **12**(1), 369–400.

Jagodzinski, M., Breitbart, A., Wehmeier, M., Hesse, E., Haasper, C., Krettek, C., Zeichen, J., Hankemeier, S. (2008) Influence of perfusion and cyclic compression on proliferation and differentiation of bone marrow stromal cells in 3-dimensional culture. *Journal of Biomechanics*. **41**(9), 1885–1891.

Janmey, P.A. (1998) The cytoskeleton and cell signaling: component localization and mechanical coupling. *Physiological reviews*. **78**(3), 763–81.

Janssen, F.W., Van Dijkhuizen-Radersma, R., Van Oorschot, A., Oostra, J., De Bruijn, J.D., Van Blitterswijk, C.A. (2010) Human tissue-engineered bone produced in clinically relevant amounts using a semi-automated perfusion bioreactor system: A preliminary study. *Journal of Tissue Engineering and Regenerative Medicine*. **4**(1), 12–24.

Janssen, F.W., Oostra, J., Oorschot, A. van, van Blitterswijk, C.A. (2006) A perfusion bioreactor system capable of producing clinically relevant volumes of tissue-engineered bone: In vivo bone formation showing proof of concept. *Biomaterials*. **27**(3), 315–323.

Jikko, A., Harris, S.E., Chen, D., Mendrick, D.L., Damsky, C.H. (1999) Collagen integrin receptors regulate early osteoblast differentiation induced by BMP-2. *Journal of Bone and Mineral Research*. **14**(7), 1075–1083.

Jin, E.J., Choi, Y.A., Kyun Park, E., Bang, O.S., Kang, S.S. (2007) MMP-2 functions as a negative regulator of chondrogenic cell condensation via down-regulation of the FAK-integrin α1 interaction. *Developmental Biology*. **308**(2), 474–484.

Jones, J.I., Clemmons, D.R. (1995) Insulin-like growth factors and their binding proteins: Biological actions. *Endocrine Reviews*. **16**(1), 3–34.

Jones, J.R. (2015) Reprint of: Review of bioactive glass: From hench to hybrids. *Acta Biomaterialia*. **23**(S), S53–S82.

Juhász, T., Matta, C., Somogyi, C., Katona, É., Takács, R., Soha, R.F., Szabó, I.A., Cserháti, C., Sződy, R., Karácsonyi, Z., Bakó, É., Gergely, P., Zákány, R. (2014) Mechanical loading stimulates chondrogenesis via the PKA/CREB-Sox9 and PP2A pathways in chicken micromass cultures. *Cellular Signalling*. **26**(3), 468–482.

Kalajzic, I., Braut, A., Guo, D., Jiang, X., Kronenberg, M.., Mina, M., Harris, M.., Harris, S.., Rowe, D.. (2004) Dentin matrix protein 1 expression during osteoblastic differentiation, generation of an osteocyte GFP-transgene. *Bone*. **35**(1), 74–82.

Kamel, M.A., Picconi, J.L., Lara-Castillo, N., Johnson, M.L. (2010) Activation of β-catenin signaling in MLO-Y4 osteocytic cells versus 2T3 osteoblastic cells by fluid flow shear stress and PGE2: Implications for the study of mechanosensation in bone. *Bone*. **47**(5), 872–81.

Karageorgiou, V., Kaplan, D. (2005) Porosity of 3D biomaterial scaffolds and osteogenesis. *Biomaterials*. **26**(27), 5474–5491.

Karsenty, G. (2008) Transcriptional control of skeletogenesis. *Annual Review of Genomics and Human Genetics*. **9**(1), 183–196.

Kasten, A., Müller, P., Bulnheim, U., Groll, J., Bruellhoff, K., Beck, U., Steinhoff, G., Möller, M., Rychly, J. (2010) Mechanical integrin stress and magnetic forces induce biological responses in mesenchymal stem cells which depend on environmental factors. *Journal of Cellular*

Biochemistry. **111**(6), 1586–1597.

Kasten, P., Beyen, I., Niemeyer, P., Luginbühl, R., Bohner, M., Richter, W. (2008) Porosity and pore size of β-tricalcium phosphate scaffold can influence protein production and osteogenic differentiation of human mesenchymal stem cells: An in vitro and in vivo study. *Acta Biomaterialia*. **4**(6), 1904–1915.

Katz, S., Boland, R., Santillán, G. (2006) Modulation of ERK 1/2 and p38 MAPK signaling pathways by ATP in osteoblasts: Involvement of mechanical stress-activated calcium influx, PKC and Src activation. *The International Journal of Biochemistry & Cell Biology*. **38**(12), 2082–2091.

Kearney, E.M., Prendergast, P.J., Campbell, V.A. (2008) Mechanisms of Strain-Mediated Mesenchymal Stem Cell Apoptosis. *Journal of Biomechanical Engineering*. **130**(6), 061004.

Keaveny, T.M., Morgan, E.F., Niebur, G.L., Yeh, O.C. (2001) Biomechanics of trabecular bone. *Annual Review of Biomedical Engineering*. **3**(1), 307–333.

Kim, C.H., You, L., Yellowley, C.E., Jacobs, C.R. (2006) Oscillatory fluid flow-induced shear stress decreases osteoclastogenesis through RANKL and OPG signaling. *Bone*. **39**(5), 1043–1047.

Kim, J., Ma, T. (2012) Perfusion regulation of hMSC microenvironment and osteogenic differentiation in 3D scaffold. *Biotechnology and Bioengineering*. **109**(1), 252–261.

Kim, S.-S., Sun Park, M., Jeon, O., Yong Choi, C., Kim, B.-S. (2006) Poly(lactide-co-glycolide)/hydroxyapatite composite scaffolds for bone tissue engineering. *Biomaterials*. **27**(8), 1399–1409.

Klein-Nulend, J., Bakker, A.D., Bacabac, R.G., Vatsa, A., Weinbaum, S. (2013) Mechanosensation and transduction in osteocytes. *Bone*. **54**(2), 182–190.

Knight, M.M., Toyoda, T., Lee, D.A., Bader, D.L. (2006) Mechanical compression and hydrostatic pressure induce reversible changes in actin cytoskeletal organisation in chondrocytes in agarose. *Journal of Biomechanics*. **39**(8), 1547–1551.

Knothe Tate, M.L., Knothe, U., Niederer, P. (1998) Experimental elucidation of mechanical load-induced fluid flow and its potential role in bone metabolism and functional adaptation. *American Journal of the Medical Sciences*. **316**(3), 189–195.

Koç, O.N., Lazarus, H.M. (2001) Mesenchymal stem cells: heading into the clinic. *Bone marrow transplantation*. **27**(3), 235–9.

Kock, L.M., Malda, J., Dhert, W.J.A., Ito, K., Gawlitta, D. (2014) Flow-perfusion interferes with chondrogenic and hypertrophic matrix production by mesenchymal stem cells. *Journal of Biomechanics*. **47**(9), 2122–2129.

Kuboki, Y., Jin, Q., Takita, H. (2001) Geometry of carriers controlling phenotypic expression in BMP-induced osteogenesis and chondrogenesis. *The Journal of bone and joint surgery. American volume*. **83**–**A Suppl**(Pt 2), S105–S115.

Kular, J., Tickner, J., Chim, S.M., Xu, J. (2012) An overview of the regulation of bone remodelling at the cellular level. *Clinical Biochemistry*. **45**(12), 863–873.

Lacroix, D., Prendergast, P.J. (2002) A mechano-regulation model for tissue differentiation during fracture healing: Analysis of gap size and loading. *Journal of Biomechanics*. **35**(9), 1163–1171.

Lacroix, D., Prendergast, P.J., Li, G., Marsh, D. (2002) Biomechanical model to simulate tissue differentiation and bone regeneration: application to fracture healing. *Medical and*

Biological Engineering and Computing. **40**(1), 14–21.

Lal, H., Verma, S.K., Smith, M., Guleria, R.S., Lu, G., Foster, D.M., Dostal, D.E. (2007) Stretch-induced MAP kinase activation in cardiac myocytes: Differential regulation through β1-integrin and focal adhesion kinase. *Journal of Molecular and Cellular Cardiology*. **43**(2), 137–147.

Lan Levengood, S.K., Polak, S.J., Wheeler, M.B., Maki, A.J., Clark, S.G., Jamison, R.D., Wagoner Johnson, A.J. (2010) Multiscale osteointegration as a new paradigm for the design of calcium phosphate scaffolds for bone regeneration. *Biomaterials*. **31**(13), 3552–3563.

Langer, R., Vacanti, J.P. (1993) Tissue engineering. *Science (New York, N.Y.)*. **260**(5110), 920–6.

Lannutti, J., Reneker, D., Ma, T., Tomasko, D., Farson, D. (2007) Electrospinning for tissue engineering scaffolds. *Materials Science and Engineering: C*. **27**(3), 504–509.

Lanyon, L.E. (1992) Control of bone architecture by functional load bearing. *Journal of Bone and Mineral Research*. **7**(S2), S369–S375.

Lanyon, L.E. (1993) Osteocytes, strain detection, bone modeling and remodeling. *Calcified Tissue International*. **53**(S1), S102–S107.

Lanyon, L.E., Rubin, C.T. (1984) Static vs dynamic loads as an influence on bone remodelling. *Journal of Biomechanics*. **17**(12), 897–905.

Lara-Castillo, N., Kim-Weroha, N.A., Kamel, M.A., Javaheri, B., Ellies, D.L., Krumlauf, R.E., Thiagarajan, G., Johnson, M.L. (2015) In vivo mechanical loading rapidly activates β-catenin signaling in osteocytes through a prostaglandin mediated mechanism. *Bone*. **76**, 58–66.

Lawrence, D.A. (1996) Transforming growth factor-beta: a general review. *European cytokine network*. **7**(3), 363–74.

Lee, D.Y., Yeh, C.R., Chang, S.F., Lee, P.L., Chien, S., Cheng, C.K., Chiu, J.J. (2008) Integrin-mediated expression of bone formation-related genes in osteoblast-like cells in response to fluid shear stress: Roles of extracellular matrix, Shc, and mitogen-activated protein kinase. *Journal of Bone and Mineral Research*. **23**(7), 1140–1149.

Lee, J., Abdeen, A.A., Tang, X., Saif, T.A., Kilian, K.A. (2015) Geometric guidance of integrin mediated traction stress during stem cell differentiation. *Biomaterials*. **69**, 174–183.

LeGeros, R.Z. (2002) Properties of osteoconductive biomaterials: Calcium phosphates. *Clinical Orthopaedics and Related Research*. **395**(395), 81–98.

Lenormand, P., Sardet, C., Pages, G., L'Allemain, G., Brunet, A., Poysségur, J. (1993) Growth Factors Induce Nuclear Translocation of MAP Kinases (p42 mapk and p44 mapk) but not of Their Activator MAP Kinase Kinase (p45 mapkk) in Fibroblasts. *The Journal of Cell Biology*. **122**(5), 1079–1088.

Li, D., Tang, T., Lu, J., Dai, K. (2009) Effects of Flow Shear Stress and Mass Transport on the Construction of a Large-Scale Tissue-Engineered Bone in a Perfusion Bioreactor. *Tissue Engineering Part A*. **15**(10), 2773–2783.

Li, G.-R., Deng, X.-L., Sun, H., Chung, S.S.M., Tse, H.-F., Lau, C.-P. (2006) Ion channels in mesenchymal stem cells from rat bone marrow. *Stem cells (Dayton, Ohio)*. **24**(6), 1519–28.

Li, J., Duncan, R.L., Burr, D.B., Gattone, V.H., Turner, C.H. (2003) Parathyroid Hormone Enhances Mechanically Induced Bone Formation, Possibly Involving L-Type Voltage-Sensitive Calcium Channels. *Endocrinology*. **144**(4), 1226–1233.

Li, J., Duncan, R.L., Burr, D.B., Turner, C.H. (2002) L-Type Calcium Channels Mediate

Mechanically Induced Bone Formation In Vivo. *Journal of Bone and Mineral Research*. **17**(10), 1795–1800.

Li, J., Zhao, Z., Liu, J., Huang, N., Long, D., Wang, J., Li, X., Liu, Y. (2010) MEK/ERK and p38 MAPK regulate chondrogenesis of rat bone marrow mesenchymal stem cells through delicate interaction with TGF-β1/Smads pathway. *Cell Proliferation*. **43**(4), 333–343.

Li, J.P., Li, S.H., Van Blitterswijk, C.A., de Groot, K. (2005) A novel porous Ti6Al4V: Characterization and cell attachment. *Journal of Biomedical Materials Research Part A*. **73A**(2), 223–233.

Li, Y.J., Batra, N.N., You, L., Meier, S.C., Coe, I. a, Yellowley, C.E., Jacobs, C.R. (2004) Oscillatory fluid flow affects human marrow stromal cell proliferation and differentiation. *Journal of orthopaedic research : official publication of the Orthopaedic Research Society*. **22**(6), 1283–1289.

Liao, S.S., Cui, F.Z., Zhang, W., Feng, Q.L. (2004) Hierarchically Biomimetic Bone Scaffold Materials: Nano-HA/Collagen/PLA Composite. *J Biomed Mater Res Part B: Appl Biomater*. **69**, 158–165.

Liu, C.X., Abedian, R., Meister, R., Haasper, C., Hurschler, C., Krettek, C., von Lewinski, G., Jagodzinski, M. (2012) Influence of perfusion and compression on the proliferation and differentiation of bone mesenchymal stromal cells seeded on polyurethane scaffolds. *Biomaterials*. **33**(4), 1052–1064.

Liu, D., Genetos, D.C., Shao, Y., Geist, D.J., Li, J., Ke, H.Z., Turner, C.H., Duncan, R.L. (2008) Activation of extracellular-signal regulated kinase (ERK1/2) by fluid shear is Ca2+- and ATP-dependent in MC3T3-E1 osteoblasts. *Bone*. **42**(4), 644–652.

Liu, J., Zhao, Z., Li, J., Zou, L., Shuler, C., Zou, Y., Huang, X., Li, M., Wang, J. (2009) Hydrostatic pressures promote initial osteodifferentiation with ERK1/2 not p38 MAPK signaling involved. *Journal of Cellular Biochemistry*. **107**(2), 224–232.

Liu, L., Shao, L., Li, B., Zong, C., Li, J., Zheng, Q., Tong, X., Gao, C., Wang, J. (2011) Extracellular signal-regulated kinase1/2 activated by fluid shear stress promotes osteogenic differentiation of human bone marrow-derived mesenchymal stem cells through novel signaling pathways. *The International Journal of Biochemistry & Cell Biology*. **43**(11), 1591–1601.

Liu, L., Zong, C., Li, B., Shen, D., Tang, Z., Chen, J., Zheng, Q., Tong, X., Gao, C., Wang, J. (2012) The interaction between b1 integrins and ERK1/2 in osteogenic differentiation of human mesenchymal stem cells under fluid shear stress modelled by a perfusion system. *Journal of tissue engineering and regenerative medicine*. **4**(8), 85–96.

Loh, Q.L., Choong, C. (2013) Three-Dimensional Scaffolds for Tissue Engineering Applications: Role of Porosity and Pore Size. *Tissue Engineering Part B: Reviews*. **19**(6), 485–502.

Lu, Z.F., Zreiqat, H. (2010) Beta-tricalcium phosphate exerts osteoconductivity through α2β1 integrin and down-stream MAPK/ERK signaling pathway. *Biochemical and Biophysical Research Communications*. **394**(2), 323–329.

Ma, T., Li, Y., Yang, S.-T., Kniss, D.A. (2000) Effects of pore size in 3-D fibrous matrix on human trophoblast tissue development. *Biotechnology and Bioengineering*. **70**(6), 606–618.

Mackie, E.J., Ahmed, Y.A., Tatarczuch, L., Chen, K.-S., Mirams, M. (2008) Endochondral ossification: How cartilage is converted into bone in the developing skeleton. *The International Journal of Biochemistry & Cell Biology*. **40**(1), 46–62.

Malone, A.M.D., Anderson, C.T., Tummala, P., Kwon, R.Y., Johnston, T.R., Stearns, T., Jacobs,

C.R. (2007) Primary cilia mediate mechanosensing in bone cells by a calcium-independent mechanism. *Proceedings of the National Academy of Sciences of the United States of America*. **104**(33), 13325–13330.

Mandracchia, V.J., Nelson, S.C., Barp, E.A. (2001) Current concepts of bone healing. *Clinics in podiatric medicine and surgery*. **18**(1), 55–77.

Marcacci, M., Kon, E., Moukhachev, V., Lavroukov, A., Kutepov, S., Quarto, R., Mastrogiacomo, M., Cancedda, R. (2007) Stem Cells Associated with Macroporous Bioceramics for Long Bone Repair: 6- to 7-Year Outcome of a Pilot Clinical Study. *Tissue Engineering*. **13**(5), 947–955.

Marieb, E.N., Hoehn, K. (2007) *Human anatomy and physiology*. Pearson Benjamin Cummings.

Marra, K.G., Szem, J.W., Kumta, P.N., Dimilla, P.A., Weiss, L.E. (1999) In vitro analysis of biodegradable polymer blend/hydroxyapatite composites for bone tissue engineering. *J Biomed Mater Res*. **47**, 324–335.

Mastrogiacomo, M., Scaglione, S., Martinetti, R., Dolcini, L., Beltrame, F., Cancedda, R., Quarto, R. (2006) Role of scaffold internal structure on in vivo bone formation in macroporous calcium phosphate bioceramics. *Biomaterials*. **27**(17), 3230–3237.

Matta, C., Zákány, R., Mobasheri, A. (2015) Voltage-Dependent Calcium Channels in Chondrocytes: Roles in Health and Disease. *Current Rheumatology Reports*. **17**(7), 43.

McBeath, R., Pirone, D.M., Nelson, C.M., Bhadriraju, K., Chen, C.S. (2004) Cell Shape, Cytoskeletal Tension, and RhoA Regulate Stem Cell Lineage Commitment. *Developmental Cell*. **6**(4), 483–495.

McCoy, R.J., O'Brien, F.J. (2010) Influence of Shear Stress in Perfusion Bioreactor Cultures for the Development of Three-Dimensional Bone Tissue Constructs: A Review. *Tissue Engineering Part B: Reviews*. **16**(6), 587–601.

McGarry, J.G., Klein-Nulend, J., Prendergast, P.J. (2005) The effect of cytoskeletal disruption on pulsatile fluid flow-induced nitric oxide and prostaglandin E2 release in osteocytes and osteoblasts. *Biochemical and Biophysical Research Communications*. **330**(1), 341–348.

Meinel, L., Karageorgiou, V., Fajardo, R., Snyder, B., Shinde-Patil, V., Zichner, L., Kaplan, D., Langer, R., Vunjak-Novakovic, G. (2004) Bone Tissue Engineering Using Human Mesenchymal Stem Cells: Effects of Scaffold Material and Medium Flow. *Annals of Biomedical Engineering*. **32**(1), 112–122.

Mellor, L.F., Baker, T.L., Brown, R.J., Catlin, L.W., Oxford, J.T. (2014) Optimal 3D Culture of Primary Articular Chondrocytes for Use in the Rotating Wall Vessel Bioreactor. *Aviation, Space, and Environmental Medicine*. **85**(8), 798–804.

Mitra, D., Whitehead, J., Yasui, O.W., Leach, J.K. (2017) Bioreactor culture duration of engineered constructs influences bone formation by mesenchymal stem cells. *Biomaterials*. **146**, 29–39.

Miyanishi, K., Trindade, M.C.D., Lindsey, D.P., Beaupré, G.S., Carter, D.R., Goodman, S.B., Schurman, D.J., Smith, R.L. (2006) Dose- and Time-Dependent Effects of Cyclic Hydrostatic Pressure on Transforming Growth Factor-β3-Induced Chondrogenesis by Adult Human Mesenchymal Stem Cells *in Vitro*. *Tissue Engineering*. **12**(8), 2253–2262.

Miyauchi, A., Notoya, K., Mikuni-Takagaki, Y., Takagi, Y., Goto, M., Miki, Y., Takano-Yamamoto, T., Jinnai, K., Takahashi, K., Kumegawa, M., Chihara, K., Fujita, T. (2000) Parathyroid hormone-activated volume-sensitive calcium influx pathways in mechanically

loaded osteocytes. *Journal of Biological Chemistry*. **275**(5), 3335–3342.

Mobasheri, A., Carter, S.D., Martín-Vasallo, P., Shakibaei, M. (2002) Integrins and stretch activated ion channels; putative components of functional cell surface mechanoreceptors in articular chondrocytes. *Cell Biology International*. **26**(1), 1–18.

Mullender, M., El Haj, A.J., Yang, Y., van Duin, M.A., Burger, E.H., Klein-Nulend, J. (2004) Mechanotransduction of bone cells in vitro: Mechanobiology of bone tissue. *Medical and Biological Engineering and Computing*. **42**(1), 14–21.

Murakami, S., Kan, M., McKeehan, W.L., de Crombrugghe, B. (2000) Up-regulation of the chondrogenic Sox9 gene by fibroblast growth factors is mediated by the mitogen-activated protein kinase pathway. *Proceedings of the National Academy of Sciences of the United States of America*. **97**(3), 1113–8.

Murphy, C.M., Haugh, M.G., O'Brien, F.J. (2010) The effect of mean pore size on cell attachment, proliferation and migration in collagen–glycosaminoglycan scaffolds for bone tissue engineering. *Biomaterials*. **31**(3), 461–466.

Mygind, T., Stiehler, M., Baatrup, A., Li, H., Zou, X., Flyvbjerg, A., Kassem, M., Bünger, C. (2007) Mesenchymal stem cell ingrowth and differentiation on coralline hydroxyapatite scaffolds. *Biomaterials*. **28**(6), 1036–1047.

Nakashima, K., Zhou, X., Kunkel, G., Zhang, Z., Deng, J.M., Behringer, R.R., De Crombrugghe, B. (2002) The novel zinc finger-containing transcription factor Osterix is required for osteoblast differentiation and bone formation. *Cell*. **108**(1), 17–29.

Nakashima, T. (2011) Evidence for osteocyteregulation of bone homeostasis through RANKL expression. *Nat. Med.*. **17**, 1231–1234.

Nakayama, H., Numakawa, T., Ikeuchi, T., Hatanaka, H. (2008) Nicotine-induced phosphorylation of extracellular signal-regulated protein kinase and CREB in PC12h cells. *Journal of Neurochemistry*. **79**(3), 489–498.

Ng, L.-J., Wheatley, S., Muscat, G.E.., Conway-Campbell, J., Bowles, J., Wright, E., Bell, D.M., Tam, P.P.., Cheah, K.S.., Koopman, P. (1997) SOX9 Binds DNA, Activates Transcription, and Coexpresses with Type II Collagen during Chondrogenesis in the Mouse. *Developmental Biology*. **183**(1), 108–121.

Nishi, M., Matsumoto, R., Dong, J., Uemura, T. (2013) Engineered bone tissue associated with vascularization utilizing a rotating wall vessel bioreactor. *Journal of Biomedical Materials Research Part A*. **101A**(2), 421–427.

Noel, D., Gazit, D., Bouquet, C., Apparailly, F., Bony, C., Plence, P., Millet, V., Turgeman, G., Perricaudet, M., Sany, J., Jorgensen, C. (2008) Short-Term BMP-2 Expression Is Sufficient for In Vivo Osteochondral Differentiation of Mesenchymal Stem Cells. *Stem Cells*. **22**(1), 74–85.

Norvell, S.M., Alvarez, M., Bidwell, J.P., Pavalko, F.M. (2004) Fluid Shear Stress Induces ?-Catenin Signaling in Osteoblasts. *Calcified Tissue International*. **75**(5), 396–404.

Olszta, M.J., Cheng, X., Jee, S.S., Kumar, R., Kim, Y.-Y., Kaufman, M.J., Douglas, E.P., Gower, L.B. (2007) Bone structure and formation: A new perspective. *Materials Science and Engineering: R: Reports*. **58**(3–5), 77–116.

Papadimitropoulos, A., Piccinini, E., Brachat, S., Braccini, A., Wendt, D., Barbero, A., Jacobi, C., Martin, I. (2014) Expansion of Human Mesenchymal Stromal Cells from Fresh Bone Marrow in a 3D Scaffold-Based System under Direct Perfusion. *Perfusion. PLoS ONE*. **9**(7).

Parekkadan, B., Milwid, J.M. (2010) Mesenchymal stem cells as therapeutics. *Annual review of biomedical engineering*. **12**, 87–117.

Park, J.S., Chu, J.S., Tsou, A.D., Diop, R., Tang, Z., Wang, A., Li, S. (2011) The effect of matrix stiffness on the differentiation of mesenchymal stem cells in response to TGF-β. *Biomaterials*. **32**(16), 3921–3930.

Patel, N., Best, S.M., Bonfield, W., Gibson, I.R., Hing, K.A., Damien, E., Revell, P.A. (2002) A comparative study on the in vivo behavior of hydroxyapatite and silicon substituted hydroxyapatite granules. *Journal of Materials Science: Materials in Medicine*. **13**(12), 1199–1206.

Patel, N., Brooks, R.A., Clarke, M.T., Lee, P.M.T., Rushton, N., Gibson, I.R., Best, S.M., Bonfield, W. (2005) In vivo assessment of hydroxyapatite and silicate-substituted hydroxyapatite granules using an ovine defect model. *Journal of Materials Science-Materials in Medicine*. **16**(5), 429–440.

Pautke, C., Schieker, M., Tischer, T., Kolk, A., Neth, P., Mutschler, W., Milz, S. (2004) Characterization of osteosarcoma cell lines MG-63, Saos-2 and U-2 OS in comparison to human osteoblasts. *Anticancer research*. **24**(6), 3743–8.

Pavalko, F.M., Chen, N.X., Turner, C.H., Burr, D.B., Atkinson, S., Hsieh, Y.F., Qiu, J., Duncan, R.L. (1998) Fluid shear-induced mechanical signaling in MC3T3-E1 osteoblasts requires cytoskeleton-integrin interactions. *The American journal of physiology*. **275**(6), 1591–601.

Pek, Y.S., Wan, A.C.A., Ying, J.Y. (2010) The effect of matrix stiffness on mesenchymal stem cell differentiation in a 3D thixotropic gel. *Biomaterials*. **31**(3), 385–391.

Phinney, D.G., Prockop, D.J. (2007) Concise Review: Mesenchymal Stem/Multipotent Stromal Cells: The State of Transdifferentiation and Modes of Tissue Repair-Current Views. *Stem Cells*. **25**(11), 2896–2902.

Pietak, A.M., Reid, J.W., Stott, M.J., Sayer, M. (2007) Silicon substitution in the calcium phosphate bioceramics. *Biomaterials*. **28**(28), 4023–4032.

Pisanti, P., Yeatts, A.B., Cardea, S., Fisher, J.P., Reverchon, E. (2012) Tubular perfusion system culture of human mesenchymal stem cells on poly- L- lactic acid scaffolds produced using a supercritical carbon dioxide-assisted process. *Journal of Biomedical Materials Research Part A*. **100A**(10), 2563–2572.

Plotnikov, A., Zehorai, E., Procaccia, S., Seger, R. (2011) The MAPK cascades: Signaling components, nuclear roles and mechanisms of nuclear translocation. *Biochimica et Biophysica Acta - Molecular Cell Research*. **1813**(9), 1619–1633.

Polak, S.J., Rustom, L.E., Genin, G.M., Talcott, M., Wagoner Johnson, A.J. (2013) A mechanism for effective cell-seeding in rigid, microporous substrates. *Acta Biomaterialia*. **9**(8), 7977–7986.

Pommerenke, H., Schmidt, C., Dürr, F., Nebe, B., Lüthen, F., Muller, P., Rychly, J. (2002) The mode of mechanical integrin stressing controls intracellular signaling in osteoblasts. *Journal of bone and mineral research : the official journal of the American Society for Bone and Mineral Research*. **17**(4), 603–611.

Porter, A.E., Patel, N., Skepper, J.N., Best, S.M., Bonfield, W. (2003) Comparison of in vivo dissolution processes in hydroxyapatite and silicon-substituted hydroxyapatite bioceramics. *Biomaterials*. **24**(25), 4609–4620.

Porter, A.E., Patel, N., Skepper, J.N., Best, S.M., Bonfield, W. (2004) Effect of sintered silicate-substituted hydroxyapatite on remodelling processes at the bone-implant interface. *Biomaterials*. **25**(16), 3303–3314.

Porter, B.D., Lin, A.S.P., Peister, A., Hutmacher, D., Guldberg, R.E. (2007) Noninvasive image

analysis of 3D construct mineralization in a perfusion bioreactor. *Biomaterials*. **28**, 2525–2533.

Prodanov, L., te Riet, J., Lamers, E., Domanski, M., Luttge, R., van Loon, J.J.W.A., Jansen, J.A., Walboomers, X.F. (2010) The interaction between nanoscale surface features and mechanical loading and its effect on osteoblast-like cells behavior. *Biomaterials*. **31**(30), 7758–7765.

Qi, X., Liu, J.-G., Chang, Y., Xu, X.-X. (2004) Comparative study on seeding methods of human bone marrow stromal cells in bone tissue engineering. *Chinese medical journal*. **117**(4), 576–80.

Raghothaman, D., Leong, M.F., Lim, T.C., Toh, J.K.C., Wan, A.C.A., Yang, Z., Lee, E.H. (2014) Engineering cell matrix interactions in assembled polyelectrolyte fiber hydrogels for mesenchymal stem cell chondrogenesis. *Biomaterials*. **35**(9), 2607–2616.

Rao, P.K., Kumar, R.M., Farkhondeh, M., Baskerville, S., Lodish, H.F. (2006) Myogenic factors that regulate expression of muscle-specific microRNAs. *Proceedings of the National Academy of Sciences*. **103**(23), 8721–8726.

Rawlinson, S.C.F., Pitsillides, A.A., Lanyon, L.E. (1996) Involvement of different ion channels in osteoblasts' and osteocytes' early responses to mechanical strain. *Bone*. **19**(6), 609–614.

Reddi, A.H. (1998) Role of morphogenetic proteins in skeletal tissue engineering and regeneration. *Nature Biotechnology*. **16**(3), 247–252.

Rizzo, V., Sung, A., Oh, P., Schnitzer, J.E. (1998) Rapid mechanotransduction in situ at the luminal cell surface of vascular endothelium and its caveolae. *The Journal of biological chemistry*. **273**(41), 26323–9.

Robinson, J.A., Chatterjee-Kishore, M., Yaworsky, P.J., Cullen, D.M., Zhao, W., Li, C., Kharode, Y., Sauter, L., Babij, P., Brown, E.L., Hill, A.A., Akhter, M.P., Johnson, M.L., Recker, R.R., Komm, B.S., Bex, F.J. (2006) Wnt/beta-catenin signaling is a normal physiological response to mechanical loading in bone. *The Journal of biological chemistry*. **281**(42), 31720–8.

Robling, A.G., Hinant, F.M., Burr, D.B., Turner, C.H. (2002) Improved Bone Structure and Strength After Long-Term Mechanical Loading Is Greatest if Loading Is Separated Into Short Bouts. *Journal of Bone and Mineral Research*. **17**(8), 1545–1554.

Rodan, G.A., Noda, M. (1991) Gene expression in osteoblastic cells. *Crit Rev Eukaryot Gene Expr*. **1**(2), 85–98.

Roelofsen, J., Klein-Nulend, J., Burger, E.H. (1995) Mechanical stimulation by intermittent hydrostatic compression promotes bone-specific gene expression in vitro. *Journal of Biomechanics*. **28**(12), 1493–1503.

Roskoski, R. (2012) ERK1/2 MAP kinases: Structure, function, and regulation. *Pharmacological Research*. **66**(2), 105–143.

Rubin, J., Fan, X., Biskobing, D.M., Taylor, W.R., Rubin, C.T. (1999) Osteoclastogenesis is repressed by mechanical strain in an in vitro model. *Journal of Orthopaedic Research*. **17**(5), 639–645.

Rubin, J., Murphy, T.C., Fan, X., Goldschmidt, M., Taylor, W.R. (2002) Activation of Extracellular Signal-Regulated Kinase Is Involved in Mechanical Strain Inhibition of RANKL Expression in Bone Stromal Cells. *Journal of Bone and Mineral Research*. **17**(8), 1452–1460.

Rubin, J., Rubin, C., Jacobs, C.R. (2006) Molecular pathways mediating mechanical signaling in bone. *Gene*. **367**, 1–16.

Rustom, L.E., Boudou, T., Lou, S., Pignot-Paintrand, I., Nemke, B.W., Lu, Y., Markel, M.D., Picart, C., Wagoner Johnson, A.J. (2016) Micropore-induced capillarity enhances bone distribution in vivo in biphasic calcium phosphate scaffolds. *Acta Biomaterialia*. **44**, 144–154.

Ryder, K.D., Duncan, R.L. (2001) Parathyroid Hormone Enhances Fluid Shear - Induced [Ca2+]i Signaling in Osteoblastic Cells Through Activation of Mechanosensitive and Voltage-Sensitive Ca2+ Channels. . **16**(2), 240–248.

Saftig, P., Hunziker, E., Wehmeyer, O., Jones, S., Boyde, A., Rommerskirch, W., Moritz, J.D., Schu, P., von Figura, K. (1998) Impaired osteoclastic bone resorption leads to osteopetrosis in cathepsin-K-deficient mice. *Proceedings of the National Academy of Sciences of the United States of America*. **95**(23), 13453–8.

Salasznyk, R.M., Williams, W.A., Boskey, A., Batorsky, A., Plopper, G.E. (2004) Adhesion to Vitronectin and Collagen I Promotes Osteogenic Differentiation of Human Mesenchymal Stem Cells. *J Biomed Biotechnol*. **2004**(1), 24–34.

Schindeler, A., McDonald, M.M., Bokko, P., Little, D.G. (2008) Bone remodeling during fracture repair: The cellular picture. *Seminars in Cell and Developmental Biology*. **19**(5), 459–466.

Schlaepfer, D.D., Hauck, C.R., Sieg, D.J. (1999) Signaling through focal adhesion kinase. *Progress in Biophysics and Molecular Biology*. **71**(3–4), 435–478.

Schwarz, R.P., Goodwin, T.J., Wolf, D.A. (1992) Cell culture for three-dimensional modeling in rotating-wall vessels: An application of simulated microgravity. *Journal of Tissue Culture Methods*. **14**(2), 51–57.

Sen, B., Styner, M., Xie, Z., Case, N., Rubin, C.T., Rubin, J. (2009) Mechanical loading regulates NFATc1 and beta-catenin signaling through a GSK3beta control node. *The Journal of biological chemistry*. **284**(50), 34607–17.

Service, R.F. (2000) Tissue engineers build new bone. *Science (New York, N.Y.)*. **289**(5484), 1498–500.

Shahrezaie, M., Moshiri, A., Shekarchi, B., Oryan, A., Maffulli, N., Parvizi, J. (2018) Effectiveness of tissue engineered three-dimensional bioactive graft on bone healing and regeneration: an in vivo study with significant clinical value. *Journal of Tissue Engineering and Regenerative Medicine*. **12**(4), 936–960.

Shao, Y., Alicknavitch, M., Farach-Carson, M.C. (2005) Expression of voltage sensitive calcium channel (VSCC) L-type Cav1.2 (α1C) and T-type Cav3.2 (α1H) subunits during mouse bone development. *Developmental Dynamics*. **234**(1), 54–62.

Sikavitsas, V.I., Bancroft, G.N., Holtorf, H.L., Jansen, J.A., Mikos, A.G. (2003) Mineralized matrix deposition by marrow stromal osteoblasts in 3D perfusion culture increases with increasing fluid shear forces. *Proceedings of the National Academy of Sciences of the United States of America*. **100**(25), 14683–8.

Sikavitsas, V.I., Bancroft, G.N., Lemoine, J.J., Liebschner, M.A.K., Dauner, M., Mikos, A.G. (2005) Flow Perfusion Enhances the Calcified Matrix Deposition of Marrow Stromal Cells in Biodegradable Nonwoven Fiber Mesh Scaffolds. *Annals of Biomedical Engineering*. **33**(1), 63–70.

Sikavitsas, V.I., Bancroft, G.N., Mikos, A.G. (2002) Formation of three-dimensional cell/polymer constructs for bone tissue engineering in a spinner flask and a rotating wall vessel bioreactor. *Journal of Biomedical Materials Research*. **62**(1), 136–148.

Sikavitsas, V.I., Temenoff, J.S., Mikos, A.G. (2001) Biomaterials and bone

mechanotransduction. *Biomaterials*. **22**(19), 2581–2593.

Silber, J.S., Anderson, D.G., Daffner, S.D., Brislin, B.T., Leland, J.M., Hilibrand, A.S., Vaccaro, A.R., Albert, T.J. (2003) Donor site morbidity after anterior iliac crest bone harvest for single-level anterior cervical discectomy and fusion. *Spine*. **28**(2), 134–9.

da Silva, H.M., Mateescu, M., Damia, C., Champion, E., Soares, G., Anselme, K. (2010) Importance of dynamic culture for evaluating osteoblast activity on dense silicon-substituted hydroxyapatite. *Colloids and Surfaces B: Biointerfaces*. **80**(2), 138–144.

Sittichockechaiwut, A., Scutt, A.M., Ryan, A.J., Bonewald, L.F., Reilly, G.C. (2009) Use of rapidly mineralising osteoblasts and short periods of mechanical loading to accelerate matrix maturation in 3D scaffolds. *Bone*. **44**(5), 822–829.

Skerry, T.M., Lanyon, L.E., Bitensky, L., Chayen, J. (1989) Early strain-related changes in enzyme activity in osteocytes following bone loading in vivo. *Journal of Bone and Mineral Research*. **4**(5), 783–788.

Smalt, R., Mitchell, F.T., Howard, R.L., Chambers, T.J. (1997) Induction of NO and prostaglandin E2 in osteoblasts by wall-shear stress but not mechanical strain. *The American journal of physiology*. **273**(4 Pt 1), E751-8.

Sodek, J., Ganss, B., McKee, M.D. (2000) Osteopontin. *Critical Reviews in Oral Biology & Medicine*. **11**(3), 279–303.

Song, K., Li, L., Li, W., Zhu, Y., Jiao, Z., Lim, M., Fang, M., Shi, F., Wang, L., Liu, T. (2015) Three-dimensional dynamic fabrication of engineered cartilage based on chitosan/gelatin hybrid hydrogel scaffold in a spinner flask with a special designed steel frame. *Materials Science and Engineering: C*. **55**, 384–392.

Song, K., Li, W., Yanxia, Z., Hong, W., Ze, Y., Mayasari, L., Tianqing, L. (2014) Dynamic Fabrication of Tissue-Engineered Bone Substitutes Based on Derived Cancellous Bone Scaffold in a Spinner Flask Bioreactor System. *Applied Biochemistry and Biotechnology*. **174**(4), 1331–1343.

Song, K., Yang, Z., Liu, T., Zhi, W., Li, X., Deng, L., Cui, Z., Ma, X. (2006) Fabrication and detection of tissue-engineered bones with bio-derived scaffolds in a rotating bioreactor. *Biotechnology and Applied Biochemistry*. **45**(2), 65.

Stephens, J.S., Cooper, J.A., Phelan, F.R., Dunkers, J.P. (2007) Perfusion flow bioreactor for 3D in situ imaging: Investigating cell/biomaterials interactions. *Biotechnology and Bioengineering*. **97**(4), 952–961.

Street, J., Bao, M., deGuzman, L., Bunting, S., Peale, F. V, Ferrara, N., Steinmetz, H., Hoeffel, J., Cleland, J.L., Daugherty, A., van Bruggen, N., Redmond, H.P., Carano, R.A.D., Filvaroff, E.H. (2002) Vascular endothelial growth factor stimulates bone repair by promoting angiogenesis and bone turnover. *Proceedings of the National Academy of Sciences of the United States of America*. **99**(15), 9656–61.

Sunters, A., Armstrong, V.J., Zaman, G., Kypta, R.M., Kawano, Y., Lanyon, L.E., Price, J.S. (2010) Mechano-transduction in osteoblastic cells involves strain-regulated estrogen receptor α-mediated control of insulin-like growth factor (IGF) I receptor sensitivity to ambient IGF, leading to phosphatidylinositol 3-kinase/AKT-dependent Wnt/LRP5 receptor-i. *Journal of Biological Chemistry*. **285**(12), 8743–8758.

Sweedy, A., Bohner, M., Baroud, G. (2018) Multimodal analysis of *in vivo* resorbable CaP bone substitutes by combining histology, SEM, and microcomputed tomography data. *Journal of Biomedical Materials Research Part B: Applied Biomaterials*. **106**(4), 1567–1577.

Szpalski, C., Sagebin, F., Barbaro, M., Warren, S.M. (2013) The influence of environmental factors on bone tissue engineering. *Journal of Biomedical Materials Research - Part B Applied Biomaterials*. **101**(4), 663–675.

Tanaka, N., Ohno, S., Honda, K., Tanimoto, K., Doi, T., Ohno-Nakahara, M., Tafolla, E., Kapila, S., Tanne, K. (2005) Cyclic Mechanical Strain Regulates the PTHrP Expression in Cultured Chondrocytes via Activation of the Ca2+ Channel. *Journal of Dental Research*. **84**(1), 64–68.

Tang, X., Teng, S., Liu, C., Jagodzinski, M. (2017) Influence of hydrodynamic pressure on the proliferation and osteogenic differentiation of bone mesenchymal stromal cells seeded on polyurethane scaffolds. *Journal of Biomedical Materials Research Part A*. **105**(12), 3445–3455.

Teitelbaum, S.L. (2007) Osteoclasts: What Do They Do and How Do They Do It? *The American Journal of Pathology*. **170**(2), 427–435.

Termine, J.D., Kleinman, H.K., Whitson, S.W., Conn, K.M., McGarvey, M.L., Martin, G.R. (1981) Osteonectin, a bone-specific protein linking mineral to collagen. *Cell*. **26**(1), 99–105.

Thompson, W.R., Majid, A.S., Czymmek, K.J., Ruff, A.L., Garcia, J., Duncan, R.L., Farach-Carson, M.C. (2011) Association of the a α2δ1Subunit With Cav3.2 Enhances Membrane Expression and Regulates Mechanically Induced ATP Release in MLO-Y4 Osteocytes. *Journal of Bone and Mineral Research*. **26**(9), 2125–2139.

Thompson, W.R., Rubin, C.T., Rubin, J. (2012) Mechanical regulation of signaling pathways in bone. *Gene*. **503**(2), 179–193.

Thomson, R.C., Yaszemski, M.J., Powers, J.M., Mikos, A.G. (1996) Fabrication of biodegradable polymer scaffolds to engineer trabecular bone. *Journal of Biomaterials Science, Polymer Edition*. **7**(1), 23–38.

Tripathi, G., Basu, B. (2012) A porous hydroxyapatite scaffold for bone tissue engineering: Physico-mechanical and biological evaluations. *Ceramics International*. **38**(1), 341–349.

Tu, Q., Valverde, P., Chen, J. (2006) Osterix enhances proliferation and osteogenic potential of bone marrow stromal cells. *Biochemical and Biophysical Research Communications*. **341**(4), 1257–1265.

Turner, C.H., Pavalko, F.M. (1998) Mechanotransduction and functional response of the skeleton to physical stress: The mechanisms and mechanics of bone adaptation. *Journal of Orthopaedic Science*. **3**(6), 346–355.

Vance, J., Galley, S., Liu, D.F., Donahue, S.W. (2005) Mechanical Stimulation of MC3T3 Osteoblastic Cells in a Bone Tissue-Engineering Bioreactor Enhances Prostaglandin E_2 Release. *Tissue Engineering*. **11**(11–12), 1832–1839.

Varma, S., Orgel, J.P.R.O., Schieber, J.D. (2016) Nanomechanics of Type I Collagen. *Biophysical journal*. **111**(1), 50–6.

Vetsch, J.R., Betts, D.C., Müller, R., Hofmann, S., Fyhrie, D., Steinfeld, A., O'Brien, F., Meinel, L., Vunjak-Novakovic, G., Kaplan, D. (2017) Flow velocity-driven differentiation of human mesenchymal stromal cells in silk fibroin scaffolds: A combined experimental and computational approach G. Reilly, ed. *PLOS ONE*. **12**(7), e0180781.

Volkmer, E., Drosse, I., Otto, S., Stangelmayer, A., Stengele, M., Kallukalam, B.C., Mutschler, W., Schieker, M. (2008) Hypoxia in Static and Dynamic 3D Culture Systems for Tissue Engineering of Bone. *Tissue Engineering Part A*. **14**(8), 1331–1340.

Wainwright, S., Biggs, W., Currey, J., Gosline, J. (1982) *Mechanical Design in Organisms*. Princeton University Press.

Walker, L.M., Publicover, S.J., Preston, M.R., Said Ahmed, M.A., El Haj, A.J. (2000) Calcium-channel activation and matrix protein upregulation in bone cells in response to mechanical strain. *Journal of cellular biochemistry*. **79**(4), 648–661.

Wang, B., Du, T.Y., Wang, Y.C., Yang, C.B., Zhang, S., Cao, X.S. (2011) Focal adhesion kinase signaling pathway is involved in mechanotransduction in MG-63 Cells. *Biochemical and Biophysical Research Communications*. **410**(3), 671–676.

Wang, L., Ma, X.-Y., Zhang, Y., Feng, Y.-F., Li, X., Hu, Y.-Y., Wang, Z., Ma, Z.-S., Lei, W. (2014) Repair of Segmental Bone Defect Using Totally Vitalized Tissue Engineered Bone Graft by a Combined Perfusion Seeding and Culture System H. A. Awad, ed. *PLoS ONE*. **9**(4), e94276.

Wang, L., Seshareddy, K., Weiss, M.L., Detamore, M.S. (2009) Effect of Initial Seeding Density on Human Umbilical Cord Mesenchymal Stromal Cells for Fibrocartilage Tissue Engineering. *Tissue Engineering Part A*. **15**(5), 1009–1017.

Wang, T.W., Wu, H.C., Wang, H.Y., Lin, F.H., Sun, J.S. (2009) Regulation of adult human mesenchymal stem cells into osteogenic and chondrogenic lineages by different bioreactor systems. *Journal of Biomedical Materials Research - Part A*. **88**(4), 935–946.

Wang, Y.C., Uemura, T., Dong, R., Kojima, H., Tanaka, J., Tateishi, T. (2003) Application of perfusion culture system improves in vitro and in vivo osteogenesis of bone marrow-derived osteoblastic cells in porous ceramic materials. *Tissue Engineering*. **9**(6), 1205–1214.

Ward Jr., D.F., Salasznyk, R.M., Klees, R.F., Backiel, J., Agius, P., Bennett, K., Boskey, A., Plopper, G.E. (2007) Mechanical Strain Enhances Extracellular Matrix-Induced Gene Focusing and Promotes Osteogenic Differentiation of Human Mesenchymal Stem Cells Through an Extracellular-Related Kinase-Dependent Pathway. *Stem Cells and Development*. **16**(3), 467–480.

Wen, L., Wang, Y., Wang, H., Kong, L., Zhang, L., Chen, X., Ding, Y. (2012) L-type calcium channels play a crucial role in the proliferation and osteogenic differentiation of bone marrow mesenchymal stem cells. *Biochemical and Biophysical Research Communications*. **424**(3), 439–445.

Woodard, J.R., Hilldore, A.J., Lan, S.K., Park, C.J., Morgan, A.W., Eurell, J.A.C., Clark, S.G., Wheeler, M.B., Jamison, R.D., Wagoner Johnson, A.J. (2007) The mechanical properties and osteoconductivity of hydroxyapatite bone scaffolds with multi-scale porosity. *Biomaterials*. **28**(1), 45–54.

Wu, Q.Q., Chen, Q. (2000) Mechanoregulation of chondrocyte proliferation, maturation, and hypertrophy: ion-channel dependent transduction of matrix deformation signals. *Experimental cell research*. **256**(2), 383–391.

Xia, L., Zhang, N., Wang, X., Zhou, Y., Mao, L., Liu, J., Jiang, X., Zhang, Z., Chang, J., Lin, K., Fang, B. (2016) The synergetic effect of nano-structures and silicon-substitution on the properties of hydroxyapatite scaffolds for bone regeneration. *J. Mater. Chem. B*. **4**(19), 3313–3323.

Xu, B., Song, G., Ju, Y., Li, X., Song, Y., Watanabe, S. (2012) RhoA/ROCK, cytoskeletal dynamics, and focal adhesion kinase are required for mechanical stretch-induced tenogenic differentiation of human mesenchymal stem cells. *Journal of Cellular Physiology*. **227**(6), 2722–2729.

Xu, S., Du, P., Xie, Y., Yue, Y. (2008) Cell distribution in a scaffold with random architectures under the influence of fluid dynamics. *Journal of Biomaterials Applications*. **23**(3), 229–245.

Xynos, I.D., Hukkanen, M.V.J., Batten, J.J., Buttery, L.D., Hench, L.L., Polak, J.M. (2000) Bioglass ®45S5 Stimulates Osteoblast Turnover and Enhances Bone Formation In Vitro: Implications and Applications for Bone Tissue Engineering. *Calcified Tissue International*.

67(4), 321–329.

Yan, Y., Gong, Y., Guo, Y., Lv, Q., Guo, C., Zhuang, Y., Zhang, Y., Li, R., Zhang, X. (2012) Mechanical Strain Regulates Osteoblast Proliferation through Integrin-Mediated ERK Activation G. Pintus, ed. *PLoS ONE*. **7**(4), e35709.

Yang, J., Cao, C., Wang, W., Tong, X., Shi, D., Wu, F., Zheng, Q., Guo, C., Pan, Z., Gao, C., Wang, J. (2010) Proliferation and osteogenesis of immortalized bone marrow-derived mesenchymal stem cells in porous polylactic glycolic acid scaffolds under perfusion culture. *Journal of Biomedical Materials Research - Part A*. **92**(3), 817–829.

Yang, M., Xiao, L., Liao, E., Wang, Q., Wang, B., Lei, J. (2014) The role of integrin-β / FAK in cyclic mechanical stimulation in MG-63 cells. *Int J Clin Exp Pathol*. **7**(11), 7451–7459.

Yao, Z., Seger, R. (2009) The ERK signaling cascade-views from different subcellular compartments. *BioFactors*. **35**(5), 407–416.

Yeatts, A.B., Both, S.K., Yang, W., Alghamdi, H.S., Yang, F., Fisher, J.P., Jansen, J.A. (2014) In Vivo Bone Regeneration Using Tubular Perfusion System Bioreactor Cultured Nanofibrous Scaffolds. *Tissue Engineering Part A*. **20**(1–2), 139–146.

Yeatts, A.B., Fisher, J.P. (2011) Bone tissue engineering bioreactors: Dynamic culture and the influence of shear stress. *Bone*. **48**(2), 171–181.

Yoon, Y.M., Oh, C.D., Kim, D.Y., Lee, Y.S., Park, J.W., Huh, T.L., Kang, S.S., Chun, J.S. (2000) Epidermal growth factor negatively regulates chondrogenesis of mesenchymal cells by modulating the protein kinase C-alpha, Erk-1, and p38 MAPK signaling pathways. *The Journal of biological chemistry*. **275**(16), 12353–9.

Yoshikawa, T., Ohgushi, H., Tamai, S. (1996) Immediate bone forming capability of prefabricated osteogenic hydroxyapatite. *Journal of Biomedical Materials Research*. **32**(3), 481–492.

You, J., Reilly, G.C., Zhen, X.C., Yellowley, C.E., Chen, Q., Donahue, H.J., Jacobs, C.R. (2001) Osteopontin gene regulation by oscillatory fluid flow via intracellular calcium mobilization and activation of mitogen-activated protein kinase in MC3T3-E1 osteoblasts. *Journal of Biological Chemistry*. **276**(16), 13365–13371.

Young, S.R.L., Gerard-O'Riley, R., Kim, J.B., Pavalko, F.M. (2009) Focal Adhesion Kinase Is Important for Fluid Shear Stress-Induced Mechanotransduction in Osteoblasts. *Journal of Bone and Mineral Research*. **24**(3), 411–424.

Yourek, G., McCormick, S.M., Mao, J.J., Reilly, G.C. (2010) Shear stress induces osteogenic differentiation of human mesenchymal stem cells. *Regenerative Medicine*. **5**(5), 713–724.

Yu, H.-S., Won, J.-E., Jin, G.-Z., Kim, H.-W. (2012) Construction of Mesenchymal Stem Cell–Containing Collagen Gel with a Macrochanneled Polycaprolactone Scaffold and the Flow Perfusion Culturing for Bone Tissue Engineering. *BioResearch Open Access*. **1**(3), 124–136.

Yu, X., Botchwey, E.A., Levine, E.M., Pollack, S.R., Laurencin, C.T. (2004) Bioreactor-based bone tissue engineering: the influence of dynamic flow on osteoblast phenotypic expression and matrix mineralization. *Proceedings of the National Academy of Sciences of the United States of America*. **101**(31), 11203–8.

Yuan, H., Fernandes, H., Habibovic, P., de Boer, J., Barradas, A.M.C., de Ruiter, A., Walsh, W.R., van Blitterswijk, C.A., de Bruijn, J.D. (2010) Osteoinductive ceramics as a synthetic alternative to autologous bone grafting. *Proceedings of the National Academy of Sciences of the United States of America*. **107**(31), 13614–9.

Zehorai, E., Yao, Z., Plotnikov, A., Seger, R. (2010) The subcellular localization of MEK and

ERK-A novel nuclear translocation signal (NTS) paves a way to the nucleus. *Molecular and Cellular Endocrinology*. **314**(2), 213–220.

Zhang, T., Wen, F., Wu, Y., Goh, G.S.H., Ge, Z., Tan, L.P., Hui, J.H.P., Yang, Z. (2015) Cross-talk between TGF-beta/SMAD and integrin signaling pathways in regulating hypertrophy of mesenchymal stem cell chondrogenesis under deferral dynamic compression. *Biomaterials*. **38**, 72–85.

Zhang, Y., Pizzute, T., Pei, M. (2014) A review of crosstalk between MAPK and Wnt signals and its impact on cartilage regeneration. *Cell and Tissue Research*. **358**(3), 633–649.

Zhang, Z., Messana, J., Hwang, N.S.H., Elisseeff, J.H. (2006) Reorganization of actin filaments enhances chondrogenic differentiation of cells derived from murine embryonic stem cells. *Biochemical and Biophysical Research Communications*. **348**(2), 421–427.

Zhao, F., Chella, R., Ma, T. (2007) Effects of shear stress on 3-D human mesenchymal stem cell construct development in a perfusion bioreactor system: Experiments and hydrodynamic modeling. *Biotechnology and Bioengineering*. **96**(3), 584–595.

Zhao, F., Ma, T. (2005) Perfusion bioreactor system for human mesenchymal stem cell tissue engineering: Dynamic cell seeding and construct development. *Biotechnology and Bioengineering*. **91**(4), 482–493.

Zhao, F., Vaughan, T.J., Mcnamara, L.M. (2015) Multiscale fluid–structure interaction modelling to determine the mechanical stimulation of bone cells in a tissue engineered scaffold. *Biomechanics and Modeling in Mechanobiology*. **14**(2), 231–243.